Zonal flows in plasma—a review

2005 Plasma Phys. Control. Fusion 47 R35

(http://iopscience.iop.org/0741-3335/47/5/R01)

INSTITUTE OF PHYSICS PUBLISHING PLASMA PHYSICS AND CONTROLLED FUSION

Plasma Phys. Control. Fusion **47** (2005) R35–R161 doi:10.1088/0741-3335/47/5/R01

TOPICAL REVIEW

Zonal flows in plasma—a review

P H Diamond[1], S-I Itoh[2], K Itoh[3] and T S Hahm[4]

[1] University of California San Diego, La Jolla, CA 92093-0319, USA
[2] Institute for Applied Mechanics, Kyushu University 87, Kasuga 816-8580, Japan
[3] National Institute for Fusion Science, Toki 509-5292, Japan
[4] Princeton University, Plasma Physics Laboratory, Princeton, NJ 08543, USA

Received 10 January 2005
Published 1 April 2005
Online at stacks.iop.org/PPCF/47/R35

Abstract

A comprehensive review of zonal flow phenomena in plasmas is presented. While the emphasis is on zonal flows in laboratory plasmas, planetary zonal flows are discussed as well. The review presents the status of theory, numerical simulation and experiments relevant to zonal flows. The emphasis is on developing an integrated understanding of the dynamics of drift wave–zonal flow turbulence by combining detailed studies of the generation of zonal flows by drift waves, the back-interaction of zonal flows on the drift waves, and the various feedback loops by which the system regulates and organizes itself. The implications of zonal flow phenomena for confinement in, and the phenomena of fusion devices are discussed. Special attention is given to the comparison of experiment with theory and to identifying directions for progress in future research.

This review article is dedicated to the memory of Professor Marshall N Rosenbluth

(Some figures in this article are in colour only in the electronic version)

Contents

1. Introduction

Zonal flows, by which we mean azimuthally symmetric band-like shear flows, are a ubiquitous phenomena in nature and the laboratory. The well-known examples of the Jovian belts and zones, and the terrestrial atmospheric jet stream are familiar to nearly everyone—the latter especially to travellers enduring long, bumpy airplane rides against strong head winds. Zonal flows are also present in the Venusian atmosphere (which rotates faster than the planet does!) and occur in the solar tachocline, where they play a role in the solar dynamo mechanism. In the laboratory, the importance of sheared $\boldsymbol{E} \times \boldsymbol{B}$ flows to the development of L-mode confinement, the L-to-H transition and internal transport barriers (ITBs) is now well and widely appreciated.

While many mechanisms can act to trigger and stimulate the growth of sheared electric fields (i.e. profile evolution and transport bifurcation, neoclassical effects, external momentum injection, etc) certainly one possibility is via the self-generation and amplification of $\boldsymbol{E} \times \boldsymbol{B}$ flows by turbulent stresses (i.e. the turbulent transport of momentum). Of course, this is the same mechanism as that responsible for zonal flow generation. It should be emphasized that it is now widely recognized and accepted that zonal flows are a key constituent in nearly all cases

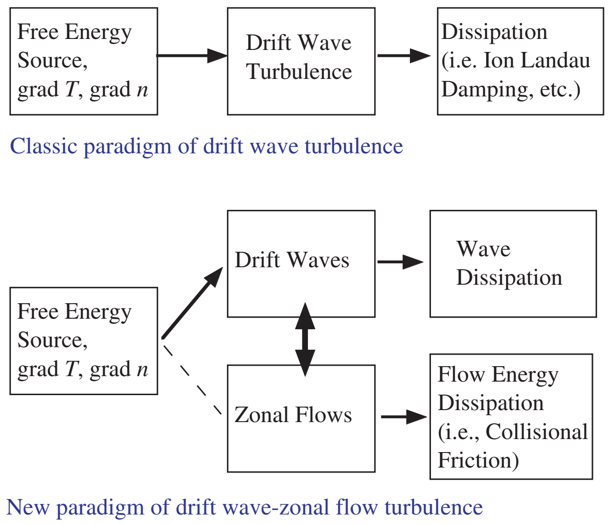

Figure 1. New paradigm for the plasma turbulence.

and regimes of drift wave turbulence—indeed, so much so that this classic problem is now frequently referred to as 'drift wave–zonal flow turbulence'. This paradigm shift occurred on account of the realization that zonal flows are ubiquitous in dynamical models used for describing fusion plasmas (i.e. ITG, TEM, ETG, resistive ballooning and interchange, etc) in all geometries and regimes (i.e. core, edge, etc), and because of the realization that zonal flows are a critical agent of self-regulation for drift wave transport and turbulence. Both theoretical work and numerical simulation made important contributions to this paradigm shift. Indeed, for the case of low collisionality plasmas, a significant portion of the available free energy is ultimately deposited in the zonal flows. Figure 1 presents energy flow charts which illustrate the classic paradigm of drift wave turbulence and the new paradigm of drift wave–zonal flow turbulence. The study of zonal flow has had a profound impact on fusion research. For instance, the proper treatment of the zonal flow physics has resolved some of the confusion [1] concerning the prospect of burning plasma, as has been discussed by Rosenbluth and collaborators in conjunction with the design of the International Thermonuclear Experimental Reactor (ITER). At the same time, the understanding of the turbulence–zonal flow system has advanced the understanding of self-organization processes in nature.

We note here that, while zonal flows have a strong influence on the formation of transport barriers, the dynamics of barriers and transitions involve evolutions of both the mean $\boldsymbol{E} \times \boldsymbol{B}$ flow as well as the zonal $\boldsymbol{E} \times \boldsymbol{B}$ flow. The topics of mean E_{r} dynamics, transport barriers and confinement regime transitions are beyond the scope of this review.

In the context of tokamak plasmas, zonal flows are $n = 0$ electrostatic potential fluctuations with finite radial wavenumber. Zonal flows are elongated, asymmetric vortex modes, and thus have zero frequency. They are predominantly poloidally symmetric as well, though some coupling to low-m sideband modes may occur. On account of their symmetry, zonal flows cannot access expansion free energy stored in temperature, density gradients, etc, and are not subject to Landau damping. These zonal flows are driven *exclusively* by nonlinear interactions, which transfer energy from the finite-n drift waves to the $n = 0$ flow. Usually, such nonlinear interactions are three-wave triad couplings between two high $\boldsymbol{k}$ drift waves and one low $\boldsymbol{q} = q_{\mathrm{r}}\hat{r}$ zonal flow excitation. In position space, this energy transfer process is simple one whereby

Reynolds work is performed on the flow by the wave stresses. Two important consequences of this process of generation follow directly. First, since zonal flow production is exclusively via nonlinear transfer from drift waves, zonal flows must eventually decay and vanish if the underlying drift wave drive is extinguished. Thus, zonal flows differ in an important way from mean $\boldsymbol{E} \times \boldsymbol{B}$ flows, which can be sustained in the absence of turbulence (and are, in strong H-mode and ITB regimes). Second, since zonal flows are generated by nonlinear energy transfer *from* drift waves, their generation naturally acts to *reduce* the intensity and level of transport caused by the primary drift wave turbulence. Thus, zonal flows necessarily act to *regulate and partially suppress* drift wave turbulence and transport. This is clear from numerical simulations, which universally show that turbulence and transport levels are reduced when the zonal flow generation is (properly) allowed. Since zonal flows cannot tap expansion free energy, are generated by nonlinear coupling from drift waves, and damp primarily (but not exclusively) by collisional processes, they constitute a significant and benign (from a confinement viewpoint) reservoir or repository for the available free energy of the system.

Another route to understanding the effects of zonal flow on drift waves is via the shearing paradigm. From this standpoint, zonal flows produce a spatio-temporally complex shearing pattern, which naturally tends to distort drift wave eddies by stretching them, and in the process generates large k_{r}. Of course, at smaller scales, coupling to dissipation becomes stronger, resulting in a net stabilizing trend. The treatment of zonal flow shearing differs from that for mean flow shearing on account of the complexity of the flow pattern. Progress here has been facilitated by the realization that a statistical analysis is possible. This follows from the fact that the autocorrelation time of a drift wave-packet propagating in a zonal flow field is usually quite short, and because the drift wave rays are chaotic. Hence, significant advances have been made on calculating the 'back reaction' of zonal flows on the underlying drift wave field within the framework of random shearing, using wave kinetics and quasilinear theory. Conservation of energy between drift waves and zonal flows has been proved for the theory, at the level of a renormalized quasilinear description. Thus, it is possible to close the 'feedback loop' of wave–flow interactions, allowing a self-consistent analysis of the various system states, and enabling an understanding of the mechanisms and routes for bifurcation between them.

From a more theoretical perspective, the drift wave–zonal flow problem is a splendid example of *two* generic types of problems frequently encountered in the dynamics of complex systems. These are the problems of nonlinear interaction between two classes of fluctuations of disparate scale, and the problems of self-organization of structures in turbulence. The drift wave–zonal flow problem is clearly a member of the first class, since drift waves have high frequency and wavenumber ($k_\perp \rho_{\mathrm{i}} \sim 1$, $\omega_k \sim \omega*$) in comparison to zonal flows ($q_r \rho_{\mathrm{i}} \ll 1$, $\Omega \sim 0$). Another member of this group, familiar to most plasma physicists, is the well-known problem of Langmuir turbulence, which is concerned with the interaction between high frequency plasma waves and low frequency ion acoustic waves. As is often the case in such problems, fluctuations on one class of scales can be treated as 'slaved' to the other, thus facilitating progress through the use of averaging, adiabatic theory and projection operator techniques. In the case of the drift wave–zonal flow problem, great simplification has been demonstrated via the identification of a conserved drift wave population density (i.e. action-like invariant) which is adiabatically modulated by the sheared flows. Indeed, though superficially paradoxical, it seems fair to say that such disparate scale interaction problems are, in some sense, more tractable than the naively 'simpler' problem of Kolmogorov turbulence, since the ratio of the typical scales of the two classes of fluctuations may be used to constitute a small parameter, which is then exploited via adiabatic methodology.

Of course, it is patently obvious that the zonal flow problem is one of self-organization of a large structure in turbulence. Examples of other members of this class include transport barrier and profile formation and dynamics, the origin of the solar differential rotation, the famous magnetic dynamo problem (relevant, in quite different limits, to the sun, earth, galaxy and reversed field pinch), and the formation of profiles in turbulent and swirling pipe flow. Table 1 summarizes these related structure formation phenomena, illustrating the objective of this review. Most of these problems are attacked at the simplest level by considering the stability of an ensemble or 'gas' of ambient turbulence to a seed perturbation. For example, in the dynamo problem, one starts by considering the stability of some state of magnetohydrodynamic (MHD) turbulence to a seed magnetic field. In the zonal flow problem, one correspondingly considers the stability of a gas of drift waves to a seed shear. The incidence of instability means that the initial vortex tilt will be re-enforced, thus amplifying the seed perturbation. It should be noted that the zonal flow formation phenomenon is related to, but not quite the same as, the well-known inverse cascade of energy in a two-dimensional fluid, which leads to large scale vortex formation. This is because the inverse cascade proceeds via a local coupling in wavenumber space, while zonal flow generation occurs via non-local transfer of energy between small and large scales. Indeed, zonal shear amplification is rather like the familiar α-effect from dynamo theory, which describes a non-local transfer of magnetic helicity to large scale. We also note that the initial stage of pattern formation instability meets only part of the challenge to a theoretical description of structure formation, and that one must subsequently 'close the loop' by understanding the mechanisms of saturation of the zonal flow instability. The saturation of zonal flows driven by drift wave turbulence is now a subject of intensive theoretical and computational investigation, worldwide.

As a related phenomena, convective cells have been subject to intensive study for a long time. The convective cell is a perturbation which is constant along the magnetic field line but changes in the direction perpendicular to the magnetic field. Such a structure is known to be induced by background drift wave turbulence. The zonal flow can be considered as a particular example of an anisotropic convective cell. However, the convective cells of greatest interest as agents of transport are localized in the poloidal direction and extended radially, which is the opposite limit of anisotropy from that of the zonal flow. Such cells are commonly referred to as *streamers*.

As the zonal flow problem is a member of a large class of rapidly expanding research topics, the perspective of this review is composed as follows. First, we present detailed explanations of the physical understanding of drift wave–zonal flow turbulence. Second, we also stress the view that studies on toroidal plasma turbulence enhance our understanding of turbulent structure formation in nature. In this sense, this review is a companion paper to recent reviews on the magnetic dynamo problem which, taken together, present a unified view that addresses the mystery of structure formation in turbulent media. Third, the impact of direct nonlinear simulation (DNS) is discussed in the context of understanding zonal flow physics, although a survey of DNS techniques themselves is beyond the scope of this review. It is certainly the case that DNS studies have significantly furthered our understanding of drift wave–zonal flow turbulence. For these reasons, examples are mainly chosen from the realm of core plasma (i.e. drift wave) turbulence. In order to maintain transparency and to be concise, this review is limited in scope. Studies of edge turbulence and of general convective cell physics are not treated in depth here. While these topics are closely related to the topic of this review, extensive introductory discussions, which are too lengthy for this paper, are necessary. Hence, details of these important areas are left for future reviews.

This paper reviews zonal flow dynamics, with special emphasis on the theory of drift wave–zonal flow turbulence and its role in plasma confinement. The remainder of this review paper is organized as follows. Section 2 presents a heuristic overview of the essentials of zonal flow physics, including shearing, generation mechanisms, and multiple states and bifurcations.

Table 1. Comparison between zonal flow in plasmas, dynamo, electromagnetic (EM) flow generation and flow structure formation.

Name of concept	Name	Main small-scale fluctuations	Generated global structure	Examples	Equations in fluid limit, fundamental drive	Coverage by this review
Electromagnetic flow drive	Flow dynamo	EM and pressure fluctuations (drift waves)	Flow	Zonal flow in toroidal plasmas	MHD equations Plasma response Pressure gradient	Yes
	MHD flow dynamo	EM and flow fluctuations	Magnetized flow	Bipolar jets	MHD equation Gravitational force Coriolis force	No
Flow generation	Neutral flow 'dynamo'	Small-scale thermal convection	Zonal flow	Jobian belt Tidal current Jet stream, etc	Navier–Stokes equation Thermal convection Coriolis force	Yes
	Flow structure formation	Small-scale convection	Structured flow	Swirling flow Asymmetry in pipe flow	Navier–Stokes equation Drive of axial flow	Partly
Magnetic dynamo	Dynamo	Fluid motion (thermal convection)	Magnetic field	Geodynamo Solar dynamo	MHD equation Thermal convection Coriolis force	No
	Magnetic structure formation	Magnetic fluctuations (kink, tearing)	Magnetic field	RFP torus	MHD equation External toroidal current	No

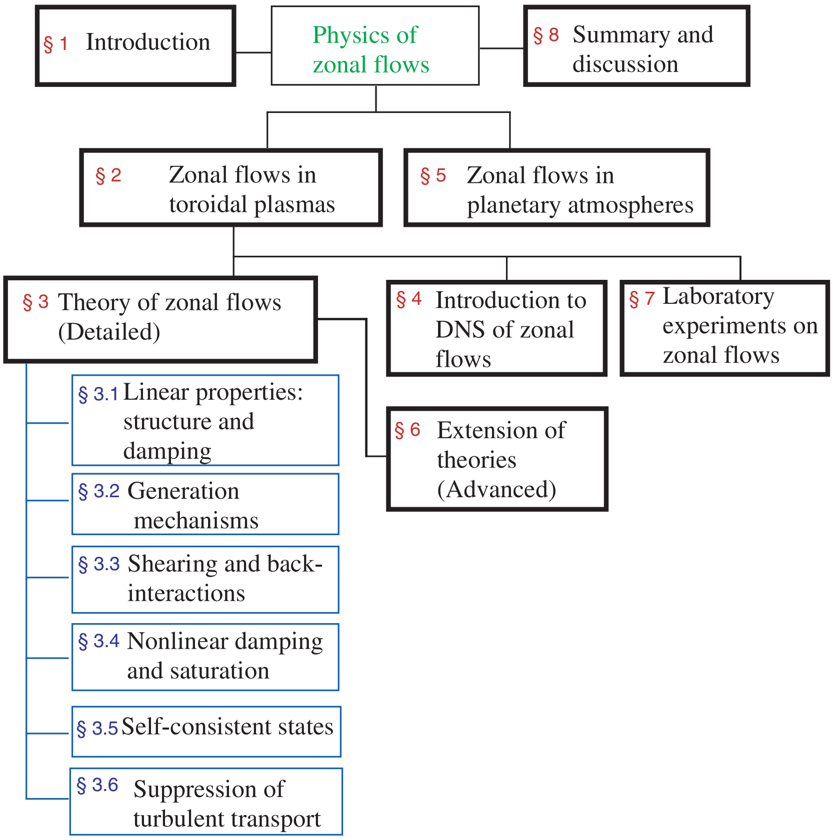

Figure 2. Road map for the review.

Section 2 is aimed at general readers, non-specialists and others who want only to read a brief executive summary. Section 3 presents a detailed description of the theory of drift wave–zonal flow turbulence. Section 3.1 discusses neoclassical collisional friction damping. Section 3.2 is concerned with drive and amplification, from a number of perspectives and approaches. In particular, both coherent and broad-band modulational stability calculations are explained in detail, and extensions to regimes where waves are trapped in the flows are discussed as well. Section 3.3 describes the feed back of zonal flows on drift waves, while section 3.4 discusses nonlinear saturation mechanisms. An emphasis is placed upon unifying the various limiting models. Section 3.5 presents a unified, self-consistent description of the various systems and the bifurcation transitions between them. Section 3.6 deals with the effect of the zonal flows on transport. Section 4 gives an overview of what numerical simulations have elucidated about zonal flow dynamics in magnetized plasmas. Section 5 gives an introduction to zonal flow phenomena in nature. Special emphasis is placed upon the well-known and visually compelling example of belt and band formation in the atmosphere of Jupiter. Section 6 discusses advanced extensions of the theory, including statistical and probabilistic approaches and non-Markovian models. Section 7 surveys the state of experimental studies of zonal flow phenomena in magnetically confined plasma. Section 8 gives a statement of conclusions, an assessment of the current state of our understanding and presents suggestions for the future direction of research. These structures are illustrated in the roadmap of figure 2. We note that an extended version of the paper may be found in the form of a preprint [2].

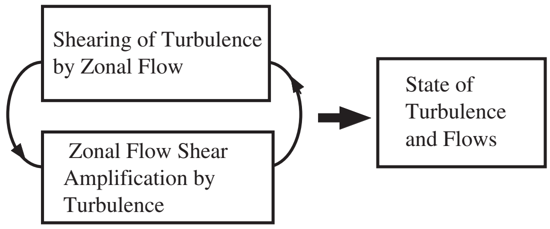

Figure 3. Mutual interaction of drift waves and zonal flows.

2. Basic physics of zonal flows: a heuristic overview

2.1. Introduction

We present an introduction to the basic physics of zonal flows. This section is directed toward a general audience, which may include plasma and fusion experimentalists and other non-specialists, as well as readers who desire only an 'executive summary' of this paper. Some of the relevant, pioneering work on zonal flows can be found in [3–8]. The emphasis here is on physical reasoning and intuition, rather than on formalism and rigorous deduction. This section begins with a discussion of shearing [9–13] by a spectrum of zonal flows and its effect on the primary drift wave spectrum. Considerations of energetics, in the quasi-linear approximation [14, 15], are then used to describe and calculate the rate of amplification of zonal shears by turbulence. We then discuss some basic features of the dynamical system of waves and zonal flows, and its various states (figure 3). Using the example of drift wave turbulence with a spatial scale length of ρ_{i}, the basic characteristics of zonal flows are summarized in table 2. This table serves as a guide for the explanations in the following sections. In the study of zonal flows, three principal theoretical approaches have been applied. These are: (i) wave kinetic and adiabatic theory, (ii) parametric (modulational) theory and (iii) envelope formalism. In this section, an explanation in the spirit of wave kinetics and adiabatic theory is given. The wave kinetic theory, as well as parametric theory are described in depth in section 3. The envelope formalism is discussed in section 6.

2.2. Basic dynamics of zonal flows

The zonal flow is a toroidally symmetric electric field perturbation in a toroidal plasma, which is constant on the magnetic surface but rapidly varies in the radial direction, as is illustrated in figure 4. The associated $\boldsymbol{E} \times \boldsymbol{B}$ flow is in the poloidal direction, and its sign changes with radius. The zonal flow corresponds to a strongly asymmetric limit of a convective cell. The key element in the dynamics of zonal flows is the process of shearing of turbulent eddies by flows with a larger scale (i.e. with shear lengths $L_{\mathrm{s}} > \Delta x_{\mathrm{c}}$, where Δx_{c} is the eddy scale). The fact that such shearing acts to reduce turbulence and transport is what drives the strong current interest in zonal flows. In the case of a smooth, mean shear flow, it is well-known that shearing tilts eddies, narrowing their radial extent and elongating them (figure 5). In some simulations, sheared flows are observed to break up the large eddies associated with extended modes. At the level of eikonal theory, this implies that the radial wavenumber of the turbulence increases linearly in time, i.e.

$$k_{\mathrm{r}} = k_{\mathrm{r}}^{(0)} - k_\theta \frac{\partial V_\theta(r)}{\partial r} t. \tag{2.1}$$

Table 2. Characteristics of zonal flow.

Spatio-temporal structures	
eigenfunction	electrostatic perturbation is dominant; $\tilde{n}_{\rm i}/n_0 \simeq 0$
radial wave length $q_{\rm r}^{-1}$	$a\rho_{\rm i} > q_{\rm r}^{-2} > \rho_{\rm i}^2$ or $q_{\rm r} \sim {\rm O}(0.1)\rho_{\rm i}^{-1}$, weak poloidal asymmetry
radial coherence length	can be $\sim\sqrt{a\rho_{\rm i}}$ (see also section 6.4)
real frequency $\Omega_{\rm ZF}$	$\Omega_{\rm ZF} \simeq 0$
autocorrelation time	$\nu_{\rm ii}\varepsilon^{-1}$, and see section 3.5.1
amplitude	average vorticity is order $\rho_{\rm i}^{-1} V_{\rm d}$ (section 3.5)
Phase diagram for ZF	
appearance: see sections 3.2.1 and 3.2.2	
significant impact for turbulent transport: $q_{\rm r} V_{\rm ZF} > \Delta\omega_k$ (see section 3.5)	
Microfluctuation that is the origin of ZF	
all instability in the range of ω_*; $\rho_{\rm i}$ and $\rho_{\rm e}$	
partition between ZF and turbulence: see sections 3.5.1 and 3.5.6	
Impact on turbulence	
significant impact if $q_{\rm r} V_{\rm ZF} > \Delta\omega_k$ (see section 3.5)	
scattering of drift wave-packet in (x, k_x) space if $\omega_{\rm bounce} > \Delta\omega_k$ (sections 3.4.6 and 3.4.7)	
Interactions between ZFs	
through modifying microfluctuations; no direct condensation/cascade so far	

As a consequence, the eddies necessarily must increase the strength of their coupling to small scale dissipation, thus tending to a quench of the driving process. In addition, the increase in $k_{\rm r}$ implies a decrease in $\Delta x_{\rm c}$, thus reducing the effective step size for turbulent transport [16].

In the case of zonal flows, the physics is closely related, but different in detail, since zonal flow shears nearly always appear as elements of a spatially complex (and frequently temporally complex) pattern (figure 6) [17–19]. This presents a significant complication to any theoretical description. Fortunately, the problem is greatly simplified by two observations. First, the drift wave spectrum is quite broad, encompassing a range of spatial scales from the profile scale $L_\perp$ to the ion gyro-radius $\rho_{\rm i}$, and a range of time scales from $(D_{\rm B}/L_\perp^2)^{-1}$ to $L_\perp/c_{\rm s}$. Here $D_{\rm B} = \rho_{\rm s} c_{\rm s}$. In contrast, the dynamically relevant part of the zonal flow spectrum has quite a low frequency and large extent, so that a scale separation between the drift waves and zonal flows clearly exists. Second, the 'rays' along which the drift waves propagate can easily be demonstrated to be chaotic, which is not surprising, in view of the highly turbulent state of the drift wave spectrum. Δk, the width of the drift wave spectrum satisfies $\Delta k \rho_{\rm i} \sim 1$. Thus, the effective lifetime of the instantaneous pattern 'seen' by a propagating drift wave group packet is $|\Delta(q_{\rm r} v_{\rm g})|^{-1}$. Here, $q_{\rm r}$ is the radial wavenumber of the zonal flow and $v_{\rm g}$ is the group velocity of the drift waves. This implies that the effective lifetime of the instantaneous shearing pattern, as seen by the wave-packet, is $\tau_{\rm ac} \sim |\Delta(q_{\rm r} v_{\rm g})|^{-1}$. For virtually any relevant parameters, this time scale is shorter than the time scale for shearing, trapping, etc of the wave-packet. Note that, on account of ray chaos, no 'random phase' assumption for zonal flow shears is necessary [20]. Thus, the shearing process in a zonal flow field can be treated as a random, diffusive process, consisting of a succession of many short kicks, which correspond to shearing events,

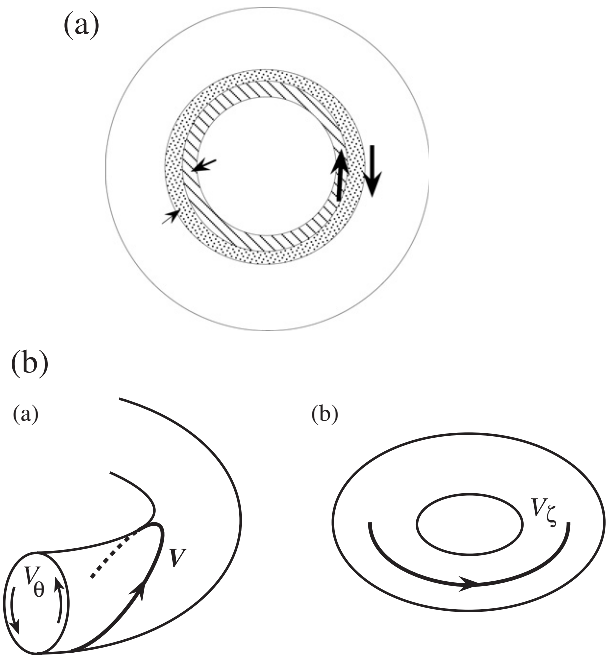

Figure 4. Zonal electric field and zonal flow. The poloidal cross-section of toroidal plasma is illustrated. The hatched region and the dotted region denote the positive and negative charges, respectively: (*a*) The flow perturbation in the poloidal cross-section. (*b*) A birds-eye view of the net flow associated with the zonal perturbation is illustrated.

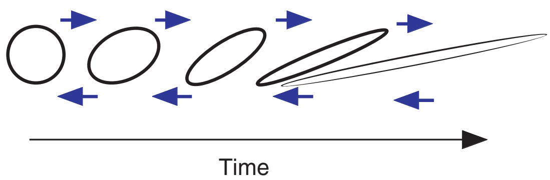

Figure 5. Shearing of the vortex.

so, the mean square wavenumber increases as

$$\langle \delta k_{\mathrm{r}}^2 \rangle = D_k t, \tag{2.2a}$$

$$D_k = \sum_q |k_\theta V_\theta q_{\mathrm{r}}|^2 \tau_{k,q}, \tag{2.2b}$$

where $\langle \cdots \rangle$ represents the average, $V_{\theta,q}$ represents the q-Fourier components of the poloidal flow velocity and $\tau_{k,q}$ is the time of (triad) interaction between the zonal flow and the drift wave-packet. This diffusion coefficient D_k is simply the mean square shear in the flow induced Doppler shift of the wave (weighted by the correlation time of the wave-packet element with the zonal flow shear), on the scale of zonal flow wavenumber q [21]. Thus, in contrast to the case of coherent shearing for which the radial wavenumber increases linearly with time, the root mean square (rms) wavennumber increases $\sim t^{1/2}$. However, the basic trend toward coupling to smaller scales in the drift wave spectrum persists. Furthermore, this evolution is adiabatic, on account of the separation in time and space scales between drift waves and zonal

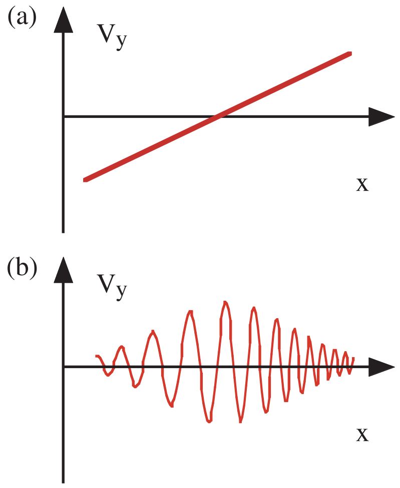

Figure 6. Sheared mean flow (*a*) and zonal flows, (*b*) are illustrated.

flows mentioned above. The use of adiabatic approximation methods greatly simplifies the calculations [22–24].

As noted above, much of the interest in zonal flows is driven by the fact that they regulate turbulence via shearing. However, it is certainly true that all low-n modes in a spectrum of drift wave turbulence will shear and strain the larger-n, smaller-scale fluctuations. Indeed, non-local shearing–straining interactions are characteristic of two-dimensional turbulence once large scale vortices are established, as argued by Kraichnan and shown in simulations by Borue and Orszag. This, in turn, naturally motivates the questions: what is so special about zonal flows (with $n = 0$)? and why are other low-n modes not given equal consideration as regulators of drift wave turbulence? There are at least *three* answers to this very relevant and interesting question. These are discussed below.

First, zonal flows may be said to be the '*modes of minimal inertia*'. This is because zonal flows, with $n = 0$ and $k_\parallel = 0$, are not screened by Boltmann electrons, as are the usual drift-ITG (ITG = ion temperature gradient) modes. Hence, the potential vorticity of a zonal flow mode is simply $q_r^2 \rho_s^2 \hat{\phi}_q$, as opposed to $(1 + k_\perp^2 \rho_s^2)\hat{\phi}_{\underline{k}}$, so that zonal flows have lower effective inertia than standard drift waves do. The comparatively low effective inertia of zonal flows means that large zonal flow velocities develop in response to drift wave drive, unless damping intervenes. In this regard, it is also worthwhile to point out that in the case of electron temperature gradient (ETG) turbulence, *both* zonal flows and ETG modes involve a Boltzmann ion response $\hat{n}_i/n_o = -|e|\hat{\phi}/T_i$, since $k_\perp \rho_i \gg 1$ for ETG. Hence, it is no surprise that zonal flow effects are less dramatic for ETG turbulence then for its drift-ITG counterpart, since for ETG, zonal flows have an effective inertia *comparable* to other modes.

Second, zonal flows, with $n = 0$ and $k_\parallel = 0$, are *modes of minimal Landau damping*. This means that the only linear dissipation acting on zonal flows for asymptotic times (i.e. $t \to \infty$) is due to collisions. In particular, no linear, time-asymptotic dissipation acts on zonal flows in a collisionless system.

Third, since zonal flows have $n = 0$, they are intrinsically incapable of driving radial $\boldsymbol{E} \times \boldsymbol{B}$ flow perturbations. Thus, they cannot tap expansion free energy stored in radial gradients. Thus, zonal flows do not cause transport or relaxation, and so constitute a *benign repository* for free energy. In contrast, other low n-modes necessarily involve a trade-off between shearing (a 'plus' for confinement) and enhanced transport (a 'minus').

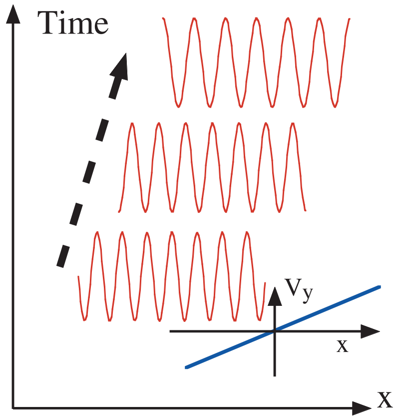

Figure 7. Drift wave in sheared flow field. When a drift wave-packet is propagating in the x-direction in the presence of flow shear, $\mathrm{d}V_y/\mathrm{d}x > 0$, the wavenumber k_x changes.

Having established the physics of shearing, it is illuminating to present a short, 'back-of-an-envelope' type demonstration of zonal flow instability. For other approaches, see the cited literature [25–31]. Consider a packet of drift waves propagating in an ensemble of quasi-stationary, random zonal flow shear layers, as shown in figure 6(*b*). Take the zonal flows as slowly varying with respect to the drift waves (i.e. $\Omega \ll \omega_k$), i.e. as quasi-stationary. Here, Ω is the rate of the change or frequency of the zonal flow and ω_k is the characteristic frequency of drift waves. The spatially complex shearing flow will result in an increase in $\langle k_\mathrm{r}^2\rangle$, the mean square radial wave vector (i.e. consider a random walk of k_r, as described above). In turn the generic drift wave frequency $\omega_{*\mathrm{e}}/(1 + k_\perp^2\rho_\mathrm{s}^2)$ must then decrease. Here, ρ_s is the ion gyro-radius at the electron temperature. Since $\Omega \ll \omega_k$, the drift wave action density $N_k = E(k)/\omega_k$ is conserved, so that *drift wave energy must also decrease*. As the total energy of the system of waves and flows is also conserved (i.e. $E_\mathrm{wave} + E_\mathrm{flow} = \mathrm{const}$, as shown in section 3.2.2), *it thus follows that the zonal flow energy must*, in turn, *increase*. Hence, the *initial perturbation is reinforced*, suggestive of *instability*. Note that the simplicity and clarity of this argument support the assertion that zonal flow generation is a robust and ubiquitous phenomenon.

A slightly larger envelope is required for a 'physical argument' which is also quantitatively predictive. Consider a drift wave-packet propagating in a sheared flow field, as shown in figure 7. Take $\omega_k > |V_\mathrm{E}'|$ and $|k| > |V_\mathrm{E}'/V_\mathrm{E}|$, so that wave action density is conserved (i.e. $N(k) = N_0$), a constant. (V_E is the $\boldsymbol{E}\times\boldsymbol{B}$ velocity and V_E' is its radial derivative.) Thus, for constant N, wave energy density evolves according to:

$$\frac{\mathrm{d}}{\mathrm{d}t}\varepsilon(k) \cong \left(\frac{2k_\mathrm{r}k_\theta\rho_\mathrm{s}^2}{1+k_\perp^2\rho_\mathrm{s}^2}\right)V_\mathrm{E}'\varepsilon(k). \tag{2.3}$$

Equation (2.3) states that the drift wave-packet loses or gains energy due to work on the mean flow via wave induced Reynolds stress [32]. Note that $k_\mathrm{r}k_\theta E(k) \sim \langle\tilde{V}_\mathrm{r}\tilde{V}_\theta\rangle$, the Reynolds stress produced by $\boldsymbol{E}\times\boldsymbol{B}$ velocity fluctuations. Note as well that the factor $k_\mathrm{r}k_\theta E(k)V_\mathrm{E}'$ is rather obviously suggestive of the role of triad interactions in controlling fluctuation–flow energy exchange. For zonal flows, the shear is random and broad-band, so that $V_\mathrm{E} \to \tilde{V}_\mathrm{E}$, $N \to \langle N\rangle + \tilde{N}$ and $NV_\mathrm{E}' \to \langle\tilde{N}\tilde{V}_\mathrm{E}'\rangle$. Hence, equation (2.3) may be rewritten as:

$$\frac{\mathrm{d}}{\mathrm{d}t}\varepsilon(k) = -V_{\mathrm{g},r}k_\theta\langle\tilde{V}_\mathrm{E}'\tilde{N}\rangle. \tag{2.4}$$

To complete the argument, the correlator $\langle \tilde{N} \tilde{V}_{\mathrm{E}}' \rangle$ must now be calculated. To this end, we use the wave kinetic equation (WKE)

$$\frac{\partial N}{\partial t} + (\boldsymbol{V}_{\mathrm{g}} + \boldsymbol{V}) \cdot \nabla N - \frac{\partial}{\partial \boldsymbol{x}}(\omega + k_\theta V_{\mathrm{E}}) \cdot \frac{\partial N}{\partial \boldsymbol{k}} = \gamma_k N - \frac{\Delta\omega_k N^2}{N_0} \tag{2.5}$$

and the methodology of quasi-linear theory to obtain:

$$k_\theta \langle V_{\mathrm{E}}' \tilde{N} \rangle = D_{\mathrm{K}} \frac{\partial \langle N \rangle}{\partial k_{\mathrm{r}}} \tag{2.6a}$$

$$D_{\mathrm{K}} = k_\theta^2 \sum_q q^2 |V_{\mathrm{E},q}^2| R(k, q) \tag{2.6b}$$

$$R(k, q) = \frac{\gamma_k}{(q V_{\mathrm{g},r})^2 + \gamma_k^2}. \tag{2.6c}$$

The term $\Delta\omega_k N^2/N_0$ represents drift wave nonlinear damping via self-interaction of the drift waves (i.e. inverse cascade by *local* interaction). Here q is the radial wavenumber of the zonal flow, and equilibrium balance in the absence of flow has been used to relate $\Delta\omega_k$ to γ_k. γ_k is the growth rate of the drift mode. The wave energy then evolves according to:

$$\frac{\mathrm{d}\varepsilon(k)}{\mathrm{d}t} = \frac{2\rho_{\mathrm{s}}^2 D_{\mathrm{K}} k_{\mathrm{r}}}{(1 + k_\perp^2 \rho_{\mathrm{s}}^2)^2} \frac{\partial \langle N \rangle}{\partial k_{\mathrm{r}}}. \tag{2.7}$$

As the total energy of the stationary wave–flow system is conserved,

$$\frac{\mathrm{d}}{\mathrm{d}t}\left(\sum_k \varepsilon(k) + \sum_q |\tilde{V}_q|^2 \right) = 0.$$

The zonal flow generation rate is thus determined to be

$$\gamma_q = -2q^2 c_{\mathrm{s}}^2 \sum_q \frac{k_\theta^2 \rho_{\mathrm{s}}^2}{(1 + k_\perp^2 \rho_{\mathrm{s}}^2)^2} R(k, q) k_{\mathrm{r}} \left(\frac{\partial \langle \eta \rangle}{\partial k_{\mathrm{r}}} \right) \tag{2.8a}$$

$$\langle \eta \rangle = (1 + k_\perp^2 \rho_{\mathrm{s}}^2) \langle \varepsilon \rangle. \tag{2.8b}$$

Here $\langle \eta \rangle$ is the mean potential enstrophy density of the drift wave turbulence, (i.e. $\eta(\underline{k}) = (1 + k_\perp^2 \rho_{\mathrm{s}}^2)^2 |\phi_{\underline{k}}|^2$) and may be thought of as the population density of drift wave vortices. Note that for toroidally and poloidally symmetric shears, $\mathrm{d}k_\theta/\mathrm{d}t = 0$, so that the conventional wave action density $N(k)$ and the potential enstrophy density $\eta(k)$ are *identical*, up to a constant factor.

The result given above in equation (2.8*a*), obtained by transparent physical reasoning, is identical to that derived previously by formal modulational stability arguments. Note that $\partial\langle \eta \rangle/\partial k_{\mathrm{r}} < 0$ (a condition which is virtually always satisfied in two-dimensional or drift wave turbulence) is required for zonal flow growth. In addition, the argument above reveals that drift wave ray chaos provides the key element of irreversibility, which is crucial to the wave–flow energy transfer dynamics. Here ray chaos requires overlap of the $\Omega/q_{\mathrm{r}} = V_{\mathrm{g}}$ resonances in D_k, a condition easily satisfied for finite lifetime drift wave eddies and (nearly) zero frequency zonal flows (i.e. $\Delta\omega_k \gg \Omega$) [33]. Under these conditions neighbouring drift wave rays diverge exponentially in time, thus validating the use of stochastic methodology employed here [34]. In the case where rays are not chaotic, envelope perturbation formalism [35, 36], methods from the theory of trapping [37–39] or parametric instability theory [40] must be used to calculate zonal flow generation.

2.3. Self-consistent solution and multiple states

At this point, we have identified the two principal elements of the physics of the drift wave–zonal flow system. These are:

(i) The shearing of drift wave eddies by the complex zonal flow field, resulting in a diffusive increase in $\langle k_r^2 \rangle$ and coupling to dissipation, reduction in transport, etc,

(ii) the amplification of zonal flow shears by modulational instability of the drift wave to a 'test' or seed shear.

Note that (i) and (ii) are, to some extent, different views of the same process of energy transfer from the short wavelength drift wave spectrum to the long wavelength zonal flow spectrum. This process of drift wave energy depletion results in a diffusive *increase* in the mean square radial wavenumber of drift waves, and a transfer of drift wave population density to small scale. In view of the fact that the drift wave population density is equivalent to the potential enstrophy density, we see that the process of zonal flow generation is not unlike the dual cascade phenomenon familiar from two-dimensional hydrodynamics. Here, the growth of zonal flow shears corresponds to the inverse energy cascade, while the increase in rms of k_r is similar to the forward enstrophy cascade [41]. Unlike the case of two-dimensional hydrodynamics, zonal shear amplification is a *non-local* coupling process in wavenumber space.

To proceed, we now examine the coupled evolution for $\langle N \rangle$, the drift wave quanta density, and the zonal flow spectrum. These evolve according to:

$$\frac{\partial}{\partial t}\langle N \rangle - \frac{\partial}{\partial k_r} D_k \frac{\partial}{\partial k_r}\langle N \rangle = \gamma_k \langle N \rangle - \frac{\Delta\omega_k}{N_0}\langle N \rangle^2, \tag{2.9a}$$

$$\frac{\partial}{\partial t}|\phi_q|^2 = \Gamma_q \left[\frac{\partial \langle N \rangle}{\partial k_r}\right]|\phi_q|^2 - \gamma_d |\phi_q|^2 - \gamma_{NL}[|\phi_q|^2]|\phi_q|^2. \tag{2.9b}$$

Equation (2.9*a*) is simply the quasi-linear Boltzmann equation for $\langle N \rangle$, while equation (2.9*b*) describes zonal flow potential growth and damping by modulational instability (the first term—proportional to the drift wave population gradient $\partial\langle N \rangle/\partial k_r$), collisional damping (the second term—due to the friction between trapped and circulating ions) [42, 43] and nonlinear damping of zonal flows (the third term—which schematically represents a number of different candidate zonal flow saturation processes). Note here that γ_{NL} is an unspecified function of zonal flow intensity, and thus can represent a nonlinear damping process such as turbulent viscous damping, etc. Together, equations (2.9*a*) and (2.9*b*) constitute a simple model of the coupled evolution dynamics. This 'minimal' model could be supplemented by transport equations which evolve the profiles used to calculate γ_k, the drift wave growth rate (i.e. $\gamma_k = \gamma_k[n^{-1}\mathrm{d}n/\mathrm{d}r, T^{-1}\mathrm{d}T/\mathrm{d}r, \ldots]$) [44]. The minimal system has the generic structure of a 'predator–prey' model, where the drift waves correspond to the prey population and the zonal flows correspond to the predator population [45–49]. As usual, the prey breeds rapidly (i.e. γ_k is fast), and supports the predator population as the food supply for the latter (i.e. $\Gamma_q = \Gamma_q[\langle N \rangle]$). The predators regulate the prey by feeding upon them (i.e. Γ_q and D_k conserve energy with each other) and are themselves regulated by predator death (at rate γ_d) and predator–predator competition ($\gamma_{NL}[|\phi_q|^2]$). Taken together, equations (2.9*a*) and (2.9*b*) describe a self-regulating system with multiple states.

The dynamics of the two population system are more easily grasped by considering a zero-dimensional model for population N and V^2, instead of the one-dimensional model equations

Table 3. State of drift wave–zonal flow system.

State	No flow	Flow ($\alpha_2 = 0$)	Flow ($\alpha_2 \neq 0$)
N (drift wave turbulence level)	$\frac{\gamma}{\Delta\omega}$	$\dfrac{\gamma_\mathrm{d}}{\alpha}$	$\dfrac{\gamma_\mathrm{d} + \alpha_2\gamma\alpha^{-1}}{\alpha + \Delta\omega\alpha_2\alpha^{-1}}$
V^2 (mean square flow)	0	$\dfrac{\gamma}{\alpha} - \dfrac{\Delta\omega\gamma_\mathrm{d}}{\alpha^2}$	$\dfrac{\gamma - \Delta\omega\gamma_\mathrm{d}\alpha^{-1}}{\alpha + \Delta\omega\alpha_2\alpha^{-1}}$
Drive/excitation mechanism	Linear growth	Linear growth	Linear growth Nonlinear damping of flow
Regulation/inhibition mechanism	Self-interaction of turbulence	Random shearing, self-interaction	Random shearing, self-interaction
Branching ratio $\frac{V^2}{N}$	0	$\dfrac{\gamma - \Delta\omega\gamma_\mathrm{d}\alpha^{-1}}{\gamma_\mathrm{d}}$	$\dfrac{\gamma - \Delta\omega\gamma_\mathrm{d}\alpha^{-1}}{\gamma_\mathrm{d} + \alpha_2\gamma\alpha^{-1}}$
Threshold (without noise)	$\gamma > 0$	$\gamma > \Delta\omega\gamma_\mathrm{d}\alpha^{-1}$	$\gamma > \Delta\omega\gamma_\mathrm{d}\alpha^{-1}$

for $\langle N(k)\rangle$ and $|\phi_q|^2$. The zero-dimensional simplified model is this

$$\frac{\partial}{\partial t}N = \gamma N - \alpha V^2 N - \Delta\omega N^2, \tag{2.10a}$$

$$\frac{\partial}{\partial t}V^2 = \alpha N V^2 - \gamma_\mathrm{d} V^2 - \gamma_\mathrm{NL}(V^2)V^2. \tag{2.10b}$$

The states of the system are set by the fixed points of the model, i.e. when $\partial N/\partial t = \partial V^2/\partial t = 0$. There are (at least) two classes of fixed points for the system. The state with finite fluctuations and transport, but no flow is that with $N = \gamma/\Delta\omega$, $V^2 = 0$. This corresponds to a state where turbulence saturates by local, nonlinear interactions. A second state, with flow, is that with

$$N = \alpha^{-1}(\gamma_\mathrm{d} + \gamma_\mathrm{NL}(V^2)), \tag{2.11a}$$

$$V^2 + \alpha^{-2}\Delta\omega\gamma_\mathrm{NL}(V^2) = \alpha^{-1}(\gamma - \Delta\omega\gamma_\mathrm{d}\alpha^{-1}). \tag{2.11b}$$

Note that the general form $\gamma_\mathrm{NL}(V^2)$ allows limit cycle solutions. Given the physically plausible assumption that $\gamma_\mathrm{NL}(V^2) > 0$ and increases with V^2 as $V^2 \to \infty$, the Poincare–Bendixon theorem implies that limit cycle solutions to (2.10a) and (2.10b) can be identified by the appearance of unstable centres as fixed points of those equations. In general, the appearance of such limit cycle attractors is due to the effects of time delays in the dynamical system of zonal flows and drift waves. For the especially simple case where $\gamma_\mathrm{NL}(V^2) \sim \alpha_2 V^2$, the solution reduces to:

$$N = \frac{\gamma_\mathrm{d} + \alpha_2\gamma\alpha^{-1}}{\alpha + \Delta\omega\alpha_2\alpha^{-1}}, \tag{2.12a}$$

$$V^2 = \left[\frac{\gamma - \Delta\omega\gamma_\mathrm{d}\alpha^{-1}}{\alpha + \alpha_2\Delta\omega\alpha^{-1}}\right]. \tag{2.12b}$$

Even this highly over-simplified model contains a wealth of interesting physics. The properties of the two states are summarized in table 3, which we now discuss. Access to the state of no flow requires only primary linear instability, i.e. $\gamma > 0$, while access to states with finite flow requires $\gamma > \Delta\omega\gamma_\mathrm{d}/\alpha$, so that the excitation of the underlying drift waves is sufficient to amplify the flow shear against collisional damping. In the no flow state, $N \sim \gamma/\Delta\omega$, consistent with the traditional picture of saturation of turbulence and transport via the balance of linear growth with nonlinear damping. With the presence of flow, $N \sim \gamma_{\rm d}\alpha^{-1}$, which directly ties the *turbulence level* to the *flow damping* [50]. This follows the fact that *in the finite flow state, the turbulence level is regulated by the shear flow, which is, in turn, itself controlled by the flow damping. Thus, the fluctuation level is ultimately set by the flow damping*! This prediction has been confirmed by several numerical simulations [51]. In the finite flow state, V^2 is set by the *difference* between the wave growth and flow damping. Thus, the branching ratio of the zonal flow to drift wave energy scales as $\gamma/\gamma_{\rm d}$. In particular, for $\gamma_{\rm d} \to 0$, the *dominant ultimate repository* of expansion free energy *are the zonal flows, whose energy exceeds that of the drift waves*. Note that the ratio $\gamma/\gamma_{\rm d}$ is the key control parameter for manipulating the fluctuation energy branching ratio. It is interesting to note that the rather special 'Dimits shift' regime [52], which is a state very close to marginal stability in an effectively collisionless system, corresponds to the somewhat ill-defined case where both $\gamma \to 0$ and $\gamma_{\rm d} \to 0$, i.e. weak flow damping and drift waves near their marginal point. The Dimits shift was discovered by DNS of ITG mode-driven turbulence in the collisionless limit. In the Dimits shift regime, the drift wave fluctuations are just above the linear stability threshold and nearly quenched by zonal flow effects which are large, on account of weak flow damping at low collisionality. The Dimits shift regime is characterized by a large imbalance between the energy in zonal flows and in $n \neq 0$ fluctuations (with zonal flow energy much larger), which gives the appearance of a 'shift' (i.e. increase) in the effective threshold for ITG turbulence and transport. Thus, it is not surprising that the Dimits shift regime merits special attention. Detailed discussion of the Dimits shift regime is given in section 3.

It is especially interesting to comment on the effects of nonlinear zonal flow damping, for which $\alpha_2 \neq 0$. The details of this process are a subject of intense ongoing research, and will be discussed extensively later in this review. Candidate mechanisms include Kelvin–Helmholtz (KH)-like instabilities of the zonal flows (which could produce a turbulent viscosity, resulting in flow damping) [53–55], drift wave trapping, etc. Whatever the details, the effect of nonlinear flow damping is to limit the intensity of the zonal flow spectrum. Since energy is conserved between drift waves and zonal flows (within the time scales of the evolution of zonal flow), this is equivalent to enhancing the fluctuation levels, in comparison to the case where $\alpha_2 = 0$. This is, indeed, the case in the rhs column of table 3, where we see the effect of finite α_2 is to enhance N and reduce V^2 in comparison to the case where $\alpha_2 = 0$. Thus, nonlinear flow damping may be viewed as a 'return' of expansion free energy to the drift wave 'channel', which thus lowers the branching ratio V^2/N.

2.4. General comments

It should be clear that the drift wave–zonal flow problem is a particular example of the more general problem of describing the nonlinear interaction between, and turbulence in, two classes of phenomena of disparate-scale, and of understanding structure formation and self-organization in such systems. Such problems are ubiquitous, and notable examples in plasma physics are Langmuir turbulence and caviton formation, magnetic field generation and the dynamo problem, and the formation of ionospheric structures, just to name a few. It is interesting to note that the separation in spatio-temporal scales often facilitates progress on such problems, via the use of adiabatic invariants, or systematic elimination of degrees of freedom using the methodology of Zwanzig–Mori theory, etc. Thus, such nominally 'more complex' problems are often easier than the so-called classic 'simple' problems, such as homogeneous turbulence. The general theory of turbulence in systems with multiple bands of interacting disparate scales is reviewed in [56]. The Langmuir turbulence and collapse problems are reviewed in [57]. The theory of the dynamo problem is discussed in great detail in [58–63].

3. Theory of zonal flow dynamics

In this section, the theory of zonal flow dynamics is discussed in detail. As shown in the heuristic discussion of section 2, the essence of the drift wave–zonal flow system dynamics is that several mechanisms are at work simultaneously. The synergy of these mechanisms results in the (self) organization of the self-regulating state. Here, we present a step-by-step discussion of the theory of the basic elements, which are:

(i) linear damping (especially collisional) of the zonal flow

(ii) mechanisms for the excitation of zonal flows by background turbulence

(iii) mechanisms by which the spectrum of zonal flow shears limits and reacts back upon the underlying drift wave turbulence

(iv) nonlinear damping and saturation mechanisms for zonal flow, especially in collisionless or very low collisionality regimes

(v) the type of self-organized states which are realized from the interaction of elements (i)–(iv)

(vi) the effect of zonal flows on turbulent transport.

Elements (i)–(vi) are discussed below. Related illustrations, tests and analyses utilizing numerical simulation are presented in section 4.

The remainder of section 3 is organized as follows. Section 3.1 presents the theory of linear collisional damping of zonal flows—scale independent collisional damping is a key energy sink. Special emphasis is placed upon the key, pioneering work of Rosenbluth and collaborators. Section 3.2 presents the theory of zonal flow generation by modulational instability of the ambient drift wave spectrum. The theory is developed for both the coherent (i.e. parametric modulational) and broadband, turbulent (i.e. wave kinetic) limits. Critical time scales which quantitatively identify these regimes are identified and discussed. The relations and connections (vis-a-vis energetics) between modulational instability and shearing, k-space diffusion, etc, are discussed and a unifying framework is presented. Emphasis here is on electrostatic turbulence and zonal flows, but related discussions of electromagnetic turbulence, zonal flows and geodesic acoustic modes (GAMs) are also included. The relationship between zonal magnetic field dynamics and the classical dynamo problem is discussed. In section 3.3, the theory of shearing and its effects on turbulence are discussed, for both mean field and random (i.e. zonal flow) shearing. This discussion is important in its own right (as an element in system self-regulation) and as a foundation for understanding the impact of zonal flows on turbulent transport, etc. In section 3.4, zonal flow saturation is discussed, with special emphasis placed upon collisionless or low collisionality regimes. As with generation, several different applicable models are discussed, each in the context of its regime of relevance as defined by time scales, degrees of freedom, etc. In particular, tertiary instability, nonlinear wave-packet scattering, wave trapping and other mechanisms are discussed. After explaining the elementary processes, a unifying classification of various possible system states is suggested in terms of the Chirikov parameter and Kubo number, which characterize the turbulent state. This classification scheme gives a global perspective on the nonlinear theory of zonal flows. In section 3.5, the system dynamics of zonal flows and turbulence are presented. In the final section 3.6, the effects of zonal flows on turbulent transport are discussed. Special attention is given to zonal-flow-induced modification of the cross-phase and upon the scaling of the turbulent transport flux with zonal flow parameters, such as shear strength, flow correlation time, etc.

3.1. Linear dynamics of zonal flow modes

Zonal flows are, first and foremost, plasma eigenmodes, albeit modes which are *linearly stable*. In this subsection, we discuss the linear response of the plasma to a low frequency electric field perturbation which is constant on a magnetic surface. This corresponds to the $m = n = 0$ component, where m and n are the poloidal and toroidal mode numbers, respectively. Two relevant regimes are explained. One is that of the slowly varying response, for which $|\partial/\partial t| \ll \omega_{\mathrm{t}} \equiv v_{\mathrm{Ti}}/qR$, where ω_{t} is the ion transit frequency and V_{Ti} is the thermal velocity of ions, $V_{\mathrm{Ti}} = \sqrt{T_{\mathrm{i}}/m_{\mathrm{i}}}$. In this case, the perturbation is called a zonal flow. The plasma response is incompressible, and the poloidal $\boldsymbol{E} \times \boldsymbol{B}$ velocity is associated with a toroidal return flow. The other is a fast-varying regime, where $|\partial/\partial t| \sim \omega_{\mathrm{t}}$. In this case, poloidal asymmetry leads to plasma compression, so as to induce an oscillation in the range of ω–ω_{t}. This oscillation is called the GAM. We first describe the zonal flow and then explain the geodesic acoustic mode. The damping of these modes by collisions and ion Landau damping is explained. In this section (and throughout the review), we use the word 'damping' for the linear response mechanisms (e.g. collisional damping or collisionless damping, like Landau damping). The nonlinear mechanisms that induce the decay of regulate the flow are called 'saturation mechanisms' or, if necessary for clarity, 'nonlinear damping mechanisms'.)

3.1.1. Zonal flow eigenmode.

In drift-ITG mode (ion temperature gradient turbulence [64]), zonal flows have an electrostatic potential $\tilde{\phi}$ which is constant on a magnetic surface, and so have $m = n = 0$, $k_{\|} = 0$. Because of the vanishing $k_{\|}$, the electron response is no longer a Boltzmann response, so that the relation $\tilde{n}/n \simeq e\tilde{\phi}/T$ no longer holds. The density perturbation is usually a small correction, in comparison with the potential perturbation. Certain collisionless trapped electron mode (CTEM) regimes may be an exception to this. Thus, zonal flows correspond to a highly anisotropic limit of the more general 'convective cell mode' [5, 65]. As discussed in section 2, zonal flows (but not GAMs) can be thought of as convective cells of minimum inertia, minimum Landau damping and minimum transport [66].

The spatial structure of the zonal flow is described here. The electrostatic perturbation is constant on each magnetic surface. Each q_{r} (q_{r} r: radial wavenumber) component has the linear dispersion relation [5, 65]

$$\omega = 0. \tag{3.1.1}$$

The vanishing real frequency is easily understood. The electrostatic perturbation with $m = n = 0$ does not cause acceleration along the magnetic surface. The linear polarization drift disappears, consistent with the ordering of $\omega \ll \omega_{\mathrm{t}}$.

The plasma produces an $\boldsymbol{E} \times \boldsymbol{B}$ flow, $V_{\boldsymbol{E}\times\boldsymbol{B}} = -E_{\mathrm{r}}/B$. This flow is directed mainly in the poloidal direction. Because of toroidicity, this flow component induces the compression of plasma. To maintain incompressibility, this compression is compensated by a return flow *along* the field line, so:

$$\boldsymbol{V} = -\frac{E_{\mathrm{r}}}{B}\begin{pmatrix} 0 \\ 1 \\ -2q\cos\theta \end{pmatrix} \tag{3.1.2}$$

to leading order in inverse aspect ratio $\varepsilon = r/R$ [48]. This flow pattern is illustrated in figure 4. On account of the secondary flow along the magnetic field line, the zonal flow in a toroidal plasma is subject to a stronger damping then those in slab plasmas.

The density perturbation remains a small correction. For the range of scales comparable to the ion gyro-radius, it can be given as:

$$\frac{\tilde{n}_{\rm i}}{n} \simeq q_{\rm r}^2 \rho_{\rm i}^2 \frac{e\tilde{\phi}}{T}. \tag{3.1.3}$$

3.1.2. Geodesic acoustic mode. Toroidal effects have been studied in conjunction with the neoclassical transport theory [67–75], as reviewed in [76–78]. When one constructs an eigenmode in the regime of fast variation, $|\partial/\partial t| \sim \omega_{\rm t}$, one finds the GAM [68]. The GAM is a perturbation for which the $m = n = 0$ electrostatic potential is linearly coupled (by toroidal effects) to the $m = 1, n = 0$ sideband density perturbation.

Working in the framework of standard fluid equations, one begins with, as governing equations, the continuity equation and the equation of motion

$$\frac{\partial}{\partial t} n + \nabla \cdot n\boldsymbol{V}_\perp + \nabla_\parallel n V_\parallel = S - \nabla \cdot \Gamma, \tag{3.1.4}$$

$$n m_{\rm i} \left(\frac{\partial}{\partial t} \boldsymbol{V} + \boldsymbol{V} \cdot \nabla \boldsymbol{V} \right) = -\nabla p + \boldsymbol{J} \times \boldsymbol{B} + S m_{\rm i} \boldsymbol{V}, \tag{3.1.5}$$

together with the charge neutrality condition $\nabla \cdot \boldsymbol{J} = 0$ and Ohm's law

$$\boldsymbol{E} + \boldsymbol{V} \times \boldsymbol{B} = 0. \tag{3.1.6}$$

$p = nT$ is the pressure, and the temperature gradient is neglected for simplicity. The source terms S and Γ represent the (equilibrium) particle source and flux, respectively. These can induce acceleration of the zonal flow if they are not homogeneous on a magnetic surface. The so-called Stringer spin-up [69] is such an acceleration phenomenon. In this subsection, we do not describe the response to S and Γ, but restrict ourselves to the dynamics of GAM eigenmode.

The key mechanism for generating the GAM is seen in equation (3.1.5) [68, 79]. If one takes the poloidal component of equation (3.1.5), one obtains $\int {\rm d}s R^2 |\nabla_\psi|^{-1} \boldsymbol{B}_p \times (n m_{\rm i} {\rm d}\boldsymbol{V}/{\rm d}t + T \nabla n) = 0$. This relation is trivial in a cylindrical plasma. However, in toroidal plasmas, toroidicity induces coupling between the $m = n = 0$ component of the electrostatic potential and the $m = 1, n = 0$ component of the density perturbation. The dispersion relation given as:

$$\Omega^2 - \frac{2c_{\rm s}^2}{R^2} - q_\parallel^2 c^2 = 0. \tag{3.1.7}$$

The resulting mode is the geodesic acoustic mode, the frequency of which is higher than the ion acoustic wave, and is given by

$$\omega_{\rm GAM}^2 \simeq 2c_{\rm s}^2 R^{-2} (1 + q^{-2}/2). \tag{3.1.8}$$

The density perturbation can be rewritten as

$$\frac{\tilde{n}}{n_0} = -\left(\sqrt{2} q_{\rm r} p_{\rm s} \frac{e\tilde{\phi}}{T_{\rm e}} \right) \sin\theta. \tag{3.1.9}$$

The dispersion relation equation (3.1.7) was derived for general toroidal magnetic configurations in [68]. The second term was given as the product of an integral of the geodesic curvature multiplied by a relative perturbation amplitude. This is the reason that this mode is called the geodesic acoustic mode or GAM.

3.1.3. Collisional damping process. The mechanism of collisional damping of zonal flows is now explained. In a slab plasma, the damping rate of the zonal flow is given by $\mu_i q_r^2$, i.e. in proportion to the ion viscosity $\mu_i = \upsilon_{ii}\rho_i^2$. However, in toroidal plasmas, the damping rate is independent of scale. (See, e.g. for a review [76–78].) Progress in the theory of the H-mode, [32, 80, 81] has stimulated a revival of detailed calculation [32, 42, 81–93] of neoclassical damping rates. In this subsection, we first describe stationary flow which is realized by the balance of collisional drag with pressure gradient drive. Relaxation processes are then discussed. The case with $|\partial/\partial t| \ll \omega_t \equiv v_{\mathrm{Thi}}/qR$ is discussed first. The case of rapidly varying response (GAM), $|\partial/\partial t| \sim \omega_t$, is explained next.

(i) Stationary flow driven by pressure gradient. The fluid velocity in an inhomogeneous toroidal flow, projected on the poloidal cross-section is expressed as

$$V_\theta = \frac{\varepsilon}{q}\bar{V}_\parallel + V_{\boldsymbol{E}\times\boldsymbol{B}} + V_{\mathrm{d}} + V_{\mathrm{dT}}. \tag{3.1.10}$$

Here $V_{\boldsymbol{E}\times\boldsymbol{B}}$ is the $\boldsymbol{E} \times \boldsymbol{B}$ drift velocity, V_{d} is the diamagnetic drift velocity, V_{dT} is the ITG drift velocity, so that $V_{\mathrm{d}} = T/eBL_n$, $V_{\mathrm{dT}} = T/eBL_T$, $L_n^{-1} = -\mathrm{d}(\ln n)/\mathrm{d}r$ and $L_T^{-1} = -\mathrm{d}(\ln T_{\mathrm{i}})/\mathrm{d}r$, and $\bar{V}_\parallel$ is the average of $V_\parallel$ on a magnetic surface. In the absence of torques (e.g. orbit loss, external momentum injection, etc), $\varepsilon q^{-1}\bar{V}_\parallel$ is an $\mathrm{O}(\varepsilon^2)$ correction with respect to $V_{\boldsymbol{E}\times\boldsymbol{B}}$ (see, e.g. [92]). The equilibrium velocity is obtained as $V_\theta = C_{\mathrm{H}} V_{\mathrm{dT}}$ where C_{H} is a numerical coefficient, shown by Hazeltine to be [73] $C_{\mathrm{H}} \simeq 1.17$ (banana), $C_{\mathrm{H}} \simeq -0.5$ (plateau), $C_{\mathrm{H}} \simeq -2.1$ (Pfirsch–Schlüter). Thus, the $\boldsymbol{E} \times \boldsymbol{B}$ drift velocity is given as

$$V_{\boldsymbol{E}\times\boldsymbol{B}} = (C_{\mathrm{H}} - 1)V_{\mathrm{d}T} - V_{\mathrm{d}} \tag{3.1.11}$$

if there is no other force to drive plasma poloidal rotation. The velocity scales with the (density and temperature) diamagnetic drift velocity. The radial electric field is easily deduced from this relation, and is given by:

$$E_{\mathrm{r}} = (C_{\mathrm{H}} - 1)\frac{T}{eL_T} - \frac{T}{eL_n}. \tag{3.1.12}$$

The radial electric field is of the order of ion temperature gradient divided by the electron charge, if the stationary state is governed by collisional transport processes.

(ii) Damping rate. The deviation of the radial electric field from the result given by equation (3.1.12) is determined by the balance between damping and driving torques. Here we survey the theories of collisional damping.

Collisional damping of zonal flows is controlled by ion–ion collision processes. When a small element of phase-space fluid originally on the low field side moves to the high field side, it is 'stretched' in the direction of the perpendicular velocity, $v_\perp$, since $v_\perp$ increases due to the conservation of magnetic moment. On account of ion–ion collisions, the deformed distribution tends to recover isotropy, which is shown by a thick solid line. In this relaxation process, thermalization of ordered poloidal motion occurs, and so the poloidal velocity is damped. From this argument, it is clear that this *damping rate is independent of the radial structure of the flow*. This is *not* diffusive damping.

In the Pfirsch–Schluter regime, the damping rate is given as

$$\gamma_{\mathrm{damp}} = \omega_t^2 \nu_{\mathrm{ii}}^{-1}. \tag{3.1.13}$$

The mean free length in the poloidal direction, which is determined by ion collisions, is inversely proportional to ν_{ii}. Note that here $\gamma_{\mathrm{damp}} = D_\parallel/(qR)^2 = \omega_t^2/\nu_{\mathrm{ii}}$ is simply the time for parallel diffusion of one connection length.

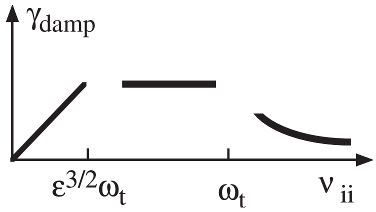

Figure 8. Schematic drawing of the collisional damping rate for the zonal flow.

In the banana regime, stronger damping occurs due to collisions between transiting ions and banana ions, because magnetically trapped particles do *not* circulate freely in the poloidal direction. Reference [83] found, by using an improved evaluation of eigenfunctions, that the damping rate increases as the toroidicity ε becomes small. A fitting formula was proposed as, $\gamma_{\mathrm{damp}} \simeq 1.5\nu_{\mathrm{ii}}^{D}(v)/\sqrt{\varepsilon}$, where $\nu_{\mathrm{ii}}^{D}(v)$ is the energy-dependent pitch-angle scattering coefficient. In [85], an evaluation of the damping rate showed that the ε-dependence is more. (The numerical solution in [85] can be fit by $\gamma_{\mathrm{damp}}/\nu_{\mathrm{ii}} \propto \varepsilon^{-\alpha}$ with $\alpha \simeq 0.85$ for $0.2 < \varepsilon < 0.8$.) An alternative fit

$$\gamma_{\mathrm{damp}} \simeq \frac{\nu_{\mathrm{ii}}^{D}(v)}{\varepsilon} \tag{3.1.14}$$

was also proposed. DNS of the drift kinetic equation [92] has supported the conclusion that γ_{damp} is a decreasing function of ε. It has also been pointed out that collisional damping induces a real part of the total oscillation frequency for the zonal flow, so that $\omega = \omega_{\mathrm{r}} + \mathrm{i}\gamma_{\mathrm{damp}}$, $\omega_{\mathrm{r}} \simeq \nu_{\mathrm{ii}}$ [85].

In the plateau regime, the dissipation rate is controlled by the transit frequency ω_t and

$$\gamma_{\mathrm{damp}} \simeq \omega_t h(\varepsilon), \tag{3.1.15}$$

where $h(\varepsilon)$ is weakly dependent on toroidicity. Direct numerical calculation has shown that $h(\varepsilon) \sim \varepsilon^{\alpha}$, and a small positive parameter is observed in the range of $\alpha \sim 1/3$ [92].

Collisionless damping, if it exists, would influence poloidal rotation in high temperature plasmas. The damping rate vanishes in the limit of $\nu_{\mathrm{ii}} \to 0$, in quiescent plasmas [42]. The drive by turbulence (zonal flow drive) and other torque (e.g. orbit loss, external force, etc) could balance collisional damping. Figure 8 summarizes the scaling trends of the collisional damping rate.

The question of what the collisional damping rate is in the limit of high poloidal velocity has attracted attention. It was noted that the damping rate γ_{damp} can depend on the poloidal velocity, if V_θ becomes of the order of $\varepsilon v_{\mathrm{Thi}}/q$. The damping rate then becomes *a decreasing function* of V_θ [81, 94]. This is a possible origin of a bifurcation of the radial electric field. (Examples include [95].) This mechanism, and the consequences of it, are explained in [48].

(iii) Geodesic acoustic mode. The GAM is also subject to collisional damping. After solving the drift kinetic equation with the ordering of $|\partial/\partial t| \sim \omega_{\mathrm{t}}$, the dispersion relation has been obtained in [92] as

$$\omega^2 - \frac{7}{8}\frac{c_{\mathrm{s}}^2}{R^2} + \mathrm{i}\frac{\nu_{\mathrm{ii}}}{\omega}\frac{c_{\mathrm{s}}^2}{R^2} = 0. \tag{3.1.16}$$

(As compared to equation (3.1.7), the GAM frequency is evaluated with a slightly different numerical coefficient. This arises because the velocity moment is taken after the drift kinetic equation is solved.) The damping rate of the GAM is estimated from equation (3.1.16) to be

$$\gamma_{\mathrm{damp}}^{\mathrm{GAM}} \simeq \tfrac{4}{7}\nu_{\mathrm{ii}}. \tag{3.1.17}$$

The banana ions do not explicitly play a role in GAM damping, because the GAM frequency is much faster than the bounce frequency of banana ions.

3.1.4. Rosenbluth–Hinton undamped component of zonal flows in collsionless plasmas. An accurate treatment of the damping of self-generated zonal flows is an outstanding issue in predicting confinement. Rosenbluth and Hintons' (RH) analytic calculation has shown that linear collisionless kinetic mechanisms do *not* damp the zonal flows completely [42]. This prediction was later verified by various gyrokinetic codes [52, 96–98], while gyrofluid models [99, 100] incorrectly predicted a total collisionless decay of poloidal rotation. A modification of the gyrofluid approximation was attempted later, but only part of the RH undamped flow has been recovered to date [101].

As discussed at the beginning of this section, zonal flow can be viewed as a superposition of GAMs with a characteristic real frequency on the order of $\omega_{\mathrm{r}} \sim v_{\mathrm{Thi}}/R$ and with a corresponding ion Landau damping rate $\omega_{\mathrm{r}} \exp(-q^2/2)$, and a zero frequency component to which the RH calculation applies. (The damping occurs due to the transit time magnetic pumping [72, 93]. One can identify the oscillation and decay of GAMs as well as the non-zero asymptotic level of zonal flows predicted by RH.)

The RH calculation, which is based on the gyrokinetic equation, consists of following the long time evolution of the zonal flow with an assigned finite initial value. Concentrating on the long term behaviour $t \gg \omega_{\mathrm{b,i}}^{-1}$, RH calculates the bounce-averaged gyrokinetic response to an initial perturbation. The nonlinear gyrokinetic Vlasov equation for zonal flow component with $q = (q_{\mathrm{r}}, 0, 0)$, i.e. $n = m = 0$ can be written as

$$\left[\frac{\partial}{\partial t} + (v_\parallel \hat{b} + \boldsymbol{v}_{\mathrm{d}}) \cdot \nabla - C_{\mathrm{ii}}\right] f_{\mathrm{i},\boldsymbol{q}} + \frac{e}{T} F_0 (v_\parallel \hat{b} \cdot \nabla + \boldsymbol{v}_{\mathrm{d}} \cdot \nabla)\phi_{\boldsymbol{q}} = S_{\mathrm{i},\boldsymbol{q}}, \tag{3.1.18}$$

where $\phi_{\boldsymbol{q}}$ is the electrostatic potential of the zonal flow; $f_{\mathrm{i},\boldsymbol{q}}$ and F_0 are the perturbed and unperturbed distribution functions of ions, respectively; and nonlinear interactions of ITGs with $\boldsymbol{k}, \boldsymbol{k}'$ are considered as a noise source $S_{\mathrm{i},\boldsymbol{q}}$ for zonal flows. Of course, equation (3.1.18) should include a response renormalization, as well as noise. The corresponding gyrokinetic Poisson's equation (i.e. the quasi-neutrality condition expressed in terms of the guiding centre density $n_{\mathrm{i},\boldsymbol{q}}$ and polarization density) is $-n_0(e/T_{\mathrm{i}})\rho_{\mathrm{i}}^2 q_{\mathrm{r}}^2 \phi_{\boldsymbol{q}} + n_{\mathrm{i},\boldsymbol{q}} = n_{e,\boldsymbol{q}}$, where $n_{e,\boldsymbol{q}} = 0$, for the adiabatic electron response with zonal flows, and the long wavelength approximation for zonal flow $\rho_{\mathrm{i}}^2 q_{\mathrm{r}}^2 \ll 1$ have been used.

In RH, a bounce-average of equation (3.1.18) has been performed for a high aspect ratio, circular tokamak geometry with $\rho_{\mathrm{i}}^2 q_{\mathrm{r}}^2 \ll \rho_{\theta,\mathrm{i}}^2\, q_{\mathrm{r}}^2 \ll 1$. ($\rho_{\theta,\mathrm{i}}$ is the ion gyro-radius at the poloidal magnetic field.) The detailed calculation is not repeated here. The main result is that an initial zonal flow potential $\phi_{\boldsymbol{q}}(0)$ will be reduced to a level $\phi_{\boldsymbol{q}}(t)$ as $t \to \infty$, due to the neoclassical enhancement of polarization shielding:

$$\frac{\phi_{\boldsymbol{q}}(t)}{\phi_{\boldsymbol{q}}(0)} = \frac{1}{1 + 1.6\varepsilon^{-1/2} q^2}. \tag{3.1.19}$$

In physical terms, the usual polarization shielding associated with finite Larmor radius effect in a short term (after a few gyro-periods) $\sim \rho_{\mathrm{i}}^2 q_{\mathrm{r}}^2$ is replaced by the neoclassical polarization shielding associated with the finite banana width of trapped ions at long time (after a few bounce periods), $\sim\varepsilon^{1/2}\rho_{\mathrm{b,i}}^2 q_{\mathrm{r}}^2 \sim \varepsilon^{-1/2}\rho_{\theta,\mathrm{i}}^2 q_{\mathrm{r}}^2$. ($\rho_{\mathrm{b,i}}$ is the banana width of ions.) An accurate calculation of the coefficient 1.6 requires a kinetic calculation which includes the contribution from passing particles, but the correct scaling can be deduced from considering only trapped ions.

The result in equation (3.1.19) has been useful in benchmarking various gyrokinetic codes. After such a test, which is explained in section 4, the RH result has turned out to be highly relevant, as indicated by numerous nonlinear simulations.

3.1.5. Further details of collisional damping of zonal flows. A frequently asked question about zonal flow in toroidal geometry is: why is the radial electric field $E_{\rm r}$ not associated with zonal flow balanced by the toroidal flow, eventually satisfying the radial force balance $E_{\rm r} = V_\theta B_{\rm t}$?

To elucidate the relation between the RH result and this question, one should consider the ion–ion collisional effect for the longer-term behaviour of zonal flows [43]. RH identified several temporal-asymptotic phases of zonal flow response to an initial zonal flow potential $\phi_{\boldsymbol q}(0)$, which consist of:

(i) For times longer than a few ion bounce-times, the zonal flow potential reduces to a non-zero residual value given by equation (3.1.19) due to a collisionless kinetic process which includes the ion Landau damping of GAMs, transit time magnetic pumping and neoclassical enhancement of polarization shielding.

(ii) For times of the order of $\varepsilon\tau_{\rm ii}$, where $\tau_{\rm ii}$ is the ion–ion collisional time, the potential and poloidal flow decay due to pitch-angle scattering in a trapped-passing boundary layer. Most of the collisional poloidal flow decay occurs in this phase (as confirmed by simulation [50]), and zonal flow is mostly in the poloidal direction, up to this phase.

(iii) For times comparable to $\varepsilon^{1/2}\tau_{\rm ii}$, the potential approaches a non-zero steady state value $\phi_{\boldsymbol q}(t) = \phi_{\boldsymbol q}(0)B_p^2B_{\rm t}^{-2}$, consistent with $E_{\rm r} = V_\theta B_{\rm t}$, and the poloidal flows decays approximately exponentially.

(iv) For times longer than $\tau_{\rm ii}$, damping of poloidal flow is due to energetic ions with small collisional rates, resulting in a slow non-exponential decay due to ion drag. Note that the collisional damping of the toroidal flow is a higher order process.

The main conclusion is that most of the collisional decay occurs on the time scale in phase (ii). Thus *one can define the net effective collisional decay time of zonal flow as* $1.5\varepsilon\tau_{\rm ii}$, following RH.

As illustrated in appendix A, there exists a near isomorphism between ITG turbulence and ETG turbulence. One crucial difference is that, while the adiabatic electron density response due to electron thermalization along the magnetic field is zero for ITG zonal flows, the adiabatic ion density response due to demagnetization is non-zero for ETG zonal flows. Interesting consequences for ETG zonal flow damping, related to this difference, have been investigated in [102].

3.2. Generation mechanism

The zonal flow is driven by nonlinear processes in the fluctuation spectrum or ensemble of wave-packets in the range of the drift wave frequency. In this subsection, several elementary processes for generation of zonal flow are presented. The mechanism for zonal flow generation includes both parametric instability of a single drift wave and modulational instability of a spectrum of drift waves. The modulational instability can be calculated via both eikonal theory and wave kinetics, and by envelope formalism.

3.2.1. Generation by parametric instability. A single drift wave (plane wave) is shown to be unstable to parametric perturbations [5, 103]. Via parametric instability, the drift wave can generate convective cells for which the parallel wavenumber vanishes, $k_\| = 0$. The zonal flow is a special example, corresponding to extreme anisotropy of a convective cell with $q_r \gg q_\theta \sim q_\parallel \sim 0$. Note that the parametric instability process is the usual one, familiar from weak turbulence theory, with the feature that one of the 'daughter waves' has zero frequency. In this subsection, parametric instability of a simple drift wave $\tilde{\phi}(\boldsymbol{x}, t) = \tilde{\phi}_{d0} \exp(\mathrm{i}\boldsymbol{k}_{d0} \cdot \boldsymbol{x} - \mathrm{i}\omega_{d0}t) + \mathrm{c.c}$ is discussed.

Zonal flow in slab plasma. Two possible parametric instabilities occur for a plane drift wave. In the study of parametric instability in slab plasmas, we use the coordinates (x, y, z) where x is in the direction of the radius and z is in the direction of magnetic field. One is the parametric decay instability [5, 103]. The primary drift wave, denoted by the wavenumber $\boldsymbol{k}_{d0}$ and frequency ω_{d0}, where the suffix d stands the drift wave, can induce a pairing of a convective cell (wavenumber $\boldsymbol{q}$ and frequency Ω) and a secondary drift wave (wavenumber $\boldsymbol{k}_{d1}$ and frequency ω_{d1}). This process occurs if conditions $\boldsymbol{k}_{d1} + \boldsymbol{q} = \boldsymbol{k}_{d0}$, $\omega_{d1} + \Omega = \omega_{d0}$ and $k_{d0}^2 > k_{d1}^2$ are satisfied. The growth rate of parametric decay instability is easily shown to be:

$$\gamma_{di} = c_s \rho_s |\boldsymbol{k}_{d0} \times \boldsymbol{q}| \sqrt{\frac{T_e}{T_i} \frac{k_{d0}^2 - k_{d1}^2}{q^2} \frac{e\tilde{\phi}_{d0}}{T_e}}, \tag{3.2.1}$$

where $\tilde{\phi}_{d0}$ is the amplitude of the electrostatic potential perturbation associated with the primary drift wave. The parametric decay instability is not effective for generating zonal flow. The beat condition requires $q_x = 2k_{d0,x}$ and $k_{d1,x} = -k_{d0,x}$. However, for this combination of wave vectors, the relation $k_{d0}^2 = k_{d1}^2$ is forced, so the growth rate of parametric decay vanishes. Thus, the zonal flow is not driven by the parametric decay instability.

The other possible parametric process is the modulational instability [25, 104–108]. In this case, the primary drift wave (denoted by $\boldsymbol{k}_{d0}$ and ω_{d0}) couples to the (modulating) zonal flow (q and Ω) and so induces two secondary drift waves. The two induced drift waves are denoted by d+ and d−, and have wavenumbers

$$\boldsymbol{k}_{d+} = \boldsymbol{k}_{d0} + \boldsymbol{q}, \qquad \text{and} \qquad \boldsymbol{k}_{d-} = \boldsymbol{q} - \boldsymbol{k}_{d0}. \tag{3.2.2}$$

The modulational instability means that the radial structure of the wave function primary drift wave is modified when the zonal flow is excited. We employ the potential vorticity conservation equation (i.e. the Charney–Hasegawa–Mima equation)

$$\frac{\partial}{\partial t}(n - \Delta_\perp \phi) + [\phi, (n - \Delta_\perp \phi)] + \frac{\partial}{\partial y}\phi = 0, \tag{3.2.3}$$

where $[\phi, g] \equiv (\hat{b} \times \nabla_\perp \phi) \cdot \nabla g$ ($\hat{\boldsymbol{b}}$: unit vector in the direction of the magnetic field) represents the advective nonlinear term, and the normalizations of space in unit of ρ_s and time in units of $L_n c_s^{-1}$, together with $n \equiv (L_n/\rho_s)\tilde{n}/n_0$, $\phi \equiv (L_n/\rho_s)e\tilde{\phi}/T_e$, are employed for simplicity. In the case of co-existing drift waves and zonal flows,

$$\phi = \phi_d + \phi_{ZF} \qquad \text{and} \qquad n = n_d + n_{ZF}. \tag{3.2.4}$$

Equation (3.2.3) is then separated into the vorticity equation for drift waves and the zonal flows. The density response is given by the Boltzmann relation for drift waves $n_d = \phi_d$. For zonal flows, the continuity equation holds, so that $\partial n_{ZF}/\partial t + \langle [\phi, n] \rangle = 0$. That is,

$$n_{ZF} = 0 \tag{3.2.5}$$

so long as $\Omega \neq 0$. Thus the vorticity equation for the zonal flow reduces to the Euler equation for a two-dimensional fluid. The parametric modulational dispersion relation is obtained as

$$(\omega_{d0} - \omega_{d+} + \Omega)(\omega_{d0} + \omega_{d-} - \Omega) = \frac{|\boldsymbol{k}_{d0\perp} \times \boldsymbol{q}|^2}{q^2}(1 + k_{d0\perp}^2 - q^2)^2 \left(\frac{\boldsymbol{k}_{d+\perp}^2 - \boldsymbol{k}_{d0\perp}^2}{1 + \boldsymbol{k}_{d+\perp}^2} + \frac{\boldsymbol{k}_{d-\perp}^2 - \boldsymbol{k}_{d0\perp}^2}{1 + \boldsymbol{k}_{d-\perp}^2} \right) |\phi_{d0}|^2. \tag{3.2.6}$$

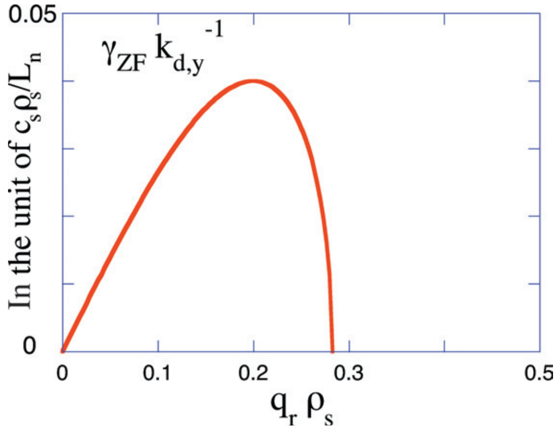

Figure 9. Growth rate of the zonal flow for the parametric modulational instability. A case of $e\tilde{\phi}_{d0}/T_e = 0.2\rho_s/L_n$ and $k_{d,x} = 0$ is shown.

where $\omega_{d+} = k_{d0,y}(1 + k_{d+}^2)^{-1}$, and $\omega_{d-} = k_{d0,y}(1 + k_{d-}^2)^{-1}$. In the limit of a long wavelength of the zonal flow, $|\boldsymbol{q}| \ll |\boldsymbol{k}_{d\perp}|$, the condition for the instability to exist can be simplified to

$$\phi_{d0} > \frac{|\boldsymbol{k}_{d0,y}|q^2}{\sqrt{2}|\boldsymbol{k}_{d0\perp} \times \boldsymbol{q}|}. \tag{3.2.7}$$

The growth rate of the secondary perturbation is given from equation (3.2.6) and is expressed in the long wavelength limit as

$$\gamma_{ZF} = \sqrt{2}|\boldsymbol{k}_{d0\perp} \times \boldsymbol{q}|\sqrt{\phi_{d0}^2 - \frac{|k_{d0,y}|^2 q^4}{2|\boldsymbol{k}_{d0\perp} \times \boldsymbol{q}|^2}}. \tag{3.2.8}$$

In the case that the drift wave is propagating nearly in the poloidal direction, $k_{d,x} \simeq 0$, equation (3.2.8) is simplified to

$$\gamma_{ZF} = k_{d0\perp} q_x \sqrt{2\phi_{d0}^2 - q_x^2}. \tag{3.2.9}$$

The maximum growth rate is given as $\gamma_{ZF} \simeq k_{d0\perp}\phi_{d0}^2$ for $|\boldsymbol{q}| \simeq \phi_{d0}$. Figure 9 shows a plot of the growth rate of the modulational instability as a function of the wavenumber of the zonal flow. It is unstable in the long wavelength region. If the growth rate of the parametric instability is larger than the collisional damping, growth of the zonal flow can occur.

Tokamak plasma. In tokamak plasma, a single drift wave eigenmode is not a plane wave, but is given by a ballooning eigenfunction. Ballooning modes are similar to Bloch wavefunctions, familiar from condensed matter physics. A ballooning mode has a single n-value (toroidal mode number—the 'good' quantum number in the direction of symmetry), and consists of a set of coupled poloidal harmonics, vibrating together with a fixed phase relation, which defines the radial wavenumber. A similar analysis has been developed, and toroidal effects influence the coupling coefficients [25]. The pump wave is expressed as [109]

$$\tilde{\phi}_0(\boldsymbol{r}, t) = \exp(-\mathrm{i}n\zeta - \mathrm{i}\omega_0 t)\sum_m \Phi_0(m - nq)\exp(\mathrm{i}m\theta) + \mathrm{c.c.}, \tag{3.2.10}$$

where m and n are the poloidal and toroidal mode numbers, respectively, and $\Phi_0(m - nq)$ represents the poloidal harmonic wavefunction. As in the case of slab plasma, a single toroidal mode number n is kept. The zonal flow $\tilde{\phi}_{\mathrm{ZF}}$ and two nonlinear sidebands of the toroidal drift waves ($\tilde{\phi}_+$ and $\tilde{\phi}_-$) may occur by modulational instability. They are given as

$$\tilde{\phi}_{\mathrm{ZF}}(\boldsymbol{r},t) = \exp(\mathrm{i}q_\mathrm{r}r - \mathrm{i}\Omega t)\Phi_{\mathrm{ZF}} + \mathrm{c.c.} \tag{3.2.11a}$$

$$\tilde{\phi}_+(\boldsymbol{r},t) = \exp(-\mathrm{i}n\zeta - \mathrm{i}\omega_0 t + \mathrm{i}q_\mathrm{r}r - \mathrm{i}\Omega t)\sum_m \Phi_+(m-nq)\exp(\mathrm{i}m\theta) + \mathrm{c.c.} \tag{3.2.11b}$$

$$\tilde{\phi}_-(\boldsymbol{r},t) = \exp(-\mathrm{i}n\zeta + \mathrm{i}\omega_0 t + \mathrm{i}q_\mathrm{r}r - \mathrm{i}\Omega t)\sum_m \Phi_-(m-nq)\exp(\mathrm{i}m\theta) + \mathrm{c.c.} \tag{3.2.11c}$$

This form is physically equivalent to the corresponding one in subsection (i), but the toroidicity-induced coupling affects the structure of the eigenfunction. (The subscript ‘d’ denoting drift waves is dropped in order to reduce the complexity of notation.)

The modulational instability is analysed by a procedure similar to that for the slab plasma. One obtains a dispersion relation for the modulational instability, namely

$$(\omega_0 - \omega_+ + \Omega)(\omega_0 - \omega_- - \Omega) = \gamma_{\mathrm{mod}}^2, \tag{3.2.12}$$

where

$$\gamma_{\mathrm{mod}}^2 = \frac{(2+\eta_\mathrm{i})}{1.6\varepsilon^{3/2}}\frac{B_\theta^2}{B_\zeta^2}k_\theta^2 q_\mathrm{r}^2 c_\mathrm{s}^2 \rho_\mathrm{s}^2 |\tilde{\phi}_0^2|, \tag{3.2.13}$$

$|\tilde{\phi}_0^2| = \langle\sum_m |\Phi_0|^2\rangle$ is the amplitude of the primary drift wave, and the difference of the eigenfrequencies is second order in the wavenumber of the zonal flow q_r, i.e. $|\omega_0 - \omega_\pm| \simeq \omega_0 q_\mathrm{r}^2 \rho_\mathrm{s}^2$. The factor of $B_\theta^2/(1.6\varepsilon^{3/2}B_\zeta^2)$ in equation (3.2.13) is a consequence of the structure of the dielectric constant of the plasma in toroidal geometry. If $\gamma_{\mathrm{mod}}^2 > (\omega_0 - \omega_+)^2$ holds, one obtains the growth rate

$$\Omega = \mathrm{i}\sqrt{\gamma_{\mathrm{mod}}^2 - (\omega_0 - \omega_+)^2}, \tag{3.2.14}$$

using $\omega_+ = \omega_-$. The growth rate of the zonal flow has a similar dependence on q_r as is illustrated in figure 9. An estimate of the wavenumber at which the growth rate is maximum is estimated to be $q_\mathrm{r} \simeq k_\theta \hat{s}$, where $\hat{s}$ is the shear parameter. Finally, on account of the confluence of nonlinear beat-induced coupling with linear, toroidicity-induced coupling, interaction with neighbouring poloidal harmonics is possible, and has no slab counterpart. For this reason, parametric modulational instability in a tokamak has sometimes been referred to as ‘four-wave coupling’. This name is slightly confusing, and the reader should keep in mind that, really, only *three* independent n modes are involved, as in the case of parametric modulational instability in a slab.

As is the case for the slab plasmas, the zonal flow is expected to be amplified if the growth rate equation (3.2.14) is larger than the collisional damping, as explained in section 3.1.3, $\sqrt{\gamma_{\mathrm{mod}}^2 - (\omega_0 - \omega_+)^2} > \gamma_{\mathrm{mod}}$.

3.2.2. Zonal flow generation by a spectrum of drift wave turbulence. While the simplified, truncated-degree-of-freedom models discussed in section 2 can elucidate and encapsulate some aspects of the physics of zonal flow generation, the physically relevant problem requires an understanding of the answer to the question: under what conditions is a *spectrum* of drift wave turbulence unstable to a test zonal shear? Note that in this respect, the zonal flow generation problem resembles the well-known magnetic dynamo problem, which seeks to answer the question of: when is a spectrum of MHD turbulence unstable to a ‘test’ magnetic field? In the (relevant) case of generation by a spectrum of drift waves, the test zonal flow might interact with a broad spectrum of primary drift wave fluctuations, each of which has a finite self-correlation

Table 4. Analogy between weak Langmuir turbulence and zonal flow generation.

Langmuir turbulence	Drift waves and zonal flows
High frequency population:	
plasmon/electron plasma wave	Drift wave $\omega_k = \omega_{*\mathrm{e}}(1 + k_\perp^2 \rho_\mathrm{s}^2)$
Low frequency structure:	
phonon/ion acoustic	Zonal flow
Drive Mechanism:	
ponderomotive pressure	Turbulent Reynolds stress
Wave population distribution:	
action: plasmon number	Potential enstrophy i.e., drift-ion number $N = (1 + k_\perp^2 \rho_\mathrm{s}^2)^2 \left\lvert \frac{e\phi}{T} \right\rvert^2$
Modulational instability criterion:	
population inversion needed	Population inversion unnecessary
Regulator:	
ion Landau damping of phonon	Collisional damping of zonal flow

time. Thus, a statistical, random phase approximation (RPA)-type theory is necessary. The essence of such a theory is to derive the zonal flow growth rate by:

(a) first averaging the zonal flow evolution equation (i.e. mean field evolution equation) over an ensemble of drift wave realizations to relate $\partial\phi_{\mathrm{ZF}}/\partial t$ to $\langle\hat{\phi}_{\mathrm{DW}}^2\rangle$, thus obtaining an equation for mean field evolution in the presence of wave (i.e. pondermotive) pressures and stresses,

(b) then computing the response of the drift wave spectrum to the test zonal flow shear, thus 'closing the feedback loop'.

This procedure, which is typical of that followed in the course of modulational stability calculations, ultimately rests upon:

(a) the separation in *time* scales between the low frequency zonal flow and the higher frequency drift waves (i.e. $\Omega_{\mathrm{ZF}} \ll \omega_{\underline{k}}$). This time scale separation enables the use of adiabatic theory (i.e. eikonal theory and wave kinetics) to compute the response of the primary drift wave spectrum to the test shear, and justifies the neglect of drift wave diffraction. Note that the parametric instability calculation, discussed in section 3.2, also rests upon such an assumption of time scale separation.

(b) the assumption of quasi-Gaussian distribution of drift wave phases.

It is worthwhile to note that the weak turbulence theory of zonal flow growth is quite closely related to the classic problem of weak Langmuir turbulence [110]. In Langmuir turbulence, low frequency test phonons (i.e. ion acoustic waves) grow by depleting the energy of a bath of ambient plasmons (i.e. plasma waves). Since $\omega_{\mathrm{pe}} \gg qc_{\mathrm{s}}$, the zonal flow is the analogue of the ion-acoustic wave, while the drift waves are the analogue of the plasma wave. Table 4 presents a detailed comparison and contrast of the weak Langmuir turbulence and zonal flow problems. We will return to table 4 later, after discussing the theory of zonal flow growth.

(i) Zonal flow growth. As previously noted, the basic dynamics of zonal flows are governed by the two-dimensional Navier–Stokes equation, since the density perturbation associated with the zonal flow is negligibly small. Alternatively, the zonal flow structure is essentially two-dimensional, as is a convective cell. Thus, in de-dimensionalized units, the zonal flow potential

evolves according to a two-dimensional fluid equation:

$$\frac{\partial}{\partial t}\nabla_{\mathrm{r}}^{2}\phi_{\mathrm{ZF}} = \frac{-\partial}{\partial r}\langle\tilde{v}_{r_{\mathrm{d}}}\nabla^{2}\tilde{\phi}_{\mathrm{d}}\rangle - \underline{\underline{\gamma}}_{\mathrm{d}}\nabla_{\mathrm{r}}^{2}\phi_{\mathrm{ZF}}. \tag{3.2.15}$$

Here $\underline{\underline{\gamma}}_{\mathrm{d}}$ is a generic damping operator, which may be a scalar coefficient or an integro-differential operator. Physically, equation (3.2.15) tells us that zonal flow vorticity evolves due to the spatial flux of drift wave vorticity $\Gamma_{u} = \langle\tilde{v}_{r_{\mathrm{d}}}\nabla^{2}\tilde{\phi}_{\mathrm{d}}\rangle$. This observation is important, as it establishes there is no *net* flow generation or momentum increase, up to boundary through put terms. Rather, zonal 'flow generation' is really a process of flow *shear amplification*. Zonal flow evolution (i.e. velocity profile evolution) is transparently a process driven by vorticity *transport*, just as temperature and density profile evolution are driven by thermal and particle fluxes. Equation (3.2.15) may be rewritten as:

$$\frac{\partial}{\partial t}\nabla_{\mathrm{r}}^{2}\tilde{\phi}_{\mathrm{ZF}} = \frac{1}{B}\frac{\partial^{2}}{\partial r^{2}}\int d^{2}k k_{\mathrm{r}}k_{\theta}|\phi_{k}^{\mathrm{d}}|^{2} - \underline{\underline{\gamma}}_{\mathrm{d}}(\nabla_{\mathrm{r}}^{2}\tilde{\phi}_{\mathrm{ZF}}). \tag{3.2.16}$$

Equation (3.2.16) directly relates the evolution of zonal flow potential to the slow variation of the drift wave intensity envelope. By 'slow variation' we refer to the fact that $|\phi_{\underline{k}}^{\mathrm{d}}|^{2}$ varies on a scale larger than upon which $\phi_{\underline{k}}^{\mathrm{d}}$ does, i.e. $k_{\mathrm{r}} > (1/|\phi_{\underline{k}}^{\mathrm{d}}|^{2})\partial|\phi_{\underline{k}}^{\mathrm{d}}|^{2}/\partial r$. Also, it is now clear that the scale of the drift wave intensity envelope is what sets the scale of the zonal flow.

Since wave population density (alternatively the 'density of waves') is conserved along wave ray trajectories, tracking the evolution of N, the density of waves, is particularly useful in evaluating the response of the drift wave spectrum to modulation by a test shear. The convenience of $N(\boldsymbol{k}, \boldsymbol{r}, t)$ follows, of course, from the fact that N obeys a Boltzmann equation, with characteristic equations given by the eikonal equations for a drift wave. In most cases, $N(\boldsymbol{k}, \boldsymbol{r}, t)$ is the wave action density $N = \varepsilon/\omega_{k}$, where ε is the wave energy density. In the case of drift wave turbulence, this question is complicated by the fact that drift wave turbulence supports *two* quadratic conserved quantities, namely the energy density $\varepsilon = (1 + k_{\perp}^{2}\rho_{\mathrm{s}}^{2})^{2}|\phi_{\underline{k}}^{\mathrm{d}}|^{2}$ and the potential enstrophy density $Z = (1 + k_{\perp}^{2}\rho_{\mathrm{s}}^{2})^{2}|\phi_{k}^{\mathrm{d}}|^{2}$. Thus, one can count either the local 'wave' density, given by the action density $N = (1 + k_{\perp}^{2}\rho_{\mathrm{s}}^{2})^{2}|\phi_{k}^{\mathrm{d}}|^{2}/\omega_{k}$, or the local 'vortex density' (i.e. 'roton' number), given by $N_{\mathrm{r}} = (1 + k_{\perp}^{2}\rho_{\mathrm{s}}^{2})^{2}|\phi_{k}^{\mathrm{d}}|^{2}$. However, for zonal flow shears (which have $q_{\theta} = 0$), k_{θ} is unchanged by flow shearing, since $\mathrm{d}k_{y}/\mathrm{d}t = -\partial(k_{\theta}V_{\mathrm{ZF}}(x))/\partial y = 0$. The action density then becomes $N = (1 + k_{\perp}^{2}\rho_{\mathrm{s}}^{2})^{2}|\phi_{\underline{k}}^{\mathrm{d}}|^{2}/\omega_{*\mathrm{e}}$ where $\omega_{*\mathrm{e}}$ is an irrelevant constant multiplier, thus rendering both counts of exciton density the same. Hence, we can rewrite the zonal flow evolution equation equation (3.2.16) as [15, 19, 111]:

$$\frac{\partial}{\partial t}\tilde{V}_{\mathrm{ZF}}' = \frac{1}{B^{2}}\frac{\partial^{2}}{\partial r^{2}}\int \mathrm{d}^{2}k\frac{k_{\mathrm{r}}k_{\theta}}{(1 + \rho_{\mathrm{s}}^{2}k_{\perp}^{2})^{2}}\frac{\delta N}{\delta\tilde{V}_{\mathrm{ZF}}'}(k, r, t)\tilde{V}_{\mathrm{ZF}}' - \gamma_{\mathrm{damp}}[\tilde{V}_{\mathrm{ZF}}'], \tag{3.2.17}$$

where $\tilde{V}_{\mathrm{ZF}}' = \partial\tilde{V}_{\mathrm{ZF}}/\partial r$, and, at the level of coherent response theory for the modulation of N by $\tilde{V}_{\mathrm{ZF}}$, $\tilde{N}$ is given by $\tilde{N}(\boldsymbol{k}, \boldsymbol{r}, t) = (\delta N/\delta\tilde{V}_{\mathrm{ZF}}')\tilde{V}_{\mathrm{ZF}}'$. Note that equation (3.2.17) relates shear amplification to the extent to which the modulation, induced in the drift wave population N by $\tilde{V}_{\mathrm{ZF}}'$, tends to drive a Reynolds stress, which *re-enforces* the initial perturbation. An *affirmative answer* to this question establishes that the drift wave spectrum is *unstable* to the growth of a seed zonal velocity shear.

The modulational response $\delta N/\delta\tilde{V}_{\mathrm{ZF}}'$ may now be calculated by linearizing the WKE for N, which can formally be written as (by taking a model of nonlinear damping as $\gamma_{\mathrm{NL}}N = \Delta\omega_{k}N^{2}/N_{0}$):

$$\frac{\partial N}{\partial t} + (\underline{v}_{\mathrm{g}} + \underline{\tilde{V}}_{\mathrm{ZF}})\cdot\underline{\nabla}N - \frac{\partial}{\partial\underline{x}}(\omega + \underline{k}\cdot\underline{\tilde{V}}_{\mathrm{ZF}})\cdot\frac{\partial N}{\partial\underline{k}} = \gamma_{\underline{k}}N - \frac{\Delta\omega_{\underline{k}}}{N_{0}}N^{2} \tag{3.2.18}$$

with characteristic equations for $\underline{x}$ and $\underline{k}$ evolution given by: $\mathrm{d}\boldsymbol{x}/\mathrm{d}t = \boldsymbol{v}_{\mathrm{g}} + \tilde{\boldsymbol{V}}_{\mathrm{ZF}}$, $\mathrm{d}\boldsymbol{k}/\mathrm{d}t = -\mathrm{d}(\omega+\boldsymbol{k}\cdot\tilde{\boldsymbol{V}}_{\mathrm{ZF}})/\mathrm{d}x$. For an ansatzed reference equilibrium spectrum $N_0(k)$, one has $\gamma_{\underline{k}} = \Delta\omega_{\underline{k}}$, so that the linearized form of the WKE for zonal flow shears becomes:

$$\frac{\partial \tilde{N}}{\partial t} + v_{\mathrm{g}}\frac{\partial \tilde{N}}{\partial r} + \gamma_{\underline{k}}\tilde{N} = \frac{\partial}{\partial x}(k_\theta \tilde{V}_{\mathrm{ZF}})\frac{\partial\langle N\rangle}{\partial k_{\mathrm{r}}}. \tag{3.2.19}$$

Here $\langle N\rangle$ is the equilibrium value of the wave spectrum. Note that the $+\gamma_{\underline{k}}\tilde{N}$ damping term arises from a partial cancellation between $\gamma_{\underline{k}}\tilde{N}$ and $-2\Delta\omega_{\underline{k}}\langle N\rangle\tilde{N}/N_0$, after using the approximate relations $\Delta\omega_{\underline{k}} \simeq \gamma_{\underline{k}}$ and $N_0 = \langle N\rangle$. It follows that the modulation $\tilde{N}_{q,\Omega}$ induced by $\tilde{V}_{\mathrm{ZF}}$ is given by

$$\tilde{N}_{q,\Omega} = \frac{-qk_\theta\tilde{V}_{\mathrm{ZF}}}{(\Omega - qv_{\mathrm{g}} + \mathrm{i}\gamma_{\underline{k}})}\frac{\partial\langle N\rangle}{\partial k_{\mathrm{r}}}$$

so the modulational instability eigenfrequency is given by

$$\Omega = \frac{+q^2}{B^2}\int\frac{\mathrm{d}^2kk_\theta^2}{(\Omega - qv_{\mathrm{g}} + \mathrm{i}\gamma_{\underline{k}})}k_{\mathrm{r}}\frac{\partial\langle N\rangle/\partial k_{\mathrm{r}}}{(1+k_\perp^2\rho_{\mathrm{s}}^2)^2} - \mathrm{i}\gamma_{\mathrm{d}}. \tag{3.2.20}$$

This finally implies that the zonal flow growth rate is given by

$$\Gamma_q = \frac{-q^2}{B^2}\int\mathrm{d}k^2\frac{k_\theta^2}{(1+k_\perp^2p_{\mathrm{s}}^2)^2}\frac{\gamma_{\underline{k}}}{(\Omega - qv_{\mathrm{g}})^2+\gamma_{\underline{k}}^2}\left(\frac{k_{\mathrm{r}}\partial\langle N\rangle}{\partial k_{\mathrm{r}}}\right) - \gamma_{\mathrm{d}}. \tag{3.2.21}$$

Several aspects of the structure of the zonal flow growth are apparent from equation (3.2.21). First, *note that growth requires* $\partial N/\partial k_{\mathrm{r}} < 0$. This condition is satisfied for virtually any realistic equilibrium spectral density for drift wave turbulence. In contrast to the well-known case of Langmuir turbulence, a population inversion (i.e. $\partial N/\partial k_{\mathrm{r}} > 0$) is *not* required for growth of zonal flows by RPA modulational instability. This is a consequence of the fact that $\omega_{\underline{k}}$ *decreases* with increasing k_{r} for drift waves, while $\omega_{\underline{k}}$ *increases* with increasing k for Langmuir waves (i.e. see section 2). Thus, induced diffusion of k_{r} will deplete the drift wave population and drive zonal flows for $\mathrm{d}\langle N\rangle/\mathrm{d}k_{\mathrm{r}} < 0$, while induced diffusion of k_{r} will deplete the plasmon population for $\mathrm{d}\langle N\rangle/\mathrm{d}k > 0$.

It is also interesting to note that the leading behaviour of the zonal flow growth has the form of negative viscosity or negative diffusion, i.e.

$$\Gamma_q \simeq q^2D(q), \tag{3.2.22}$$

where

$$D(q) \cong \frac{-1}{B^2}\int\mathrm{d}^2k\frac{k_\theta^2\gamma_{\underline{k}}}{(1+k_\perp^2\rho_{\mathrm{s}}^2)^2}\frac{k_{\mathrm{r}}}{(\Omega - qv_{\mathrm{g}})^2+\gamma_{\underline{k}}^2}\frac{\partial\langle N\rangle}{\partial k_{\mathrm{r}}}. \tag{3.2.23}$$

This is, of course, consistent with expectations based upon the well-known inverse cascade of energy in two-dimensional, although we emphasize that zonal flow growth is non-local in wavenumber, and strongly anisotropic, in contrast to the inverse cascade. An order-of-magnitude estimate of equation (3.2.22) is given with the help of equation (3.2.23). Assuming that $k_\perp^2\rho_{\mathrm{s}}^2 < 1$ and that $\gamma_{\underline{k}} > qv_{\mathrm{g}}$, integration by parts yields

$$D(q) \simeq \frac{k_\theta^2}{B^2}\frac{1}{\gamma_{\mathrm{drift}}}|\tilde{\phi}_{\mathrm{d}}|^2 = \frac{c_{\mathrm{s}}^2\rho_{\mathrm{s}}^2}{\gamma_{\mathrm{drift}}}k_\theta^2\left|\frac{e\tilde{\phi}_{\mathrm{d}}}{T}\right|^2. \tag{3.2.24}$$

This value is of the same order of magnitude in comparison to other transport coefficients driven by turbulent drift waves. However, it should be noted that zonal flow growth occurs over a region of size q^{-1}, while conventional transport coefficients quantify the rate of diffusion across a profile scale length. Thus, zonal flow dynamics are *mesoscopic* phenomena, occurring on spatial scales between those of the turbulence correlation length and characteristic scale lengths of the profiles.

(ii) Energy conservation property. It is appropriate to demonstrate here that the RPA theory of zonal flow growth, presented above, manifestly conserves energy. Equations (3.2.22) and (3.2.23) give

$$\frac{\mathrm{d}}{\mathrm{d}t}|\tilde{V}_{\mathrm{ZF}}|^2 = \sum_q 2\Gamma_q |\tilde{V}_{\mathrm{ZF}_q}|^2 = \frac{-2}{B^2}\sum_q \int \mathrm{d}^2k \frac{q^2|k_\theta \tilde{V}_{\mathrm{ZF}_q}|^2}{(1+k_\perp^2\rho_\mathrm{s}^2)^2} R(q,\Omega)\frac{\partial\langle N\rangle}{\partial k_\mathrm{r}}, \tag{3.2.25}$$

$$R(q,\Omega) = \frac{\gamma_k}{(\Omega - qV_\mathrm{g})^2 + \gamma_k^2}. \tag{3.2.26}$$

The corresponding rate of change of the mean drift wave energy is

$$\frac{\mathrm{d}}{\mathrm{d}t}\langle\varepsilon\rangle = \int \mathrm{d}^2k \frac{1}{(1+k_\perp^2\rho_\mathrm{s}^2)}\frac{\mathrm{d}}{\mathrm{d}t}\langle N(k,t)\rangle. \tag{3.2.27}$$

Since a spectrum of sheared zonal flows induces diffusion of the drift wave population in radial wavenumber, one can write:

$$\frac{\mathrm{d}\langle N\rangle}{\mathrm{d}t} = \frac{\partial}{\partial r}D_{K,K}\frac{\partial\langle N\rangle}{\partial r}, \tag{3.2.28}$$

$$D_{K,K} = \sum_q \frac{1}{B^2}k_\theta^2|\tilde{V}_{\mathrm{ZF}}|^2 q^2 R(q,\Omega). \tag{3.2.29}$$

Proceeding to integrate by parts, we obtain

$$\frac{\mathrm{d}\langle\varepsilon\rangle}{\mathrm{d}t} = \int \mathrm{d}^2k \frac{2k_\mathrm{r}}{(1+k_\perp^2\rho_\mathrm{s}^2)^2} D_{K,K}\frac{\partial\langle N\rangle}{\partial k_\mathrm{r}}. \tag{3.2.30}$$

It is thus abundantly clear that $\mathrm{d}(|\tilde{V}_{\mathrm{ZF}}|^2 + \langle\varepsilon\rangle)/\mathrm{d}t = 0$, so the theory conserves energy. Having thus rigorously established energy conservation, we will make use of this actively in the future to simplify calculations.

3.2.3. Relation between the RPA and single mode description. It is appropriate, at this point, to establish some connection or correspondence between the coherent modulation instability calculation discussed in section 3.2.1 and the RPA calculation discussed here in section 3.2.2. To this end, it is interesting to note that the zonal flow growth rate equation (3.2.20) may be re-expressed as a frequency, i.e.

$$\Omega = -\int \mathrm{d}^2k \frac{\gamma_{\mathrm{coh}}^2(q,k)}{(\Omega - qv_\mathrm{g} + \mathrm{i}\gamma_{\underline{k}})}, \tag{3.2.31}$$

where $\gamma_{\mathrm{coh}}^2(q,k) = (k_\theta^2 q^2 k_\mathrm{r}/(B^2(1+k_\perp^2\rho_\mathrm{s}^2)^2))\partial\langle N\rangle/\partial k_\mathrm{r}$. Here the effect of $\partial/\partial k_\mathrm{r}$ on $(1 + k_\perp^2\rho_\mathrm{s}^2)^{-2}$ and R has been neglected. In this limit, then equation (3.2.31) can be rewritten as

$$\Omega(\Omega - qv_\mathrm{g}) = -\gamma_{\mathrm{mod}}^2, \tag{3.2.32}$$

where $\gamma_{\mathrm{mod}}^2 = k_\theta^2 q_\mathrm{r}^2\langle N\rangle(1+k_\perp^2\rho_\mathrm{s}^2)^{-2}$. This form is essentially the same as those obtained from the parametric analyses of modulational instability, and gives the zonal flow growth rate as $\gamma_{\mathrm{ZF}}^2 = \gamma_{\mathrm{mod}}^2 - (qv_\mathrm{g})^2$, which is equivalent to equation (3.2.9). The result in the case of the plane drift wave corresponds to the limiting case where the lifetime of the primary drift waves, $\gamma_{\mathrm{drift}}^{-1}$, is much longer than the growth rate of the zonal flow. We emphasize, however, that the validity of the coherent calculation not only requires that $\gamma_{\mathrm{mod}} > \gamma_{\underline{k}}$, but also $\gamma_{\mathrm{mod}} > q(\mathrm{d}v_\mathrm{g}/\mathrm{d}k)\Delta k$.

Here $(q(\mathrm{d}v_{\mathrm{g}}/\mathrm{d}k)\Delta k)^{-1}$ is the autocorrelation of a dispersive drift wave-packet in the zonal flow strain field. It measures the time for a packet of width Δk to disperse as it propagates radially across a zonal flow of scale q^{-1}. Thus, validity of the coherent modulational theory requires *both* proximity to marginal stability of the primary drift wave spectrum (so $\gamma_{\mathrm{mod}} > \gamma_{\underline{k}}$), and a narrow spectrum (so that $\gamma_{\mathrm{mod}} > q(\mathrm{d}v_{\mathrm{gr}}/\mathrm{d}k)\Delta k$).

Building upon these considerations, one may construct an interpolation formula:

$$\Omega\left(\Omega - q\frac{\partial\omega}{\partial k_{\mathrm{r}}} + \mathrm{i}\gamma_{\mathrm{drift}}\right) = -\gamma_{\mathrm{mod}}^2, \tag{3.2.33}$$

noticing that the coefficient $D_{k_{\mathrm{r}},k_{\mathrm{r}}}$ defined by equation (3.2.29) satisfies the relation $D_{k_{\mathrm{r}},k_{\mathrm{r}}} \simeq q_{\mathrm{r}}^{-2}\gamma_{\mathrm{mod}}^2\gamma_{\mathrm{drift}}^{-1}$, within the approximation of equation (3.2.32). Equation (3.2.33) covers various ranges. In the limit of plane wave, $\gamma_{\mathrm{drift}} < \gamma_{\mathrm{mod}}$, the reactive instability equation (3.2.9) or (3.2.14) is recovered, where $\gamma_{\mathrm{ZF}} \sim \gamma_{\mathrm{mod}} \propto q_{\mathrm{r}}$ holds. In the opposite limit, $\gamma_{\mathrm{drift}} > \gamma_{\mathrm{mod}}$, diffusive growth ($\gamma_{\mathrm{ZF}} \sim \gamma_{\mathrm{mod}}^2 \propto q_{\mathrm{r}}^2$) results.

It might be useful here to note the cut-off of the zonal flow growth at large q_{r}. It is explained in the case of plane drift wave (parametric modulational instability) by equation (3.2.9) or figure 9. A similar expression is obtained in the limit of RPA. In the expression of the zonal flow growth rate in the RPA limit, e.g. equation (3.2.26), the response function is evaluated by $R(q,\Omega) \sim 1/\gamma_{\boldsymbol{k}}$. The lowest order correction of the wave dispersion is written as $R(q,\Omega) \sim \gamma_{\boldsymbol{k}}^{-1}(1 - q_{\mathrm{r}}^2 v_{gr}^2\gamma_{\boldsymbol{k}}^{-2} + \cdots)$. Thus one has an expression of γ_{ZF}, $\gamma_{\mathrm{ZF}} = D(q_{\mathrm{r}} = 0)q_{\mathrm{r}}^2(1 - q_{\mathrm{r}}^2 q_{r0}^{-2})$, where $q_{r0}^2 = v_{gr}^{-2}\gamma_{\boldsymbol{k}}^2$ represents the effect of the dispersion of the drift waves. This is an expansion of equation (3.2.22) with respect to $q_{\mathrm{r}}^2 q_{r0}^{-2}$.

3.2.4. Zonal flow drive by poloidal asymmetry. The particle flux driven by drift wave fluctuations could be poloidally asymmetric. If such an asymmetry exists in the background drift waves, a poloidal flow is induced in tokamak plasmas. This mechanism was first noted by Stringer [69] and is called the Stringer spin-up. We briefly explain it here.

The continuity equation (3.1.4) describes the flow on the magnetic surface if there is poloidal asymmetry in the net source term $S - \nabla\cdot\Gamma$. Poloidal asymmetry of $S - \nabla\cdot\Gamma$ appears, if the particle flux is not uniform in θ. We write

$$S - \nabla\cdot\Gamma = \langle S - \nabla\cdot\Gamma\rangle + (S - \nabla\cdot\Gamma)_a F(\theta), \tag{3.2.34}$$

where $\langle\cdots\rangle$ is a poloidal average, and $F(\theta)$ is a function describing the poloidally inhomogeneous part, so $\langle F(\theta)\rangle = 0$. The magnitude of poloidal asymmetry, $(S - \nabla\cdot\Gamma)_a$, and the shape of $F(\theta)$ are taken as prescribed here. In steady state, this inhomogeneity induces a secondary flow on the magnetic surface $V_{\mathrm{a},\parallel}$. The asymmetric flow $V_{\mathrm{a},\parallel}$ is given by: $V_{\mathrm{a},\parallel} = qRn_0^{-1}(S - \nabla\cdot\Gamma)_a\int_0^\theta \mathrm{d}\theta\, F(\theta)$.

In the presence of this flow, the parallel component of equation (3.1.5) is affected, in that the $r^{-1}V_\theta\partial V_\parallel/\partial\theta$ term in $\boldsymbol{V}\cdot\nabla\boldsymbol{V}$ does not vanish. As a result, one has the dispersion relation

$$\Omega^3 - \omega_{\mathrm{GAM}}^2\Omega = -\mathrm{i}\frac{2c_{\mathrm{s}}^2}{Rr}\gamma_{\mathrm{as}}, \tag{3.2.35}$$

where γ_{as} is the net particle 'production' rate of the asymmetric source, i.e.

$$\gamma_{\mathrm{as}} = \frac{1}{n_0}(S - \nabla\cdot\Gamma)_a\int_0^{2\pi}\frac{\mathrm{d}\theta}{2\pi}\cos\theta\, F(\theta). \tag{3.2.36}$$

This result shows that instability is possible if $F(\theta)$ has an in–out asymmetry, like $F(\theta) \sim \cos\theta$.

Equation (3.2.36) predicts two possible types of instabilities. One is growth of the zero frequency zonal flow with $\Omega \ll \omega_{\mathrm{GAM}}$. In this case, equation (3.2.36) reduces to

$$\Omega \simeq \mathrm{i}\frac{1}{\omega_{\mathrm{GAM}}^2}\frac{2c_s^2}{Rr}\gamma_{\mathrm{as}} \simeq \mathrm{i}\frac{R}{r}\gamma_{\mathrm{as}}, \tag{3.2.37}$$

which shows that poloidally symmetric flow spins up if $\gamma_{\mathrm{as}} > 0$. The other case corresponds to the excitation of the GAM. For the branch with $\gamma \simeq \omega_{\mathrm{GAM}}$, equation (3.2.35) gives an approximate solution

$$\Omega \simeq \omega_{\mathrm{GAM}} - \mathrm{i}\frac{1}{\omega_{\mathrm{GAM}}^2}\frac{c_s^2}{Rr}\gamma_{\mathrm{as}} \simeq \omega_{\mathrm{GAM}} - \mathrm{i}\frac{R}{2r}\gamma_{\mathrm{as}}. \tag{3.2.38}$$

The GAM is destabilized if $\gamma_{\mathrm{as}} < 0$. We note that the growth rate of the axisymmetric flow, equation (3.2.37) or (3.2.38) does not depend on the radial extent of the flow, i.e. $\gamma_{\mathrm{as}} \propto (q_{\mathrm{r}})^0$. where q_{r} is the radial wavenumber of the zonal flow. Hence, the Stringer spin-up mechanism can be important for the case of small q_{r}. The collisional damping rate in section 3.1.3 is also independent of q_{r}. Comparing equations (3.1.14) with (3.1.17), the excitation of a GAM with long radial wavelength is expected to occur if $\gamma_{\mathrm{as}} < \nu_{\mathrm{ii}}$. It has recently been pointed out that the shearing of the background turbulence by GAM induces poloidal asymmetry of the particle flux Γ and that this mechanism can cause the GAM instability, and

$$\mathrm{Im}(\Omega) \propto q_{\mathrm{r}}^2. \tag{3.2.39}$$

In this case, the growth rate is proportional to q_{r}^2 and coefficients are given in [112].

3.2.5. Influence of turbulent momentum transport on the secondary flow. As is shown in section 3.1.1, the zonal flow is associated with a secondary flow along the magnetic field line that cancels the divergence of the perpendicular flow. The viscous damping of this secondary flow due to toroidicity acts as a damping rate of the zonal flow, in addition to the collisional damping. This damping rate is rewritten as [48]

$$\gamma_{\mathrm{damp}} = \mu_{\parallel}(1 + 2q^2)q_{\mathrm{r}}^2, \tag{3.2.40}$$

where $\mu_{\parallel}$ is the turbulent shear viscosity for the flow along the field line, and q is the safety factor. Of course, $\mu_{\parallel}$ is a function of the drift wave intensity, and thus can be suppressed in the regime of strong zonal flows, such as the Dimits shift. The Pfirsch–Schlüter coefficient $1+2q^2$ is replaced by $1+1.6q^2/\sqrt{\varepsilon}$ in the collisionless limit. This damping term has dependencies on the wavenumber q_{r} and the intensity of the primary drift wave turbulence, which are similar to those of the growth rate, given in section 3.2.3. The dependence on geometrical factors differs from γ_{ZF}. Therefore the safety factor q (and thus the $B_\theta(r)$ profile!) can play an important role in determining the domain of zonal flow growth.

3.2.6. Electromagnetic effects. The discussion in the previous subsections is cast in the framework of the electrostatic limit, in the interest of transparency of argument. Plasma turbulence supports magnetic perturbations, and electromagnetic effects also have important roles in the physics of zonal flows. One of the effects is known as the 'finite-β effect' on drift waves [113], where β is the ratio of the plasma pressure to the magnetic field pressure, $\beta = 2\mu_0 B^{-2} p$. Frequently, the magnetic stress tends to compete against the Reynolds stress, thus reducing zonal flow growth. The other is the generation of the (poloidally symmetric) magnetic field bands by plasma turbulence. The generation of the magnetic field that has a symmetry (on a larger scale than that of the background turbulence) has been known as the mean field dynamo. This dynamo is more akin to a 'mesoscale dynamo' then to a mean field or small scale dynamo. Since the magnetic fields so generated have zonal symmetry and structure, we refer to them as *zonal fields*. The study of zonal fields is a new direction from which to approach the dynamo problem [60–63].

In the broad context of the zonal flows, two directions of research are explained here. One is finite-β effects on drift waves and the zonal flow generation by them. This is discussed in the context of parametric decay instability. The other is the magnetic field generation by drift-Alfven waves. The zonal field calculation is approached using the methods of statistical theory. Here, two examples are arranged as follows:

Subject	Mechanisms for zonal flow growth
Zonal flow generation by finite-β drift waves	Modulational instability of a plane drift Alfven wave
Zonal magnetic field generation	Random Alfven wave refraction of Alfven wave turbulence

(i) Finite-β effect on the drift waves. In the finite-β plasmas, coupling between the drift wave and shear Alfven wave occurs so as to form a drift-Alfven mode. The dispersion relation of this mode has been given as

$$1 + k_y^2\rho_s^2 - \frac{\omega_*}{\omega} - \frac{\omega(\omega - \omega_*)}{k_\parallel^2 V_A^2} = 0, \tag{3.2.41}$$

where V_A is Alfven wave velocity.

The plane drift Alfven mode is also unstable to modulations. The method explained in section 3.2.1 has been applied to the finite-β case [114–116]. Introducing the vector potential perturbation ψ (the component of the vector potential in the direction of main magnetic field), one writes the plane wave as $(\phi, \psi)_0 = (\phi_0, \psi_0)\exp(\mathrm{i}k_y y + \mathrm{i}k_\parallel z - \mathrm{i}\omega_0 t)$, where the subscript 0 stands for the primary wave with real frequency ω_0 given by (3.2.41). The modulational perturbation thus follows

$$\begin{pmatrix}\phi\\ \psi\end{pmatrix}_{\mathrm{m}} = \begin{pmatrix}\phi_{\mathrm{ZF}}\\ \psi_{\mathrm{ZF}}\end{pmatrix}\exp(\mathrm{i}q_x x - \mathrm{i}\Omega t) + \begin{pmatrix}\phi_+\\ \psi_+\end{pmatrix}\exp(\mathrm{i}q_x x + \mathrm{i}k_y y + \mathrm{i}k_\parallel z - \mathrm{i}\omega_+ t)$$
$$+ \begin{pmatrix}\phi_-\\ \psi_-\end{pmatrix}\exp(\mathrm{i}q_x x - \mathrm{i}k_y y - \mathrm{i}k_\parallel z - \mathrm{i}\omega_- t), \tag{3.2.42}$$

where ϕ_{ZF} is the electrostatic potential perturbation that induces zonal flow, ψ_{ZF} generates the zonal magnetic field, Ω is the frequency of the zonal flow and field, and (ϕ_+, ψ_+) and (ϕ_-, ψ_-) are the upper and lower drift-Alfven mode sidebands.

As was explained in section 3.2.1, nonlinearity induces the coupling between the primary wave and the modulations. In the electromagnetic case, the primary nonlinearities consist of the convective nonlinearity $V_\perp \cdot \nabla$ in the Lagrange time derivative, and the nonlinearity in $\nabla_\parallel$, due to the bending of magnetic field lines [117, 118]. A set of bilinear equations for the variables (ϕ_0, ψ_0), $(\phi_{\mathrm{ZF}}, \psi_{\mathrm{ZF}})$, (ϕ_+, ψ_+) and (ϕ_-, ψ_-) was derived. By using the estimate of $k_\parallel \sim 1/qR$, the growth rate of the zonal flow together with the zonal field $\gamma_{\mathrm{ZF}} = \mathrm{Im}\,\Omega$ is given by

$$y_{\mathrm{ZF}} = q_x k_y \rho_s^2 \omega_{\mathrm{ci}} |\phi_0| \left(M_A(1 - \hat{\omega}_0^2 k_y^2 \rho_s^2 \hat{\beta}) + M_B \hat{\omega}_0^2 q_x^2 k_2^2 \rho_s^4 \hat{\beta} - \frac{q_x^2 \rho_s^4 \hat{\omega}_0^2}{2L_n^2 |\phi_0|^2} \right)^{1/2} \tag{3.2.43}$$

with coefficients

$$M_{\mathrm{A}} = C^{-1}(1 - \hat{\omega}_0(2\hat{\omega}_0 - 1)k_y^2\rho_{\mathrm{s}}^2\hat{\beta} + (q_x^2 - k_y^2)k_\perp^{-2}(1 - \hat{\omega}_0^{-1} - k_y^2\rho_{\mathrm{s}}^2)),$$

$$M_{\mathrm{B}} = -2k_y^2C^{-1}k_\perp^{-2}(1 - \hat{\omega}_0^{-1} + k_y^2\rho_{\mathrm{s}}^2), \qquad C = 1 + k_y^2\rho_{\mathrm{s}}^2 - \hat{\omega}_0(3\hat{\omega}_0 - 2)k_y^2\rho_{\mathrm{s}}^2\hat{\beta},$$

where $|\phi_0| = |e\tilde{\phi}_0/T|$, $\hat{\omega}_0 = \omega_0/\omega*$ and $\hat{\beta} = \beta(qR/L_n)^2/2$ are used for convenience to elucidate finite-β effects. The coefficient $\hat{\beta}$ represents the ratio of the frequency to the shear-Alfven wave frequency, i.e. $(\omega_*/k_\| V_{\mathrm{A}})^2 \simeq k_y^2\rho_{\mathrm{s}}^2\hat{\beta}$.

This set of equations is cast in terms of the parameters we now list: the amplitude of the pump wave $|\phi_0| = |e\tilde{\phi}_0/T|$; the wavenumber of the pump wave $k_y\rho_{\mathrm{s}}$; the wavenumber of the zonal flow $q_x\rho_{\mathrm{s}}$; and the normalized pressure, $\hat{\beta}$. The fourth parameter appears as a result of finite β. In the limit of $\hat{\beta} \to 0$, the results of section 3.2.2 are recovered. In the limit of small $\hat{\beta}$, equation (3.2.43) tells that the growth rate of the zonal flow decreases as β increases. This has also been discussed in terms of 'Alfvenization' of the zonal flow drive [119]. In addition to the Reynolds stress, the divergence of the Maxwell stress is known to induce a force on plasmas. The signs of the divergences of the Reynolds stress and Maxwell stress are opposite for the drift-Alfven waves. For the shear-Alfven wave, the relation $\tilde{v} \propto \beta$ holds. This implies a cancellation of the Reynolds stress and Maxwell stress, and the consequent quenching of the zonal flow drive. Thus, the finite-β effect, which introduces a coupling between the shear-Alfven wave and drift wave, causes magnetic field perturbations that reduce the drive of the zonal flow for fixed value of $|\phi_0| = |e\tilde{\phi}_0/T|$. Equation (3.2.43) includes terms quadratic in $\hat{\beta}$, which exceed the linear term on $\hat{\beta}$, as $\hat{\beta}$ increases. In [115], it has been shown that the zonal flow growth rate starts to increase if $\hat{\beta}$ exceeds a critical value, $\hat{\beta} > \hat{\beta}_{\mathrm{c}}$, $\hat{\beta}_{\mathrm{c}} \simeq 2k_y^{-2}\rho_{\mathrm{s}}^{-2}$. The origin of the reduction of turbulent transport at the high beta value that has been observed in DNS [115] is attributed to this. We note here that an analogous effect in the theory of differential rotation in stars is referred to as 'omega (Ω) quenching.'

Another application of this type of analyses has been given for the Alfven ITG mode [120]. The same structure of modulational instability (3.2.9) was found [114] in that case.

(ii) Zonal magnetic field generation. The amplitude of the zonal magnetic field ψ_{ZF} is shown to 'seed' the growth of modulational instability [114]. This effect is important for zonal field growth. In the problem of the dynamo in space and astrophysical objects, the electric resistance by collisions along the field line is weak enough that zonal magnetic field generation can have substantial impact. The regime of low resistivity is also relevant to toroidal plasmas. In addition, nonlinear MHD instability, like the neoclassical tearing mode [121], which illustrates the critical role of the current profile in turbulent plasmas, can be 'seeded' by zonal field. Thus, the study of zonal magnetic field that is associated with, and similar to, the zonal flow has attracted attention.

An analysis of zonal field modulational instability is briefly illustrated here, and provides an introduction to further study of dynamo and field amplification problems. The equation for the 'mean field' is here considered to be that for the vector potential component in the direction of the strong (toroidal) magnetic field [122]. The equation is given by the $V_\|$ moment of the electron drift kinetic equation, which is:

$$(1 - \delta_{\mathrm{e}}^2\nabla_\perp^2)\frac{\partial}{\partial t}\psi_{\mathrm{ZF}} - \left\langle \tilde{E}_\| \frac{\tilde{n}}{n} \right\rangle + \frac{\partial}{\partial r}\Gamma_{J,r} = \eta_\| \nabla_\perp^2 \psi_{\mathrm{ZF}}. \qquad (3.2.44)$$

Here δ_{e} is the collisionless electron skin depth, c/ω_{pe}, $\langle \tilde{E}_\| \tilde{n}/n \rangle$ gives the average parallel acceleration, $\Gamma_{J,r}$ stands for the turbulent flux of current in the x direction, and $\eta_\|$ is the collisional resistivity. $\Gamma_{J,r}$ is closely related to the mean magnetic helicity flux. By using quasi-linear theory as applied to the drift-kinetic equation, the terms $\langle \tilde{E}_\parallel \tilde{n}/n \rangle$ and $\Gamma_{J,r}$, which contribute to the generation of the mean magnetic field, are easily shown to be

$$\left\langle \tilde{E}_\parallel \frac{\tilde{n}}{n} \right\rangle = -\frac{\pi T_\mathrm{e}}{e} \sum_k \frac{2k_\perp^2 \rho_\mathrm{s}^2}{2 + k_\perp^2 \rho_\mathrm{s}^2} \frac{k_\parallel}{|k_\parallel|} \omega_k^2 f_0 \left(\frac{\omega_k}{k_\parallel} \right) N_k, \tag{3.2.45}$$

$$\Gamma_{J,r} = \frac{\pi T_\mathrm{e}}{\Omega} \sum_k \frac{2k_\perp^2 \rho_\mathrm{s}^2}{2 + k_\perp^2 \rho_\mathrm{s}^2} \frac{k_y \omega_k^3}{k_\parallel |k_\parallel|} f_0 \left(\frac{\omega_k}{k_\parallel} \right) N_k, \tag{3.2.46}$$

where Ω is the time derivative of the zonal field, $(\partial/\partial t)\psi_\mathrm{ZF} = -\mathrm{i}\Omega\psi_\mathrm{ZF}$, $f_0(\omega_k/k_\parallel)$ is the unperturbed distribution function of plasma particles at the resonant phase velocity, $v_\parallel = \omega_k/k_\parallel$, and N_k is the action density of the kinetic shear-Alfven wave (i.e. the ratio of the wave energy density divided by the wave frequency) given by;

$$N_k = \frac{2 + k_\perp^2 \rho_\mathrm{s}^2}{2\omega_k} k_\perp^2 \rho_\mathrm{s}^2 \left| \frac{e\tilde{\phi}_k}{T_\mathrm{e}} \right|^2. \tag{3.2.47}$$

Note that $\Gamma_{J,r} \to 0$ as $k_\perp \rho \to 0$ (i.e. in the ideal MHD limit). This is a consequence of the fact that, on resonance, $\Gamma_{J,r} \propto |\tilde{E}_\parallel|^2$, which vanishes for ideal Alfven waves. Thus, zonal field dynamics are explicitly dependent on $\tilde{E}_\parallel$ of the underlying waves. As usual, N may be thought of as a wave population density. The sensitivity of the weighting factor to finite-gyro-radius effects is due to the influence of the dispersion relation $\omega_k^2 = k_\parallel^2 v_\mathrm{A}^2 (1 + k_\perp^2 \rho_\mathrm{s}^2)$ on the phase relation ψ/ϕ for kinetic shear-Alfven waves. The modulation of the action density N_k resulting in the imposition of a seed zonal magnetic field is calculated by the same procedure of section 3.2.2. The wave-packet evolves according to the WKE

$$\frac{\partial}{\partial t} N_k + v_\mathrm{g} \frac{\partial N}{\partial x} - \frac{\partial}{\partial x} \omega_k \cdot \frac{\partial N}{\partial k_x} = C(N), \tag{3.2.48}$$

where $C(N)$ stands for wave damping. The dispersion relation for the kinetic Alfven wave satisfies equation (3.2.41), and the group velocity is given as $v_{\mathrm{g},r} = k_\parallel^2 v_\mathrm{A}^2 \omega_k^{-1} k_x \rho_\mathrm{s}^2$. (The kinetic shear Alfven wave is a forward-going wave.) Therefore the perturbation in the wave frequency caused by the imposition of the zonal magnetic field δB_x is given by $\delta\omega_k \omega_k^{-1} = k_y k_\parallel^{-1} B_0^{-1} \delta B_x$, i.e. a simple modulation of Alfven speed, where B_0 stands for the unperturbed magnetic field and the relation $\delta k_\parallel = k_y \delta B_x B_0^{-1}$ is used. By use of this frequency modulation, the modulation of the wave action density δN_k is easily shown to be

$$\delta N_k = \frac{\mathrm{i}\omega_k}{\Omega - q_x v_{\mathrm{g},x} + \mathrm{i}\gamma_\mathrm{KSAW}} \frac{k_y}{k_\parallel} \frac{q_x^2 \delta\psi_\mathrm{ZF}}{B_0} \frac{\partial N_k}{\partial k_x}, \tag{3.2.49}$$

where damping rate γ_KSAW is introduced as $C(N) = \gamma_\mathrm{KSAW} N$ in equation (3.2.48). Substitution of equation (3.2.49) into equations (3.2.45) and (3.2.46) gives the response of $\langle \tilde{E}_\parallel \tilde{n}/n \rangle$ and $\Gamma_{J,r}$, to the imposition of ψ_ZF, i.e. $\delta\langle \tilde{E}_\parallel \tilde{n}/n \rangle$ and $\delta\Gamma_{J,r}$. If the forms of $\delta\langle \tilde{E}_\parallel \tilde{n}/n \rangle$ and $\delta\Gamma_{J,r}$ are substituted into equation (3.2.44), a closed equation for ψ_ZF follows. This equation determines the eigenvalue Ω, by which equation (3.2.44) is rewritten as

$$\frac{\partial}{\partial t} \psi_\mathrm{ZF} = -\mathrm{i}\Omega\psi_\mathrm{ZF} - \frac{q_\mathrm{r}^2 \eta_\parallel}{1 + q_\mathrm{r}^2 \delta_\mathrm{e}^2} \psi_\mathrm{ZF}. \tag{3.2.50}$$

The growth rate $\mathrm{Im}\,\Omega$ can be re-expressed as [122];

$$\mathrm{Im}\,\Omega = \frac{4\pi c_\mathrm{s}^2 \delta_\mathrm{e}^2 q_\mathrm{r}^2}{v_{\mathrm{th},e}(1 + q_\mathrm{r}^2 \delta_\mathrm{e}^2)} \sum_k \frac{(1 + k_\perp^2 \rho_\mathrm{s}^2)^{5/2}}{2 + k_\perp^2 \rho_\mathrm{s}^2} \frac{k_\perp^2 k_y^2}{|k_\parallel^2|} \frac{\partial^2}{\partial k_x^2} \left(\frac{\langle \omega_k N_k \rangle}{\sqrt{1 + k_\perp^2 \rho_\mathrm{s}^2}} \right) f_0. \tag{3.2.51}$$

This result has a similar structure to the case of zonal flow generation, equations (3.2.22) and (3.2.23) in its dependence on q_r^2, and on the wave population spectrum (i.e. the k_x—derivative of N_k). It shows that zonal magnetic field instability is driven by a negative slope of $\langle \omega_k N_k \rangle / \sqrt{1 + k_\perp^2 \rho_s^2}$. This condition is usually satisfied, without inversion of populations for Alfvenic MHD.

As was the case for zonal flow drive by drift waves, the drive of the zonal magnetic field is also subject to damping by the collisional resistivity. If the growth rate $\gamma_{\mathrm{ZF}} = \mathrm{Im}\,\Omega$ equation (3.2.50) exceeds the resistive damping rate, i.e. $\gamma_{\mathrm{ZF}} > q_r^2 \eta_\parallel / (1 + q_r^2 \delta_e^2)$, the zonal magnetic field grows. This driving mechanism of mesoscale magnetic perturbation by microscopic turbulence can have an impact on global MHD instabilities in toroidal plasmas by secondary perturbations, such as neoclassical tearing modes.

3.2.7. Comparison with MHD mean field dynamo theory. It is instructive to compare the results for zonal field growth with those of dynamo theory, in MHD, which is another outstanding problem in structure formation in an axial vector field due to turbulence.

In the mean field MHD dynamo theory, the mean magnetic field $\langle \boldsymbol{B} \rangle$ and vorticity $\langle \boldsymbol{\omega} \rangle$ evolve (for incompressible turbulence) according to: [60, 62, 63]

$$\frac{\mathrm{d}\langle \boldsymbol{B} \rangle}{\mathrm{d}t} = \nabla \times \langle \tilde{\boldsymbol{V}} \times \tilde{\boldsymbol{B}} \rangle + \eta_\parallel \nabla^2 \langle \boldsymbol{B} \rangle, \tag{3.2.52}$$

$$\frac{\mathrm{d}\langle \boldsymbol{\omega} \rangle}{\mathrm{d}t} = \nabla \times \left\langle \frac{\tilde{\boldsymbol{B}} \cdot \nabla \tilde{\boldsymbol{B}}}{4\pi n_i m_i} - \tilde{\boldsymbol{V}} \cdot \nabla \tilde{\boldsymbol{V}} \right\rangle + \nu \nabla^2 \langle \boldsymbol{\omega} \rangle \tag{3.2.53}$$

where ν is a molecular viscosity. The essence of the mean field electrodynamic theory is to approximate the averages of the nonlinear terms, quadratic in fluctuation amplitude, by some effective transport coefficient times a mean field quantity. In many ways this procedure for a closure approximation is quite similar to the familiar case of quasilinear theory, which is a closure of the Vlasov hierarchy. While relatively minor, technical variations abound, most mean field dynamo theories predict

$$\frac{\mathrm{d}\langle \boldsymbol{B} \rangle}{\mathrm{d}t} = \nabla \times (\alpha \langle \tilde{\boldsymbol{B}} \rangle - \beta \langle \boldsymbol{J} \rangle) + \eta_\parallel \nabla^2 \langle \boldsymbol{B} \rangle, \tag{3.2.54}$$

$$\frac{\mathrm{d}\langle \boldsymbol{\omega} \rangle}{\mathrm{d}t} = \nu_{\mathrm{eff}} \nabla^2 \omega + \nu \nabla^2 \omega. \tag{3.2.55}$$

Here alpha (α) is the familiar pseudo-scalar, proportional to turbulent helicity, and β and ν_{eff} are turbulent resistivity and viscosity, respectively. Note that β is positive but ν_{eff} is *not* positive definite, since it is clear from equation (3.2.53) that turbulence effects on $\langle \omega \rangle$ must vanish if $\tilde{\boldsymbol{V}} = \tilde{\boldsymbol{B}} / \sqrt{4\pi n_i m_i}$, i.e. a state of maximal cross helicity. This is identical to the cancellation of the Reynolds and Maxwell stresses which occurs for zonal flow generation by Alfven waves. Additional contributions to $\langle \tilde{\boldsymbol{V}} \times \tilde{\boldsymbol{B}} \rangle$ and $\langle \tilde{\boldsymbol{B}} \cdot \nabla \tilde{\boldsymbol{B}} / 4\pi n_i m_i - \tilde{\boldsymbol{V}} \cdot \nabla \tilde{\boldsymbol{V}} \rangle$ may enter. These correspond to mean vorticity effects on $\langle \boldsymbol{B} \rangle$ and mean magnetic field effects on $\langle \omega \rangle$, respectively.

An important, relatively recent development in the theory of mean field electrodynamics was motivated by questions of self-consistency and conservation of magnetic helicity. These considerations together suggest that α should be quenched, as compared to its kinematic value, and that the quench should be proportional to the magnetic Reynolds number R_{M}. While this question is still controversial, both theory and computation suggest that

$$\alpha = \frac{\alpha_{\mathrm{kin}}}{(1 + R_M^\sigma \langle V_A \rangle^2 / \langle \tilde{V}^2 \rangle)}, \tag{3.2.56}$$

where α_{kin} is the kinematic alpha coefficient $\alpha_{\text{kin}} \simeq \langle \tilde{V} \cdot \tilde{\omega} \rangle \tau_{\text{c}}$, τ_{c}, is the correlation time and $\sigma \simeq 1$. It is useful to note that equation (3.2.56) may be rewritten as $\alpha = \alpha_{\text{kin}} \eta_{\parallel} / (\eta_{\parallel} + \tau_{\text{c}} \langle V_{\text{A}} \rangle^2)$. This expression emphasizes that mean field growth is ultimately tied to *collisional resistivity*, as it is only the latter which breaks the freezing-in of field and fluid in MHD.

(i) Correspondence of driving terms. Comparing the results of equation (3.2.51) with equation (3.2.54), one finds that the physics of zonal field generation in part (ii) of section 3.2.6 has a deep connection to the physics of mean field dynamos. In order to clarify the relation of zonal magnetic field generation, equations (3.2.51) and (3.2.51), to the MHD dynamo problem, equations (3.2.50) and (3.2.51) may be rewritten by the use of $B_\theta = \mathrm{d}\psi_{\text{ZF}}/\mathrm{d}r$, so

$$\frac{\partial}{\partial t} B_\theta = -\eta_{\text{ZF}} \nabla^2 B_\theta, \tag{3.2.57}$$

where

$$\eta_{\text{ZF}} = -\frac{4\pi c_{\text{s}}^2 \delta_{\text{e}}^2}{v_{\text{th,e}}(1 + q_{\text{r}}^2 \delta_{\text{e}}^2)} \sum_k \frac{(1 + k_\perp^2 \rho_{\text{s}}^2)^{5/2}}{2 + k_\perp^2 \rho_{\text{s}}^2} \frac{k_\perp^2 k_y^2}{|k_\parallel|} \frac{\partial^2}{\partial k_x^2} \left(\frac{\langle \omega_k N_k \rangle}{\sqrt{1 + k_\perp^2 \rho_{\text{s}}^2}} \right) f_0. \tag{3.2.58}$$

Here, the collisional resistivity $\eta_\parallel$ is dropped and the q_{r}^2 in equation (3.2.51) is rewritten as $-\nabla^2$, noting that the generated field depends only on the radius r. The sign of η_{ZF} (i.e. corresponding to a *negative resistivity*) is positive for 'normal', i.e. one with $\partial^2/\partial k_x^2 (\langle \omega_k N_k \rangle / \sqrt{1 + k_\perp^2 \rho_{\text{s}}^2}) < 0$, but becomes negative (corresponding to positive dissipation) if $\partial^2/\partial k_x^2 (\langle \omega_k N_k \rangle / \sqrt{1 + k_\perp^2 \rho_{\text{s}}^2}) > 0$, as for a population inversion. If one considers the $\beta \boldsymbol{J}$ term in equation (3.2.54), the induction equation can be written as

$$\left. \frac{\mathrm{d}\boldsymbol{B}}{\mathrm{d}t} \right|_{\beta\text{-dynamo}} = \beta \nabla^2 \boldsymbol{B}. \tag{3.2.59}$$

Comparing equations (3.2.57) and (3.2.59), one finds that the electromotive force for zonal field generation corresponds to the $\beta \boldsymbol{J}$ -term in the mean field induction equation. The driving takes the form of a *negative* coefficient η_{ZF} of turbulent resistivity. What is interesting is that the sign of the turbulent resistivity varies with the spectrum slope. Thus, the zonal field 'dynamo' is really a process of flux or current coalescence, somewhat akin to the inverse cascade of mean-square magnetic flux predicted for two-dimensional and three-dimensional reduced MHD. This process conserves total magnetic flux, unlike an alpha dynamo, which amplifies magnetic flux via the stretch–twist–fold cycle. Note that there is a clear correspondence between zonal flow and zonal field generation. Zonal field generation is, simply put, related to the inverse transfer of magnetic flux while zonal flow generation is related to the inverse transfer of fluid energy.

The relationship to the drive of zonal flow vorticity is also discussed. The growth of the zonal flow vorticity, e.g. equations (3.2.22) and (3.2.23). Comparing equations (3.2.22) with (3.2.55), we see that the drive of zonal flow vorticity by drift waves corresponds to a turbulent viscosity in mean field MHD (the first term in rhs of equation (3.2.55). As in the case of the magnetic field, the viscosity-like term ($D_{\text{rr}} \nabla^2 U_q$) in equation (3.2.22) has the opposite sign to the usual turbulent viscosity, *a la* Prandtl. The MHD dynamo theory has also shown that the zonal flow can be driven by the curvature of plasma current, and its possible role in the ITB formation has been discussed [123]. A corresponding term in the zonal flow problem will be obtained by retaining the ψ_{ZF}-term in equation (3.2.42) in calculating the evolution of ϕ_{ZF}. This is a subject for future research.

(ii) Other contrasts. *Mesoscale character.* The zonal magnetic field and zonal flow both have a mesoscale character. That is, while they can have a coherence length on a mesoscale, i.e. one which is equal to the system size, in the poloidal and toroidal directions along the magnetic field, the radial wave length can be as short as that of the microscopic fluctuations. In MHD dynamo theory, research has concentrated on the large scale dynamo (having a characteristic scale length of the system size) or on the small scale dynamo, which has a microscopic scale length usually set by the dissipation scale. The problem of the zonal field and zonal flow generation sits in an intermediate regime that connects both large and small scales. However, zonal structures are highly anisotropic.

In addition, the symmetry of the generated field also influences the turbulent driving terms. For instance, the generated zonal magnetic field in section 3.2.6 is dependent on only one radial dimension, and the toroidal magnetic field is unchanged. Under such constraints of symmetry, Cowling's theorem guarantees that an α-dynamo term cannot appear.

Collisionless dynamo. Both zonal magnetic field and zonal flow couple to collisionless dissipation. In the case of zonal fields, collisionless dissipation (i.e. in particular, Landau damping) regulates both magnetic helicity and current transport. This first, genuinely 'collisionless dynamo' theory is notable since Landau resonance is a natural alternative to resistive diffusion for decoupling the magnetic field and plasma, in low-collisionality regimes. Of course, one should also recognize that Landau damping is not a panacea for the problems confronting dynamo theory. For example, here, zonal magnetic field growth occurs via the product of the $|\tilde{E}_\parallel|^2$ spectrum and Landau damping, i.e. $\eta_{\mathrm{ZF}} \sim \sum |\tilde{E}_\parallel|^2 \delta(\omega - k_\parallel V_\parallel)$. As a consequence, zonal field growth is limited by the size of $\tilde{E}_\parallel$ (which vanishes in ideal MHD), since coupling of fields to particles enters via the latter. Thus in progressing from MHD to kinetics, one in a sense exchanges the 'freezing-in law' difficulty for the $\tilde{E}_\parallel \sim 0$ difficulty.

Tertiary instability. As is discussed in section 3.5, one possible route to zonal flow saturation is via generalized Kelvin–Helmholtz (GKH) instability of the flow. Such an instability is an example of a tertiary instability, i.e. parasitic instability driven by a secondary instability. We may speculate that the tertiary instability of the zonal field is similar to a 'micro-tearing mode', and is driven by relaxation of the current and temperature profile of the zonal field. Of course, given the narrow radial extent of the zonal field, such tertiary micro-tearing modes are almost certainly temperature gradient driven. Note that such instabilities will also produce zonal current filamentation, which may contribute to the seeding of neoclassical tearing modes, as well. More generally, tertiary micro-tearing instabilities offer another possible route to dynamo saturation. Of course, just as magnetic shear severely inhibits the GKH instability of zonal flows, it can also be expected to restrict the viability of tertiary micro-tearing. Detailed research on tertiary micro-tearing is necessary to quantitatively address the speculations presented here.

Role of global parameters in turbulent coefficients. One of the goals of the study of structure formation in turbulent media is to relate the turbulent driving coefficients (e.g. α, β, ν_{eff} in MHD turbulence theory, or γ_{ZF} and χ_{turb} in the problem of zonal flow and drift wave turbulence) to relevant dimensionless parameters characteristic of the system, such as ρ_{i}/a, Rayleigh number, Taylor number, etc. In this direction of research, explicit analytic formulae have been obtained for the problem of zonal flow and drift wave turbulence. This is a significant achievement of the cumulative research effort on turbulence theory. In addition, in this area of research, one can find cross-disciplinary similarities, such as transport suppression by the inhomogenous $E \times B$ flow and 'α -suppression' in MHD dynamo theory.

The noticeable difference in the sign of corresponding terms in the zonal flow problem and the dynamo problem may be viewed as originating from the differences in the nature of the turbulence. In the MHD dynamo, turbulent dynamo coefficients are evaluated based on three-dimensional turbulence, since the theory is constructed for a weak magnetic field. On the other hand, the turbulence which is analysed for the source of zonal flow is quasi-two-dimensional, on account of the strong toroidal field, which is externally imposed. The unification of the dynamo problem and the zonal flow problem is an outstanding key future challenge for turbulence theory.

3.3. Shearing and back reaction of flows on turbulence

In magnetized plasmas, if flow shear exists together with a pressure gradient (a source of turbulence) the flow shear may suppress the turbulence driven by pressure-gradient relaxation. The back reaction, by both externally generated and self-generated shear flow, on pressure-gradient-driven turbulence, is a key mechanism that governs the turbulent state and the transport. Of course, flow shear itself may be a source of instability, such as the familiar KH instability. However, magnetic shear tends to mitigate or quench velocity-shear-driven instabilities, so they are not of too great a concern to confinement systems.

3.3.1. Effect of flow shear on linear stability. The first step in analysing the back interaction of sheared flow on turbulence is linear stability theory. The linear effect of sheared flow on the pressure-gradient-driven instability has been exhaustively surveyed in the literature [16]. Indeed, the Richardson problem of shear flow and buoyancy, which leads to the definition of the Richardson number $R_{\mathrm{i}} \equiv (g/L_n)(\mathrm{d}V_y/\mathrm{d}x)^{-2}$, is a classic example of the competition between processes (i.e. density or potential temperature-gradient-driven buoyancy and shearing). (Here the gravity $\boldsymbol{g}$ is in the direction of density gradient, x-direction.) Readers are recommended to refer to [16] for details of the various linear mechanisms. Some key elementary processes are explained here.

One characteristic mechanism for shear suppression is via a deformation of the eigenfunction. In the presence of velocity shear, the eigenfunctions are deformed, so that the wave length in the direction of the gradient becomes smaller. As a result of this, the linear growth rate decreases. (In other words, the fundamental mode, which has the largest growth rate, is forced to couple to higher modes, which are much more stable than the fundamental.) Consideration of the symmetry explains how the stabilizing effect usually appears at second order in velocity shear, i.e. $\sim (\mathrm{d}V_y/\mathrm{d}x)^2$, so the stabilizing trend does not depend on the sign of $\mathrm{d}V_y/\mathrm{d}x$. This mechanism works for the Rayleigh–Benard instability in neutral fluids [124–126] and for plasma instabilities driven by pressure, density and temperature inhomogeneities [127–136]. For non-resonant or hydrodynamic process, stabilization is possible, if the heuristic condition

$$|V'_{E\times B}| \sim \gamma_{\mathrm{L}0} \tag{3.3.1}$$

is satisfied, where $\gamma_{\mathrm{L}0}$ is the linear growth rate in the limit of $V'_{E\times B} = 0$. It is *very important* to realize that *this is only an approximate criterion.* This order-of-magnitude estimate is consistent with the results of simulations of *linear dynamics* with sheared flow [19, 137].

In collisionless plasmas, another type of stabilization mechanism occurs via wave–particle resonance. The ion orbit can be modified by an inhomogeneous electric field, so Landau damping may be enhanced, and very strong ion Landau resonance takes place if the electric field shear is large enough [138]. For instance, ion Landau damping, which is usually a stabilizing effect, enters via the wave–particle resonant denominator $\mathrm{i}/(\omega - k_\parallel v_\parallel)$, so that wave–ion resonance occurs at $x_{\mathrm{i}} = \omega/v_{\mathrm{Th\,i}}k'_\parallel$ ($k'_\parallel = \partial k_\parallel/\partial x$). In the presence of sheared $\boldsymbol{E}\times\boldsymbol{B}$ flow, the shear flow Doppler shift renders the resonance equal to $\mathrm{i}/(\omega - k_\parallel v_\parallel - k_\theta x \partial V_\theta/\partial x)$. Then, with velocity shear, the ion Landau resonance point is shifted to $x_{\mathrm{i}} = \omega/(v_{\mathrm{Thi}}k'_\parallel + k_\theta \partial V_\theta/\partial x)$, so that the resonance is stronger. Thus, electric field shear can significantly enhance the effect of ion Landau damping. Drift reversal of trapped particles due to an inhomogeneous electric field also influences stability. The toroidal drift velocity of trapped ions is modified by a factor $(1 + 2u_g)$, where $u_g = \rho_{pi} v_{thi}^{-1} B_p^{-1} (dE_r/dr)$. If the condition $u_g < -\frac{1}{2}$ is satisfied, trapped particles drift as if the magnetic curvature were favourable. The trapped-ion mode is thus stabilized by drift reversal in the range of $u_g < -1$. Note that this stabilization mechanism is asymmetric with respect to the sign of E_r' [139].

If flow shear becomes too strong, KH-type instability may occur [126]. The evolution from drift instability to KH instability has been confirmed for drift wave–zonal flow and other plasma systems [131].

3.3.2. Effect on turbulence amplitude. In the model equation for a passive scalar advected by background fluctuations, the effects of rapidly changing fluctuations are included in the turbulent transport coefficient, which is a measure of turbulent mixing. The equation of the test field $\tilde{X}$ in the presence of the sheared flow thus has the form

$$\frac{\partial}{\partial t}\tilde{X} + \bar{V}_y(x)\frac{\partial}{\partial y}\tilde{X} - D\nabla^2\tilde{X} = \tilde{S}^{\text{ext}}, \tag{3.3.2}$$

where $\bar{V}_y(x)$ is the sheared flow in figure 6(*a*), D is the diffusion coefficient due to the small scale fluctuations, and $\tilde{S}^{\text{ext}}$ represents the source. The stretching of contours of constant test perturbations occurs, and the turbulence level (i.e. $\tilde{X}$), the cross-phase, and the flux are suppressed by $\partial\bar{V}_y/\partial x$ (i.e. E_r' in magnetized plasmas). The mean velocity is in the y-direction (poloidal direction), and is sheared in the x-direction (radial direction). The sheared velocity is expressed as

$$V_y = S_v x \tag{3.3.3}$$

in local coordinates. The flow shear is interpreted as $S_v = r\,\mathrm{d}(E_r/Br)/\mathrm{d}r$ in cylindrical geometry. The expression for toroidal plasmas has been derived [11] and is $S_v = (r/q)(\mathrm{d}/\mathrm{d}r)(qE_r/rB)$.

(i) Mean flow—constant stretching and decorrelation rate. We first consider the case where the mean flow shear S_v varies much more slowly than the autocorrelation time of turbulent fluctuations, and varies smoothly in space (i.e. on scales longer than that of the turbulence correlation function). In this case, S_v may be taken as constant. The influence of the convection term $\bar{V}_y(x)\partial/\partial y$ in equation (3.3.2) is treated by using shearing coordinates [140]. The Lagrangian time derivative in equation (3.3.2) is given as $\partial/\partial t + \bar{V}_y(x)\partial/\partial y \to \partial/\partial t + S_v x\partial/\partial y$. Shearing coordinates annihilate the operator $(\partial/\partial t + S_v x\partial/\partial y)$ via the transformation

$$k_x \to k_x^{(0)} + k_y S_v t, \tag{3.3.4}$$

where $k_x^{(0)}$ is defined at $t = 0$. Note that shearing coordinates are quite analogous to Roberts and Taylor twisted slicing coordinates, which annihilate the operator $\boldsymbol{B}\cdot\nabla$.

The increase in the perpendicular wavenumber is also observed in the laboratory frame. After time t, a circular element is stretched to an, the minor axis of which is given by $L_\perp = L/\sqrt{1 + S_v^2 t^2}$. The reduction in $L_\perp$ is equivalent to the growth of the perpendicular wavenumber, so that the characteristic perpendicular wavenumber for the test field $\tilde{X}$ is effectively enhanced by a factor $(1 + S_v^2 t^2)$ [9, 141–143],

$$k_{\perp\text{eff}}^2 = k_\perp^2(1 + S_v^2 t^2). \tag{3.3.5}$$

Again, this is quite analogous to the familiar expression for $k_\perp^2$ of ballooning modes, i.e. $k_\perp^2 = k_\theta^2(1 + \hat{s}^2(\theta - \theta_0)^2)$. Time-asymptotically, then

$$k_{\perp\mathrm{eff}} \propto k_\perp S_v t. \tag{3.3.6}$$

The change of the wavenumber is linear in time, i.e. *ballistic*.

The diffusivity D implies a random walk due to the background fluctuations. The influence of the shear flow on diffusivity will be discussed in section 3.6. One simple, direct method to determine the relevant time scales is to analyse the random motion in shearing coordinates. The correlation time τ_{cor} in the presence of random motion but in the absence of shear is $\tau_{\mathrm{cor}}^{-1} = k_\perp^2 D$, the wavenumber increases in time so that the correlation time becomes shorter in the presence of the shear flow, since $k_\perp$ is stretched, as shown in equation (3.3.9). Equation (3.3.6) holds for long times, if $k_\perp S_v t > 1$. Then the effective correlation time is just

$$\frac{1}{\tau_{\mathrm{cor,eff}}} = Dk^{(0)^2}(1 + S_v^2 \tau_{\mathrm{cor,eff}}^2). \tag{3.3.7}$$

Thus, if $S_v \tau_{\mathrm{cor,eff}} > 1$,

$$\frac{1}{\tau_{\mathrm{cor,eff}}} = k^{(0)^{2/3}} D^{1/3} S_v^{2/3}, \tag{3.3.8}$$

which is the enhanced decorrelation rate, resulting from the coupling of shearing and turbulent decorrelation. This result is similar to those of Dupree (1966) and Hirshman–Molvig (1979) [144], all of which involve decorrelation via scattering of action coupled to differentially rotating phase-space flow. If $S_v \tau_{\mathrm{cor,eff}} > 1$,

$$\frac{1}{\tau_{\mathrm{cor,eff}}} = k_\perp^{(0)^2} D(1 + S_v^2 \tau_{\mathrm{cor}}^{(0)^2} + \cdots), \tag{3.3.9}$$

which recovers the shear-free result. Note that the hybrid decorrelation due to the shear flow is effective if S_v reaches the level $Dk_{\perp 0}^2$. For a constant D, the relation

$$S_v \geqslant Dk_{\perp 0}^2 \tag{3.3.10}$$

indicates that decorrelation by shear flow is more effective than decorrelation by turbulent diffusion alone.

The reduction of the correlation length leads to suppression of the fluctuation amplitude of the test field $\tilde{X}$, as

$$\langle \tilde{X}^2 \rangle \approx \frac{1}{1 + S_v^2 \tau_{\mathrm{cor}}^2} \langle \tilde{X}^2 \rangle_{\mathrm{ref}} = \frac{1}{1 + S_v^2 \tau_{\mathrm{cor}}^2} \tau_{\mathrm{cor}}^{(0)} \lim_{\ell \to 0} S^{\mathrm{ext}}(\ell) \tag{3.3.11}$$

assuming that the magnitude of the source term $\lim_{\ell \to 0} S^{\mathrm{ext}}(\ell)$ is unaffected.

(ii) Random stretching and decorrelation rate. In the presence of zonal flows or the GAMs, the shearing velocity is *not* constant in time. Moreover, even a slowly varying ensemble of zonal flow modes can result in drift wave ray chaos due to overlap of $\Omega = q_{\mathrm{r}} v_{\mathrm{g}}$ resonances, thus validating the assumption of stochastic dynamics. As an analytic idealization then, we take S_v as a stochastic variable, $\langle S_v \rangle = 0$, where $\langle S_v \rangle$ is a long-time average of S_v, $\langle \ldots \rangle = \lim_{t \to \infty} t^{-1} \int_0^t \mathrm{d}t \ldots$ (see figure 10). We write

$$S_v = \gamma_v \sqrt{\tau_{\mathrm{ac}}} w(t), \tag{3.3.12}$$

where γ_v denotes the instantaneous magnitude of the zonal flow shear, $w(t)$ is the temporal coherence function and τ_{ac} is the autocorrelation time of the (random) zonal flow. Obviously $w(t)$ is constant for $t < \tau_{\mathrm{ac}}$ and fluctuates drastically for $t > \tau_{\mathrm{ac}}$.

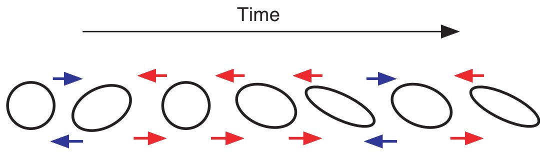

Figure 10. Random shearing flow and stretching. Shear flow (denoted by blue arrows or red arrows) is rapidly changing in time.

The stretching of an eddy in the y-direction is now a stochastic process. The statistical average is given by $\langle L_l^2 \rangle \approx L^2 + L^2 \gamma_v^2 \tau_{\mathrm{ac}} t$, or

$$\langle k_\perp^2 \rangle = k_\perp^{(0)^2} + D^{(K)} t, \qquad \text{where } D^{(K)} = k_\perp^{(0)^2} \gamma_v^2 \tau_{\mathrm{ac}}. \tag{3.3.13}$$

A similar argument as in the previous subsection applies to this diffusive shearing case. We have an equation for the decorrelation rate in the presence of the stochastic shear flow as

$$\frac{1}{\tau_{\mathrm{cor}}} = D k_\perp^{(0)^2} (1 + \gamma_v^2 \tau_{\mathrm{ac}} t) \tag{3.3.14}$$

and $\tau_{\mathrm{cor}}^{-1} \simeq D k_\perp^{(0)^2} \gamma_v^2 \tau_{\mathrm{ac}} t$ for long times. Thus, if $\tau_{\mathrm{cor}} > \gamma_v^{-2} \tau_{\mathrm{ac}}^{-1}$, we have

$$\frac{1}{\tau_{\mathrm{cor}}} \simeq (D k_\perp^{(0)^2} \gamma_v^2 \tau_{\mathrm{ac}})^{1/2}. \tag{3.3.15}$$

Note that this is a 'doubly diffusive' hybrid decorrelation rate, combining a random walk in radius with one in k_{r}. If, on the other hand, $\tau_{\mathrm{cor}} < \gamma_v^{-2} \tau_{\mathrm{ac}}^{-1}$, $\tau_{\mathrm{cor}}^{-1} \simeq D\, k_\perp^{(0)^2}$ as usual. It is important to note here that τ_{ac}, the autocorrelation time of the pattern of zonal flow shears that a drift wave-packet actually sees, is given by $\min\{\Delta\Omega, \Delta(q_{\mathrm{r}} v_{\mathrm{g}}(k))\}$. Thus, the strength of zonal flow induced shear decorrelation is sensitive to the structure of the zonal flow spectrum and zonal flow pattern.

(iii) Stochastic Doppler shift. There might be a case for which the radial wave length of the GAM is much longer than the wave length of the test mode, while the flow changes in time very rapidly. In such a case, in addition to the flow shear (as is discussed in (ii), in this subsection), the stochastic Doppler shift is also effective in reducing the turbulence level [16, 145–147].

In the forced stochastic oscillator equation (3.3.1), the Doppler shift term is given by the random Doppler shift,

$$\frac{\partial}{\partial t} \tilde{X}_k + \mathrm{i} \tilde{\omega}_k \tilde{X}_k - D_k \nabla^2 \tilde{X}_k = \tilde{S}_k^{\mathrm{ext}}. \tag{3.3.16}$$

The impact of stochastic frequency shift is characterized by the parameter

$$\Gamma_l = \tau_{\mathrm{ac},l} \langle \tilde{\omega}_k^2 \rangle, \tag{3.3.17}$$

where $\tau_{\mathrm{ac},l}$ is the autocorrelation time of the longer wavelength fluctuations $\tilde{v}_l$ [147].

In the limit of rapidly changing background fluctuations, $\tau_{\mathrm{ac},l} \ll \tau_{\mathrm{cor}}$, one obtains that the decorrelation of the test field occurs with the rate of $\tau_{\mathrm{cor}}^{-1} + \Gamma_l$. One then finds that the fluctuation level is suppressed by the stochastic Doppler shift due to the longer wavelength fluctuations. The suppression factor is

$$\frac{1}{1 + \tau_{\mathrm{D}} \Gamma_l} = \frac{1}{1 + \tau_{\mathrm{D}} \tau_{\mathrm{ac},l} \langle \tilde{\omega}_k^2 \rangle} \qquad (\text{for } \tau_{\mathrm{ac},l} \ll \tau_{\mathrm{D}}), \tag{3.3.18}$$

assuming that the source $\lim_{\ell \to 0} S^{\mathrm{ext}}(\ell)$ is unchanged.

In the large amplitude limit of random oscillation (or long correlation time $\tau_{\mathrm{ac},l}$), $\tau_{\mathrm{ac},l}^2\langle\tilde{\omega}_k^2\rangle > 1$, one has

$$I \sim \sqrt{\frac{\pi}{2}}\frac{1}{\sqrt{\langle\tilde{\omega}_k^2\rangle}}\lim_{\ell\to 0} S^{\mathrm{ext}}(\ell). \tag{3.3.19}$$

A reduction by the factor $1/\tau_{\mathrm{cor}}\sqrt{\langle\tilde{\omega}_k^2\rangle}$ is obtained.

3.3.3. Symmetry between zonal flow drive and turbulence suppression. After overviewing the back-interaction of flows on turbulence, we now visit the issue of symmetry between zonal flow drive and turbulence suppression.

When the drift waves are stochastic in time, the random stretching induces diffusion of drift wave fluctuations in k_{r} space. As is discussed in section 3.2.2, one then has

$$\frac{\partial}{\partial t}W_{\mathrm{drift}}\bigg|_{\mathrm{ZF}} = -\frac{\partial}{\partial t}W_{\mathrm{ZF}}\bigg|_{\mathrm{drift}} \tag{3.3.20}$$

for the drift wave energy, $W_{\mathrm{drift}} = \sum_k \omega_k\langle N_k\rangle$, and the kinetic energy of the zonal flow $W_{\mathrm{ZF}} = \sum_{q_x}\tilde{V}_{\mathrm{ZF},q_x}^2$.

From these considerations, we see that the symmetry between the coefficient α in equations (2.10*a*) and (2.10*b*) comes from the conservation of energy in the coupling between the drift wave fluctuations and zonal flow. The suppression of drift wave fluctuations by the shear associated with the zonal flow can be alternatively described as an energy transfer from drift wave fluctuations to zonal flow fluctuations. This relation holds for the case where the quasi-linear theory for N is applicable.

3.3.4. Poloidal asymmetry. While we focus almost exclusively on zonal flows which are symmetric in both the toroidal and poloidal directions in this review paper, sometimes it is necessary to take into account a weak poloidal variation of zonal flows, or a poloidally varying large-scale convective cell, when we study the shearing of smaller turbulence eddies by larger coherent structures. The examples include:

(i) Strong toroidal-rotation-induced centrifugal force can introduce the poloidal-angle dependence of the electrostatic potential associated with the mean $\boldsymbol{E}\times\boldsymbol{B}$ flow [148, 149].
(ii) Shearing of smaller-scale eddies by larger-scale convective cells ($n \sim m \sim \mathrm{O}(1)$) including a sideband of the zonal flow, such as $\phi_{n=0,m=1}$, etc.
(iii) Shearing of smaller-scale turbulence (originating from high-k instabilities) by larger-scale turbulence (originating from low-k instabilities); for instance, shearing of ETG or CDBM turbulence by ITG-TIM (trapped ion mode) turbulence. (A more detailed discussion is made in section 3.4.6.)
(iv) Poloidally inhomogeneous toroidal flow induced by pressure anisotropy [150].

Rapid poloidal variation (rather than radial) is associated with streamers, which are beyond the scope of this review, but briefly discussed in section 6. For these situations, one could construct a model problem of shearing by considering an electrostatic potential $\phi(r,\theta)$ which varies in both radius and poloidal angle. The relevant quantities are:

$$\omega_{E,rr} = -\frac{\partial^2}{\partial r^2}\phi(r,\theta), \qquad \omega_{E,\theta r} = -\frac{1}{r}\frac{\partial^2}{\partial\theta\partial r}\phi(r,\theta) \tag{3.3.21a}$$

$$\omega_{E,r\theta} = -\frac{\partial^2}{\partial rqr\partial\theta}\phi(r,\theta), \qquad \omega_{E,\theta\theta} = -\frac{1}{qr^2}\frac{\partial^2}{\partial\theta^2}\phi(r,\theta), \tag{3.3.21b}$$

where q is the safety factor. These illustrate the 'tensor' nature of the shearing ω_E by convective cells. From these generalizations, the standard theories of shearing, addressing the reduction of the radial correlation length, can be extended to study the deformations of eddies in every direction [151] including the change in the correlation length in the direction parallel to the magnetic field [150].

Following the procedure in [9], the two-point correlation evolution equation has been derived in general toroidal geometry [151]

$$\frac{\partial}{\partial t}C_{12} + \left\{(\psi_{-}\omega_{E,\psi\psi} + \eta_{-}\omega_{E,\theta\psi})\frac{\partial}{\partial\zeta_{-}} + (\psi_{-}\omega_{E,\psi\theta} + \eta_{-}\omega_{E,\theta\theta})\frac{\partial}{\partial\psi_{-}} - D_{\mathrm{eff}}\frac{\partial^2}{\partial\zeta_{-}^2}\right\}C_{12} = S_2. \tag{3.3.22}$$

Here, $C_{12} = \langle\delta H(1)\delta H(2)\rangle$ the correlation function of the fluctuating quantity δH, and D_{eff} is the ambient turbulence-induced relative diffusion of two nearby points: $(\psi_1, \eta_1, \zeta_1)$ and $(\psi_2, \eta_2, \zeta_2)$ in flux coordinates. Other notations follow those of [151]. In contrast to the usual case of a flux function $\phi(r)$, where only the radial shear of the $\boldsymbol{E}\times\boldsymbol{B}$ angular frequency (itself mainly in the poloidal direction), $\omega_{E,\psi\psi} = -\partial^2\phi/\partial\psi^2 = \partial(E_{\mathrm{r}}/RB_\theta)/\partial\psi$ appears in the two-point correlation evolution, equation (3.3.22) and describes the 'tensor' character of the shearing process when ϕ is a function of both ψ and $\theta\cdot\omega_{E,\alpha\beta}$ with subscripts ψ and θ for α, β is a natural flux coordinate generalization of equation (3.3.21). By taking the moments and following the standard procedure of calculating the exponentiation rate of two nearby points, one can derive that the shape of turbulent eddies are distorted due to the various components of the shear tensor in the following way [151]:

$$\Delta r^2 = \Delta r_0^2\left(1 + \frac{\omega_E^2}{\Delta\omega_k(\Delta\omega_k + \omega_{E,\psi\theta})}\right)^{-1} \quad \text{and} \quad \Delta\eta^2 = \Delta\eta_0^2\left(1 + \frac{(\Delta\eta_0/\Delta\zeta_0)^2\omega_{E,\theta\psi}^2}{\Delta\omega_k(\Delta\omega_k + \omega_{E,\psi\theta})}\right)^{-1}, \tag{3.3.23}$$

where $\Delta\omega_k$ is the decorrelation rate of ambient turbulence and $\omega_E = -(\Delta\psi_0/\Delta\zeta_0)(\partial^2\phi/\partial\psi^2)$ is the $\boldsymbol{E}\times\boldsymbol{B}$ shearing rate in general toroidal geometry [11]. Note that equation (3.3.23) shows the reduction in parallel correlation length due to poloidal asymmetry which has been found independently in [150]. The tensor character of the shearing process has been also recognized in the problem of the shearing of small ETG eddies by larger ITG eddies, which is discussed in section 3.4.6.

Unlike decorrelation via the shear in $\boldsymbol{E}\times\boldsymbol{B}$ zonal flow, it can be shown from the symmetry of the two-point correlation function that there is no net decorrelation mechanism due to the flow curvature associated with the second radial derivative of the zonal flow [152].

3.4. Nonlinear damping and saturation: low collisionality regimes

In this section, nonlinear mechanisms which limit or saturate the growth of zonal flows are described. Research in this direction has been particularly stimulated by the challenge of understanding how zonal flow growth is controlled in low or zero collisionality regimes, for which the energy density of zonal flows can substantially exceed the energy density of drift waves, i.e. $|\tilde{V}_{\mathrm{ZF}}^2| \gg \int \omega_k N_k\,\mathrm{d}k$. Several possibilities exist, including:

(a) Tertiary instability—i.e. a secondary instability of the zonal flow (itself a product of the secondary instability), rather like the familiar KH instability of a sheared flow. Such a tertiary KH instability will *return* energy to the $m \neq 0$ fluctuations, thus limiting zonal flow growth.

(b) Nonlinear wave-packet scattering—i.e. a process by which a drift wave-packet undergoes multiple nonlinear interactions with the zonal flow, thereby exchanging energy with, and regulating the growth of, the zonal flows. Such scattering processes are quite similar to nonlinear wave–particle interaction, familiar from weak turbulence theory. This process also returns energy to $m \neq 0$ fluctuations.

(c) nonlinear wave-packet trapping—i.e. the process by which modulational instability is saturated due to deflection of drift wave trajectories by finite amplitude zonal flows. This process is analogous to the trapping of particles by a finite amplitude waves in a Vlasov plasma, and acts to nonlinearly quench the zonal flow growth process by terminating the *input of energy* to the zonal flow.

(d) adjustment of system dynamics—i.e. an 'umbrella label' under which the various routes by which the system evolves toward a stationary state via adjustment of the global dynamics may be collectively described. Examples include the possibility of either multi-dimensional (i.e. repetitive bursts or limit cycle) or strange (i.e. chaotic) attractors, in contrast to the naively expected fixed point. Another possibility is adjustment (via predator–prey competition) to exploit available, albeit weak, dissipation. Generally, mechanisms in (d) work in synergy with mechanisms in (a)–(c).

		Degrees of freedom		Correlation time			
Sub-section	Key concept	Drift wave	Zonal flow	Drift wave	Zonal flow	Coherent structure	Next sub-section
3.4.1	Tertiary inst.	—	1	Long	Long	—	—
3.4.2	Dithering	Small	1	Long	Long	Dynamics	3.5.2
3.4.4	Diffusion model	Large	Large	Short	Short	No	3.5.3
3.4.5	Predator–prey model						3.5.1
3.4.6	Wave trapping	Large	Large	Long	Long	Yes	3.5.4
3.4.7	Collisionless satu.	Large	Large	Short	Long	Yes	3.5.5

3.4.1. Tertiary instability. One mechanism for nonlinear saturation of zonal flows is turbulent viscous damping of the flow, originating either from background drift wave turbulence, or from instability of the zonal flow. As the zonal flow is itself the product of a 'secondary' instability in the ensemble of 'primary' drift waves, instability of the zonal flow is called *tertiary* instability [153]. These tertiary instabilities of the flow may be thought of as GKH instabilities, which relax the profile of generalized potential vorticity and so mix and transport zonal flow momentum, thus damping the flow. Interest in GKH instabilities was sparked by consideration of the so-called Dimits shift regime, where the overwhelming preponderance of available free energy is channeled into zonal flows (i.e. $E_{\mathrm{ZF}}/E_{\mathrm{DW}} \simeq \gamma_{\mathrm{L}}/\gamma_{\mathrm{damp}}$), in turn, naturally raising the question of what sort of consideration of stability will *ultimately limit* zonal flow shears. Of course, proximity to, or excedence of, the GKH stability boundary results in the onset of momentum transport and turbulent viscosity.

The actual GKH is driven by both $\boldsymbol{E} \times \boldsymbol{B}$ velocity and ITGs, since both enter the total potential vorticity $\nabla^2(\phi + \tau T_{\mathrm{i}}/2)$ (where $\tau = T_{\mathrm{e}}/T_{\mathrm{i}}$). However, it is instructive to first consider the simpler limit of $\tau \to 0$. In that case, flute-like ($k_{\|} \to 0$) modes with low but finite m (i.e.

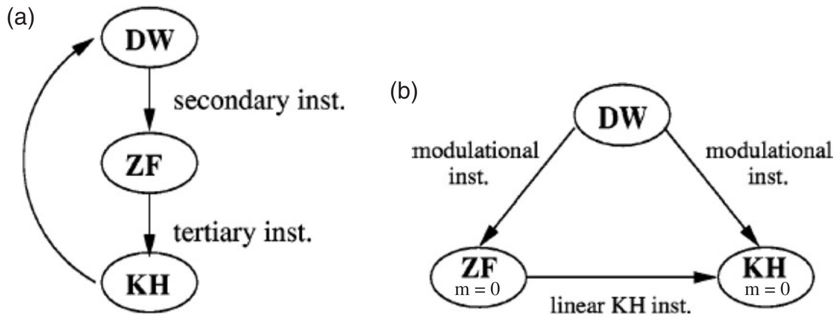

Figure 11. The contrast of the linear view of the GKH modes (*a*) to a more general case where GKH modes are generated by both linear and nonlinear modulational instabilities (*b*). The linear view is hierarchical in that GKH is generated by the linear instability of zonal flows (ZF), which are already generated by DW. In general, GKH modes can, however, be generated directly from DW by modulational instability.

$m \neq 0$) evolve according to

$$\left(\frac{\partial}{\partial t} + V_{\mathrm{ZF}} \cdot \nabla\right) \nabla^2 \phi_{\mathrm{KH}} + V_{\mathrm{KH}} \cdot \nabla \nabla^2 \phi_{\mathrm{ZF}} = \left(\frac{\partial^2}{\partial x^2} - \frac{\partial^2}{\partial y^2}\right) \langle \tilde{V}_x \tilde{V}_y \rangle + \frac{1}{2} \frac{\partial^2}{\partial x \partial y} (\langle \tilde{V}_y^2 \rangle - \langle \tilde{V}_x^2 \rangle). \tag{3.4.1}$$

Here the lhs describes the linear growth of the KH instabilities and the rhs represents drive by drift wave stresses. Equation (3.4.1) thus states that $m \neq 0$ GKH fluctuations (which transport and mix zonal flow momentum) can be excited *either* by instability of the zonal flow *or* by drift wave Reynolds stress. This suggests that, in contrast to the hierarchical scenario (figure 11(*a*)) of primary → secondary → tertiary instability described above, the process for generation of $m \neq 0$ modes may be non-hierarchical (figure 11(*b*)), whereby low but non-zero m modes are generated *both* by KH instability of the zonal flow *and* by modulational instability of the drift wave spectrum. The direct drive by drift waves is briefly discussed in section 6. The relative importance of the hierarchical and non-hierarchical scenarios is a topic of ongoing research. An existing result indicates that the modulational drive of $m \neq 0$ modes results in momentum transport significantly in excess of the KH driven transport, but further research into this question is necessary before reaching a definitive conclusion.

Regarding KH instabilities, it is instructive to start by considering a simple case with zonal potential $\phi_{\mathrm{ZF}} = \bar{\phi}\cos(q_x x)$, perturbed by a KH perturbation, $\phi_{\mathrm{KH}} = \sum_n \hat{\phi}_n \cos(n q_x x + q_y y)$ (q_x is the wavenumber of the zonal flow, and q_y is the poloidal wavenumber of the KH instability.) The perturbation is easily shown to grow at the rate

$$\gamma_{\mathrm{KH}}^2 = \bar{\phi}^2 q_x^2 q_y^2 \left(\frac{q_x^2 - q_y^2}{q_x^2 + q_y^2}\right). \tag{3.4.2}$$

Thus, $\gamma_{\mathrm{KH}} > 0$ requires $q_x^2 > q_y^2$, i.e. *the poloidal wavelength of the KH mode must exceed the radial scale of the zonal flow*. This of course favours long-wavelength instability. For $q_y^2 \ll q_x^2$, note that γ_{KH} reduces to $\gamma_{\mathrm{KH}} \sim |q_y V_{\mathrm{ZF}}|$. Note that γ_{KH} scales with V_{ZF}, not with $\mathrm{d}V_{\mathrm{ZF}}/\mathrm{d}x$ [104, 154].

Of course, the example discussed above is over-simplified, as it omits magnetic shear, electron dissipation, and many other effects. In particular, magnetic shear is quite strongly stabilizing, as it works against the interchange of vorticities at an inflection point, which is the basic mechanism of the KH and the elementary process which underlies the well-known Rayleigh inflection-point criterion. The strong sensitivity of the KH to magnetic shear is nicely illustrated later in section 4. (Figure 39 of section 4 shows the disruption of the zonal flow pattern in the regimes of weak magnetic shear and its persistence in regions of strong magnetic shear [54].) In order to examine the effect of shear on tertiary KH modes, the energy transfer budget and zonal flow pattern of a shearless and sheared system were compared in [155]. In the shear-free system, transfers of energy from zonal flows to drift waves occurred, and disruption of the zonal flow pattern was evident in the flow visualizations. In the sheared system, no back-transfer of energy occurred and the flow pattern persisted.

In the plasma of interest, $\tau \neq 0$, so the generalized potential vorticity is $\nabla^2(\Phi)$, where $\Phi \equiv \phi + \tau T_{\mathrm{i}}/2$. The system is described by the equations

$$\frac{\partial}{\partial t}\nabla^2\Phi + [\Phi, \nabla^2\Phi] = \frac{\tau^2}{4}[T, \nabla^2 T], \tag{3.4.3a}$$

$$\frac{\partial}{\partial t}T + [\Phi, T] = 0. \tag{3.4.3b}$$

Here $[g, h]$ is the Poission bracket. Note that, to the lowest order in τ, this system corresponds to a statement of conservation of potential vorticity in flows with generalized velocity $\boldsymbol{V} = \nabla\Phi \times \hat{z}$. Here, the temperature gradient, as well as $\boldsymbol{E} \times \boldsymbol{B}$ shear, can drive instability. A similar analysis as before gives

$$\gamma_{\mathrm{KH}}^2 = \frac{1}{2}\left(\bar{\phi} + \frac{\tau}{2}\bar{T}\right)^2 q_x^2 q_y^2 \left(\frac{q_x^2 - q_y^2}{q_x^2 + q_y^2}\right). \tag{3.4.4}$$

Note that the *phase* between the zonal potential and zonal temperature is *crucial* to the result. This phase is determined by several factors, including the zonal flow generation mechanism (i.e. which sets the ratio of growth for $\bar{\phi}$ and $\bar{T}$) and the Rosenbluth–Hinton damping mechanism (i.e. which suggests that certain values of phase damp more rapidly than others). While one study suggests a good correlation between the stability boundary for GKH and the termination of the Dimits shift regime (see, e.g. figure 37 in section 4 [156]), the parameter space for this problem has not been systematically explored, and so the 'bottom line' remains controversial. Moreover, other linear stability studies which retain ion Landau damping suggest that even for steep $\partial\bar{T}/\partial x$, tertiary instability growth is very weak and the scale of mixing is quite small [157]. Thus, tertiary instability and its effect on zonal flow saturation remain open problems, where further study is needed.

With these as yet inconclusive findings in mind, it is interesting to note that another, related, route to exciting momentum transport and the back-transfer of energy from zonal flows to waves exists and has not been explored. This mechanism exploits the situation that GKH modes, while not strongly unstable, are neither heavily damped, and the fact that noise emission from primary drift waves is abundant. Thus, one has a situation where noise is emitted into slow modes, sitting close to criticality, so that large transport can occur *without* linear instability. Moreover, the effective noise bath will be enhanced by self-consistent inclusion of GKH effects. Finally, noise emission can also produce localized defects in the flow, which in turn drive small-scale relaxation and momentum transport.

3.4.2. Model of small plane waves. As is explained in section 3.2.2, dynamics of a plane drift wave explain the zonal flow growth if the decorrelation rate of drift waves γ_{drift} is very small. Within this framework, one can construct a model composed of three drift waves and one zonal flow. The example of toroidal drift waves of section 3.2.2 is explained.

The quasi-linear effects of the secondary waves on the primary drift wave are given by [25]. Replacing variables from a set of [$\Phi_0(\xi)$, $\Phi_{\rm ZF}$, $\Phi_+(\xi)$ and $\Phi_-(\xi)$] to [P, Z, S and Ψ] which are defined as $P = \langle (e\Phi_0/T)^2\rangle$, $Z = \Phi_{\rm ZF}$ and $\Phi_+(\xi)/\Phi_0(\xi) = S\exp(\mathrm{i}\Psi)$ with suitable normalizations, a closed set of equations results are given as:

$$\frac{\mathrm{d}P}{\mathrm{d}\tau} = P - 2ZS\cos(\Psi), \tag{3.4.5a}$$

$$\frac{\mathrm{d}Z}{\mathrm{d}\tau} = -\frac{\gamma_{\rm damp}}{\gamma_{\rm L}}Z + 2PS\cos(\Psi), \tag{3.4.5b}$$

$$\frac{\mathrm{d}S}{\mathrm{d}\tau} = -\frac{\gamma_{\rm side}}{\gamma_{\rm L}}S + ZP\cos(\Psi), \tag{3.4.5c}$$

$$\frac{\mathrm{d}\Psi}{\mathrm{d}\tau} = \frac{(\omega_0 - \Omega_+)}{\gamma_{\rm L}} - \frac{ZP}{S}\sin(\Psi), \tag{3.4.5d}$$

where the normalized time is $\tau = \gamma_{\rm L}t$, $\gamma_{\rm L}$ is the linear growth rate of the primary mode, $\gamma_{\rm damp}$ is the collisional damping rate of the zonal flow, $\gamma_{\rm side}$ is the sideband damping rate and $\omega_0 - \Omega_+$ is the frequency mismatch of the sideband and primary mode.

Equations (3.4.5b)–(3.4.5d) describe the parametric excitation for a fixed pump amplitude. The coupling to the primary wave, equation (3.4.5a), describes the nonlinear stabilizing effect of the driven zonal flow on the growth rate of the zonal flow $\gamma_{\rm ZF}$. Reference [158] describes the fully nonlinear evolution of this type of system.

3.4.3. Nonlinear coupled equation for a large number of drift waves. If the number of excited drift wave modes are very small, so that the drift wave can be treated as a monochromatic pump, a simple model like section 3.4.2 applies. In real plasmas, however, the primary fluctuations (drift waves) have a large number of degrees of freedom, and an analysis treating the drift wave spectrum is necessary.

Equations (3.2.16) and (3.2.18) describe the coupled dynamics of the drift wave action and the vorticity of the zonal flow, $N_k = (1 + k_\perp^2\rho_{\rm s}^2)^2|\phi_k|^2$ and $U \equiv \mathrm{d}V_{\rm ZF}/\mathrm{d}r$, respectively. Taking into account of the collisional damping of zonal flow (section 3.1.3), the dynamical equation for the zonal flow vorticity

$$\left(\frac{\partial}{\partial t} + \gamma_{\rm damp}\right)U = \frac{\partial^2}{\partial r^2}\frac{c^2}{B^2}\int \mathrm{d}^2k\frac{k_\theta k_{\rm r}}{(1 + k_\perp^2\rho_{\rm s}^2)^2}N_k \tag{3.4.6}$$

and that of the drift wave spectral density

$$\frac{\partial}{\partial t}N_k + \boldsymbol{v}_{\rm g}\cdot\frac{\partial N_k}{\partial \boldsymbol{x}} - \frac{\partial\omega_{k0}}{\partial \boldsymbol{x}}\cdot\frac{\partial N_k}{\partial \boldsymbol{k}} - \gamma_{\rm drift}N_k = k_\theta\frac{\partial N_k}{\partial k_{\rm r}}U \tag{3.4.7}$$

are derived as before, where $\boldsymbol{v}_{\rm g} \equiv \partial\omega_k/\partial\boldsymbol{k}$ is the group velocity of the drift wave, and $\gamma_{\rm drift}$ represents the linear instability and the nonlinear damping rate that causes saturation of the drift wave (in the absence of zonal flow).

In the following subsections, the evolution of drift waves and zonal flow is explained in several limiting cases.

3.4.4. Diffusion limit. We first discuss the case where the autocorrelation time of the drift wave $\tau_{\rm ac,d}$ and that of the zonal flow $\tau_{\rm ac,ZF}$ are much shorter than the time scale determined by $\gamma_{\rm ZF}^{-1}$, where $\gamma_{\rm ZF}^{-1}$ is the characteristic time scale of the linear zonal flow instability. It is very important to keep in mind that we also use this ordering as a tractable model of the case where the zonal flow spectrum is slowly varying, but spatially complex. Thus, this limit is of broader interest than one may initially think. Note that the validity of the equivalence between spatial complexity and short autocorrelation time follows from the fact that it is the *net dispersion* in $\Omega - q_r v_{gr}$ which is of interest. Thus, even if $\Delta\Omega$ is small, the existence of fine scale zonal flows can guarantee that $\Delta(q v_{gr})$ is large, so that the zonal flow–drift wave autocorrelation time is correspondingly short. The autocorrelation time of the drift wave, $\tau_{\mathrm{ac,d}} \simeq \gamma_{\mathrm{drift}}^{-1}$, is determined by the drift wave self-nonlinearity, and is taken as prescribed in this review. The time scale orderings are written as

$$\gamma_{\mathrm{drift}} \gg \gamma_{\mathrm{ZF}}, \qquad \tau_{\mathrm{ac,ZF^{-1}}} \gg \gamma_{\mathrm{ZF}}. \tag{3.4.8}$$

In this case, the phase of each mode composing the drift wave fluctuation is considered to be random and the spectral density or modal number distribution function N_k is calculated (i.e. no phase information). Fourier components of the zonal flow, U_{q_r}, induce random Doppler shifts in the drift waves, because the autocorrelation time of U_{q_r} is short. The coefficient $k_\theta U$ in the rhs of equation (3.4.7) can be considered as a random frequency modulation.

The term $k_\theta U \partial N_k/\partial k_r$ in equation (3.4.7) changes rapidly in time and is approximated as random. The average within the 'long time scale', $\gamma_{\mathrm{ZF^{-1}}}$, is evaluated according to the analysis of section 3.3.2. By employing a quasi-linear treatment for random stretching from section 3.3.2(ii), one has [111] $k_\theta U(\partial N_k/\partial k_r) \simeq (\partial/\partial k_r)(D_{kk}(\partial N_k/\partial k_r))$, where D_{kk} is given by equation (3.2.29). For further simplification, the response of drift waves on the lhs of equation (3.4.7) can be rewritten, in terms of the linear growth term and nonlinear self-interaction term, as $(\partial N_k \partial t) + \boldsymbol{v}_g \cdot (\partial N_k/\partial \boldsymbol{x}) - (\partial\omega_{k0}/\partial \boldsymbol{x}) \cdot (\partial N_k/\partial \boldsymbol{k}) = \gamma_L N_k - \gamma_{NL} N_k$, where γ_L is the linear growth rate and γ_{NL} is the nonlinear damping rate. With this formal expression, equation (3.4.7) reduces to the diffusion equation for the drift wave spectrum

$$\left(\frac{\partial}{\partial t} - \gamma_L + \gamma_{NL}\right) N_k - \frac{\partial}{\partial k_r}\left(D_K \frac{\partial N_k}{\partial k_r}\right) = 0. \tag{3.4.9}$$

The evolution of the zonal flow is given by negative diffusion and collisional damping (as is explained in section 3.2.2), as

$$\left(\frac{\partial}{\partial t} + \gamma_{\mathrm{damp}}\right) |U_{q_r}|^2 = \frac{\partial^2}{\partial r^2} \sum_k D_q \frac{\partial}{\partial k_r} N_k |U_{q_r}|^2, \tag{3.4.10}$$

where the coefficient D_q is calculated in section 3.2.2 to be $D_q = B^{-2} k_\theta^2 k_r (1 + k_\perp^2 \rho_s^2)^{-2} R(q_r, k)$.

3.4.5. Predator–prey model. The system of equations (3.4.9) and (3.4.10) describes the interaction between the drift wave and zonal flow. This is an example of a two-component, self-regulating system. As the 'primary' fluctuation, the drift wave grows by its own instability mechanism. The drift wave fluctuation energy is transformed into the energy of the zonal flow via the secondary instability process. In this sense, a correspondence of the form:

$$\begin{aligned} &\text{drift wave fluctuation}\langle N\rangle = \sum_k N_k \leftrightarrow \text{prey} \\ &\text{zonal flow energy}\langle U^2\rangle = \sum_{q_r} |U_{q_r}|^2 \leftrightarrow \text{predator} \end{aligned} \tag{3.4.11}$$

holds.

A low degree of freedom model can be deduced from equations (3.4.9) and (3.4.10). In integrating equations (3.4.9) and (3.4.10) in wavenumber space, a Krook approximation is used to write: $\sum_k \partial/\partial k_r (D_{kk} \partial N_k/\partial k_r) \simeq -\alpha \langle U^2\rangle\langle N\rangle$. With this simplification, and by use of the energy concervation relation in section 3.3.3, equations (3.4.6) and (3.4.7) can be modelled as

$$\left(\frac{\partial}{\partial t} - \gamma_{\mathrm{L}} + \gamma_{\mathrm{N}}\right)\langle N\rangle = -\alpha\langle U^2\rangle\langle N\rangle, \tag{3.4.12}$$

$$\left(\frac{\partial}{\partial t} + \gamma_{\mathrm{damp}}\right)\langle U^2\rangle = \alpha\langle U^2\rangle\langle N\rangle, \tag{3.4.13}$$

where γ_{L} and γ_{NL} are typical numbers for the linear and nonlinear rates. As is explained, the collisional damping rate γ_{damp} does *not* depend on the scale q_{r}, as it is a drag, not a viscosity.

The evolution of the wave–zonal flow system critically depends on the nonlinear damping of drift waves. The simplest form of the nonlinear damping rate of the drift wave may be chosen as $\gamma_{\mathrm{NL}}\langle N\rangle = \gamma_2\langle N\rangle^2$. By these simplifications, one has a two-dimensional predator–prey model of the form

$$\frac{\partial}{\partial t}\langle N\rangle = \gamma_{\mathrm{L}}\langle N\rangle - \gamma_2\langle N\rangle^2 - \alpha\langle U^2\rangle\langle N\rangle, \tag{3.4.14}$$

$$\frac{\partial}{\partial t}\langle U^2\rangle = -\gamma_{\mathrm{damp}}\langle U^2\rangle + \alpha\langle U^2\rangle\langle N\rangle. \tag{3.4.15}$$

A tractable model with a small number of degrees of freedom can be constructed in the diffusion limit, as well.

3.4.6. Coherent nonlinear drift wave–zonal flow interactions (1)—wave trapping. The growth of the zonal flow is influenced by the finite amplitude zonal flow on the drift waves, even if tertiary instability is not induced. The presence of the zonal flow induces higher order deformation of the drift wave spectra, which causes the modification of the growth rate of the zonal flow. This is, of course, analogous to the modification of the distribution function structure due to nonlinear resonant particle dynamics in Vlasov plasma problems. An analogy holds, and may be summarized by:

Drift wave–zonal flow problem		One-dimensional Vlasov problem
N_k	$\leftrightarrow$	$\tilde{f}(v)$
k_{r}	$\leftrightarrow$	v
$k_\theta U(x)$	$\leftrightarrow$	$e\tilde{E}(x)$

(3.4.16)

where U is the vorticity of the zonal flow, $U = \partial V_{\mathrm{ZF}}/\partial x$. A more thorough comparison is summarized in table 5.

As in the case of particle trapping in a wave field, the trapping of drift wave-packet in the zonal flow field can take place. This phenomena thus has an influence on the evolution of zonal flow. Bounce motion of drift wave rays occurs, as is explained in appendix A. In this subsection, we review the nonlinear process that is relevant when the lifetime of the drift wave and that of zonal flow are long compared to both γ_{ZF} and the bounce frequency ω_{bounce} (the explicit form of which is given in appendix A), i.e. when

$$\gamma_{\mathrm{drift}} \ll \gamma_{\mathrm{ZF}}, \omega_{\mathrm{bounce}}, \qquad \tau_{\mathrm{ac,ZF}}^{-1} \ll \gamma_{\mathrm{ZF}}, \omega_{\mathrm{bounce}}. \tag{3.4.17}$$

This is the opposite limit to section 3.4.4, where waves and zonal flows are assumed to be randomized rapidly during their mutual interaction, as in the quasi-linear problem. Another limit is that the lifetime of drift waves is much shorter than the trapping time, but the coherence time of the zonal flow is longer than $\gamma_{\mathrm{ZF}}^{-1}$. This limit is discussed in the next subsection (section 3.4.7).

The coupled dynamical equations for the drift wave fluctuations and the zonal flow component are given following the argument of equations (3.4.6) and (3.4.7). The vorticity

Table 5. Analogy of one-dimensional Vlasov and drift wave–zonal flow problems.

	One-dimensional Vlasov plasma with Langmuir waves	Drift wave-packets in zonal flow field
Constituents	Particle	$\Leftrightarrow$ Drift wave-packet
	Langmuir wave spectrum	$\Leftrightarrow$ Zonal shear spectrum
	Particle velocity v	$\Leftrightarrow$ Packet group velocity v
	Real space x	$\Leftrightarrow$ Wavenumber k_x
Time scales		
Autocorrelation time τ_{ac}	$\min\left\{\left(k\Delta\left(\frac{\omega}{k}\right)\right)^{-1}, (\Delta(kv))^{-1}\right\}$	$\min\{(\Delta\Omega)^{-1}, (\Delta(q_x v_{\mathrm{g}}))^{-1}\}$
Nonlinear time	Trapping time $\left(\frac{e\tilde{\phi}_{\mathrm{L}}}{m}\right)^{-1}$	Turnover time $\tau_\perp = q_x \tilde{V}_{\mathrm{ZF}}, \omega_{\mathrm{bounce}}^{-1}$
Decorrelation time τ_{c}	$(k^2 D)^{-1/3}$	$\min\left\{\gamma_k^{-1}, k^2/D_k, \left(q_x^2 D_k \left(\frac{\mathrm{d}v_{\mathrm{g}}}{\mathrm{d}k}\right)^2\right)^{-1/3}\right\}$
Relaxation time	$\Delta v^2 D_v^{-1}$	$\frac{\Delta k^2}{D_k}$
Resonance	Wave-particle $\omega/k = v$	Wave-packet–shear flow
and		$v_{\mathrm{g}}(k) = \frac{\Omega}{q_x}$
irreversibility	Phase-space overlap $\leftrightarrow$ Orbit chaos	Group-shear resonance overlap $\leftrightarrow$ Ray chaos
Theoretical descriptions		
Stochasticity/quasi-linear	$\tau_{\mathrm{ac}} < \tau_\perp$, orbit chaos, Random acceleration Velocity diffusion	$\tau_{\mathrm{ac}} < \tau_\perp$, ray chaos, Random shearing Diffusive refraction
Weak turbulence	Induced scattering $\leftrightarrow$ Nonlinear Landau damping of particles	Induced scattering of wave-packets in zonal flow field
Coherent/trapping	$\tau_{\mathrm{ac}} > \tau_\perp$, particle bounce motion Trapping oscillations $\rightarrow$ BGK mode	$\tau_{\mathrm{ac}} > \tau_\perp$, ray trapping Ray trapping oscillations $\rightarrow$ BGK wave-packet
Trapping in turbulence	Granulations, clumps $\rightarrow$ Fokker–Planck drag	Wave population granulations $\rightarrow$ Wave kinetic drag

equation that relates the zonal flow to the wave population, (3.4.6) and the WKE, together form a nonlinear dynamical system

$$\left(\frac{\partial}{\partial t} + \gamma_{\mathrm{damp}}\right) U = \frac{\partial^2}{\partial r^2}\frac{1}{B^2}\int \mathrm{d}^2 k \frac{k_\theta k_{\mathrm{r}}}{(1 + k_\perp^2 \rho_{\mathrm{s}}^2)^2} N_k, \tag{3.4.18a}$$

$$\frac{\partial}{\partial t} N_k + \boldsymbol{v}_{\mathrm{g}} \cdot \frac{\partial N_k}{\partial \boldsymbol{x}} = k_\theta \frac{\partial N_k}{\partial k_{\mathrm{r}}}(1 + k_\perp^2 \rho_{\mathrm{i}}^2) U, \tag{3.4.18b}$$

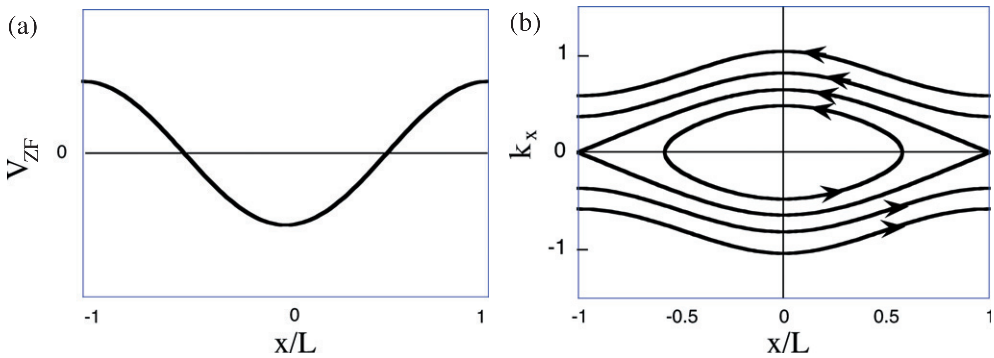

Figure 12. Trapping of wave-packets in the trough of zonal flow velocity. The spatial profile of zonal flow velocity (*a*) and trajectories in phase-space (*b*).

where the 'screening' effect of a finite gyro-radius is retained, $\bar{U} = U + \rho_s^2 \, \mathrm{d}^2U/\mathrm{d}r^2$. In comparison with equation (3.4.7), the linear growth and nonlinear damping of drift waves are dropped, because the case of coherent waves is studied here.

This set of equations (3.4.18*a*) and (3.4.18*b*) has a similar structure to the Vlasov equation that describes wave–particle interactions (such as plasma waves, etc). The term $k_\theta U(x)$ in equation (3.4.18*b*) is the counterpart of acceleration in the phase-space. That is, equation (3.4.18*b*) has a similar structure to the one-dimensional Vlasov equation, and equation (3.4.18*b*) is the analogue of the Poisson equation. With this analogy in mind, one can study a (Bernstein–Greene–Kruskal) BGK-like solution with finite-amplitude zonal flow.

Consideration of drift wave ray dynamics (details are given in [38]) leads us to conclude that the drift wave-packet can be labelled by the two invariants of motion ω_{k0} and k_{y0}, i.e. $\omega_k - uk_x - k_y \bar{V}_{\mathrm{ZF}} \equiv \omega_{k0}$ and $k_y = k_{y0}$, where u is a uniform velocity $\partial/\partial t \to -u\partial/\partial x$. Note that the wavefrequency ω_k and the wavenumber k_x are modified along the path of the drift wave-packet according to the relation which is simply the dispersion relation

$$\omega_k = k_{y0}(1 + k_{y0}^2 + k_x^2)^{-1}. \tag{3.4.19}$$

By use of these two integrals of motion, (ω_{k0} and k_{y0}), an exact solution for the distribution function is given in the form:

$$N(x, k_x, k_y) = N(\omega_{k0}(x, k_x), k_{y0}). \tag{3.4.20}$$

The trapping of the drift wave-packet occurs in the trough of the zonal flow, as is explained in [38]. Figure 12 illustrates the rays of drift wave-packets in phase-space for the case in which the screened velocity $\bar{V}_{\mathrm{ZF}}$ has a sinusoidal dependence in the x-direction. The trapped region is determined by the difference $\Delta\bar{V}_{\mathrm{ZF}}$ between the maximum and minimum of $\bar{V}_{\mathrm{ZF}}$. The wavenumber on the separatrix at the minimum of $\bar{V}_{\mathrm{ZF}}$ is given as $k_{x0,\mathrm{sep}}^2 = \Delta\bar{V}_{\mathrm{ZF}}(1 + k_{y0}^2)^2(1 - \Delta\bar{V}_{\mathrm{ZF}}(1 + k_{y0}^2))^{-1}$ for a simple case of stationary zonal flow structure. Wave-packets which satisfy $k_{x0}^2 < k_{x0,\mathrm{sep}}^2$ are trapped in the inhomogeneous zonal flow. The bounce frequency at the bottom of the trough is seen to be

$$\omega_{\mathrm{bounce}} = \sqrt{\frac{2\rho_s^2 k_y q_r}{1 + \rho_s^2 k_y^2}\omega_{k0}\frac{\mathrm{d}\bar{V}_{\mathrm{ZF}}}{\mathrm{d}r}}. \tag{3.4.21}$$

As is the case for the trapping of resonant particles by waves in collisionless plasmas, the bounce frequency of quasi-particles (wave-packets) has a dependence like $\omega_{\mathrm{bounce}} \propto \sqrt{V_{\mathrm{ZF}}}$. The bounce frequency becomes lower as the trajectory approaches the separatrix. The assumption in this line of thought, equation (3.4.17), means that $\gamma_{\mathrm{drift}} < \omega_{\mathrm{bounce}}$ is necessary in order that wave-packet trapping is relevant. Thus, trapping of wave-packets is particularly important near marginal stability of the drift waves.

If the trapping of the wave-packet is effective, the growth of the zonal flow stops. On a trapped trajectory, the distribution function tends to approach the same value. The distribution function N_k finally recovers a symmetry with respect to k_{r}, and the rhs of equation (3.4.18*a*) vanishes. The trapping of the drift wave tends to terminate the growth of the zonal flow.

3.4.7. Coherent nonlinear drift wave–zonal flow interactions (2)—zonal flow quenching. If the zonal flow has a long lifetime, it is possible to form a coherent spatial structure through a strongly nonlinear deformation of the drift wave population density. However, the condition of equation (3.4.17) does not always hold. That is, the autocorrelation time of drift waves can be shorter than the lifetime of zonal flow structures while the zonal flows maintain their coherence, i.e.

$$\gamma_{\mathrm{drift}} > \gamma_{\mathrm{ZF}}, \omega_{\mathrm{bounce}}, \qquad \tau_{\mathrm{ac,ZF^{-1}}} \ll \gamma_{\mathrm{ZF}}. \tag{3.4.22}$$

In this subsection, we study the case where the turbulent drift wave spectrum forms a spatially coherent zonal flow structure.

The WKEs as in section 3.4.4, equation (3.4.18*a*) and equation (3.4.18*b*), are employed. An asymmetric part of N_k with respect to k_x, $\hat{N}_k$, contributes to the time evolution of U through equation (3.4.18*a*). Solving equation (3.4.18*b*) and expressing $\hat{N}_k$ in the form of a perturbation expansion

$$\hat{N}_k = \hat{N}_k^{(1)}(U) + \hat{N}_k^{(2)}(U^2) + \hat{N}_k^{(3)}(U^3) + \cdots \tag{3.4.23}$$

and substituting it into equation (3.4.18*a*), a nonlinear equation of the zonal flow vorticity U is obtained. The linear response has been obtained, as is explained in section 3.2.1, i.e. $\hat{N}_k^{(1)} = (\partial/\partial r)(k_\theta V_{\mathrm{c}})R(q_{\mathrm{r}}, \Omega)(\partial N_k/\partial k_{\mathrm{r}})$, where $R(q_{\mathrm{r}}, \Omega) = \mathrm{i}/(\Omega - q_{\mathrm{r}}v_{\mathrm{g}} + \mathrm{i}\gamma_{\mathrm{drift}})$ is the response function. Equation (3.4.23) is based on a formal expansion in the parameter $UR(q_{\mathrm{r}}, \Omega) \simeq U/\gamma_{\mathrm{drift}}$, which is ordered as small. Thus, all resonance functions, both $R(q_{\mathrm{r}}, \Omega) = \mathrm{i}/(\Omega - q_{\mathrm{r}}v_{\mathrm{g}} + \mathrm{i}\gamma_{\mathrm{drift}})$, and those corresponding to higher resonances, reduce to the simple form $R(q_{\mathrm{r}}, \Omega) \sim 1/\gamma_{\mathrm{drift}}$. Note that this approximation clearly fails, close to marginal stability of the primary drift waves, where $\gamma_{\mathrm{drift}} \to 0$. For $\gamma_{\mathrm{drift}} < \Delta(\Omega - q_{\mathrm{r}}v_{\mathrm{g}})$, resonance structure becomes important, and the analogue of phase-space density granulations form in N.

For a wide spectrum of fluctuations, one has $R(q_{\mathrm{r}}, \Omega) \to 1/\gamma_{\mathrm{drift}}$ and obtains the leading diffusion term of equation (3.2.23) of section 3.2.2. The contribution from the second-order term is small (from the considerations of symmetry), so the first contributing order is the third-order term:

$$\hat{N}_k^{(3)} \simeq U^3 R(q_{\mathrm{r}}, \Omega)^3 k_\theta^3 \frac{\partial^3 N_k}{\partial k_{\mathrm{r}}^3}. \tag{3.4.24}$$

Note that this is equivalent to the contribution which gives nonlinear Landau damping in the Vlasov problem. Recall that nonlinear Landau damping is also third order in the perturbation amplitude, involves contributions at beat wave resonances where $\omega + \omega' = (k + k')v$ and thus may be obtained from 'higher-order quasi-linear theory'. Substituting equation (3.4.24) into equation (3.4.18*a*), one obtains a nonlinear equation for the drift wave vorticity [159]

$$\frac{\partial}{\partial t}U = -D_{rr}\frac{\partial^2}{\partial r^2}U + D_3\frac{\partial^2}{\partial r^2}U^3 - \gamma_{\mathrm{damp}}U \tag{3.4.25}$$

with $D_3 = -B^{-2}\int \mathrm{d}^2k R(q_{\mathrm{r}}, \Omega)^3 k_\theta^4 k_{\mathrm{r}}(1 + k_\perp^2\rho_{\mathrm{s}}^2)^{-2}\partial^3 N_k/\partial k_{\mathrm{r}}^3$. As the spectral function is peaked near $k_{\mathrm{r}} \simeq 0$, the sign in the definition of D_3 is chosen such that D_3 is positive when D_{rr} is positive.

The quenching of the drive of the zonal flow is a characteristic mechanism in the problem of generation of the axial-vector field through turbulent transport of energy (such as dynamo problems). In the case of magnetic field generation via a dynamo, the α-suppression problem has been investigated [160]. Equation (3.4.25) is an explicit expression for the quench of the driving force of the axial vector field.

Equation (3.4.25) governs the dynamics of the (coherent) structure of the zonal flow. Further exploration of this result follows below. As is derived in section 3.2, the zonal flow growth rate γ_{ZF} (the first term in the rhs of equation (3.4.25)) behaves like: $\gamma_{\mathrm{ZF}} = D_{rr}q_{\mathrm{r}}^2 \times(1-q_{\mathrm{r}}^2/q_{r0}^2)$. Damping is induced by collisional processes (section 3.1.3) and by the turbulent diffusion of a secondary parallel flow (section 3.2.6), via $\gamma_{\mathrm{damp}} = \gamma_{\mathrm{damp}}^{\mathrm{coll}} + \mu_{\|}(1+2q^2)q_{\mathrm{r}}^2$, where $\gamma_{\mathrm{damp}}^{\mathrm{coll}}$ is the collisional damping explained in section 3.1.3, $\mu_{\|}$ is the turbulent shear viscosity for the flow along the field line, and q is the safety factor. (The coefficient $1 + 2q^2$ can take a slightly different form, depending on the plasma parameters.) Thus, equation (3.4.25) can be written in the explicit form

$$\frac{\partial}{\partial t}U + D_{rr}\left(\frac{\partial^2}{\partial r^2}U + q_{r0}^{-2}\frac{\partial^4}{\partial r^4}U\right) - D_3\frac{\partial^2}{\partial r^2}U^3 - \mu_{\|}(1+2q^2)\frac{\partial^2}{\partial r^2}U + \gamma_{\mathrm{damp}}^{\mathrm{coll}}U = 0. \tag{3.4.26}$$

Equation (3.4.26) states that the zonal flow is generated by the background turbulence and is stabilized by collisional damping, higher order dispersion and by the nonlinearity.

3.4.8. A unifying framework—shearing and wave kinetics. Building upon the studies of particular nonlinear mechanisms in various limiting cases, which are explained individually in the preceding subsections, we now propose a unifying framework for understanding the zonal flow problem. This framework is one of shearing and wave kinetics.

We now discuss the physics of stochastic shearing of primary drift waves by a spatio-temporally complex spectrum of zonal flows, in particular, and also survey the wave kinetics of drift waves in a slowly evolving spectrum of zonal flows, in general. Extensive use is made of an instructive and far-reaching analogy between the wave kinetics of a drift wave-packet in a zonal flow field and the kinetics of a particle in a Langmuir wave field in a one-dimensional Vlasov plasma. On account of the particular symmetry of the zonal flow field, both the drift wave–zonal flow and the one-dimensional Vlasov problem can be reduced to two-dimensional phase-space dynamics, for x, V and x, k_{r}, respectively. In each case, the effective frequency of the motion $\omega(J)$ is a function of the action variable J, so that the dynamics are non-degenerate, and differentially rotating flow in phase-space results. The analogy enables a unification of many analyses of shearing effects, both in the stochastic and coherent regimes. Of course, shearing dynamics are of great interest, as they constitute the mechanism by which the zonal flows regulate transport and turbulence levels, and thus merit detailed attention.

The analogy between zonal flow and Vlasov plasma is motivated by the observation of the obvious similarities between the WKE for $N(\boldsymbol{k},\boldsymbol{x},t)$ in the presence of a zonal flow spectrum $|\tilde{V}_q|^2$ and the Boltzmann equation for $f(\boldsymbol{V},\boldsymbol{x},t)$ in the presence of a Langmuir wave spectrum $|\tilde{E}_{k,\omega}|^2$. These equations are

$$\frac{\partial}{\partial t}N + v_{\mathrm{g}}\cdot\frac{\partial N}{\partial x} - \frac{\partial}{\partial x}(k_y\tilde{V})\cdot\frac{\partial N}{\partial k_x} = C(N) = \gamma_{\mathrm{drift}}N \tag{3.4.27a}$$

and

$$\frac{\partial}{\partial t}f + V\cdot\frac{\partial f}{\partial x} - \frac{\partial}{\partial x}\left(\frac{e}{m}\tilde{\phi}\right)\cdot\frac{\partial f}{\partial v} = C(f), \tag{3.4.27b}$$

where $\tilde{E}_{k,\omega} = -\partial\tilde{\phi}_{\rm L}/\partial x$ for Langmuir wave turbulence. (The subscript L stands for the Langmuir waves.) The analogy is summarized in table 5, which we now discuss. Rather clearly, the analogue of the 'particle' with velocity $\boldsymbol{v}$ in the Vlasov case is the drift wave-packet with group velocity $\boldsymbol{v}_{\rm g}(k)$, which is sheared by the zonal flow field $\tilde{V}$, itself the analogue of the Langmuir wave field. The analogue of the Boltzmann collision integral $C(f)$, which maintains a near-Maxwellian average distribution function is the wave kinetic collision integral $C(N)$, taken to have the form $\gamma_{\rm drift}N = \gamma_k N - \Delta\omega_k N^2 N_0^{-1}$ in some cases which require an equilibrium spectrum of turbulence in the absence of zonal flows.

Aspects of the dynamics can be elucidated by consideration of resonances and time scales. The analogue of the well-known wave–particle resonance $\omega/k = V$ is that for which the phase velocity of the shearing flows equals the wave-packet group velocity $v_{\rm g}(k) = \Omega/q_x$. Just as in the particle case, chaos occurs when the zonal flow–wave group resonances overlap, resulting in stochastic drift–wave-ray dynamics. Stochasticity of ray trajectories provides the crucial element of *irreversibility* in the drift wave–zonal flow interactions. Note that since zonal flow energy is concentrated at very low frequency, while the dispersion in $v_{\rm g}(k)$ is large, overlap of $v_{\rm g}(k) = \Omega/q_x$ resonances occurs at quite modest zonal flow amplitudes. Such a state of *ray chaos* naturally necessitates a stochastic description. At least four time scales govern both the wave–particle and zonal shear–wave group dynamics. These are:

(i) The spectral autocorrelation times $\tau_{\rm ac}$. In the case of the Vlasov plasma, $\tau_{\rm ac} = \min\{(k\Delta(\omega/k))^{-1}, V\Delta k\}$. These times correspond to the lifetimes of the instantaneous electric field pattern 'seen' or traversed by a particle. For the zonal shear,

$$\tau_{\rm ac} = \min\{(\Delta\Omega)^{-1}, (\Delta(q_x v_{\rm g}))^{-1}\}. \tag{3.4.28}$$

Here, $(\Delta\Omega)^{-1}$ gives the flow pattern lifetime, which is usually quite long, since $\Omega \sim 0$. However, the dispersion in the Doppler frequency shift of the wave in a propagating packet (i.e. $\Delta(q_x v_{\rm g})$) is usually quite large, resulting in short autocorrelation time, and suggests that a stochastic analysis is relevant. It is important to again stress the fact that no *a priori* postulate of randomness or noise in the zonal flow spectrum is required, since the origin of stochasticity lies in the overlap of mode-flow resonance, and *not* in any random phase assumption.

(ii) The nonlinear orbit times, which correspond to the vortex circulation times in phase or eikonal space. These correspond to the particle bounce or trapping time $(e\tilde{\phi}_{\rm L}/m)^{-1}$ in the case of the Vlasov plasma, and the shearing rate of a fluid element in a zonal flow,

$$\tau_\perp = (q_x\tilde{V}_{\rm ZF})^{-1} \tag{3.4.29}$$

or the bounce time $(\omega_{\rm bounce}^{-1})$ of a trapped wave-packet, equation (3.4.21), whichever is shorter. In the event that resonances do not overlap, and that the nonlinear orbit time is shorter than the autocorrelation time, a coherent interaction analysis of the dynamics is required.

(iii) The nonlinear decorrelation time, which quantifies the scattering time for an individual trajectory of coherence time for a resonant triad. For the Vlasov plasma, $\tau_{\rm c} = (k^2 D_{\rm V})^{-1/3}$, the well-known result first obtained by Dupree. Here $D_{\rm V}$ is the quasi-linear diffusivity in velocity space. For the zonal amplification problem,

$$\tau_{\rm c} = \min\left\{\gamma_k^{-1}, k^2/D_k, \left(q_x^2 D_k\left(\frac{{\rm d}v_{\rm g}}{{\rm dk}}\right)^2\right)^{-1/3}\right\}. \tag{3.4.30}$$

Here γ_k controls the triad coherence time. Note that γ_k appears in place of a nonlinear self-decorrelation rate $\Delta\omega_k$ via the requirement that $C(N) = 0$, to determine in N the absence of zonal flow. $D_k k^{-2}$ is the rate of diffusive scattering (i.e. random refraction) and $(q_x^2 D_k({\rm d}v_{\rm g}/{\rm d}k)^2)^{1/3}$ is the analogue of the Dupree decorrelation $(k^2 D_{\rm V})^{1/3}$ rate for a ray in a dispersive medium. (Note that D_k has the dimension of m^{-2} s^{-1}.) This arises as a

Table 6. Regimes of zonal flow–wave kinetics.

Regime	Chirikov overlap parameter $S = \Delta v_g/\Delta(\Omega/q_x)$	Kubo number $K = \tau_{ac}/\tau_\perp$	Dominant physical process
Stochastic	$S > 1$	$K \ll 1$	Stochastic rays, random shearing and refraction
Turbulent trapping	$S > 1$	$K \leqslant 1$	Stochastic rays, shearing with granulated N
Coherent	$S \ll 1$	$K > 1$	Strongly deflected rays, wave-packet trapping
BGK solution		$K \to \infty$	Wave-packet trapping
Single wave	$S \to 0$	$K \to 0$	Modulational instability

consequence of coupling between scattering in k_x (due to D_k) and the propagation at the wave group speed $v_g(k)$.

(iv) the time scale for evolution of the average population density, i.e. the macroscopic relaxation time. For the Vlasov plasma, this is $\tau_{relax} = \Delta v^2 D_V^{-1}$, where Δv is the extent of phase velocities excited, and D_V is the quasi-linear velocity space diffusion coefficient. Similarly, for the zonal flow problem,

$$\tau_{relax} = \frac{\Delta k^2}{D_k}. \tag{3.4.31}$$

The possible dynamical states of the system are classified by the ordering of the various time scales, and by whether or not the trajectories are chaotic. The four basic time scales can nearly always be ordered as

$$\min(\tau_{ac}, \tau_\perp) < \max(\tau_{ac}, \tau_\perp) \leqslant \tau_c < \tau_{relax}. \tag{3.4.32}$$

Thus, the possible system states can be classified by:

(i) The Chirikov overlap parameter

$$\mathsf{S} = \frac{\Delta v_g}{\Delta(\Omega/q_r)}. \tag{3.4.33}$$

Here, Δv_g is the width of the wave group–zonal shear resonance, and $\Delta(\Omega/q_r)$ is the spacing between resonances.

(ii) The effective Kubo number

$$\mathsf{K} = \frac{\tau_{ac}}{\tau_\perp}, \tag{3.4.34}$$

the ratio of the autocorrelation time τ_{ac} to the zonal flow shearing time $\tau_\perp$.

These ratios immediately divide the system states into three categories, which are analysed in table 6. For $\mathsf{S} > 1$ and $\mathsf{K} \ll 1$, the dynamics are stochastic, with stochastic rays, and random shearing and refraction of drift waves by zonal flows constituting the principal effect of zonal flows on the turbulence. This regime may be treated by using the method of quasi-linear theory, yielding a picture of diffusive refraction (section 3.5.4). Extensions to higher order expansions in population density perturbations $\tilde{N}$ have been implemented, and are analogous to induced scattering (i.e. nonlinear Landau damping), familiar from weak turbulence theory for the Vlasov plasma. (section 3.5.7 discusses such an extension.) For $\mathsf{S} \ll 1$ and $\mathsf{K} > 1$, the dynamics are coherent, with strongly deflected rays tracing vorticities in the (x, k_x) space. In this regime,

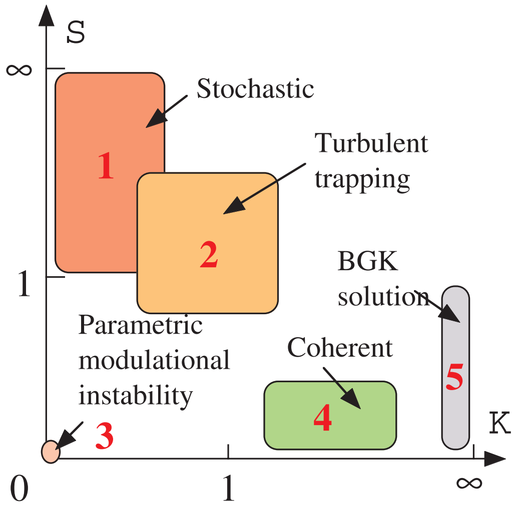

Figure 13. Parameter domains for various theoretical approaches.

the wave population density evolution will exhibit oscillations due to the 'bouncing' of trapped rays, and will asymptote to the formation of wave-packets corresponding to BGK solutions of the WKE. In this regime, zonal flow shear and wave-packets adjust to form a self-trapping state. (Section 3.5.6. Some extensions are discussed in section 6.) A third regime is that with $\mathsf{S} > 1$ and $\mathsf{K} \leqslant 1$, which corresponds to the regime of turbulent trapping. The dynamics here resembles those of the stochastic regime, except that consistent with $\mathsf{K} \leqslant 1$, closely separated wave-packets remain correlated for times $t > \tau_c$. These correlated, small-scale packets are analogous to clumps in the one-dimensional Vlasov plasma, and result in granulation of the wave-packet population density N. Such granulations necessitate the calculation of a Fokker–Planck drag, as well as diffusion, for describing the evolution of $\langle N \rangle$, i.e. the long time average. (This issue is discussed in section 6.) Likewise, self-trapped wave-packets correspond to holes or cavitons in the Vlasov plasma. Figure 13 illustrates the parameter domain and various theoretical approaches.

Having outlined the general structure of the dynamics of shearing in wave kinetics, we now proceed to discuss the regime of stochastic ray dynamics in some detail. Here, we are primarily concerned with the evolution of the mean drift wave population $\langle N(k, t) \rangle$ in the presence of the zonal flow spectrum. The salient features of the stochastic dynamics regime are given in table 7, along with their analogies for the one-dimensional Vlasov turbulence problem. Averaging the WKE yields the mean field equation for $\langle N \rangle$

$$\frac{\partial}{\partial t}\langle N \rangle - \frac{\partial}{\partial k_r}\left\langle \frac{\partial}{\partial x}(k_\theta \tilde{V}) N \right\rangle = \langle C(N) \rangle, \tag{3.4.35}$$

where the mean refraction-induced flux of $\langle N \rangle$ in k_r is given by

$$\Gamma_{k_r} = \left\langle \frac{\partial}{\partial x}(k_\theta \tilde{V}) N \right\rangle = -\mathrm{i} \sum_{q_x} q_x k_\theta \tilde{V}_{-q} \tilde{N}_q. \tag{3.4.36}$$

Proceeding in the spirit of quasi-linear theory, the expression for $\Gamma_{k_r} = \langle (\partial/\partial x)(k_\theta \tilde{V}) N \rangle = -\mathrm{i} \sum_{q_x} q_x k_\theta \tilde{V}_{-q} \tilde{N}_q$ may be calculated by iteratively substituting the response of N to V, $\delta N/\delta \tilde{V}$. Proceeding as in section 3.2, $\tilde{N}_q = q_x k_\theta \tilde{V}_q (\Omega - q_x v_g + \mathrm{i}\gamma_{\mathrm{drift}})^{-1} \partial \langle N \rangle / \partial k_x$, so that

Table 7. Comparison of stochastic dynamics.

Particles in electrostatic wave spectrum	Drift wave in zonal flow field
Diffusion coefficient	
$D_{\mathrm{r}} = \sum_k \frac{e^2}{m^2} \lvert\tilde{E}_k\rvert^2 R(k,\omega)$	$D_x = \sum_{q_x} q_x^2 k_\theta^2 \lvert\tilde{V}_q\rvert^2 R(k, q_x)$
Resonance function	
$R(k,\omega_k) = \frac{\tau_{\mathrm{c},k}^{-1}}{(\omega - kv)^2 + \tau_{\mathrm{c},k}^{-2}}$	$R(k, q_x) = \frac{\gamma_{\mathrm{drift}}}{(\Omega - q_x v_{\mathrm{g}})^2 + \gamma_{\mathrm{drift}}^2}$
Scattering field	
Wave spectrum	Zonal shear spectrum
$\sum_k \lvert\tilde{E}_k\rvert^2$	$\lvert V'_{\mathrm{ZF}}\rvert^2 = \sum_k q_x^2 \lvert\tilde{V}_{\mathrm{ZF},q}\rvert^2$
Scattered field	
Particle $v \to f(v)$	Drift wave-packet $v_{\mathrm{g}}(\boldsymbol{k}) \to N(\boldsymbol{k})$
Spectral autocorrelation rates	
$\Delta\omega^{-1} \leftrightarrow$ time for fastest slowest waves to cross	$\left(q_x \left(\frac{\mathrm{d}v_{\mathrm{g}}}{\mathrm{d}k}\right) \Delta k\right)^{-1} \leftrightarrow$ time for wave-packet to disperse while crossing flow layer
Nonlinear decorrelation rate τ_{c}^{-1}	
$k^2 D_{\mathrm{r}}$	$\max\left\{\gamma_k, D_k k^{-2}, \left(q_x^2 D_k \left(\frac{\mathrm{d}v_{\mathrm{g}}}{\mathrm{d}k}\right)^2\right)^{1/3}\right\}$
Time for particle to scatter one wave length	Lowest of times for wave-packets to diffuse one wavenumber, or to scatter through a zonal flow scale by wavenumber diffusion and propagation, or persistence time of triad

the wavenumber space flux is

$$\Gamma_{k_{\mathrm{r}}} = -D_{k_{\mathrm{r}}} \frac{\partial \langle N \rangle}{\partial k_x} \tag{3.4.37}$$

with the k-space diffusion coefficient

$$D_{k_{\mathrm{r}}} = \sum_{q_x} q_x^2 k_\theta^2 |\tilde{V}_q|^2 R(k, q_x) \tag{3.4.38}$$

and resonance function $R(k, q_x) = \gamma_{\mathrm{drift}}((\Omega - q_x v_{\mathrm{g}})^2 + \gamma_{\mathrm{drift}}^2)^{-1}$. As noted above, the resonance in question is that between the drift wave-packet with group speed $v_{\mathrm{g}}(k)$ and the phase speed of the zonal shear Ω/q_x. It is interesting to observe that this resonance appears as a limiting case of the well-known three-wave resonance denominator

$$R_{\boldsymbol{k},\boldsymbol{q},\boldsymbol{k+q}} = \frac{\mathrm{i}}{\omega_{\boldsymbol{k}} + \omega_{\boldsymbol{q}} - \omega_{\boldsymbol{k+q}} + \mathrm{i}(\Delta\omega_{\boldsymbol{k}} + \Delta\omega_{\boldsymbol{q}} + \Delta\omega_{\boldsymbol{k+q}})}. \tag{3.4.39}$$

Expanding for $|\boldsymbol{q}| < |\boldsymbol{k}|$ and replacing the broadenings by γ_{drift} then yields $R_{\boldsymbol{k},\boldsymbol{q},\boldsymbol{k+q}} = \mathrm{i}(\omega_{\boldsymbol{q}} - \boldsymbol{q} \cdot \partial\omega_{\boldsymbol{k}}/\partial\boldsymbol{k} + \mathrm{i}\gamma_{\mathrm{drift}})^{-1}$. Finally, specializing to the case $\boldsymbol{q} = q_x\hat{x}$ and rewriting $\omega_{\boldsymbol{q}} = \Omega$ then finally gives $R_{\boldsymbol{k},\boldsymbol{q},\boldsymbol{k+q}} = \mathrm{i}(\Omega - q_x v_{\mathrm{g}} + \mathrm{i}\gamma_{\mathrm{drift}})^{-1} = R(k, q_x)$. The diffusion equation for $\langle N \rangle$ may also be straightforwardly derived by a Fokker–Planck calculation. Here, one should recall that, in the absence of additional physics, the analogue of Liouvilles theorem for a stochastic Hamiltonian system implies a partial cancellation between diffusion and drag terms, leaving a result equivalent to the quasi-linear equation derived above.

Table 8. Short summary of theoretical method and description in this subsection.

Theoretical method	Nonlinear process and subsections in section 3.4	Self-consistent state explained in section 3.5
Parametric	Tertiary inst.; 3.4.1	—
instability	Dithering; 3.4.2	3.5.2
Random phase	Predator–prey; 3.4.5	3.5.1
approximation	Diffusion model; 3.4.4	3.5.3
Coherent structure	Wave trapping; 3.4.6	3.5.4
	Saturation; 3.4.7	3.4.5

In the stochastic regime, the evolution of the drift wave spectrum is simple. The k_r spectrum spreads diffusively, with $\langle \delta k_\mathrm{r}^2 \rangle = D_k t$. The random walk to larger k_r just reflects the random shearing at work on waves. The self-consistent dynamics of the drift wave–zonal flow system are then described by the mean field equation for $\langle N \rangle$ (rewriting equation (3.4.35))

$$\frac{\partial}{\partial t}\langle N \rangle - \frac{\partial}{\partial k_\mathrm{r}} D_k \frac{\partial}{\partial k_\mathrm{r}} \langle N \rangle = \langle C(N) \rangle \tag{3.4.40}$$

with equation (3.4.38) and equations for the zonal flow intensity evolution.

3.5. The drift wave–zonal flow system: self-consistent state

In previous subsections, elementary processes for zonal flow dynamics were explained. These included the linear damping process, the bilinear growth process, the back-reaction of zonal flows on drift waves, the nonlinear saturation mechanism and electromagnetic effects. Combining these elementary processes as building blocks, self-consistent states of the system are now discussed. As in the description in section 3.4, explanations here are given which note the differences in the number of degrees of freedom and in the correlation times of drift waves and zonal flows. Useful modelling of self-consistent states depends on these key factors, and the correspondence is listed in table 8.

First, models with few degrees-of-freedom are explained by focusing on two examples. One is the quite generic predator–prey model (section 3.4.5), which is valid for the case where many drift wave modes and zonal flow components are randomly excited, and their correlation times are much shorter than the characteristic time of evolution of the system. This basic model is explained in section 3.5.1. The other is the opposite case where only one drift wave is unstable (with sideband modes linearly stable). The coupled modes are thus assumed to have long coherence times (section 3.4.2), as in simple dynamical systems such as the Lorenz model. This case is explained in section 3.5.2

Next, more detailed descriptions follow. The spectral shape is of considerable importance (as discussed in sections 3.4.3 and 3.4.4), and is explained within the scope of the induced diffusion model in section 3.5.3. Coherent spatial structure is discussed in sections 3.5.4 and 3.5.5. These discussions correspond to the nonlinear mechanisms in section 3.4.6 and section 3.4.7, respectively.

3.5.1. Predator–prey model. Drift waves excite zonal flows, while zonal flows suppress drift waves. The degree of excitation or suppression depends upon the amplitudes of the drift wave and zonal flow. These interactions are modelled as a predator–prey dynamical system, for zonal flow mean square shear $\langle U^2 \rangle = \sum_{q_\mathrm{r}} |U_{q_\mathrm{r}}|^2$ and drift wave population density $\langle N \rangle = \sum_k N_k$ (see equation (3.4.9) and (3.4.10)).

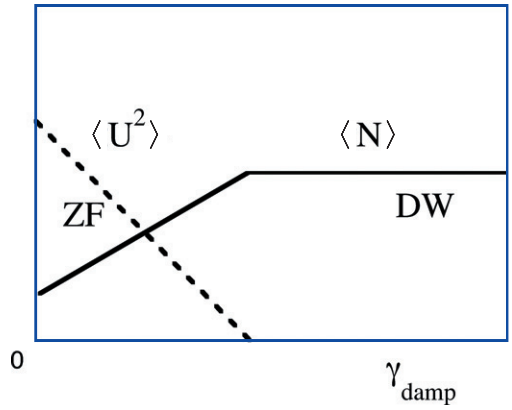

Figure 14. Amplitude of drift waves $\langle N\rangle$ and that of zonal flow $\langle U^2\rangle$ for the case where the self-nonlinear stabilization effect of zonal flow (e.g. the $\gamma_{\mathrm{NL}}(V^2)$ term in equation (2.10*b*)) exists. It shows the γ_{damp}-dependence with fixed γ_{L}.

(i) Stationary states. This system of equations (3.4.14) and (3.4.15) has two types of steady-state solution. One is the solution without zonal flow $\langle N\rangle = \gamma_{\mathrm{L}}/\gamma_2$, $\langle U^2\rangle = 0$, which results in the case of strong damping of the zonal flow, $\gamma_{\mathrm{damp}} > \alpha\gamma_{\mathrm{L}}/\gamma_2$. The other is the state with zonal flow, $\langle N\rangle = \gamma_{\mathrm{damp}}/\alpha$, $\langle U^2\rangle = \alpha^{-1}(\gamma_{\mathrm{L}} - \gamma_2\gamma_{\mathrm{damp}}\alpha^{-1})$, which is relevant when the damping rate of the zonal flow is weak,

$$0 < \gamma_{\mathrm{damp}} < \frac{\alpha}{\gamma_2}\gamma_{\mathrm{L}}. \tag{3.5.1}$$

(The case of $\gamma_{\mathrm{damp}} = 0$ needs special consideration, as is explained later.)

This system is controlled by two important parameters, i.e. the linear growth rate of the drift wave γ_{L} and the damping rate of the zonal flow γ_{damp}. In the region of low zonal flow damping rate (as for equation (3.5.1)), the zonal flow coexists with the drift wave. The other important result is the role of $(\gamma_{\mathrm{L}}, \gamma_{\mathrm{damp}})$ in determining the partition of the energy. In the region of low collisionality, where the zonal flow is excited, the drift wave amplitude is independent of the linear growth rate γ_{L}, but is controlled by the zonal flow damping rate γ_{damp}. The magnitude of the zonal flow increases if γ_{L} increases. The dependence on γ_{L} illustrates the importance of the self-nonlinearity effect of the zonal flow, which is discussed in equation (2.11). By the use of a generic form $\gamma_{\mathrm{NL}}(U^2) \sim \alpha_2 U^2$, the partition of energy between the waves and zonal flows appears in equation (2.12). The dependencies are shown, in figure 14, for the case of fixed γ_{L}, when the self-nonlinearity effect is present. The predator–prey model thus explains the most prominent features of the role of zonal flows in determining system behaviour. The possible shift of the boundary for the appearance of turbulence from $\gamma_{\mathrm{L}} = 0$ to $\gamma_{\mathrm{L}} = \gamma_{\mathrm{excite}} > 0$ (so-called Dimits shift for ITG turbulence) is discussed later.

(ii) Dynamical behaviour. Equations (3.4.14) and (3.4.15) also describe the characteristic dynamics of the system. The fixed points equations (2.12) are stable for a wide range of parameters. In some particular circumstances, different types of dynamics appear, as is categorized in [161].

Stable fixed point. At first, the stability of fixed points is explained. In cases where all of the coefficients (i.e. $\gamma_{\mathrm{L}}, \gamma_{\mathrm{damp}}, \alpha, \gamma_2$) are non-negative values, $\gamma_{\mathrm{L}} \neq 0, \gamma_{\mathrm{damp}} \neq 0$, $\alpha \neq 0, \gamma_2 \neq 0$, the fixed points are stable. For instance, the perturbation near the stationary

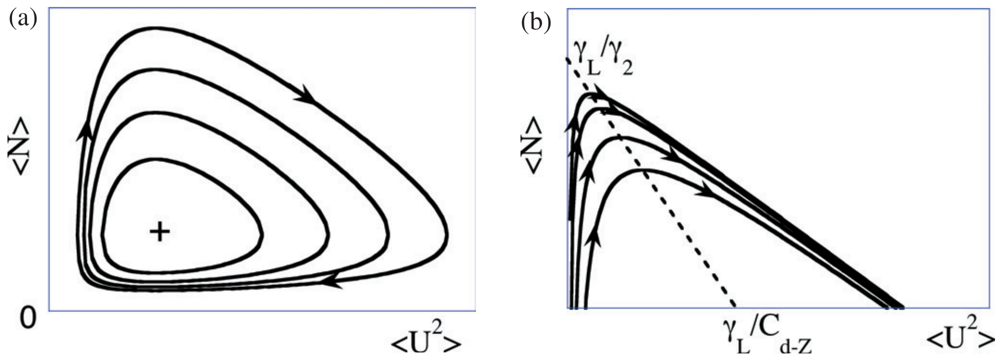

Figure 15. Phase portrait in the absence of nonlinear stabilization effect of drift waves, $\gamma_2 = 0$, [16] (*a*). Trajectory in the case of no zonal flow damping $\gamma_{\rm damp} = 0$ is shown in (*b*). Depending on the initial conditions, the system reaches different final states, in which the waves are quenched.

state,$\{\delta\langle N\rangle, \delta\langle U^2\}\rangle \propto \exp(\mathrm{i}\omega t)$ shows a damped oscillation with the frequency

$$\omega = \frac{-\mathrm{i}\gamma_{\rm damp}\gamma_2 + \mathrm{i}\sqrt{\gamma_{\rm damp}^2\gamma_2^2 - 4\gamma_{\rm damp}\gamma_{\rm L}(\alpha^2 - \alpha)}}{2\alpha}. \tag{3.5.2}$$

The imaginary part of ω is negative. Equation (3.5.2) predicts a stable fixed point. Depending on the initial conditions, transient oscillations of drift wave and zonal flow can occur. However, they decay in time and the system converges to a stationary solution.

Repetitive bursts. When the nonlinear self-stabilization effect of the drift waves is absent, i.e. $\gamma_2 = 0$, periodic bursts of the wave and flow occur. In this case, equations (3.4.14) and (3.4.15) have an integral of the motion; namely

$$\langle N\rangle - \frac{\gamma_{\rm damp}}{\gamma_{\rm L}}\ln\langle N\rangle + \langle U^2\rangle - \ln\langle U^2\rangle = \text{const} \tag{3.5.3}$$

[162, 163]. A phase portrait for the system is given in figure 15. Periodic bursts appear. The burst of the drift wave spectrum is followed by one of the zonal flow shear. However, this is unphysical for real drift wave turbulence, since the nonlinear self-interaction effects are essential to the turbulence dynamics.

Single burst and quenching of waves. When collisional damping of the zonal flow is absent, i.e. $\gamma_{\rm damp} = 0$, particular care is required, because the relation $\langle N\rangle = 0$ satisfies the rhs of equation (3.4.14). As is pointed out in [111, 161], the problem is a transient one, and the final, steady state depends on the initial condition. The trajectory $(\langle N\rangle, \langle U^2\rangle)$ satisfies, $\mathrm{d}\langle N\rangle/\mathrm{d}\langle U^2\rangle = [(\gamma_{\rm L} - \gamma_2\langle N\rangle)/\alpha\langle U^2\rangle] - 1$ which is solved to yield

$$\langle N\rangle = \frac{\gamma_{\rm L}}{\gamma_2} - \frac{\alpha}{\gamma_2 + \alpha}\langle U^2\rangle - c_0\langle U^2\rangle^{-\gamma_2/\alpha}. \tag{3.5.4}$$

Here c_0 is a constant which is determined by the value of $(\langle N\rangle, \langle U^2\rangle)$ at $t = 0$. The trajectory $(\langle N\rangle, \langle U^2\rangle)$ is shown in figure 15(*b*) for various values of the initial condition. The drift wave amplitude increases at first. Then energy is transferred to the mean square flow shear, and the wave energy is finally quenched, at a constant value of the amplitude of the flow. The state is related to the complete quench of wave energy near marginal stability, i.e. the so-called Dimits shift [52]. It may be viewed as the continuation of the trend $N/\langle U^2\rangle \sim \gamma_{\rm damp}/\gamma_{\rm L}$ to the limit where $\gamma_{\rm damp} \simeq 0$.

These features are also seen in the nonlinear coupling of different modes, having been studied in connection with L–H transition problems (e.g. [46, 164–175]). The phase portraits show differences in the underlying dynamics.

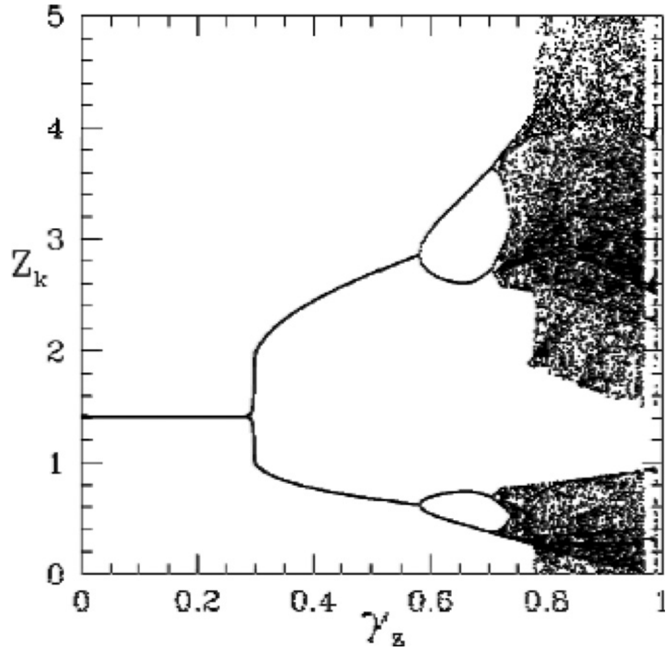

Figure 16. Normalized amplitude of zonal flow Z_k as a function of the normalized damping rate $\gamma_z = \gamma_{\mathrm{damp}}/\gamma_{\mathrm{L}}$. Quoted from [25].

3.5.2. Single instability model. When only one drift wave is unstable, the primary drift wave and sidebands maintain a long coherence time. This is the opposite limit from case (i), for which a reduced variable model applies. This case is explained in section 3.4.2. A closed set of equations is derived for the amplitude of only one unstable mode, P, the amplitude of zonal flow, Z, the relative amplitude of sideband drift wave S and the frequency mismatch Ψ as equation (3.4.5). This type of coherent interaction of model amplitudes appears in the Lorenz model, and other dynamical systems.

Equations (3.4.5a)–(3.4.5d) describe the parametric excitation for a fixed pump amplitude P, and give the zonal flow growth rate γ_{ZF}. The coupling to the primary wave, equation (3.4.5a) accounts for the stabilizing effect of (nonlinearly driven) zonal flow on the primary drift wave. This system of equations has been analysed for the problem of three-wave coupling [176]. The fixed point is given [25] by $P_* = \sqrt{\gamma_{\mathrm{damp}}\gamma_{\mathrm{L}}^{-1}}Z_*$, $Z_* = \sqrt{((\omega_0 - \Omega_+)^2 + \gamma_{\mathrm{side}}^2)/2\gamma_{\mathrm{L}}\gamma_{\mathrm{side}}}$, $S_* = \sqrt{\gamma_{\mathrm{damp}}/2\gamma_{\mathrm{side}}}Z_*$ and $\sin\Psi_* = (\omega_0 - \Omega_+)/\sqrt{(\omega_0 - \Omega_+)^2 + \gamma_{\mathrm{side}}^2}$.

For a fixed value of γ_{L} (γ_{L} is used as a normalizing parameter for obtaining equations (3.4.5a)–(3.4.5d)), the dependence of the saturation amplitude on the damping rate of zonal flow is explained by the stationary solution. The amplitude of the primary unstable drift wave increases as γ_{damp} according to: $P \propto \sqrt{\gamma_{\mathrm{damp}}}$. In the small γ_{damp} limit, the zonal flow amplitude Z_* remains constant, but the amplitudes of the primary wave and sidebands, P_* and S_*, vanish. These results are qualitatively the same as those of the model in section 3.5.1. In this model, a forward Hopf bifurcation takes place when γ_{damp} exceeds a threshold. Figure 16 illustrates the numerical calculation of the long time behaviour of the solution of equations (3.4.5a)–(3.4.5d). In the case of small γ_{damp}, the solution converges to the fixed point in the phase-space. In a limit of large γ_{damp}, the system exhibits chaos.

3.5.3. Saturation: determining the drift wave spectrum. The wave spectrum contains additional freedom, and can influence the self-consistent state. Equations (3.4.9) and (3.4.10) form a set of nonlinear diffusion equations that determine the spectra of zonal flow and drift wave [111].

The stationary state of the zonal flow is realized, as is seen from equation (3.4.10), by the balance between collisional damping and the bilinear drive by the drift waves, i.e.

$$q_{\mathrm{r}}^2 \sum_k D_q \frac{\partial}{\partial k_{\mathrm{r}}} N_k = \gamma_{\mathrm{damp}}. \tag{3.5.5}$$

On the other hand, the stationary state of the drift waves arises, as seen from equation (3.4.9), by the balance between linear drive and damping, nonlinear damping and k-space diffusion by the random zonal flows. Linear instability sits in the region of small $|k_{\mathrm{r}}|$. In the absence of diffusion, the local (in k-space) balance $\gamma_{\mathrm{L}} = \gamma_{\mathrm{NL}}$ gives the saturated state of drift waves. For a simple case of $\gamma_{\mathrm{NL}} = \gamma_2 N_k$. One has the saturation level $N_k = \gamma_{\mathrm{L}}/\gamma_2$. In the presence of random shearing by zonal flows, diffusion in the k-space occurs, and fluctuation energy is transferred to stable regions of k-space.

(i) Constant diffusivity. The case of constant diffusivity illustrates the competition between various effects. The simplest case of $\gamma_{\mathrm{NL}} = \gamma_2 N_k$ is chosen. The coefficients (γ_2, D_k,) are independent of k_{r}. The linear growth rate is also independent of k_{r}, in both the stable region ($|k_{\mathrm{r}}| > k_{rc}$) and the unstable region ($|k_{\mathrm{r}}| < k_{rc}$). In this limit, equation (3.4.9) is modelled by a simple diffusion equation

$$-\gamma_{\mathrm{L}} N_k + \gamma_2 N_k^2 - D_k \frac{\mathrm{d}^2 N_k}{\mathrm{d}k_{\mathrm{r}}^2} = 0. \tag{3.5.6}$$

This equation is solved by constructing a Sagdeev potential. The boundary conditions, $N_k = 0$ at $k = \infty$ (stable region, $|k_{\mathrm{r}}| > k_{rc}$) and $\mathrm{d}N_k/\mathrm{d}k_{\mathrm{r}} = 0$ at $k_{\mathrm{r}} = 0$ (unstable region, $|k_{\mathrm{r}}| < k_{rc}$), are natural choices.

Multiplying $\mathrm{d}N_k/\mathrm{d}k_{\mathrm{r}}$ by equation (3.5.6) and integrating over k_{r}, one has

$$\int_N^0 \frac{\mathrm{d}N_k\sqrt{D_k}}{\sqrt{\left(|\gamma_{\mathrm{L}}|N_k^2 + (2\gamma_2/3)N_k^3\right)}} = k_{\mathrm{r}} \qquad (|k_{\mathrm{r}}| > k_{rc}), \tag{3.5.7a}$$

$$\int_N^{N(0)} \frac{\mathrm{d}N_k\sqrt{D_k}}{\sqrt{\left(-\gamma_{\mathrm{L}}N_k^2 + (2\gamma_2/3)N_k^3 + \gamma_{\mathrm{L}}N(0)^2 - (2\gamma_2/3)N(0)^3\right)}} = k_{\mathrm{r}}, \qquad (|k_{\mathrm{r}}| < k_{rc}). \tag{3.5.7b}$$

Two solutions to equations (3.5.7*a*) and (3.5.7*b*) must be connected at $|k_{\mathrm{r}}| = k_{rc}$. *This continuity condition determines $N(0)$ as an eigenvalue.*

As an illustration, a case of strong linear stability in the region $|k_{\mathrm{r}}| > k_{rc}$ is described here. In this case, the connection at $|k_{\mathrm{r}}| = k_{rc}$ requires $N(k_{rc}) = 0$. That is,

$$\int_0^1 \frac{\mathrm{d}n}{\sqrt{\left(1 - n^2 + (2\gamma_2 N(0)/3\gamma_{\mathrm{L}})(n^3 - 1)\right)}} = k_{\mathrm{rc}}\sqrt{\frac{D_k}{\gamma_{\mathrm{L}}}}, \tag{3.5.8}$$

where $n(k_{\mathrm{r}}) = N_k/N(0)$ is a normalized function that describes the shape of the spectrum. This relation (3.5.8) gives a relation between $N(0)$, γ_{L} and D_k (i.e. the zonal flow amplitude), as

$$D_k = \frac{\gamma_{\mathrm{L}}}{k_{rc}^2}(\text{lhs of equation (3.5.8)})^2. \tag{3.5.9}$$

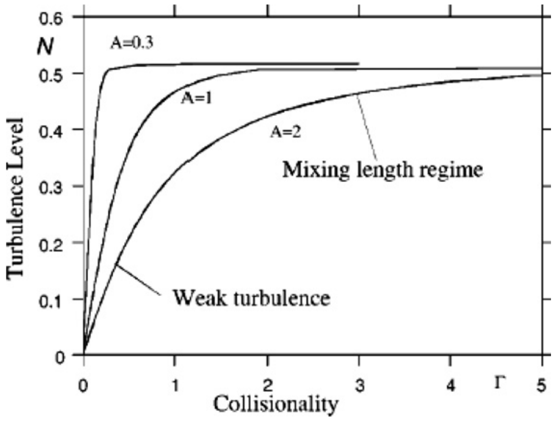

Figure 17. Amplitude of drift waves (normalized to $2\gamma_L/\gamma_2$) in the stationary state as a function of the collisional damping rate of zonal flow γ_{damp}. The horizontal axis is taken $\gamma_{\mathrm{damp}}/\gamma_L$ in the unstable region $|k_r| < k_{rc}$. In this figure, A is a parameter that is in proportion to $C_{\mathrm{d}\to\mathrm{Z}/\gamma_2}$. (quoted from [111].)

Equation (3.5.5) requires

$$\left[q_{\mathrm{r}}^2 \sum_k \frac{1}{B^2} \frac{k_\theta^2 k_{\mathrm{r}}}{(1+k_\perp^2 \rho_{\mathrm{s}}^2)} R(q_{\mathrm{r}}, k) \frac{\partial}{\partial k_{\mathrm{r}}} n(k)\right] N(0) = \gamma_{\mathrm{damp}}. \tag{3.5.10}$$

Equations (3.5.8) or (3.5.9) and (3.5.10) describes the self-consistent solution. Although the coefficient in the square bracket in equation (3.5.10) depends on γ_{damp} through the spectral shape function $N(k_{\mathrm{r}})$, equation (3.5.10) tells us that $N(0)$ increases nearly linearly with respect to γ_{damp}, in the limit of small γ_{damp}.

Figure 17 illustrates the solution of equations (3.5.8) or (3.5.9) and (3.5.10). The gradual change of the drift wave spectrum with collisional damping is demonstrated. The features in equations (3.5.8)–(3.5.10) are the ones clarified by the low-dimensional model in section 3.5.1. Direct calculation of the diffusion equation gives a smooth continuation from the collisionless regime to the regime of strong collisionality.

(ii) Numerical solution. In more realistic examples, for which γ_L and D_k depend upon the wavenumber k_{r}, a numerical solution of equation (3.5.9) is required. The solution of the full diffusion equation recovers the basic trends of the low-degrees-of-freedom model. The drift wave amplitude goes to zero if γ_{damp} approaches to zero. However, there is a quantitative difference between the two models. The result of the solution for the spectrum gives an empirical fit as [161]

$$\langle N \rangle \propto \gamma_{\mathrm{damp}^{0.75}}. \tag{3.5.11}$$

This dependence is slightly weaker than that predicted by the predator–prey model, and the analytical result in (i). This may be due to the fact that the change in spectrum shape due to finite γ_{damp} leads to the modification of the effective coupling coefficient α which is averaged over the drift wave spectrum.

Temporal evolution is also investigated by the numerical solution for $\langle N \rangle$ distribution function. In this case, the coupling coefficient α is not constant in time, on account of the change of the spectral shape, and the result in section 3.5.1 must be re-examined. By solution of the diffusion equation, the qualitative conclusion of the low-dimensional model is confirmed.

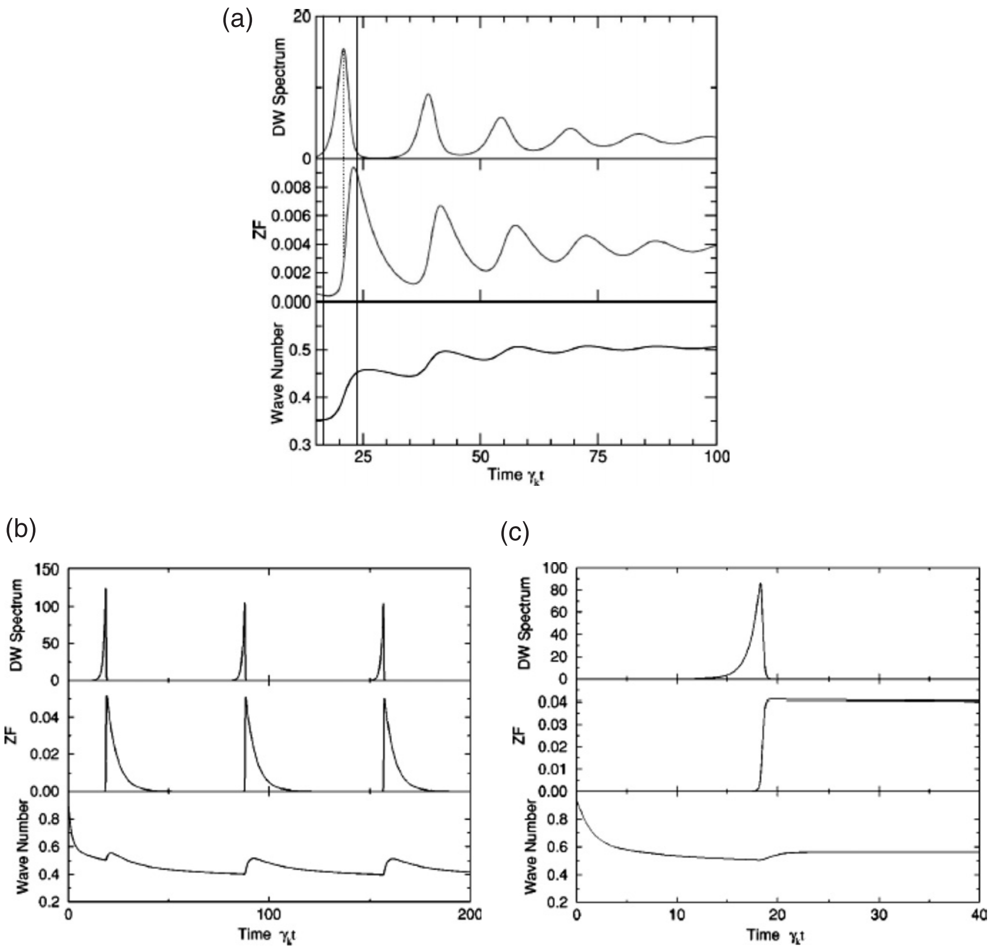

Figure 18. Temporal evolution of drift wave energy, zonal flow and the average wavenumber. Cases of $\gamma_L \neq 0$, $\gamma_{\mathrm{damp}} \neq 0$, $\gamma_2 \neq 0$ (*a*), $\gamma_2 = 0$ (*b*) and $\gamma_{\mathrm{damp}} = 0$ (*c*) are shown [161].

Specifically:

(a) the steady state is a stable fixed point, and the temporal solution converges after transient oscillations [$\gamma_L \neq 0$, $\gamma_{\mathrm{damp}} \neq 0$, $\gamma_2 = 0$];
(b) periodic bursts appear for $\gamma_L \neq 0$, $\gamma_{\mathrm{damp}} \neq 0$, $\gamma_2 = 0$, corresponding to a limit cycle attractor;
(c) a single transient burst of drift waves is quenched by zonal flow for $\gamma_L \neq 0$, $\gamma_{\mathrm{damp}} = 0$, $\gamma_2 \neq 0$, and corresponds to the Dimits shift regime.

The results are demonstrated in figure 18. Figures 18(*b*) and (*c*) correspond to the trajectories in figures 15(*a*) and (*b*), respectively. They confirm the understanding which is obtained by use of a simple model in section 3.5.1. Study of the transient phenomena by simulation [177, 178] is explained in section 4.

3.5.4. Wave trapping and BGK solution. When the coherence time of the zonal flow and drift waves is much longer than the time scale of drift wave spectral evolution, trapping of drift waves by the zonal flow may occur [38, 179–181]. For this, the relations $\gamma_{\mathrm{drift}} \ll \omega_{\mathrm{bounce}}$

and $\tau_{\mathrm{ac,ZF^{-1}}} \ll \omega_{\mathrm{bounce}}$ apply. In this case, the drift wave-packets have constants of the motions (k_{y0}, ω_{k0}) as shown in appendix A. Note that in this regime, the drift wave ray dynamics resemble those of a particle trapped in a single, large-amplitude plasma wave. Time asymptotically, then, the solution for N corresponds to a BGK solution, i.e. a time-independent solution parametrized by a finite set of constants of the motion of the ray trajectory. As with all BGK solutions, there is no guarantee a particular solution is stable or is physically accessible. Additional physical considerations must be introduced or addressed to determine stability.

In this system, there are infinite numbers of constants of motion, because the WKE (for rhs = 0), like the Vlasov equation, is time reversible. Just as irreversibility enters the collisionless Vlasov problem when phase mixing of undamped Case–Van Kampen modes leads to Landau damping of (macroscopic—i.e. velocity integrated) Langmuir wave perturbations, irreversibility enters here due to phase mixing when N is integrated over the spectral in k_{r}. The BGK solution corresponds, in principle, to the finite amplitude, time-asymptotic state of such solutions. The distribution function can thus be written in terms of the constants of motion as equation (3.4.20). Noting that the trajectories are classified into untrapped and trapped orbits, equation (3.4.20) can be rewritten as

$$N(x, k_x, k_y) = N_{\mathrm{U}}(\omega_{k0}(x, k_x), k_{y0}) + N_{\mathrm{T}}(\omega_{k0}(x, k_x), k_{y0}), \tag{3.5.12}$$

where the subscripts U and T denote the untrapped and trapped wave-packets.

The self-consistent solution is given by equations (3.4.19) and (3.5.12). One has

$$\left(u\frac{\mathrm{d}}{\mathrm{d}x} - \gamma_{\mathrm{damp}}\right) V_{\mathrm{ZF}} = -\frac{\mathrm{d}}{\mathrm{d}x}\int_{-\infty}^{\infty} \mathrm{d}k_y k_y \left\{\int_{w_{\mathrm{m}}}^{\infty} \mathrm{d}w\, J N_{\mathrm{U}} + \int_{w_{\mathrm{min}}}^{w_{\mathrm{m}}} \mathrm{d}w\, J N_{\mathrm{T}}\right\}, \tag{3.5.13}$$

where $w = -\omega_{k0}/k_{y0}$, J is the Jacobian of the transformation of variables, w_{m} is the value of w at the separatrix, and w_{min} is w at $k_x = 0$ [38].

The distribution functions N_{U} and N_{T} have infinite degrees of freedom, and flattening (i.e. plateau formation) might take place (and likely *does*) in $N_{\mathrm{T}}(\omega_{k0}(x, k_x), k_{y0})$. Choosing a particular class of the functions $N_{\mathrm{U}}(\omega_{k0}(x, k_x), k_{y0})$ and $N_{\mathrm{T}}(\omega_{k0}(x, k_x), k_{y0})$, a self-consistent solution V_{ZF} has been obtained from equation (3.5.13).

The accessibility and stability of a particular distribution function require future research.

3.5.5. Zonal flow quenching and coherent structure. If wave trapping is not complete, a coherently structured zonal flow is formed by the drift wave turbulence. This is the case for $\gamma_{\mathrm{drift}} > \gamma_{\mathrm{ZF}}$, ω_{bounce} and $\tau_{\mathrm{ac,ZF^{-1}}} \ll \gamma_{\mathrm{ZF}}$. The case where the turbulent drift wave spectrum forms such a spatially coherent zonal flow structure is discussed in this section.

If the asymmetric deformation of the distribution function $N(k_x)$ is calculated to higher order in the zonal flow vorticity U, the correction of order U^3 tends to reduce asymmetry. This is reasonable, since the third-order contribution is stabilizing. For the case of $\mathrm{U} > 0$, modification of δN is positive for $k_x > 0$, so as to increase U. The third-order term has the opposite sign, so as to suppress the growth of the zonal flow [159, 182].

Taking into account the modification of the growth rate of the zonal flow, the dynamical equation for the zonal flow is written in an explicit form as equation (3.4.26). By use of normalized variables $x = r/L, \tau = t/t_{\mathrm{Z}}$ and $\hat{\mathrm{U}} = \mathrm{U}/\mathrm{U}_0$, where $L^{-2} = q_{r0}^2(1-\mu)$, $t_{\mathrm{Z}} = D_{rr}^{-1} q_{r0}^{-2}(1-\mu)^{-2}$ and $\mathrm{U}_0^2 = D_{rr} D_3^{-1}(1-\mu)$, equation (3.4.26) is rewritten in the collisionless limit as

$$\frac{\partial}{\partial \tau}\hat{\mathrm{U}} + \frac{\partial^2}{\partial x^2}\hat{\mathrm{U}} - \frac{\partial^2}{\partial x^2}\hat{\mathrm{U}}^3 + \frac{\partial^4}{\partial x^4}\hat{\mathrm{U}} = 0. \tag{3.5.14}$$

The case that the flow is generated from a state with low noise level, where no net flow momentum exists, $(\int \mathrm{d}x \hat{\mathrm{U}} = 0)$, is studied. Here the flow evolves satisfying the condition

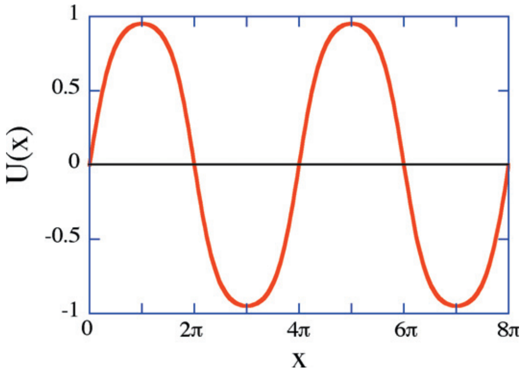

Figure 19. Coherent profile of normalized zonal flow vorticity.

$\int \mathrm{d}x\hat{\mathrm{U}} = 0$. A stationary solution of equation (3.5.14) in the domain $0 < x < d$, for the periodic boundary condition, is given by an elliptic integral as

$$\int^{\hat{\mathrm{U}}} (1 - 2u^2 + u^4 - \kappa^2)^{-1/2}\,\mathrm{d}u = \pm\frac{x}{\sqrt{2}}, \tag{3.5.15}$$

where κ is an integral constant ($0 \leqslant \kappa < 1$) given by the periodicity constraint $\int_{-u_c}^{u_c} (1 - 2u^2 + u^4 - \kappa^2)^{-1/2}\,\mathrm{d}u = d/2\sqrt{2}n$ ($n = 1, 2, 3, \ldots$. The integer n is the one which is closest to $d/n = 4\sqrt{2}\pi$.) Numerical solution of equation (3.5.14) has shown that the solution (3.5.15) is stable and is an attractor. Figure 19 illustrates the stable stationary state. Compared to a simple sinusoidal function (eigenfunction of the linear operator), the result in figure 19 has much weaker curvature at the peak, and is closer to a piecewise constant function.

The normalized function $u(x)$ is of the order of unity, so that the characteristic values of vorticity and scale length l are given as $\mathrm{U}_0 = D_{rr}^{1/2} D_3^{-1/2} (1 - \mu)^{1/2}$, and $l = q_{r0}^{-1}(1 - \mu)^{-1/2}$. The ratio D_3/D_{rr} is characterized by $D_3 \sim k_\theta^2 l^2 \Delta\omega_k^{-2} D_{rr}$. One has an estimate

$$V_0 = v_z(1 - \mu)^{1/2}. \tag{3.5.16}$$

where $v_z = \Delta\omega_k k_\theta^{-1}$. This result gives an expression for the zonal flow in terms of the decorrelation rates of drift waves. Combining this with the dynamical equation which dictates the drift wave fluctuations, e.g. equation (3.5.6), the amplitude of the self-consistent state may be derived. Further research is necessary to understand the significance of these results.

3.5.6. Shift of the boundary for drift wave excitation. When coupling with zonal flow is taken into account, the boundary in the parameter space for the excitation of turbulent transport is modified. The shift of the excitation boundary is one aspect of characteristic nonlinear interactions. The shift is noticed in the context of subcritical excitation of turbulence (see, e.g. [183–185] and a review [186]). The shift also appears for supercritical excitation [187–192]. The case of ITG coupled with zonal flow also belongs to this class of stability boundary shifts.

The mutual interaction of fluctuations with different scale lengths has been studied [187]. The component with longer wave length is called 'intermediate scale' and that with shorter wave length is called 'micro'. In the presence of mutual interaction, the phase diagram is illustrated in figure 20. The boundary for the excitation of the micro mode is no longer $\gamma_{\mathrm{L}}^{\mathrm{micro}} = 0$, but shifted to a positive value of $\gamma_{\mathrm{L}}^{\mathrm{micro}} = 0$. In the absence of the intermediate scale mode, the micro mode is excited for $\gamma_{\mathrm{L}}^{\mathrm{micro}} > 0$. However, when the intermediate scale

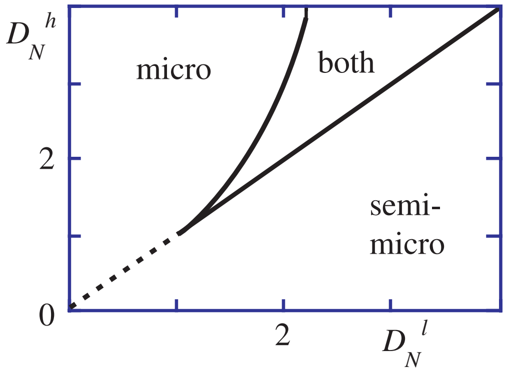

Figure 20. Phase diagram for the case of mutual interactions between intermediate scale and micro modes.

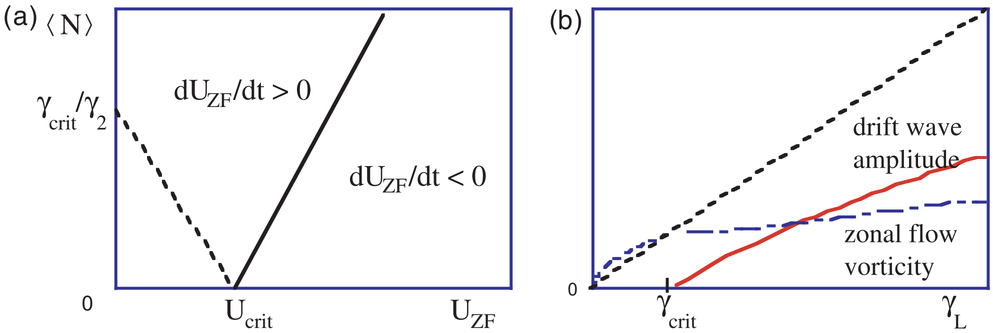

Figure 21. Marginal stability boundary for the growth of the zonal flow is shown by the solid line in the limit of $\gamma_{\mathrm{damp}} = 0$ (*a*). The dotted line indicates the marginal stability condition for the drift waves (*a*). The excited energy of waves and flows as a function of the growth rate of drift waves, in the limit of $\gamma_{\mathrm{damp}} = 0$ (*b*).

mode is excited $D^{\mathrm{intermediate}} > 0$, the micro mode is quenched in the vicinity of the stability boundary $\gamma_{\mathrm{L}}^{\mathrm{micro}} \sim 0$, and is excited at finite level only if the growth rate exceeds a substantially larger value, $\gamma_{\mathrm{crit}}^{\mathrm{micro}}$. This constitutes an upshift of the boundary for excitation of the turbulence. An analysis of the coupling between ITG and current diffusive ballooning mode is reported in [191] and the case of the ITG and ETG is given in [192]. These examples also exhibit stability boundary upshifts. (See also the simulation study [193, 194].)

In the case of drift waves coupled to zonal flow, the 'micro' fluctuation is the drift wave, and the zonal flow plays the role of the 'intermediate scale' fluctuation. For transparency of argument, we take here the limit of vanishing collisional damping of zonal flow, i.e. $\gamma_{\mathrm{damp}} = 0$. The shift of the boundary for the excitation of the drift waves from $\gamma_{\mathrm{L}}^{(\mathrm{DW})} = 0$ occurs if the zonal flow has finite amplitude for very small amplitude of the drift wave [195], i.e. $\langle \mathrm{U}^2 \rangle \neq 0$ at $\langle N \rangle = 0$. In the other limit of large growth rate, the increase of the drift wave amplitude $\langle N \rangle$ by the increase of $\gamma_{\mathrm{L}}^{(\mathrm{DW})}$ requires self-stabilization of the zonal flow. Examples of such self-nonlinear effects are the $\gamma_{\mathrm{NL}}(V^2)$ term in equation (2.10*b*) or the U^3 term in equation (3.5.14). Summarizing these, the stability boundary for the zonal flow in the $(\mathrm{U}^2, \langle N \rangle)$ plane should have the form as is illustrated in figure 21(*a*). That is, the boundary for the marginal stability condition $\mathrm{dU}_{\mathrm{ZF}}/\mathrm{d}t = 0$ (solid line in figure 21(*a*)) intersects the boundary $\langle N \rangle = 0$ at a finite

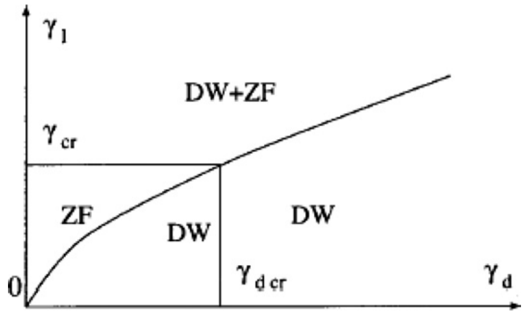

Figure 22. This diagram, indicates the regions of residual drift wave and zonal flow turbulence as well as the region where they coexist in the $(\gamma_L, \gamma_{\rm damp})$ plane.

value of the zonal flow amplitude (denoted by $\mathrm{U}_{\rm crit}$). This allows a finite amplitude of zonal flow at a very low level of drift wave fluctuation. In this circumstance, the boundary for the drift wave excitation shifts from $\gamma_{\rm L}^{\rm (DW)} = 0$ to $\gamma_{\rm L}^{\rm (DW)} = \gamma_{\rm crit} > 0$. The dotted line in figure 21(*a*) illustrates the boundary of the marginality condition for the growth of drift waves from the case of $\gamma_{\rm L}^{\rm (DW)} = \gamma_{\rm crit}$. Below the critical value of the growth rate, a steady-state solution is allowed for $\langle N\rangle = 0$. Figure 21(*b*) illustrates the partition of the energy between drift waves and zonal flow as a function of the growth rate of the drift waves. The waves are not sustained in steady state below the critical value $\gamma_{\rm L}^{\rm (DW)} < \gamma_{\rm crit}$. After the transient growth of waves, the zonal flow can be sustained at a finite value, and this level is dependent on the initial condition. If the critical growth rate is exceeded, i.e. $\gamma_{\rm L}^{\rm (DW)} > \gamma_{\rm crit}$, both waves and flows are excited. The estimate of the drift wave amplitude for the case when the excitation of zonal flow is ignored, is denoted by a thin dotted line.

Noting the presence of critical value of zonal flow vorticity $\mathrm{U}_{\rm crit}$, a phase diagram in the $(\gamma_{\rm L}, \gamma_{\rm damp})$ plane is shown schematically in figure 22 [195].

The mechanism that gives the finite values of the critical vorticity of the zonal flow has been discussed in [195]. The key is the determination of the self-nonlinear damping term for the zonal flow growth, e.g. $\gamma_{\rm NL}(\mathrm{U}_{\rm ZF}^2, \langle N\rangle)$, as in equation (2.10*b*). The marginal condition for the zonal flow growth is thus expressed as

$$\gamma_{\rm NL}\left(\mathrm{U}_{\rm ZF}^2, \langle N\rangle\right) = \alpha\langle N\rangle. \tag{3.5.17}$$

3.6. Suppression of turbulent transport

Mean shear flow and zonal flow can reduce or quench transport by altering either the turbulent fluctuations amplitude or the wave–particle correlation time, which determines the 'cross-phase' between, say $\tilde{V}_{\rm r}$ and $\tilde{n}$, in the particle flux $\Gamma_{\rm r} = \langle \tilde{n}\tilde{V}_{\rm r}\rangle$. Up till now, we have been primarily concerned with effects on the fluctuation *intensity. However, both zonal and mean shears can alter the correlation times and thus fluxes*, *even at fixed fluctuation amplitude*. In section 3.6, we examine shear flow effects on transport. We begin by considering the effect of sheared mean and zonal flows on transport of a passive scalar by an otherwise fixed or prescribed ensemble of turbulence.

3.6.1. Passive scalar transport: sheared mean flow. The average cross-field flux is given in terms of cross correlations between various fluctuation fields. For instance, the radial particle flux is given by: $\Gamma_{\rm r} = (1/B)\langle \tilde{n}\tilde{E}_\theta\rangle$. This flux, an averaged quantity, is determined by the amplitudes of density and electric field, *and* by the phase between them. In the case of electrostatic fluctuations, $\Gamma_{\rm r}$ can be written as:

$$\Gamma_{\rm r} = \frac{1}{B}|\tilde{n}||\tilde{E}_\theta|\sin\alpha \tag{3.6.1}$$

where α is the phase difference between the density and potential fluctuations. α is determined by the wave–particle correlation time and by the response function. Obviously, shifting α can reduce (or increase) the flux.

Here, we investigate the effect of mean shear on transport by analysing the response of a passive, phase-space field f (i.e. a distribution function) to a given ensemble of turbulence. A model equation for the passive advection of f in the presence of prescribed fluctuating $\tilde{\boldsymbol{v}}$ (i.e. advecting velocity field) is:

$$\frac{\partial f}{\partial t} + v_\parallel \hat{b}\cdot\nabla f + \langle \boldsymbol{V}\rangle\cdot\nabla f + \tilde{\boldsymbol{v}}\cdot\nabla f - D_{\rm c}\nabla^2 f = 0. \tag{3.6.2}$$

Here $\langle \boldsymbol{V}\rangle = V_y(x)\hat{y}$ is the mean sheared $\boldsymbol{E}\times\boldsymbol{B}$ flow, $v_\parallel$ is the parallel phase-space velocity and $D_{\rm c}$ is the collisional diffusion coefficient. We focus on strong turbulence, and consider the asymptotic limit where $D_{\rm c}\to 0$ [196, 197].

A formal solution for the cross field flux, $\Gamma_{\rm f} \equiv \langle \tilde{f}^*\tilde{v}_x\rangle$, is then given by

$$\Gamma_{\rm f} = \mathrm{Re}\sum_{\boldsymbol{k},\omega} \frac{\mathrm{i}|\tilde{v}_{x,k,\omega}|^2}{\omega - k_\parallel v_\parallel - k_y x S_v + \mathrm{i}\tau_{ck}^{-1}}\frac{\mathrm{d}}{\mathrm{d}x}f_0. \tag{3.6.3}$$

Note that equation (3.6.3) contains many time scales for irreversible dynamics, which must be considered. These are:

(a) $\Delta\omega_k$—the mode *self-correlation decay rate*, or inverse lifetime, due to nonlinear scrambling;

(b) *Doppler spread (autocorrelation) rates*: $|k\Delta(\omega/k)|$—the spectral self-spreading (autocorrelation) rate, i.e. the inverse; lifetime of the spectral pattern (reflects the effect of dispersion—linear process);
$|k_\parallel v_\parallel \Delta x|$—the parallel Doppler spread (autocorrelation) rate, i.e. the rate at which parallel Doppler shift $k_\parallel v_\parallel$ changes with radius;
$|k_y S_v \Delta x|$—the shearing Doppler spread (autocorrelation) rate, i.e. the rate at which the sheared $\boldsymbol{E}\times\boldsymbol{B}$ flow-induced Doppler shift $k_y V_{\boldsymbol{E}\times\boldsymbol{B}}$ changes with radius;

(c) *Decorrelation rates*
$k_x^2 D_x$—particle decorrelation rate for radial scattering;
$\left(k_y^2 D_x S_v^2\right)^{1/3}$—particle decorrelation rate for hybrid of radial scattering in sheared flow, i.e. due to random walk in shearing coordinates;
$\left(k_\parallel'^2 v_\parallel^2 D_x\right)^{1/3}$—particle decorrelation rate for radial scattering in a sheared magnetic field.

Here Δx is the radial spectral width, D_x is the radial test diffusion coefficient, $k_\parallel' = k_\parallel/L_{\rm s}$ and $L_{\rm s}$ is the shear length. Hereafter, parallel dynamics are ignored. Shearing becomes important when

$$\left|k_y S_v \Delta x\right| \geqslant k_x^2 D_x \sim \frac{D_x}{\Delta x^2}, \qquad \left|k_y S_v \Delta x\right| \geqslant \Delta\omega_k. \tag{3.6.4}$$

In this case, the relevant decorrelation rate is set by

$$\frac{1}{\tau_{ck}} = \left(k_y^2 D_y S_v^2\right)^{1/3}. \tag{3.6.5}$$

For $k_y S_v \Delta x \gg k_\parallel v_\parallel$, but $\left|k_y S_v \Delta x\right|$ or $|\Delta k\,\mathrm{d}\omega_k/\mathrm{d}k|$ greater than $\Delta\omega_k$ and τ_{ck}^{-1}, Γ_j, can be simplified to $\Gamma_{\rm f} \cong -\pi\sum_{\boldsymbol{k},\omega}\left|\tilde{v}_{x,\boldsymbol{k}}\right|^2\delta\left(\omega_k - k_y S_v x\right)\mathrm{d}f_0/\mathrm{d}x$. (An analytic expression

Im $\left(\omega - k_y x S_v + \mathrm{i}k_y^2 D_y\right)^{-1} \simeq -\pi\delta(\omega - k_y x S_v)$ is used.) The cross-field flux then reduces to:

$$\Gamma_\mathrm{f} \cong -\pi \int\int \mathrm{d}m\, \mathrm{d}\omega R \left|\frac{k_y}{L_\mathrm{s}}\right| \frac{|\tilde{v}_{x,\boldsymbol{k}}|^2}{|k_y S_v|} \frac{\mathrm{d}}{\mathrm{d}x} f_0. \tag{3.6.6}$$

Note that the flux depends on the spectral intensity at the resonance point $x_\mathrm{r} = \omega/k_y S_v$. The assumption that this point falls within the spectral envelope is valid if $x_\mathrm{r} < \Delta x$ or equivalently, $\omega < |k_x S_v \Delta x|$. Since we are concerned with the regimes of strong shear, this is almost always the case. In such strong shear regimes, then, Γ_f scales inversely with S_v, i.e.

$$\Gamma_\mathrm{f} \propto S_v^{-1}. \tag{3.6.7}$$

A detailed analysis in [197] established that the passive scalar amplitude perturbation scales as $\sqrt{\langle(\tilde{f}/f)^2\rangle} \propto S_v^{-5/6}$, so that

$$\sin\alpha \propto S_v^{-1/6}. \tag{3.6.8}$$

Note that the effect of even strong shear on the flux is modest ($\sim S_v^{-1}$) and its impact on the cross-phase is quite weak ($\sim S_v^{-1/6}$). Thus, the theory predicts that suppression of the cross-phase is weaker than reduction in turbulence intensity.

It is interesting to examine the scaling of D_x in the strong turbulence regime, for weak and strong shear. Noting that $\Gamma_\mathrm{f} = -D_x(\mathrm{d}/\mathrm{d}x) f_0$, we have already established that $D_x \sim S_v^{-1}$ for strong shear and weak turbulence. In the case of strong shear and strong turbulence, $\tau_{ck}^{-1} > |k_y S_v \Delta x|$, so is Γ_f given by (from equation (3.6.3)): $\Gamma_\mathrm{f} = -\mathrm{Re}\sum_{\boldsymbol{k},\omega} \tau_{ck} |\tilde{v}_{x,k,\omega}|^2 (\mathrm{d}/\mathrm{d}x) f_0$, i.e. $D_x = \tau_{ck}\langle\tilde{v}^2\rangle$. Taking equation (3.6.5) with $D_x \simeq D_y$ then gives

$$D_x \sim \frac{\langle\tilde{v}^2\rangle^{3/4}}{(k_y S_v)^{1/2}}, \tag{3.6.9}$$

which is consistent with the expected scaling $D_x \sim \omega_\mathrm{b}(\Delta x_T)^2$ where ω_b is the particle bounce time in a poloidal wavelength, and Δx_T is the resonance width in radii.

Next, for the strong turbulence, weak shear case $1/\tau_{ck} = k_x^2 D_x$, so $D_x \sim \langle\tilde{v}^2\rangle^{1/2}(k_x^2)^{-1/2}$, which is the familiar scaling for transport in strong two-dimensional turbulence, first derived by Taylor and McNamara. Finally, we also note that the regime of strong shear (i.e. $|k_y S_v \Delta x| > \tau_{ck}^{-1}, \Delta\omega_k, \omega$) but with non-resonant response has also been investigated [196]. The predictions are $\Gamma_\mathrm{f} \sim S_v^{-2}$ and $\sin\alpha \propto S_v^{-2}$. The importance of this regime is dubious, though, since strong shear naturally favours a large shearing Doppler spread which in turn suggests the applicability of standard quasilinear theory and the occurrence of a resonant interaction.

3.6.2. Passive scalar transport: zonal flows. In the previous subsection, we considered the effect of a mean shear flow on passive scalar flux and cross-phase. While understanding the case of a mean shear is necessary, it is certainly *not sufficient* for an understanding of the effects of a spectrum of zonal flows upon transport. Two additional features must be considered in the case of zonal flows. These are:

(a) the flow pattern has a finite lifetime or self-correlation time, $\tau_\mathrm{c,ZF}$;
(b) shearing occurs as a *spectrum* of scales, each corresponding to a radial zonal flow wavenumber q_r. The shearing pattern may be spatially complex.

The implication of differences (a) and (b) are that the effectiveness of shearing will be reduced (relative to that for equal strength mean flow) for short $\tau_\mathrm{c,ZF}$, and that one should expect to find $S_{v,\mathrm{rms}}$ (the rms value) replacing S_v in the quasilinear predictions given above, when $\tau_\mathrm{c,ZF} \to \infty$. The details of these calculations have quite recently appeared in the literature [198].

3.6.3. Reduction of turbulent transport. The results in sections 3.6.1 and 3.6.2 imply that the scaling of transport in a shear flow is not universal, and turbulent transport must be computed by specifying a relaxation mechanism. In addition, the amplitude of the fluctuating velocity field and characteristic correlation length must be determined simultaneously by considering the effects of E_r and $\mathrm{d}E_\mathrm{r}/\mathrm{d}r$, and their spectra. Some representative analyses of the calculation of turbulent transport are reported here.

Several analyses have been performed for ITG modes, e.g. [199–201]. An expression for the turbulent transport coefficient has been proposed [201]:

$$\chi_\mathrm{turb} \simeq \frac{(\gamma_\mathrm{L} - \omega_{E1} - \gamma_{*1})^{1/2}\gamma_\mathrm{d}^{1/2}}{k_y^2}, \tag{3.6.10}$$

where γ_L is the linear growth rate in the absence of flow shear, ω_{E1} is the $\boldsymbol{E} \times \boldsymbol{B}$ flow shear frequency, $\omega_{E1} = (r/q)(\mathrm{d}/\mathrm{d}r)(qE_\mathrm{r}/rB)$, γ_{*1} is the shear of the diamagnetic flow, and γ_d is the damping rate of a representative zonal flow mode. The latter is approximated in [195] as $\gamma_\mathrm{d} \simeq 0.3(T_\mathrm{i}/T_\mathrm{e})\omega_\mathrm{M}$ (ω_M is the toroidal magnetic drift frequency), and k_y is the poloidal wavenumber of the most unstable mode. The dependence of χ_turb on ω_{E1} is adjusted to the results of nonlinear simulation, i.e. the expression represents a fit to data.

In the case of self-sustaining CDIM turbulence, the thermal diffusivity has been predicted to be [150, 202]

$$\chi_\mathrm{turb} \sim \frac{1}{(1 + 0.5G_0^{-1}\omega_{E1}^2)} \frac{G_0^{3/2}}{s^2} \left(\frac{c}{\omega_p}\right)^2 \frac{v_{Ap}}{a}, \tag{3.6.11}$$

where $\omega_{E1} = k_\theta \tau_{A\theta} E_\mathrm{r}'/B$, G_0 is the normalized pressure gradient and $\langle k_\perp^2 \rangle \propto (1 + 0.5G_0^{-1}\omega_{E1}^2)G_0^{-1}$. As the gradient of the radial electric field becomes larger, the correlation length becomes shorter. In toroidal geometry (i.e. for the case of CDBM turbulence), the normalized parameter $\omega_{E1} = \tau_{A\theta}(\mathrm{d}E_\mathrm{r}/\mathrm{d}r)/srB$ controls the turbulence level and turbulent transport [142]. The effects of $\boldsymbol{E} \times \boldsymbol{B}$ flow shear and magnetic shear complement each other. The same shear dependence is also found for the case of ITG modes.

The ETG mode has a shorter characteristic wave length. This fact suggests that the $\boldsymbol{E} \times \boldsymbol{B}$ flow shear has a weaker effect. However, extended streamers could be affected by $\boldsymbol{E} \times \boldsymbol{B}$ shear, and the transport by ETG modes could then also be affected. Current research indicates that some transfer mechanism of ETG energy to longer scale (either, say, by streamer formation or by inverse cascade to $c/\omega_{\mathrm{p}e}$) is necessary for ETG turbulence to be of practical interest to tokamak confinement. The electron gyro-Bohm thermal diffusivity, i.e. $\chi_\mathrm{e,GB} = \rho_\mathrm{e}^2 V_\mathrm{Th,e}/L_\mathrm{Te} = \sqrt{m_\mathrm{e}/m_\mathrm{i}}\chi_\mathrm{i,GB}$, is too small to be relevant. Further study is required to understand the relation of transport by shorter wavelength turbulence to electric field shear [188, 192, 203, 204].

In addition to the inhomogeneity of flow across the magnetic surfaces, the inhomogeneity on the magnetic surface is also effective in the suppression of turbulence. The toroidal flow in tokamaks varies in the poloidal direction if a hot ion component exists. This poloidal dependence suppresses turbulence [150].

The dependence of χ_turb on ω_{E1} has also been explained experimentally. The expression

$$\chi_\mathrm{turb} \propto \frac{1}{1 + (\omega_{E1}/\gamma)^h} \tag{3.6.12}$$

has been derived analytically with an index h (γ is the decorrelation rate or instability growth rate in the absence of $\boldsymbol{E} \times \boldsymbol{B}$ shear). The index is given as $h = 2$ in the models [141–143] and as $h = 2/3$ in the strong shear limit in [9]. A nonlinear simulation has suggested a dependence similar to that in equation (3.6.8) for the case of ITG mode turbulence. Further elaboration of the theory is required in order to derive a formula which is relevant in a wide parameter region. A comparison of the index h with experimental observations has been reported [205] for when the electric field bifurcation is controlled by an external bias current. The result is in the range of $h \simeq 2$ [205], but the comparison is not yet conclusive [206–208].

3.6.4. Self-regulated state. The final solution of the turbulent transport problem requires a self-consistent solution for the turbulent heat flux and the zonal flow. The level of the turbulence-generated $\boldsymbol{E} \times \boldsymbol{B}$ shearing rate in formula in section 3.6.3, e.g. equation (3.6.12), must be determined *self-consistently* from the dynamics of the drift wave–zonal flow. Here research in this direction is discussed.

Let us illustrate the problem by the model of two scalar variables from the discussion of sections 2 and 3.4. An example is given as equation (2.10).

(i) Collisional damping limit. The simplest case is that for which the quasilinear drive of zonal flow by turbulence is balanced by collisional damping. In this case, equation (2.12*a*) gives $W_{\mathrm{drift}} = \gamma_{\mathrm{damp}}/\alpha$. The physics of this result is simple—the fluctuation level adjusts so that the zonal flow is marginally stable. That is, the saturated level of turbulence is independent of the magnitude of the drive of linear instabilities, but is controlled by the damping rate of the zonal flow. Alternatively put, the zonal flow regulates the fluctuation level and the flow damping regulates the flow, so the *flow damping* thus regulates fluctuations and transport. In this case, an analytic result is easily derived, and one obtains a stationary state in a dimensional form

$$\frac{e\tilde{\phi}}{T_{\mathrm{e}}} \simeq \sqrt{\frac{\gamma_{\mathrm{damp}}}{\omega_*}\frac{\rho_{\mathrm{s}}}{L_n}}, \tag{3.6.13}$$

where $\tilde{\phi}$ is the amplitude of fluctuations in the range of drift wave frequency and γ_{damp} is the damping rate of the zonal flow. The rhs is reduced by a factor $\sqrt{\gamma_{\mathrm{damp}}/\omega_*}$, as compared to the mixing length levels, due to zonal flow effects. Numerical simulations have confirmed the essential weak turbulence limit, i.e. $\langle (e\tilde{\phi}/T_{\mathrm{e}})^2\rangle \propto \gamma_{\mathrm{damp}}/\omega_*$, not $|e\tilde{\phi}/T_{\mathrm{e}}|_{\mathrm{rms}} \propto \gamma_{\mathrm{damp}}/\omega_*$. The damping rate of the zonal flow (γ_{damp}) is proportional to the ion–ion collision frequency in the high temperature limit (see section 3.1.3). As a result, the level of fluctuations that induces transport is controlled by ion collisions, although the fluctuation spectrum itself is composed of 'collisionless' waves. In the weak turbulence limit, the transport coefficient follows as

$$\chi_{\mathrm{i}} \simeq \frac{\gamma_{\mathrm{damp}}}{\omega_*}\frac{\rho_{\mathrm{s}}}{L_n}\frac{T}{eB} \sim \frac{\nu_{\mathrm{ii}}}{\omega_*}\frac{\rho_{\mathrm{s}}}{L_n}\frac{T}{eB}. \tag{3.6.14}$$

This scales as a gyro-reduced Bohm thermal diffusivity, 'screened' by the factor of $\gamma_{\mathrm{damp}}/\omega*$. Of course, retaining nonadiabatic electron effects complicates the question of collisionality scaling.

(ii) Nonlinear saturation mechanism. In high temperature plasmas, where $\nu_{\mathrm{ii}}/\omega_* \to 0$ holds, the saturation of the zonal flow is influenced by nonlinear processes. These processes are discussed in section 3.4. Possible nonlinear saturation processes include the trapping of drift waves in zonal flows, excitation of *tertiary* instabilities, quenching of zonal flow drive by drift wave spectrum modification, and others. The formal solution of equation (2.12) can be rewritten as $W_{\mathrm{ZF}} = \alpha\alpha_2^{-1}W_{\mathrm{drift}}$, and $W_{\mathrm{drift}} = (1 + \alpha^2\alpha_2^{-1}\Delta\omega^{-1})^{-1}\gamma_{\mathrm{L}}/\Delta\omega$. Because of the production of zonal flow, the usual fluctuation saturation level is 'screened' by the factor of $(1 + \alpha^2\alpha_2^{-1}\Delta\omega^{-1})^{-1}$ as compared to the level $\gamma_{\mathrm{L}}/\Delta\omega$. Thus, the nonlinear stabilization of turbulence may be dominated by the zonal flows shearing channel, instead of the usual mixing

process, i.e. $\alpha^2\alpha_2^{-1}\Delta\omega^{-1} > 1$. In this case, the turbulent transport coefficient is reduced by the factor of $\alpha^{-2}\alpha_2\Delta\omega$.

$$\chi_{\rm i} = \frac{\alpha_2\Delta\omega}{\alpha_2}\chi_{\rm i,0}, \tag{3.6.15}$$

where $\chi_{\rm i,0}$ is the predicted thermal conductivity in the absence of the zonal flow. Obtaining an explicit formula for the nonlinear suppression mechanism (the term α_2) is a topic of current research, and a final answer has not yet been determined. However, if one employs one example from the model of nonlinear reduction of zonal flow drive, one has

$$\chi_{\rm i} = \frac{1}{1+\tau_{\rm c}^2 v_{\rm z}^2 q_{\rm r}^2}\chi_{\rm i,0}, \tag{3.6.16}$$

where $v_{\rm z} \simeq V_{\rm d}$ is the saturation velocity of the zonal flow, $q_{\rm r}$ is the wavenumber of zonal flow and $\tau_{\rm c}$ is the correlation time of turbulence. In the vicinity of the stability boundary, where the correlation time of turbulence is expected to be very long, the reduction of turbulent transport is quite strong. If the drive of turbulent transport becomes stronger (i.e. going further from marginality) and $\tau_{\rm c} v_{\rm z} q_{\rm r} \simeq 1$ holds, then the parameter dependence of $\chi_{\rm i}$ becomes similar to that of $\chi_{\rm i,0}$.

(iii) Role of GAM. When the damping of zonal flow is strong, $\gamma_{\rm damp} > \gamma_{\rm L}\alpha/\omega_2$, the zonal flow may not be excited, but the GAM is still driven. As is discussed in section 3.3.2, the fluctuation levels are suppressed by a factor of $(1 + \tau_{\rm c}\tau_{\rm c,GAM}\langle k_\theta^2 \tilde{V}_{\rm GAM}^2\rangle)^{-1}$, where $\tilde{V}_{\rm GAM}$ is the $\boldsymbol{E} \times \boldsymbol{B}$ velocity associated with the GAM, and $\tau_{\rm c,GAM}$ is the autocorrelation time of the GAM. In the large-amplitude limit, the suppression factor is given by equation (3.3.19).

This suppression factor is derived for the condition that the source of turbulence is unchanged. As discussed in section 3.1.3, the GAM is subject to collisional damping. The saturation mechanism and saturation level of the GAM have not yet been determined. Links between the driven GAM and poloidally asymmetric cross-field transport have been suggested [209]. The accumulation of fluctuation energy in a finite poloidal region, which is coupled to zonal flow dynamics, has also been discussed [210]. The calculation of turbulent transport which is regulated by GAM is left for future research.

4. Numerical simulations of zonal flow dynamics

4.1. Introduction

DNS studies have played a crucial role in the development of research on zonal flows. The perceived synergy between the theory and DNS has been a key promoter of interest in the physics of the zonal flows. Although the technical details of direct numerical simulation techniques are beyond the scope of this review, the physical results of nonlinear simulations are reviewed here, in order to illustrate the elementary dynamics of, and processes in, the drift wave–zonal flow system.

There are several steps in reviewing the understanding which has been facilitated by DNS. These should be addressed in sequence. The first is modelling, i.e. reduction to basic equations appropriate for relevant geometry. Although the rate of development of computational power has been tremendous, the direct computational solution of the primitive nonlinear plasma equations (such as the Klimontovich or Vlasov equations in real geometry and for actual size devices) is still far beyond the computational capability of even the foreseeable future. Thus, reduced modelling has been employed to simplify the basic dynamical equations. The main representative models and hierarchical relations among them are explained in appendix B.

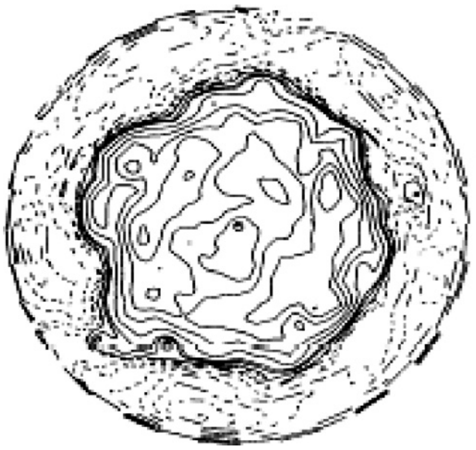

Figure 23. Contour of electrostatic potential from the simulation of [8].

(Keywords for various reduced equations are explained in this appendix.) The second is the selection of important elementary processes in zonal flow and drift wave systems. Here we focus on the following issues: (i) generation of zonal flow by turbulence, (ii) shearing of turbulence by zonal flow, (iii) coexistence of zonal flow and drift waves, (iv) nonlinear states, (v) collisional damping, (vi) dependence on global plasma parameters and (vii) nonlinear phenomena. For these elementary processes, the results of DNS are explained below. Third, several important features of zonal flows have been *discovered* by DNS studies. Therefore, the historical development is also described, though the discussion is bounded by considerations of brevity.

The observation of zonal flow by DNS has been reported in the last two decades for various types of plasma turbulence. Figure 23 is one early example [8], in which the formation of a quasi-symmetric isopotential contour, loosely resembling that of a magnetic surface, is demonstrated. These contour structures indicate the presence of a banded poloidal $\boldsymbol{E} \times \boldsymbol{B}$ flow, called a zonal flow.

It should be stressed again that the objective of the explanation here is an illustration of elementary physical processes of zonal flows. The examples are chosen primarily from the DNS of core turbulence, i.e. 'gyro-Bohm' drift-ITG turbulence. It is well-known that the progress in the DNS studies for plasma turbulence and zonal flows is not limited to this class of examples. Readers are suggested to refer to related reviews on DNS of the subject (for instance, see [211]). In the following subsections, the progress in DNS of drift-ITG turbulence with zonal flow is reviewed together with the specification of simulation methods.

4.2. Ion temperature gradient driven turbulence

4.2.1. Models and geometry. Research on zonal flows in the plasma physics simulation community has exploded in the 1990s and still continues so, to date. This happened as it became more obvious that, independent of the simulation method, simulation domain and boundary conditions, zonal flows play a dominant role in regulating ITG-driven turbulence, which is a prime candidate for the anomalous ion heat transport ubiquitously observed in most plasmas in tokamaks [18]. This progress also paralleled the advances in both gyrokinetic and gyrofluid simulation methods for various geometries. We summarize the highlights of this story in a roughly chronological order.

Exploiting the governing equations of plasma microturbulence, gyrokinetic simulations are based on the nonlinear gyrokinetic description of plasmas, in which the full charged particle kinetic dynamics in a strong magnetic field is simplified, using the disparity between the spatio-temporal scales of the phenomena of interest, and the scale of the magnetic field inhomogeneity and the gyro-period as leverage. As a consequence, the gyro-center distribution function is defined in a five-dimensional phase-space, after decoupling and elimination of the gyro-motion. The perpendicular velocity enters parametrically. The wavelengths of instabilities can be comparable to the size of an ion gyro-radius. Some DNS approaches use the particle-in-cell simulation method, which is Lagrangian in character (i.e. particles are pushed) while others use the continuum Vlasov approach which is Eulerian in character (i.e. the gyrokinetic equation is solved as a partial differential equation). While, to date, most simulations in toroidal geometry have used the conventional nonlinear gyrokinetic equation [212], which ignores the parallel acceleration nonlinearity which is formally weaker, some simulations [213] have used a fully nonlinear energy-conserving form of the nonlinear gyrokinetic equation [214]. Gyrofluid models are then derived from the gyrokinetic equations by taking moments [215]. Some kinetic effects, such as linear Landau damping and a limited form of nonlinear Landau damping, have been included in gyrofluid models while others have not. Most notably, gyrofluid models do not accurately treat nonlinear wave–particle interaction.

Regarding simulation geometry, global simulations typically use a domain which spans a macroscopic fraction of the tokamak volume. Annular domains are sometimes used as an option. Radial variation of gradient quantities, such as temperature gradient and magnetic shear, is allowed in global simulations. Of course, questions concerning mean profile evolution persist. Flux-tube simulations are restricted to a local domain of a few turbulence correlation lengths and assume the existence of a scale separation between the turbulence and equilibrium profiles, and so do not accurately represent mesoscale dynamics. Typically, radially periodic boundary conditions are used and the gradient quantities are treated as constant within a simulation domain.

4.2.2. Adiabatic electrons and conventional collisionless gyrokinetic ions. We start from the simplest case of the collisionless limit in order to explain some of the key elements of zonal flow DNS. In this subsection, illustrations are given on the issues of (i) generation of zonal flow by turbulence, (ii) shearing of turbulence by zonal flows, (iii) coexistence of zonal flow and drift waves and some aspects of (iv) dependence of dynamics on global parameters.

Historical overview. While zonal flows with large radial scales (the system size—so as to render them indistinguishable from mean flows) were observed in ITG simulations in a simple geometry in the early 1980s [216], it was in early gyrofluid [99] and gyrokinetic [217] simulations of toroidal ITG turbulence, where fluctuating sheared $\boldsymbol{E} \times \boldsymbol{B}$ flows driven by turbulence with a radial characteristic length comparable to that of ambient turbulence (several ion gyro-radii), began to appear and attract attention. These simulations were either quasi-local in the flux-tube domain [17, 19, 99, 217], or in a sheared slab geometry [156]. On the other hand, early global gyrokinetic simulations of ITG turbulence either did not address [218, 219] or did not find the effects of fluctuating $\boldsymbol{E} \times \boldsymbol{B}$ flows [220] on turbulence to be significant. The reason for this is as follows. Early global gyrokinetic simulations [219, 220] had relatively small system size (in ion gyro-radius units), and consequently had rather sharp radial variations of pressure gradient. Zonal flows with scale lengths of the system size have been the dominant feature in these simulations [220]. In other words, the simulation domain was so small that it was effectively impossible to distinguish between zonal and mean flows. Even as more

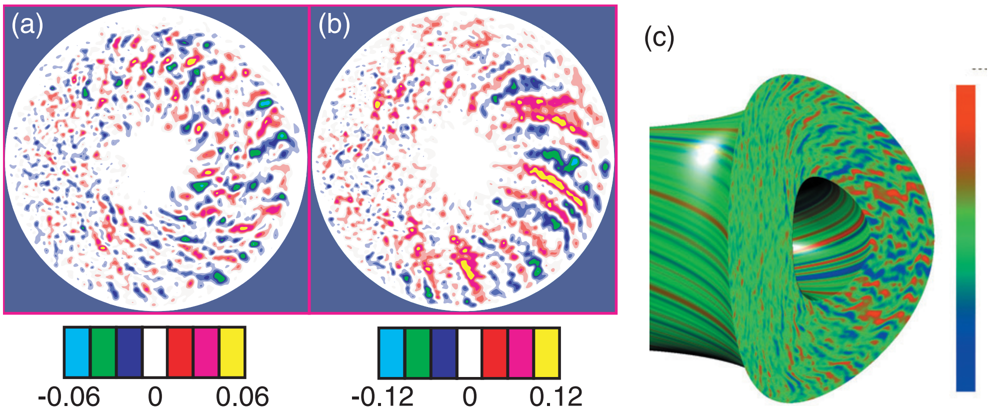

Figure 24. The radial size of turbulent eddies shown in coloured contour of ambient density fluctuation gets reduced due to the random shearing by self-generated $\boldsymbol{E} \times \boldsymbol{B}$ zonal flows from gyrokinetic particle simulation, (*a*) and (*b*) (from [18]). (*c*) is quoted from http://fusion.gat.com/comp/parallel/gyro_gallery.html.

codes were independently developed, this qualitative difference between global simulations [213, 221] and flux-tube simulations [99, 217] continued, and fomented lingering doubts as to the proper treatment and possible existence of such fluctuating flows. However, as computing power became sufficient to handle larger system size, the finer scale flows began to appear in global gyrokinetic simulations [213], although its effect on steady-state transport was not observed to be as significant as that seen in the flux tube simulations.

The importance of these small-scale zonal flows in regulating turbulence in the tokamak has begun to be widely appreciated, as gyrokinetic simulations [18] in both full torus and annulus geometry (with various boundary conditions), for which radial variations of the pressure gradient are mild, have produced results which demonstrate the importance of the fluctuating flows with qualitatively similar characteristics as those in flux-tube simulations [19, 52, 99]. The inclusion of zonal flows in gyrokinetic simulations [18] significantly reduces the steady state ion thermal transport, as reported earlier [52, 99]. Figure 24 illustrates some of the characteristic results for the effects of zonal flows on ITG turbulence. Isodensity contours are shown. Fluctuations in the presence of zonal flow, figure 24(*a*), have shorter correlation lengths and lower saturation levels, in comparison to the case where zonal flows are suppressed, figure 24(*b*). A similar illustration for non-circular plasma is reproduced as figure 24(*c*).

The dynamics of coupling between drift waves and zonal flow has been explicitly analysed by DNS. This simulation has directly tested the physics of the modulational instability process, as well. Figure 25 illustrates the *generation of zonal flow by turbulence* and the back reaction of zonal flow shear onto that turbulence. In this study, the ITG turbulence freely grows to a saturation, with zonal flows suppressed. This generates a stationary spectrum or 'gas' of ITG modes. (Thick solid line, being followed by thin solid line (*c*).) In the second run, the turbulence first develops to saturation without zonal flow, but then flow evolution is restored to the system (after $t \simeq 40\ L_n/c_s$ in this simulation). The zonal flow *then* starts to grow exponentially (thin solid line (*a*) plotted on a logarithmic scale), and reaches a new stationary state. As the amplitude of the zonal flow increases, the turbulence level decreases. (Thick solid line (*b*).) Note that the new stationary level is much smaller than the reference case. The modulational instability of a zonal flow spectrum to a test shear is thus established by the observed exponential growth. The reduction in the turbulence level confirms the expectation that the zonal flow shearing will reduce turbulence levels.

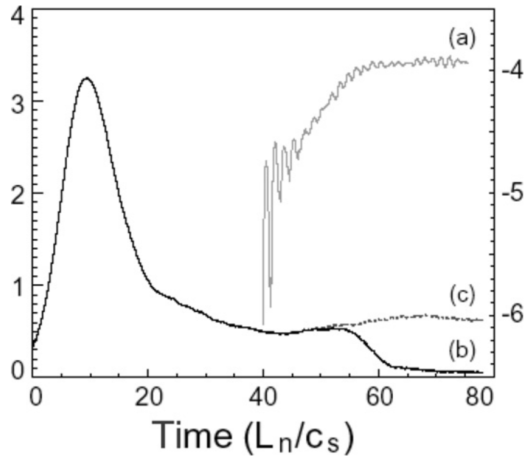

Figure 25. Temporal evolution of the amplitude of the zonal flow, on log scale (*a*), and turbulence level (*b*) and (*c*) on linear scale [15].

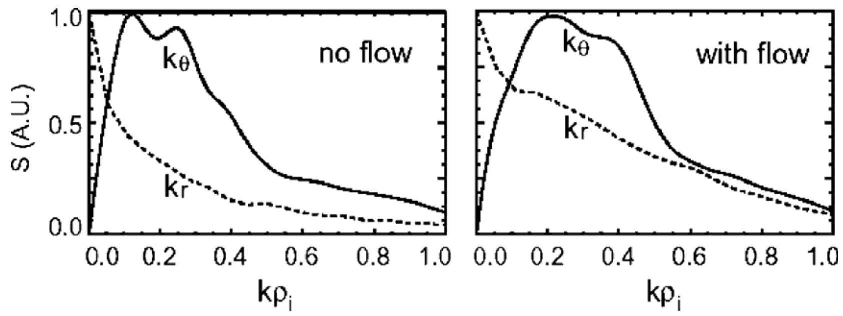

Figure 26. k_r spectrum of the ambient density fluctuation from gyrokinetic particle simulation is broadened due to random shearing of eddies by self-generated $\boldsymbol{E} \times \boldsymbol{B}$ flows (- - - -) [222].

The shearing of turbulence by zonal flow is also clear. The key mechanism of the turbulence suppression is as explained in section 3. One new significant finding from this simulation is a broadening of the k_r spectrum of turbulence due to self-consistently generated zonal flows, as shown in figure 26. It is in agreement with the expectation that an eddy's radial size will be reduced as shown by the contours of density fluctuations in figure 24. These also agree (qualitatively) with theoretical expectations of the reduction of radial correlation length due to the shearing by $\boldsymbol{E} \times \boldsymbol{B}$ flow [9, 10]. The quantitative analysis of the turbulence shearing rate is explained below.

The zonal flows observed in simulations [18, 99, 222] contained significant energy in $\boldsymbol{k} - \omega$ bands, with radial scales and frequencies comparable to those of the turbulence. It was therefore of vital importance to extend the nonlinear theory of turbulence decorrelation by the mean $\boldsymbol{E} \times \boldsymbol{B}$ flow shear [9, 10] to address the effect of rapid-time-varying $\boldsymbol{E} \times \boldsymbol{B}$ flow shear in regulating turbulence. This was needed for a better quantitative understanding of the nonlinear simulation results. An analysis of the nonlinear gyrofluid simulation results indicated that the instantaneous $\boldsymbol{E} \times \boldsymbol{B}$ shearing rate associated with self-generated zonal flows exceeds the maximum linear growth rate by an order of magnitude, while the turbulence fluctuation amplitude definitely remained above the thermal noise level, and the ion thermal transport remained significantly anomalous [222]. This was somewhat puzzling since in the cases with mean $\boldsymbol{E} \times \boldsymbol{B}$ shear flows, which are now either measured or calculated from data in existing toroidal devices, many leading experimental teams observed that their plasmas made transitions to enhanced confinement regimes [206, 223, 224] when the $\boldsymbol{E} \times \boldsymbol{B}$ shearing rate in general toroidal geometry [11] exceeded the linear growth rate of microinstabilities in the absence of the $\boldsymbol{E} \times \boldsymbol{B}$ shear. This puzzle can be resolved by considering the following points.

One thread of thought is to look at fine space–time scales of zonal flow shearing rate. Fluctuating sheared $\boldsymbol{E} \times \boldsymbol{B}$ flows play an important role in saturating the turbulence [17, 19, 99, 156, 217]. These flows are typically of radial size $k_{\mathrm{r}}\rho_{\mathrm{i}} \sim 0.1$, but contain of a broad k_{r} spectrum of shears. Since the $\boldsymbol{E} \times \boldsymbol{B}$ shearing rate is proportional to $k_{\mathrm{r}}^2\phi$, the high k_{r} component of ϕ, although small in magnitude, can contribute significantly to the $\boldsymbol{E} \times \boldsymbol{B}$ shearing rate. Indeed, for $|\phi_k|^2 \sim k^{-\alpha}$, the shear spectrum actually increases with k (until FLR effects, etc, kick in), i.e. $|V_k|^2 \sim k^{4-\alpha}$, unless $\alpha > 4$, which is unlikely. The instantaneous $\boldsymbol{E} \times \boldsymbol{B}$ shearing rate, which varies in radius and time, can be much higher than the maximum linear growth rate for a significant portion of the simulation domain. An example is shown in [145]. Of course, shearing effects depend on the lifetime of the shearing pattern, as well as on the shear strength, as discussed in section 3.6.

Specifically, using gyrofluid-simulation zonal flow spectra and time-history data to calculate the correlation time of zonal flows, the effective shearing rate in [222], which reflects the fact that fast-varying components of the zonal flow shear are relatively ineffective in shearing turbulence eddies, has been evaluated for each k_{r}. It has a broad peak at low to intermediate k_{r}, and becomes smaller at high k_{r}, as shown in figure 3 of [222]. Higher k components of the shear flows, while strong, have short correlation time. Overall, this rate is *comparable* to the linear growth rate. This seems qualitatively consistent with considerable reduction, but not the complete suppression, of turbulence (as observed in simulations). The expression for the effective shearing rate is presented in section 4.5. where we discuss the role of GAMs [68]. The instantaneous $\boldsymbol{E} \times \boldsymbol{B}$ shearing rate from global gyrokinetic particle simulations is also dominated by high k_{r} components, and varies roughly on the turbulence time scales as reported in [145]. It is much larger than the maximum linear growth rate for a significant portion of the simulation domain.

The other thread of thought is to reconsider the heuristic rule-of-thumb estimate for turbulence quenching, $\gamma_{\boldsymbol{E}\times\boldsymbol{B}} \simeq \gamma_{\mathrm{L}}$ [19]. Though handy and dandy, this formula has several limitations. First, the nonlinear theory [9–11] tells that $\gamma_{\boldsymbol{E}\times\boldsymbol{B}}$ should be compared to the turbulent decorrelation rate, γ_{NL}, not to γ_{L}. It should be noted that it is much easier to calculate γ_{L} than γ_{NL}, so that this is one reason why many experimental results were 'analysed' in this simplified context. While γ_{L} can be used as a rough measure of strength of ambient turbulence when an estimation of γ_{NL} is not available, the limitation of this approximation is obvious.

The dependence on global parameters in the *collisionless* limit is discussed here. One finding of DNS is the complete suppression of the ITG mode near the linear stability boundary. In the regime of a weak linear growth rate, the initial value problem of DNS showed that the ITG turbulence can first grow but is then quenched by the induced zonal flow. This zonal flow can be strong enough to reduce the ion thermal transport to a value which is nearly zero, within the resolution [225] of the simulation. Such transient evolution, and later quench of turbulence have been confirmed by DNS. This is the so-called Dimits shift, indicating a nonlinear upshift of the threshold for an ITG-driven thermal fluxes. In essence, the Dimits shift regime is one where expansion free energy is transferred to the zonal flows, with relatively little remaining in the drift waves. As a result, the heat flux versus gradient curve is 'upshifted'—hence the name. The Dimits shift regime is, to a large extent, a consequence of the approximation of zero or very low collisionality. A well-known example is from a simplified set of equilibrium parameters

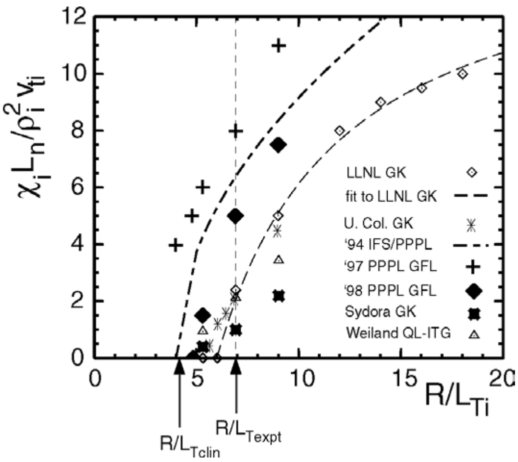

Figure 27. Dependence of ion thermal conductivity by ITG turbulence on the ion temperature gradient (collisionless limit). from [225].

from the case of DIII-D H-mode plasma [225]. For this particular set of parameters, the critical value of the ion temperature gradient has been effectively increased from $R/L_{\mathrm{Ti}} = 4$ to $R/L_{\mathrm{Ti}} = 6$ due to the undamped component of zonal flows. Note that both linear and up-shifted thresholds are, in general, functions of s/q, $T_{\mathrm{e}}/T_{\mathrm{i}}$ and R/L_n. Figure 27 illustrates the turbulent transport coefficient in a stationary state as a function of the ion temperature gradient ratio. In collisionless simulations, turbulence is completely quenched slightly above the linear stability threshold. The upshift of the threshold for the onset of turbulence is observed. When the driving source of turbulence (temperature gradient in this case) becomes larger, the turbulence level starts to increase, as summarized in figure 27.

It has been emphasized that low-frequency turbulence in confined plasmas should be considered as a self-regulating, two-component system consisting of the usual drift wave spectrum and zonal flows [15]. One of the early indications for the coexistence of the zonal flow and turbulence is shown in figure 28. In this simulation, the coexistence of drift waves (with finite k_θ, and frequencies comparable to the diamagnetic frequency) with the poloidally symmetric ($k_y = 0$) short-scale-length zonal flow perturbations (here, called radial modes) is clearly demonstrated.

The partition of the excited energy between the turbulence and the flows is explained in section 3. The partition has also been examined in the DNS. While the gyrokinetic approach is desirable for quantitative studies of this issue, as demonstrated in [225], a simpler model can illustrate the main trend. One of the examples from a fluid simulation of toroidal ITG turbulence is presented in figure 29 [226]. Near the linear stability boundary, nearly all of the energy is carried by the flow. When the temperature gradient (and consequently the linear growth rate γ_{L}) increases, both the turbulence energy and flow energy increase. As is explained in section 3.5, the rate of increment of the turbulence energy and that of the flow energy are dependent on the nonlinear saturation mechanism for the zonal flow. Theoretical analysis is in qualitative agreement in this issue of energy partition, but has yet to provide a satisfactory quantitative answer. In particular, the branching ratio between zonal flow and drift wave turbulence is set by the ratio of wave growth to flow damping (collisional and otherwise). For modest collisionality, near threshold, $E_{\mathrm{flow}}/E_{\mathrm{wave}} \sim \gamma_{\mathrm{L}}/\gamma_{\mathrm{damp}}$.

An approach to the total quench of turbulence in the Dimits shift regime has also been studied in DNS. Transient bursts of turbulence energy have been observed in direct simulations

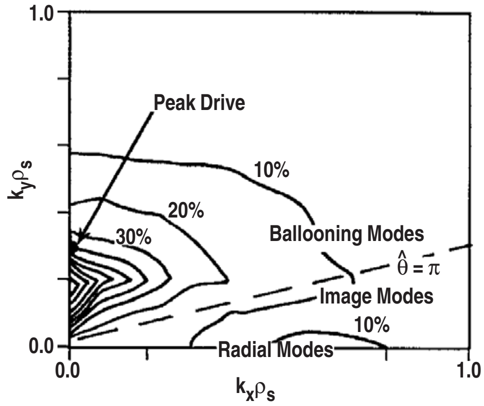

Figure 28. Contour of fluctuation spectrum from [19].

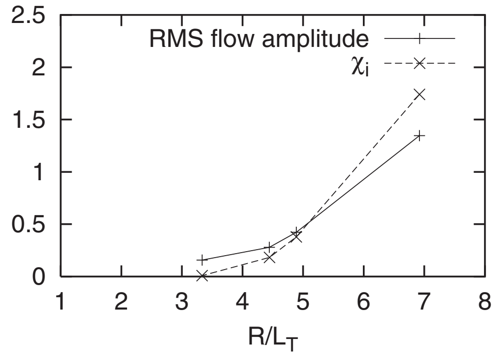

Figure 29. Dependence of the turbulence level (shown by ion thermal conductivity) and zonal flow amplitude on the ion temperature gradient. (from [226]).

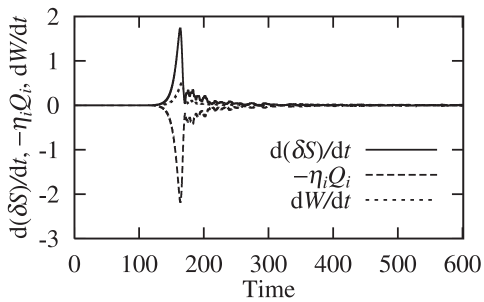

Figure 30. Transient burst of ITG turbulence and associated transport in the collisionless limit [178].

with various levels of modelling. The evolution was studied in the context of various models, e.g. in the convection problem [177] and a detailed Vlasov model of one-dimensional ITG turbulence (near the stability boundary) [178]. Figure 30 illustrates an example of the results of the Vlasov model study.

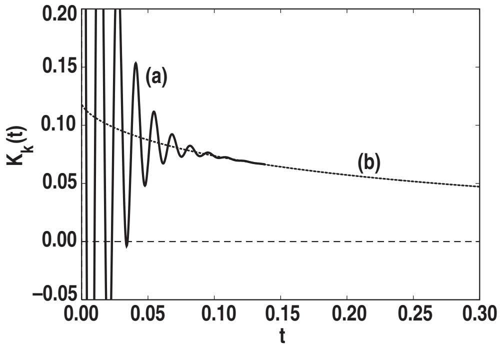

Figure 31. Transient evolution of the poloidal flow and approach to the RH zonal flow. $K(t) = \phi(t)/\phi(0)$ is the normalized potential and time is normalized to τ_{ii} (from [43]).

Before closing this subsection, a distinction caused by the models is noted. Global gyrokinetic particle simulations and flux tube gyrofluid simulations display many common features of the physics of zonal flows, despite differences in simulation methods, simulation domains and boundary conditions. However, the following quantitative difference between them exists. Short wavelength components of zonal flows are more prominent in flux-tube gyrofluid simulations, as compared to gyrokinetic simulations. However, according to estimation from nonlinear gyrofluid simulation, most of the shearing is done by the low to intermediate k_{r} part of the zonal flow spectrum. Since the long wavelength components of zonal flows are more prominent in global gyrokinetic simulations, as compared to the flux-tube gyrofluid simulations, one can speculate that the higher value of steady state ion thermal diffusivity typically observed in gyrofluid simulation (in comparison to that seen in gyrokinetic simulation) is partially due to an underestimation of the low k_{r} component of the zonal flows. These components of zonal flows which are undamped by the collisionless neoclassical process [42] were inaccurately treated as completely damped in the original gyrofluid closure [99]. This undamped component of the zonal flows [the Rosenbluth–Hinton (RH) zonal flow] is of practical importance because it can upshift the threshold value of the ion temperature gradient for ITG instability.

4.2.3. Simulations with additional effects: neoclassical damping of zonal flows, nonadiabatic electrons and velocity space nonlinearity. Other fundamental issues of the zonal flow are its neoclassical (both collisional and collisionless) damping, nonadiabatic electron effects and phase-space dynamics. We now discuss these effects.

The aforementioned example of the RH zonal flow [42] illustrates the importance of correct treatment of zonal flow damping in predicting the levels of turbulence and transport. This motivated further research on the neoclassical damping of zonal flows and its effect on turbulence. When $\boldsymbol{E} \times \boldsymbol{B}$ flow is initialized in a toroidal plasma and allowed to relax in the absence of turbulence and collisions, its poloidal component is damped due to the variation of B in the poloidal direction. The damping occurs due to the 'transit-time magnetic pumping' [72], and in the long term it evolves to a finite RH residual flow level.

The collisionless neoclassical process (transit-time magnetic pumping) induces decay of the flow. The evolution of the flow could be viewed as a superposition of the RH zonal flow of zero frequency and the GAM oscillation, which decays via transit-time magnetic pumping. In figure 31, the evolution of the electrostatic potential (averaged over the magnetic surface)

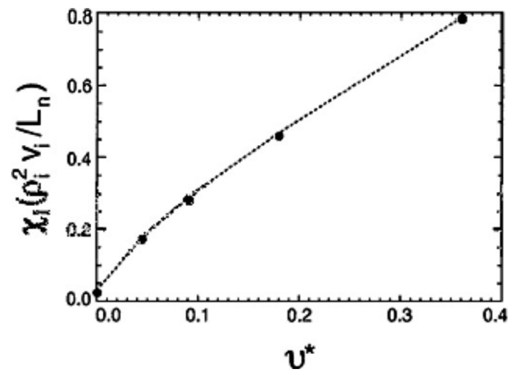

Figure 32. Ion heat conductivity in nonlinear gyrokinetic simulations with $R/L_T = 5.3$ versus the ion–ion collision frequency [51].

is illustrated, where the initial condition is chosen as a high amplitude zonal flow. A simple adiabatic electron model and the one which includes electron effects and electromagnetic effects are compared in DNS [97]. The simple model of adiabatic electrons captures an essential part of the physics, as zonal flows in this system are mostly governed by ion dynamics, more specifically the neoclassical polarization shielding [42] and geodesic curvature coupling. In the long term, the flow converges to a level predicted by neoclassical theory [42].

In the banana collisionality regime, this short (transit) time scale, collisionless damping accompanied by GAM oscillation is followed by a slower collisional damping. A decay of zonal flows due to ion–ion collisions occurs via a number of different asymptotic phases [43], but most of the damping occurs on a time scale $\tau_{ii} \simeq \varepsilon/\nu_{ii}$, as summarized in section 3.1.5.

The important role of collisional damping of zonal flows in regulating transport has been nicely demonstrated by gyrokinetic particle simulations [51]. Even a very low ion–ion collisionality, which is typical of core plasmas in present day tokamaks, was enough to enhance the turbulence level by reducing the amplitude of the zonal flows. The changes in the linear growth rates of ITG modes were negligible. Near and beyond the ITG linear threshold, collisional damping of zonal flows was responsible for a non-zero level of ion thermal transport, and thereby effectively softened the nonlinear upshift of the ITG threshold. Equivalently stated, the presence of collisional damping eliminated the Dimits shift regime. Figure 32 shows the turbulent transport coefficient as a function of the ion collisionality for the parameters of $R/L_T = 5.3$. This parameter is in the Dimits shift regime (i.e. practically no turbulent transport, although the ITG is linearly unstable) for $\upsilon_{ii} = 0$. As the ion collision frequency increases, the level of zonal flow is reduced, and the turbulent transport increases concomitantly, as predicted by theoretical models. The theory of collisional damping of the zonal flow explains this parameter dependence well. Note again that the linear growth rate γ_L is essentially not influenced by the ion collision frequency, for this set of parameters. The change of the turbulence transport is not caused by a change in γ_L, but by the damping rate of the zonal flow. It is worth emphasizing here that the turbulent transport coefficient often has very different dependence on global parameters, in comparison to those of γ_L. This is a simple consequence of self-regulation—flows damp the drift waves and collisions damp the flows, so collisions (more generally, zonal flow damping) ultimately regulate the turbulence. A schematic drawing of the self-regulation is illustrated in figure 33.

It should be noted that system states are not always fixed points. Near the threshold, the two-component system consisting of zonal flows and ambient turbulence has exhibited a

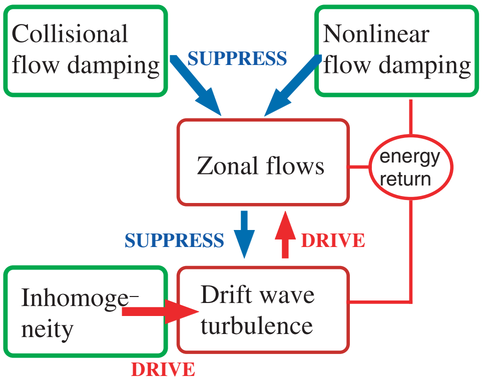

Figure 33. Schematic illustration of the self-regulation. In the circle on the right, 'energy return' indicates the process of energy return to drift waves (being investigated).

bursty cyclic behaviour, with a period proportional to the zonal flow decay time $\sim \tau_{ii} \simeq \varepsilon/\nu_{ii}$. It is interesting to note that this is a well-known feature of a predator–prey type dynamical system which has been widely used in transport barrier formation models [227, 228]. More details on the effect of collisional zonal flow damping on ITG turbulence and transport from gyrofluid simulation with flux boundary conditions were recently reported [229]. In this study, the authors reported that the increase in the zonal flow $\boldsymbol{E} \times \boldsymbol{B}$ shearing rate is responsible for the increase in the energy confinement as one decreases the collisionality. It is worthwhile noting that this simulation confirms that the transport reduction occurred via the reduction in fluctuation amplitude, via the shearing mechanism we discussed in detail in section 3.6.

We note that a theory [196] suggesting that most transport reduction due to $\boldsymbol{E}\times\boldsymbol{B}$ shear flow comes from the change in phase relation between the fluctuating radial velocity (transporter) and the quantity which is transported (transportee) has been proposed. Significant theoretical disagreements have emerged concerning this claim [197, 230]. Indeed, simulations in [229] show that the change in the cross-phase was negligible while transport varied significantly. An example is quoted in figure 34. The same conclusion can also be drawn [231] from the proportionality between transport and fluctuation intensity during the bursting phase observed in [51]. Thus, indications at present favour amplitude reduction as the primary mechanism for transport quenching.

Nonadiabatic electron response (which depends on collisionality) can also change the linear drive of ITG instability. Thus, it is of practical interest to address how the electron–ion collisions can modify transport near marginality i.e. in the Dimits shift regime via their effect on electrons. From continuum gyrokinetic simulations in flux-tube geometry [232], results indicated that the nonlinear upshift of the ITG threshold *decreases* as the electron–ion collsionality decreases, and the nonadiabatic electron contribution to the linear drive increases. At higher collsionality, nonadiabatic electron effects get weaker, and a significant nonlinear upshift occurs, as predicted by ITG simulation with adiabatic electron response. The concomitant increase in turbulence and zonal flow amplitudes due to growth enhancement from trapped electrons can be sufficient to drive the zonal flows into a strongly nonlinear regime, where collisionless (nonlinear) flow damping significantly exceeds the now familiar collisional damping, thus breaking the scaling of fluctuation intensity with collisionality. Indeed, some hints of a robust nonlinear saturation process for zonal flow were observed in a recent global PIC simulation of CTEM turbulence [233]. The influence of nonadiabatic response

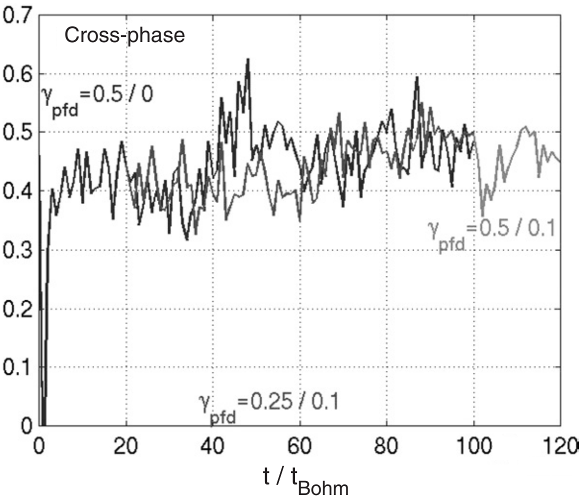

Figure 34. Cross-phase evaluated at the radial position where the ZFs are persistently localized ($r/a = 0.8$) for all the simulations with $\rho* = 0.02$ versus time. $\gamma_{\rm pfd}$, the poloidal damping rate normalized to $c_{\rm s}/qR$, is varied as indicated [229].

of electrons is also illustrated in figure 35. Two cases, without and with, are compared. The two-dimensional power spectrum of the flux surface-averaged electrostatic potential for electrostatic adiabatic electron turbulence is shown. The zonal flow spectrum is narrowly peaked about $\omega \simeq 0$, together with the peak at the GAM frequency. The spectrum for electromagnetic kinetic electron turbulence shows a more turbulent zonal flow spectrum. In the presence of nonadiabatic response of electrons, the power spectrum of the zonal flow component becomes wider [233]. Thus, seemingly paradoxically, collisionless electron effects can alter the collisionality scaling of drift wave turbulence. Of course, for larger $\upsilon_{\rm ee}$, the nonadiabatic electron response decreases, thus restoring collisionality dependence via the zonal flow damping.

Some global simulations have suggested there is an interesting link between zonal flows and 'non-locality phenomena' in drift or ITG turbulence. 'Non-local phenomena' is a catch-all which generically includes mesoscale dynamics associated with avalanches, turbulence spreading, etc. Of particular note here is turbulence spreading [234, 235], and the mesoscale patterns which form in drift–zonal flow systems. Figure 36 shows a spatially inhomogeneous, and in fact highly corrugated and structured, pattern of turbulence level intensity and zonal flow radial electric field. Simply put, the turbulence level is large in the $E_{\rm r}$ trough and relatively small in regions of strong $E_{\rm r}$ shear. Such a pattern was quite likely formed by a process where by: (i) a finite region of instability produced growing fluctuations, (ii) these fluctuations naturally drove zonal flow (with preferred radial wave length) growth, implying a concomitant decrease in their intensity levels, and the formation of fluctuation intensity *gradients*, (iii) the steepened intensity gradient in turn stimulated turbulence spreading via the spatial scattering associated with nonlinear mode coupling, and (iv) the subsequent growth of the zonal flows, following the spreading turbulence. The corrugated fluctuation intensity profile may be thought of as a 'turbulence suppression wave', which is at first propagating, and later standing. Of course, some additional physics is necessary to explain the apparent quenching of turbulence at $E_{\rm r}$ maxima. For this, zonal flow curvature effects on turbulence (which is explained in section 3.4.6) are likely candidates. Flow curvature can squeeze or dilate fluctuation wave structures, and thus has an effect which is sign-dependent.

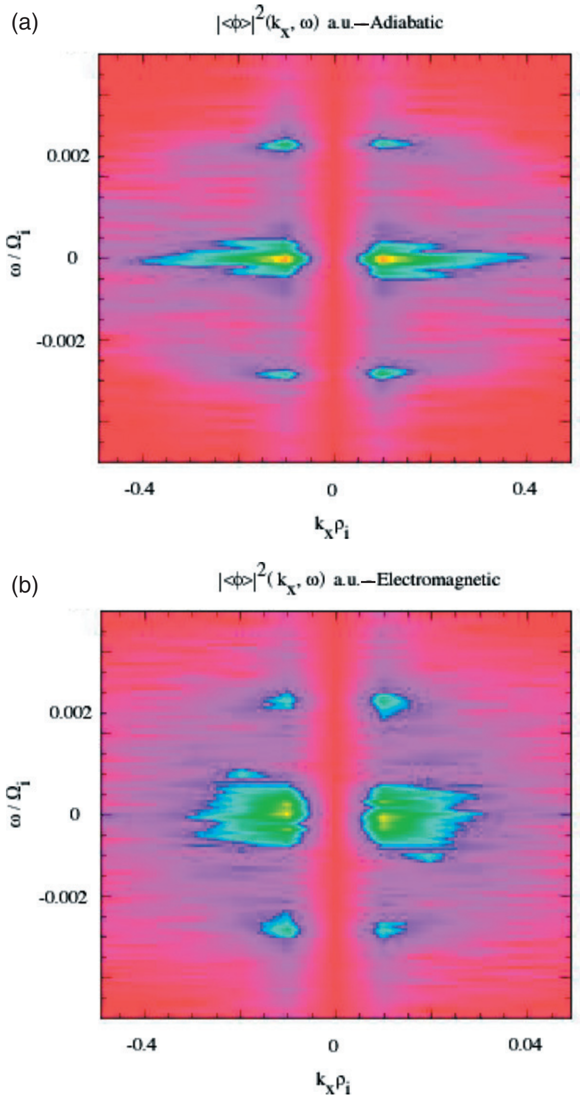

Figure 35. Frequency spectrum of the zonal flows in collisionless trapped electron mode (CTEM) turbulence. Note a peak of pure zonal flow near $\omega = 0$ and that at GAM frequency $\omega_{\mathrm{GAM}} = v_{\mathrm{Thi}}/R$. The influence of nonadiabatic response of electrons is illustrated. The case without (left) and with (right) are shown. In the presence of nonadiabatic response of electrons, the power spectrum of zonal flow component becomes wider [233].

Tertiary instabilities have been discussed in DNS results by a number of authors. For instance, the growth rate of the tertiary instability for an observed zonal flow structure has been reported in [53] and is reproduced in figure 37. The simulation has suggested the possibility that the growth of the zonal flow is quenched by the onset of the tertiary instability. (A similar argument was advanced by [237] in the case of ETG.)

Most simulations mentioned above have used the conventional nonlinear gyrokinetic equation [212], which ignores the velocity space nonlinearity. The latter is formally smaller than the $\boldsymbol{E} \times \boldsymbol{B}$ nonlinearity. It is commonly believed that this omission of velocity space nonlinearity does not cause a serious problem, if one focuses on practically oriented issues,

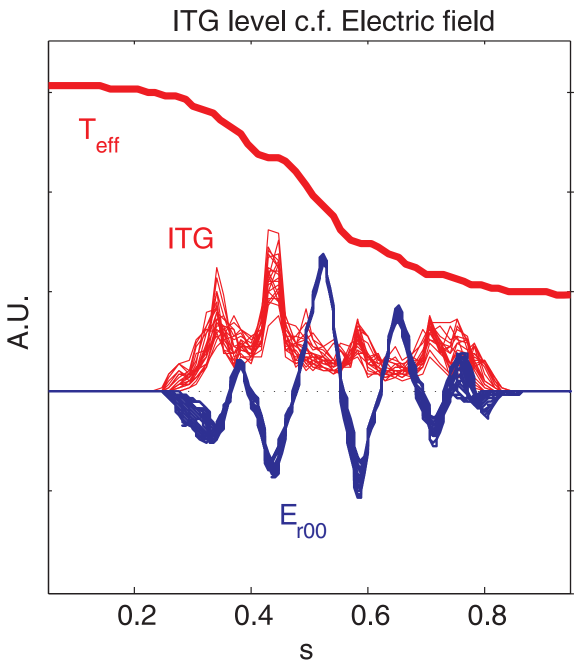

Figure 36. Snapshots of the zonal $\boldsymbol{E} \times \boldsymbol{B}$ flow, ITG amplitude and effective temperature profile in the nonlinear stage [236].

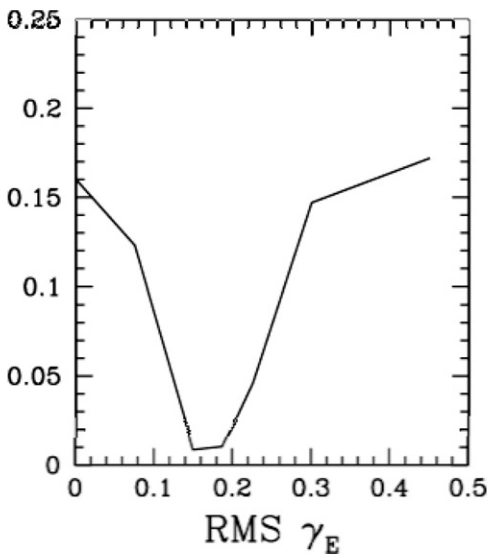

Figure 37. Growth rate of tertiary instability [53].

such as the comparisons of the linear growth rates, turbulence and transport levels in the post nonlinear saturation phase, etc. However, the conventional nonlinear gyrokinetic equation fails to obey the fundamental conservation laws, such as energy (of particles and fluctuation fields), and phase-space volume, at a non-trivial order. For longer times, well after the initial nonlinear

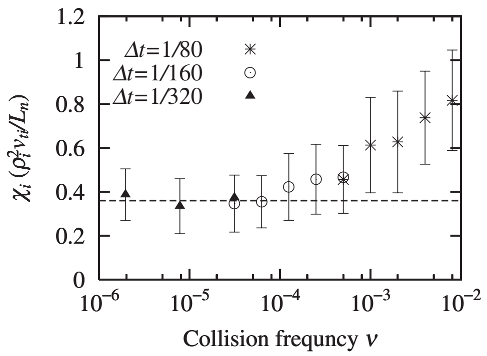

Figure 38. Asymptotic convergence of the turbulent transport in the collisionless limit from [243].

saturation of turbulence, even very small errors in the governing equation can accumulate in time, regardless of the computational method, and muddy the physics predictions. A recent simulation [236] in cylindrical geometry used a fully nonlinear energy conserving and phase-space conserving form of the nonlinear gyrokinetic equation [214]. The importance of using governing equations with proper conservation laws is demonstrated in this series of simulations, with and without velocity space nonlinearity. The authors reported that neglecting velocity space nonlinearity in an ITG simulation resulted in undesirable consequences. The energy was no longer conserved between particles and fluctuating fields, and a precious indicator of the quality of numerical integration was lost. The zonal flow pattern and the radial heat transport pattern were affected as well.

It is worthwhile noting that velocity space nonlinearity of electrons has been considered in the context of the electron drift kinetic equation for the drift wave problem in a sheared slab geometry [238]. See also the extended description in [2] on velocity space nonlinearities and the related phenomena [238–243]. In this regard, it should be appreciated that, it is not computationally straightforward to reproduce the collisionless limit by the present simulation schemes. In the case of large ion temperature gradient, strong turbulent transport is predicted even in the collisionless limit, as is illustrated in figure 27. Under this condition, Vlasov plasma simulation is performed with a sufficient resolution, and an asymptotic limit is shown to reproduce the collisionless limit, as is demonstrated in figure 38.

4.3. Electron temperature gradient-driven turbulence

ETG-driven turbulence is considered to be one of the candidates for causing anomalous electron thermal transport. Since it produces little ion thermal transport and particle transport, its possible existence cannot be easily ruled out by a variety of experimental observations on different transport channels. Fluctuations with wavelengths and frequencies as predicted by ETG theory have not been fully observed to date (except that the observed short-wave length fluctuations on TFTR by Wong *et al* [244, 245] has a possibility of being the ETG or current-diffusive ballooning mode [142]). There are plans to measure such short-wavelength fluctuations in NSTX [246], DIII-D [247] and C-Mod [248]. ETG is *almost* isomorphic to ITG in the electrostatic limit, with the role of electrons and ions reversed. If this isomorphism were perfect, ETG turbulence at electron gyro-radius ($\sim\rho_\mathrm{e}$) scale would produce electron thermal transport $\chi_\mathrm{e}^{\mathrm{ETG}} \sim \sqrt{m_\mathrm{e}/m_\mathrm{i}}\chi_\mathrm{i}^{\mathrm{ITG}}$ which is too small to be relevant to tokamak plasma experiment. Here, $\chi_\mathrm{i}^{\mathrm{ITG}}$ is ion thermal transport expected from the electrostatic ITG at the

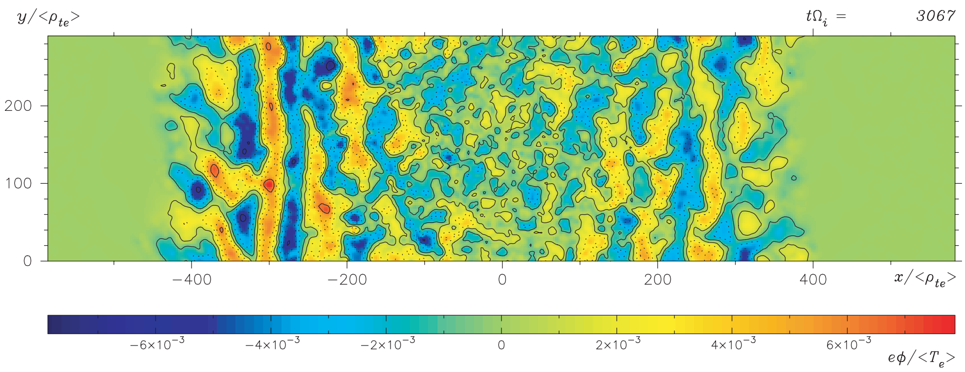

Figure 39. Two-dimensional contour of the electrostatic potential perturbation of ETG turbulence near the q-minimum surface $x = 0$ [54].

ion gyro-radius scale. A more detailed explanation for the isomorphism between ITG and ETG is given in appendix A. This isomorphism is broken if one considers zonal flows in the nonlinear regime or Debye shielding effects [54]. As stated in the preceding section, for ITG turbulence, a proper electron response with $\delta n_{\mathrm{e}}/n_0 = e(\phi - \langle\phi\rangle)/T_{\mathrm{e}}$, was essential to obtaining an enhanced zonal flow amplitude [156]. On the other hand, for ETG turbulence, the ion dynamics asymptotes to a pure adiabatic response $\delta n_{\mathrm{i}}/n_0 = -e\phi/T_{\mathrm{i}}$, as it is unmagnetized for $k_\perp \rho_{\mathrm{i}} \gg 1$. Equivalently, *both* ETG mode and ETG-driven zonal flows have adiabatic ions. For this pure adiabatic ion response, the role of the zonal flow in regulating turbulence was expected to be weaker than that for ITG turbulence. This is a consequence of the fact that the adiabatic ion response effectively *increases* the zonal flow inertia. For this case, flux-tube gyrokinetic continuum simulations suggest that radially elongated streamers can be generated and might enhance electron thermal transport significantly [249]. At present, there exists significant qualitative differences in ETG simulation results regarding the level of transport produced by ETG turbulence [250–252].

It has been reported [249] that transport is reduced significantly for negative or small magnetic shear and large Shafranov shift. See also [253–255]. Global gyrokinetic particle [54] and global gyrofluid [251] simulations in a sheared slab geometry near q_{min}, found that transport is substantially reduced in finite magnetic shear regions regardless of its sign, as compared to the region near the q_{min} surface. This result is in semi-quantitative agreement with the fact that a state with zonal flows can become unstable to KH instability, but only in the absence of the strong stabilizing influence of magnetic shear [9].

An illustration of the zonal flow is reproduced here in figure 39. This case treats the ETG turbulence in the vicinity of the radius where the magnetic shear vanishes (i.e. the 'q-minimum' surface). It is noticeable that the zonal flows are reduced in the vicinity of the minimum-q surface. Away from the minimum-q surface, the zonal flow is strongly excited. It has also been noted [54] that for some tokamak plasma parameters, the electron Debye length λ_{De} can be larger than the electron gyro-radius ρ_{e}, and thus can make a quantitative difference in ETG turbulence-driven zonal flows.

It is noteworthy that a gyrofluid simulation of ETG turbulence, which completely neglects ETG zonal flows [250], obtained a transport level only a factor of 2 or 3 higher than the insignificant value expected from a naive mixing-length estimation based on ETG turbulence at the electron gyro-radius scale $\chi_{\mathrm{e,ML}}^{\mathrm{ETG}}$ (i.e. 'electron gyro-Bohm scaling'). We note that in [249], the radial size of streamers is comparable to the size of simulation domain, invalidating the assumptions of spatial scale separation for flux-tube simulations, and that in [250], unrealistically small system size was assumed. More recent global gyrokinetic particle simulations, with system size comparable to an actual experiment, show that the transport level is quite modest (similar to the result of [250]) even in the presence of radially elongated streamers [251].

Despite recent theoretical progress on electron zonal flow damping [102], which is the electron counterpart of the ion zonal flow damping [42, 43], it appears that understanding of zonal flow physics in ETG turbulence has not matured to the level of understanding of that for zonal flows in ITG turbulence.

4.4. Fluid simulations with zonal flows

Zonal flows have been widely studied in the geophysical and planetary fluid mechanics community, as recently summarized in [256]. Zonal flow generation due to inverse cascade has been theoretically predicted [4] for the Hasegawa–Mima (HM) system [257] which is isomorphic to the quasi-geostrophic or Rossby wave equation first derived by Charney [258, 259]. Zonal flow generation observed in simulations of the HM-Rossby system as a consequence of inverse cascade is combined with the crossover at the Rhines scale [260] from a dispersive-wave-dominated, weak turbulence regime at large scales to a strong turbulence regime at small scales [261]. The Rhines scale is that scale at which the fluid particle circulation frequency (i.e. turbulent decorrelation rate) equals the three-Rossby-wave frequency mismatch. Thus, the Rhines scale, l_{Rhines}, is set by a competition between nonlinearity and dispersion (due to polarization drift). The Rossby dispersion relation, $\omega = -\beta_{\mathrm{R}} k_y k_\perp^{-2}$ (where β_{R} is a coefficient to show the gradient of Coriolis force and k_y is the wavenumber in the longitudinal direction (see section 5.2 for a more detailed explanation), implies that for scales longer than the Rhines scale, non-zero triad couplings require one component to have $k_y = 0$, meaning it is a zonal flow. Thus, for $l > l_{\mathrm{Rhines}}$, the dynamically preferred mechanism of nonlinear interaction is seen to involve zonal flow generation. The crucial role of the polarization nonlinearity in zonal flow generation was also confirmed.

Following the pioneering work on zonal flow self-generation in the Hasegawa–Wakatani (HW) system [8], turbulence-driven zonal flows have also been observed in the nonlinear simulations of various fluid turbulence models [262–267]. Their radial scales were typically of the order of a fraction of the simulation domain. In the multi-helicity case, both flows and energy transfer between flows and ambient turbulence oscillate in radius and turbulence suppression by zonal flow was weaker. Large coherent vortices around low-order rational surfaces were found to participate in the generation of zonal flows [268].

A new issue in zonal flow physics was pointed out by Wakatani in conjunction with the control of resistive wall mode (RWM) [269]. RWM stability is strongly dependent on plasma rotation. Wakatani showed that the perturbation-driven torque (divergence of the Reynolds–Maxwell stress) tends to decelerate the flow velocity at the rational surface. This would be an origin of the nonlinear instability. That is, when the plasma rotation frequency decreases, RWM becomes more unstable because the lower real frequency enhances the Ohmic dissipation in the resistive wall.

4.5. Edge turbulence

4.5.1. Outstanding issues. While zonal flow physics is well developed in the context of drift-ITG turbulence, appropriate to the core, a consistent quantitative picture of even the simulation results remains elusive for the case of edge. Several groups are currently working

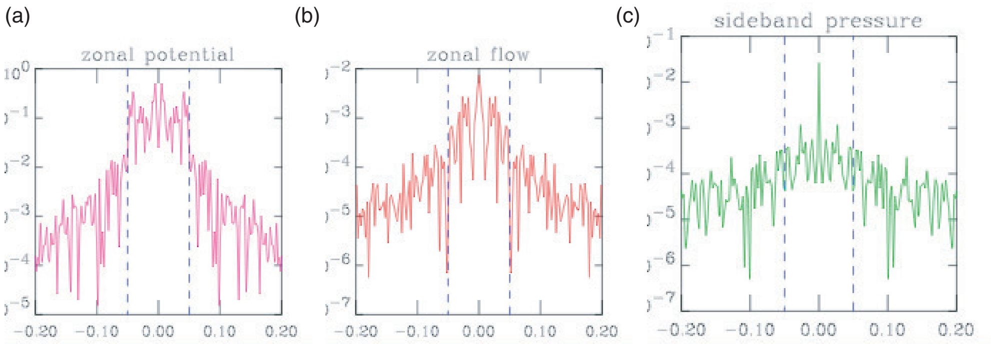

Figure 40. Frequency spectrum of the zonal flows from gyrofluid simulation of edge drift-Alfven turbulence [276]. Note a significant intensity spectrum from zero frequency all the way up to the GAO frequency ω_{GAO}, without a distinct single peak.

on this important problem, and have published mutually exclusive results and interpretations. A review of this subtopic would be premature. (One can nevertheless mention that at edge, the relative importance of the GAM and sidebands become higher. Figure 35 illustrates the coexistence of the dominant zero-frequency zonal flow and the weak GAM oscillation of the flow intensity spectrum in a core. A different set of edge turbulence simulation results, shown in figure 40, indicates (a) that the zonal electrostatic potential spectrum is more continuous and connects directly to the GAM portion of the spectrum, (b) the flow spectrum in which the GAM component is almost invisible, even on a log scale and (c) the sideband ($m = 1$) pressure perturbation, which is shown to be dominant over the zero-frequency component.) Hence, we simply refer the reader to the more detailed description in [2] and to the current literature [270–276].

4.6. Short summary of the correspondence between theoretical issues and numerical results

4.6.1. Survey of correspondence. As is stressed throughout this paper, the explanation of simulation studies in this section does not aim for an exhaustive review of the simulation of zonal flow, but rather strives to illuminate the *understanding* of zonal flow which has emerged together with the theory, and to identify to what extent the theoretical understanding has been verified by DNS. For this reason, the emphasis is on the ITG-ZF cases, and the example figures are limited. It would be useful, after listing some DNS results, to summarize the correspondence between theoretical modelling and DNS. Table 9 illustrates key issues, sections of this review and corresponding figures from DNS. It is clear that the theory and simulation have cooperated to advance the understanding of drift wave–zonal flow systems. Further research can be expected to improve understanding considerably.

4.6.2. On transport coefficients. The results of global transport studies may attract broader interest, in particular from experimentalists. A short note is added here.

The ITG mode has been studied most intensively. Simulation observations include:

(a) *Upshift of the critical temperature gradient* for the onset of turbulent transport [277–279] $\eta_{\mathrm{c,DNS}} > \eta_{\mathrm{c,lin}}$ where $\eta_{\mathrm{c,DNS}}$ is the critical temperature gradient above which turbulent transport occurs and $\eta_{\mathrm{c,lin}}$ is the linear stability boundary. In between two critical values, $\eta_{\mathrm{c,DNS}} > \eta_{\mathrm{i}} > \eta_{\mathrm{c,lin}}$, turbulent transport remains very close to zero but the zonal flow

Table 9. Correspondence between the presentations of theory and corresponding examples of computational results.

Key issue	Section for theoretical explanation	Example of computational result (figure #)
Linear process		
Eigenfrequency	Sections 3.1.1, 3.1.2	35
Collisional damping	Section 3.1.3	31
RH undamped flow	Section 3.1.4	31
Generation by turbulence	Section 3.2	23, 24, 25, 28
Growth rate	Sections 3.2.1, 3.2.2	25
Suppression of turbulence	Section 3.3	24, 25, 27
Stretching vortex	Section 3.3.2	26
Effect on cross-phase	Section 3.6.2	34
Nonlinear interaction		
Tertiary instability	Section 3.4.1	37
RPA and diffusion approach	Sections 3.4.3, 3.4.4	25
Wave trapping	Sections 3.4.6, 3.4.7	36
Broadening of ZF spectra	Section 3.4.8	40
Dynamical evolution	Sections 3.5.1, 3.5.3	
Steady state and energy partition		
Weak instability case		
complete suppression	Sections 3.5.1, 3.5.6	27
role of collisional damping	Section 3.5.1	32
quench via transient burst	Section 3.5.1	30
Strong instability	Sections 3.5.3–3.5.5	27, 29
Coherent structure	Sections 3.4.6, 3.4.7	
Other effects		
Nonadiabatic electrons		35
Electromagnetic effects	Section 3.2.6	35
ETG mode	Appendix A	39
Collisionless dissipation		38

energy dominates, for weak zonal flow damping. The determination of the critical gradient at the onset of turbulence is a subject of current research, and is explained in section 3.5.6.

(b) *Recovery* of mixing levels of χ_i at higher gradient: $\chi_i \propto (\eta_i - \eta_{c,DNS})^{1-2}$ as η_i exceeds $\eta_{c,DNS}$ [226, 277–279], and $\chi_i \propto (\eta_i - \eta_{c,DNS})^0$ as $\eta_i \gg \eta_{c,DNS}$ [277–279].

A major gap in the findings from numerical simulations of the physics of drift–ITG–zonal flow turbulence is a *systematic* exploration of at least the two-dimensional parameter space of zonal flow damping (γ_{damp}) and deviation from marginal stability (i.e. $\delta\eta_i \equiv \eta_i - \eta_{c,lin}$). A possible 'third axis' would measure the strength of nonadiabatic electron effects. Even for the pure ITG case, a systematic exploration of the $(\gamma_{damp}, \delta\eta_i)$ parameter space has not been undertaken. Such a study could help answer many questions, such as: (i) finding the cross-over point between collisional and collisionless saturation; (ii) understanding and elucidating the relevance of various nonlinear saturation mechanisms for zonal flow, such as trapping, nonlinear scattering, tertiary instability and the role of the phase between the zonal potential and zonal temperature [279]; (iii) understanding the effect of nonlinear drift wave noise on zonal flow saturation. The thorough completion of such a study should be a high priority for future DNS investigations.

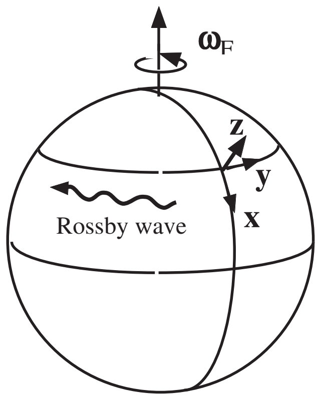

Figure 41. Rotating sphere. Coordinates on a rotating sphere are: the x-axis in the direction of latitude (from pole to equator), y-axis in the direction of longitude and z-axis in the vertical direction. Propagation of Rossby wave in the westward direction.

5. Zonal flows in planetary atmospheres

This section presents a survey of zonal flow phenomena elsewhere in nature. Special emphasis is placed upon the origin and dynamics of belts and zones in the Jovian atmosphere. The physics of the Venusian super-rotation, is discussed as well. The relationship between zonal flow generation and the magnetic dynamo problem has already been discussed in section 3.2.6. These considerations enter here, as well.

5.1. Waves in a rotating atmosphere

5.1.1. Rossby waves and drift waves. The large-scale dynamics of planetary atmospheres are those of thin layers of rapidly rotating fluids. The close similarity between drift wave dynamics and the dynamics of rapidly rotating fluids at low Rossby number (where the Rossby number, R_o, is the ratio of the vorticity or eddy turnover rate of the motion to the rotation frequency ω_F), called geostrophic fluids, has long been appreciated [4]. The interested reader is referred to [2] for an extended description of the analogy, and also to [280, 281] for further discussion. In such a regime, the fluid stream function ψ evolves according to the *quasi-geostrophic equation* (in the coordinates in figure 41):

$$\frac{\mathrm{D}}{\mathrm{D}t}\left(\nabla_\perp^2\psi - \frac{\omega_{\mathrm{F,z}}}{gH_m}\psi\right) - 2\frac{\partial\omega_{\mathrm{F,z}}}{\partial x}\frac{\partial\psi}{\partial y} = 0. \tag{5.1.1}$$

Here, the analogue of the diamagnetic frequency is the gradient of the Coriolis frequency $2\partial\omega_{\mathrm{F,z}}/\partial x$ and the analogue of the gyro-radius is the Rossby radius of deformation $\rho_R = \sqrt{gH_m}/\omega_{\mathrm{F,z}}$. H_m refers to the thickness of an atmospheric scale height. Rescaling according to $|2\rho_R\partial\omega_{\mathrm{F,z}}/\partial x|^{-1}t \rightarrow t$, $x/\rho_{\mathrm{R}} \rightarrow x$, $y/\rho_{\mathrm{R}} \rightarrow y$, and $(2|\partial\omega_{\mathrm{F,z}}/\partial x|)^{-1}\rho_{\mathrm{R}}^{-3}\psi \rightarrow \psi$, equation (5.1.1) then takes the form

$$\frac{\partial}{\partial t}(\nabla_\perp^2\psi - \psi) + [\psi, \nabla_\perp^2\psi] - \frac{\partial\psi}{\partial y} = 0, \tag{5.1.2}$$

where $[f, g] = (\nabla f \times \nabla g)\cdot\hat{z}$, which is identical to the HM equation [4, 257, 259]. Since HM systems are known to support zonal flows, it is not surprising that zonal flows are ubiquitous in planetary atmospheres.

5.1.2. Zonal flows and the Rhines scale. Because of the similarity of the normalized equation (5.1.17) to the HM equation in plasma dynamics, the understanding of the zonal flow generation, Rossby wave soliton and the suppression of the Rossby wave by zonal flow is readily extended using the methods in section 3.

There arises a critical wavenumber k_c, above which the nonlinear enstrophy cascade gives a power law spectrum as $|\psi_k|^2 \propto k^{-4}$. with $k_c = (\rho_R/4L|\psi|)^{1/3}$, where k_c is normalized, L is the horizontal gradient scale length of $\omega_{F,z}$ (in the direction of latitude) and $|\psi|$ is the normalized stream function [4]. Below this critical wavenumber, a global structure such as zonal flow appears. This scale, known as the *Rhines scale* [259], may be estimated by comparing the three-wave frequency mismatch for Rossby wave interaction with the eddy turnover rate for two-dimensional turbulence, i.e. by comparing $\Delta\omega_{MM} = \omega_k - \omega_{k'} - \omega_{k''}$ with $k\tilde{V}_k$. Note that for scales smaller than k_c^{-1}, wave dynamics are effectively irrelevant, as the eddy decorrelation rate exceeds the wave frequency. For scales longer than the Rhines scale, the turbulence is weak, so that the three-wave resonance condition must be satisfied. Since $k_\perp^2\rho_R^2$ is finite, dispersion makes this difficult. Thus, three-wave resonance is most easily achieved if one mode has $k_y = 0$, so that it is a *zonal flow*. Note that this picture suggests, that: (a) zonal flows are the ultimate repository of large scale energy of the two-dimensional inverse cascade in a geostrophic system, (b) geostrophic turbulence is a *three* component system, composed of eddies, Rossby waves and zonal flows. The significance of the Rhines length for determining the scale of zonal flow excitation is nicely illustrated in [261]. Application to the giant planets, Jupiter and Saturn, has been discussed by Hasegawa [282] and many other authors.

The nonlinearity becomes important if the normalized amplitude of vorticity $\nabla^2\psi$ becomes unity. This is the case if the flow velocity reaches the level (in the case of the earth, where $V \sim |\rho_R^2 \partial\omega_{F,z}/\partial x| \sim 50\,\mathrm{m\,s^{-1}}$ for the horizontal scale length $k_y \sim \rho_R^{-1} \sim 10^{-6}\,\mathrm{m^{-1}}$. The azimuthal mode number (i.e. corresponding to the poloidal mode number) is then in the range of a few to ten.

5.2. Zonal belts of Jupiter

One cannot have heard about or contemplate the topic of zonal flows without the vivid image of the belts of Jupiter coming to mind, at least for an instant. While several of the giant planets exhibit zonal flows in their atmospheres, we focus the discussion on the case of Jupiter, in the interests of brevity.

The planet Jupiter consists primarily of a fluid molecular hydrogen, with a solid core of metallic hydrogen. It is enormous, with an equatorial radius of 7.14×10^4 km and rotates quite rapidly, so that 1 Jovian day lasts only 9.9 h. The core of the planet is also very hot, so that the gas envelope is convectively unstable. Thus, the atmosphere is quite dynamic and turbulent. The rich variety of visible structures we normally tend to associate with the Jovian atmosphere, such as zonal belts, the Great Red Spot vortex, KH billows, etc, all live in the weather layer, a thin two-dimensional (spherical) surface layer which is stably stratified, and thus acts as a 'rigid lid' on the convectively unstable interior. Thus, the phenomena of the weather layer are the visible projections of the dynamics of the cloud tops, in turn, driven by the convective dynamics of the planetary interior, which are hidden from view. In this respect, the situation resembles that of solar physics before the advent of helioseismology, when researchers were forced to deduce aspects of the convection zone dynamics by watching their photospheric manifestations, or that in radar surveillance of ocean dynamics, where one attempts to uncover the structure of ocean internal waves and currents by studying their modulations of the surface wave field.

The turbulence of Jupiter is driven by thermal buoyancy, and is strongly affected by rotation, so that the Rossby number R_o is exceedingly low (i.e. $R_o \equiv \tilde{\omega}/\omega_F \ll 1$, where

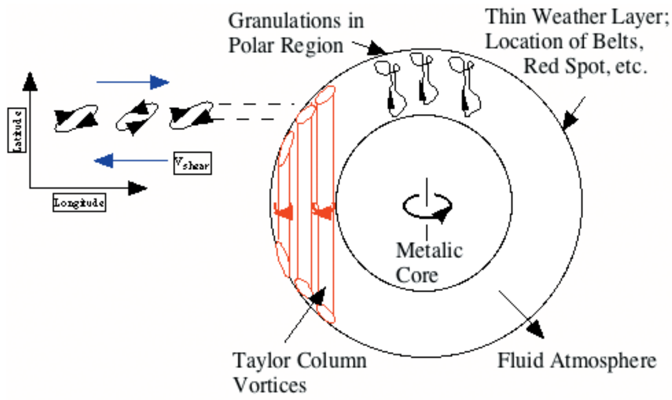

Figure 42. Schematic drawing of convection phenomena in the Jovian atmosphere. A schematic depiction of zonal belt formation in the secondary bifurcation scenario is also shown. Northern and southern projections of the Taylor column onto the weather layer with tilting modulation and bifurcation. (Based on [256].)

ω_F is the planetary rotation rote and $\tilde{\omega}$ is the vorticity of the fluid motion). Thus, the Taylor–Proudman theorem applies. This theorem states that in the presence of strong rotation, fluid flow tends to form columnar cells (i.e. 'Proudman Pillars') aligned with the axis of rotation, so as to minimize the energy expended on the bending of vortex lines. In the case of Jupiter, the cells in the interior are Taylor columns aligned with the axis of rotation of the planet. As shown in figure 42, the lower boundary condition on the columnar motion is the no-slip condition, applied at the surface of the metallic hydrogen core. This, of course, implies that an Ekman layer must connect the rigid surface to the rotating columns. The upper boundary condition is $v_z = 0$ at the weather layer, consistent with the 'rigid lid' imposed by the stable stratification there. The basic characteristics and turbulence physics of the Jovian atmosphere are summarized in table 10.

The dominant role of rotation in the dynamics of the Jovian atmosphere, together with the rigid lid and no-slip boundary conditions, imply that the evolution may be described using a two-dimensional thermal Rossby wave model, which evolves the fluid potential vorticity and the potential temperature along trajectories determined by geostrophic velocities. In this model, which is structurally similar to the curvature-driven ITG turbulence model, the free energy source is the temperature gradient, released by buoyancy drive. A critical value of the Rayleigh number $Ra_{\text{crit}} \sim O(10^4)$ [256] must be achieved for instability. Finite frequency, which enters via the diamagnetic frequency in the case of plasmas, appears here via β-effect, i.e. the gradient in the Coriolis frequency. For significant deviations from the critical Rayleigh number Ra_{crit}, large transport will result. The Jovian atmosphere is quite strongly turbulent and the effective Reynolds number of the weather layer is high. This is in sharp contrast to the case of a tokamak plasma, where the effective Reynolds number is low, i.e. $Re \sim 10$–100, at most, and the turbulence is more akin to wave turbulence than strong hydrodynamic turbulence.

Given this situation where the essential core dynamics are obscured by cloud cover, it is not surprising that (at least) two schools of thought on the origin of zonal belts have arisen. These are

(i) a secondary bifurcation approach (coherent), developed by Busse and his collaborators [256] and extended by several other authors [284–292]. This scenario accounts for the appearance of zones via the coherent modulational instability of an array of convection cells.

Table 10. Comparison and contrast of the Jovian atmosphere and toroidal system dynamics.

	Jupiter	Toroidal system
Basic characteristics		
Free energy	∇T	∇T, ∇n, etc
Rotation	$\Omega_{\mathrm{rot}} \gg \omega_k$	$\Omega_{\mathrm{c,i}} \gg \omega_k$
Rossby number	$R_{\mathrm{o}} \equiv \tilde{\omega}/\Omega_{\mathrm{rot}} \ll 1$	$R_{\mathrm{o}} = k_\perp^2 \rho_{\mathrm{i}}^2 e\tilde{\phi}/T \ll 1$
Effective Reynolds number	Strong turbulence	$R_{\mathrm{eff}} \sim$ 10–100 wave turbulence
Velocity	Geostrophic	$\boldsymbol{E} \times \boldsymbol{B}B^{-2}$
Turbulence physics		
Instability	Thermal Rossby	Drift-ITG
Frequency	β-effect	Diamagnetic
Cell structure	Taylor–Proudmann columns	Ballooning modes, extended along $\boldsymbol{B}_0$
Threshold	$R_{\mathrm{a}} > R_{\mathrm{a,c}}$	$[R/L_{\mathrm{Ti}} > R/L_{\mathrm{Ti}}]_{\mathrm{crit}}$
Eddy	Rising thermal plumes	Ballooning envelope fragments
Transport	Turbulent transport	D, $\chi \sim D_{\text{gyro-Bohm}}$
Basic structure	Belts, zones	$n = 0$, k_{r} finite, electrostatic fluctuations
Location	Surface, 'Weather layer'	Core and edge of confined plasmas
Mechanism for generation	(i) Secondary bifurcation of convection column tip cells (ii) Inverse cascade in weather layer with β-effect	Modulational instability of wave spectrum
Large-scale dissipation	Ekman friction	Rosenbluth–Hinton friction
Anisotropy	β-effect	Flow-minimal inertia
Flow and fluctuation model	Same	Flow 2D ($n = 0$) and fluctuation 3D, with $k_\parallel v_{\mathrm{th,e}} > \omega_k$
Bifurcated state	Belt formation	L-mode, ITB, ETB

(ii) the inverse cascade scenario (turbulent), developed by Hasegawa [282] and by Marcus and collaborators [283], which builds, in part, on the ideas of Rhines. This approach seeks to explain the appearance of zonal belts via an inverse energy cascade in β-plane turbulence, which is forced stochastically by the planetary atmosphere. Thus, two-dimensional turbulence is forced by rising plumes, which randomly impinge on the weather layer, thus energizing its motions.

Here, we briefly discuss the essential features of both approaches. The assumptions and logic of the two scenarios are summarized in figure 43. The key elements of Jovian zonal flow physics are listed in table 10, which includes a comparison to corresponding aspects of tokamak zonal flow physics.

Figure 42 encapsulates the quasi-coherent, secondary bifurcation scenario. The idea here is that a modulational (or 'tilting') instability occurs in the array of Taylor columnar vortices. The tilting instability is an extension of that originally analysed by Howard and Krishnamurti, and subsequently studied by many others. As a consequence, the cellular 'footprints' of these columns on the weather layer also undergo tilting instability, thus tending to amplify zonal shears and cause the development of belts. In this scenario, the number of zones is determined by the number of unstable columnar cells which 'fit' into the fluid interior region of the atmosphere. At high latitudes, near the polar regions, granules rather than belts are expected,

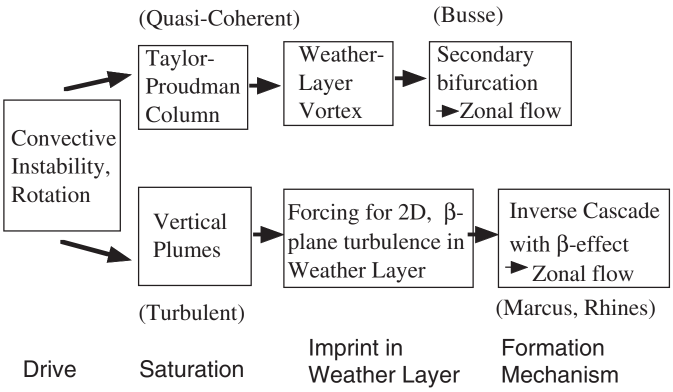

Figure 43. The assumptions and logic of the two scenarios.

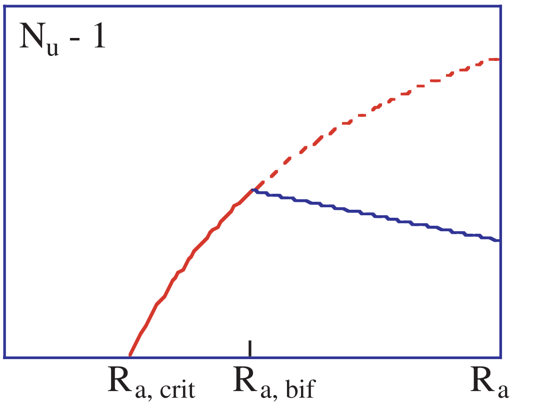

Figure 44. Cartoon of the secondary bifurcation scenario, after figure 6 of [284].

since the columnar cells sense *both* the no-slip lower boundary condition at the surface of the metallic hydrogen layer, as well as the rigid lid boundary condition at the weather layer. Thus, belts are limited to lower latitudes, where both 'ends' of the Proudman pillar pierce the weather layer. This is consistent with observations of the Jovian atmosphere.

It is interesting to note that, as Ra is increased, the bifurcation sequence closely resembles that familiar from the formation of the transport barrier. As shown in figure 44, starting from Ra_{crit}, thermal transport (as quantified by the Nusselt number N_u) increases with Ra. At a second critical Rayleigh number called Ra_{bif}, generation of secondary flows begins. This generation is accompanied by an alteration of the convection pattern structure, in that cells are tilted, sheared and distorted by the zonal flows. As Ra increases beyond Ra_{bif}, the Nusselt number decreases with increasing Ra, while the zonal flow energy increases, symptomatic of heat transport suppression and the increased channelling of free energy into zonal flows, rather than convection cells. At higher values of Ra, tertiary bifurcations, vacillations, cyclic phenomena, etc are predicted to appear, as well [256, 284–286]. This is shown in figure 44. Not surprisingly for this scenario, the mean zonal flow pattern exhibits north–south symmetry, modulo some correction for the effects of the great Red Spot, which appears in the southern hemisphere. In the Busse scenario, the scale of zonal bands is set by the eigenvalue for secondary bifurcation, implying a band scale which is set by some fraction of the box size.

The second scenario is that of an inverse cascade on a β-plane, as proposed by Marcus, building upon the ideas of Rhines. In this scenario, rising plumes from the convection zone constitute a source of forcing for the two-dimensional inverse cascade on a β-plane. The forcing term is proportional to $\omega_F \partial V_z/\partial z$, where $\partial V_z/\partial z$ is necessarily large in the weather layer, on account of the stable stratification there. On forcing scales, the nonlinearity is strong, so an inverse cascade develops toward large scales, with Kolmogorov spectrum $E(k) \sim k^{-5/3}$. Anisotropy develops as a consequence of β, via an extension of the mechanism of Rhines. The Rhines mechanism is based on the observation that on a β-plane the eddies have a finite frequency, corresponding to the Rossby wave frequency $\omega = \beta k_x k_\perp^{-2}$. At low k, such waves are strongly dispersive, so that triad interaction is severally inhibited, except for domains with $k_x = 0$. *The preference of nonlinear interaction for such states of high symmetry explains the tendency to form zonal bands*. Note that the Rhines length effectively defines the scale size on which enstrophy enters. The onset of such band formation occurs at large scales when the eddy turnover rate drops to the level of the wave frequency, i.e. $k\tilde{V} = \beta k_x k_\perp^{-2}$, so that the Rhines scale, which demarks the onset of zonal structure, is $(\tilde{V}/\beta)^{1/2}$. The inverse cascade is, in turn, damped by scale-independent Rayleigh friction, associated with Ekman damping, etc. Not surprisingly, the frictional damping plays a crucial role in the model, as the Rosenbluth–Hinton scale-independent friction term does in the plasma zonal flow problem. Marcus *et al* emphasize that three conditions are necessary for zonal flow formation, in addition to rapid rotation, convective instability and large $\partial V_z/\partial z$ in the weather layer, which we have already established. These are that the size of the vorticity advection nonlinearity must

(a) exceed the frictional damping on the forcing scale. Otherwise, energy cannot couple to the Rhines scale and thus anisotropy cannot develop.
(b) exceed the strength of the β-effect, i.e. $k_y \partial\omega_F/\partial x$ on forcing scales. Otherwise, energy will be coupled to Rossby waves, rather than zonal flows. Of course, a spectrum of Rossby waves can be unstable too, and thus amplify zonal perturbations, as discussed in this paper. The implications of this secondary mechanism have not been addressed by Marcus *et al*.
(c) exceed the viscous damping. Otherwise, energy will be dissipated so that structure formation will not be possible.

In the Marcus scenario, the number of bands is determined via energy balance by the system parameters, such as the forcing strength (related to the heat flux), the frictional damping, etc. In addition, tertiary KH instability may enter the determination of the band structure by limiting the strength of zonal vorticity. While Marcus and collaborators have assembled good computational arguments that large scale structure formation will occur if criteria (a)–(c) (above) are satisfied, further research is necessary to clarify the issues related to the details of pattern selection, such as band scale, number of bands, etc.

Predictably, work subsequent (i.e. [288–290]) to the initial efforts of Busse *et al* and Marcus *et al* paints a picture of zonal flow phenomena which combines aspects of both outlooks. Of particular note is a recent paper by Jones *et al* [288], which builds upon and extends earlier studies by Brummell and Hart [289] and Christensen [290]. In particular, Jones *et al* emphasize the importance of scale-independent frictional drag, which is isomorphic in structure to Rosenbluth–Hinton collisional damping but originates in the friction between the Proudman pillars and the weather layer and inner core. Such friction appears to play a key role in setting the *number* of zonal bands in the system, for a given set of parameters. The *width* of an *individual band*, however, is close to that of the Rhines scale, and exhibits a similar parameter scaling. This is somewhat interesting in that the other results of Jones *et al* appear consistent with the secondary bifurcation scenario of Busse, yet the band scale size is set by the competition between nonlinearity and dispersion, as predicted by Rhines and Marcus. In

Busse's scenario, the zone scale is set by the box size. Finally, Jones *et al* report the appearance of cycles or 'bursty phenomena', which are very similar to the corresponding cyclic system states discussed in section 3. As before, here the cycles consist of alternating intervals of instability growth followed by quenching by the shearing action of the zonal flows. The scale-independent damping sets the duration of the interval between the maximum of the zonal flow shear and the return of buoyancy-driven turbulence, as does the Rosenbluth–Hinton friction in the case of ITG turbulence.

A related line of work in the geophysical fluid dynamics community is concerned with three-dimensional studies of convection driven dynamos in systems bounded by rapidly rotating spheres (for example [291, 292]). In this case, several interesting phenomena appear. First, zonal magnetic fields, as discussed in section 3, can be generated and are observed. Second, both mean field $\langle \boldsymbol{J} \rangle \times \langle \boldsymbol{B} \rangle$ forces and turbulent magnetic stresses can react back on the fluid flow, causing a quench or termination of the shear amplification process. This reduction in shearing effects, in turn, leads to an *increase* in heat transport and, in some cases, an increase in dynamo activity. The latter occurs when the 'gain' due to enhanced convective turbulence levels outweighs the 'loss' of the Ω-effect (i.e. shear amplification of magnetic fields). Moreover, cyclic dynamo and zonal field evolution are observed. Ongoing work here is focused on the exploration of extremes of the possible regimes of Prandtl and magnetic Prandtl number.

5.3. Superrotation of the Venusian atmosphere

Another interesting mystery in the dynamics of planetary atmosphere is the superrotation of Venus [293, 294]. *By 'superrotation', we mean a fast zonal flow* with an *azimuthal speed in excess of the rotation velocity of the planet itself*! Indeed, Venusian winds can reach $100\,\mathrm{m\,s^{-1}}$ at altitudes of 60–70 km, which is about 60 times faster than the speed of the planet. This remarkable observation naturally suggests that the planetary wind results from some processes of self-organization of thermally driven convective flow in the Venusian atmosphere, which is similar to the mechanism of zonal flow generation.

The key questions pertinent to the generation of zonal flows in the atmosphere of Venus are: (a) what is the mechanism of symmetry breaking which seeds zonal flow generation? and (b) what are the implications of three-dimensional geometry? In this regard, note that the Venusian atmosphere is *not* thin.

Regarding (a), the conventional wisdom is that superrotation results from a tilting instability, the initial symmetry breaking for which results from the motion of the solar heating. This is called the 'moving flame mechanism'. Another possibility for symmetry breaking is convection driven flows between day and night sides of the planet (i.e. thermal winds) [295]. Other mechanisms involve thermal tidal pumping [287] and Hadley circulation pumping mechanism [296], which involves a horizontal eddy viscosity. Regarding (b), recent results [297] indicate that the moving flame mechanism is viable in two-dimensional (though the cell-temperature perturbation is a critical element of the dynamics, contrary to initial expectations), but fails in three dimensions, since the basic flow is *stable* in spherical geometry [285]. Thus, attention is shifting to the tidal pumping and Hadley mechanisms. Clearly, much further research is necessary in order to understand the superrotation of the Venusian atmosphere.

6. Extensions of theoretical models

To supplement the theory of zonal flows explained in section 3, some advanced extensions are described in this section. The first topic is the streamer, which has a lot of similarity to the zonal flow but can have a quite different influence on the drift wave turbulence and transport. The second issue is the statistical nature of the zonal flow. While the mean field instability growth associated with the negative viscosity effect, explained in section 3, is essential to the dynamics of zonal flow, noise can be important, as well. Thus, the probability density function (PDF) for the dynamical quantities in the system of drift wave–zonal flow can have non-Gaussian properties, and the noise can have great influence on some global parameters of interest (e.g. heat flux, transition boundary, etc). The third is the non-Markovian nature of the system dynamics. These issues belong in the realm of advanced research on the zonal flow, and are discussed briefly in this section. Finally, a method of theoretical analysis of the zonal flow (based on reductive perturbation theory), which is complementary to the one explained in section 3, is briefly addressed. An extended description on related development (including streamers [298–306]) is given in [2].

6.1. Noise effects and probabilistic formulations

Background turbulence that induces zonal flow has a short correlation time, so that the driving force for zonal flow has a component that rapidly changes in time. The driving force by turbulence, on the average, acts to cause the growth of the zonal flow as is explained in section 3. In addition to the 'negative viscosity effect', which drives zonal flow growth, there is noise excitation of zonal flow scales due to incoherent emission from drift waves [15, 42, 50, 307].

A systematic description of the statistical average and the noise has been given in the literature [50, 307]. A calculation using the eddy-damped-quasi-normal-Markovian (EDQNM) approach has been discussed in detail in [307]. By use of the action of drift waves N_k and the enstrophy of zonal flows Z_q, a set of balance equations for the system dynamics has been derived. Detailed calculation is left to the references, but the noise term is explained here. For long wavelength evolution, one finds

$$\frac{\partial}{\partial t} Z_q = 2\gamma_q Z_q + \dot{Z}_q^{\text{noise}}, \tag{6.1.1}$$

where γ_q is the growth rate of the zonal flow. Note that a stationary solution is possible only when $\gamma_q < 0$, which requires confrontation of the problem of nonlinear saturation of zonal flows. Here $\dot{Z}_q^{\text{noise}}$ is the long time average magnitude of the mean square of the noise term, i.e.

$$\dot{Z}_q^{\text{noise}} = q^4 \sum_q \frac{k_y^2 k_x^2}{(1 + k_\perp^2)^4} Re\theta_{q,k,-k} N_k^2, \tag{6.1.2}$$

where $\theta_{k,-k,q}$ is the triad interaction time of three waves [13, 307]. In this expression, γ_q *must* include the effect of nonlinear stabilization, so that γ_q may be negative at finite amplitude, which is necessary for any (meaningful) stationary state. By use of such a balance equation, the role of noise pumping has been analysed [50]. The possibility of bifurcation has been pointed out. Obtaining and understanding such a γ_q is a subject for ongoing research, and the full solution of this problem is left to future studies.

6.2. Statistical properties

It is well-known that a statistical approach is needed to treat the probability density function [16, 308, 309]. In order to clarify the implications of statistical theory on the understanding of the relevant phenomena, it is useful to consider models which discuss low dimensional systems. One may write a Langevin equation to study the statistical property of the quantity X which is the subject of interest:

$$\frac{\partial}{\partial \tau} X + [\Lambda_0(X) + \Lambda_1(X) w_1(\tau)] X = w_0(\tau) g. \tag{6.2.1}$$

In this equation Λ is the (nonlinear) damping rate, which can be nonlinear and which can contain multiplicative noise $w_1(\tau)$, g is the magnitude of the noise source and $w_0(\tau)$ represents the noise. (It is not necessary to specify the rhs of equation (6.2.1) as Gaussian white noise. What is necessary is that the autocorrelation time of the noise must be much shorter than the relevant time scale Λ^{-1}.)

Non-Gaussianity of the PDF is caused either by the nonlinearity in the damping rate Λ, or by the dependence of the noise source g on the quantity X, or by multiplicative noise entering via the damping rate. An example of a problem involving multiplicative noise is zonal flow growth in the presence of avalanches. This scenario is a simple example, of *multiplicative noise*. Note that multiplicative noise necessarily changes the structure of the Fokker–Planck equation, so that the PDF is, in general, non-Gaussian.

There have been some basic studies of the effect of noise on bifurcation transitions and transport barrier formation, but in general, the theory of zonal flow and transport barrier dynamics with noise remains *terra nova*. Note that the interplay of avalanches with zonal flows and barriers gives another perspective on the problem of the interplay of zonal flows and streamers, discussed previously.

6.2.1. Instantons. It has been known that the large amplitude drift wave takes a form of 'modon' [310, 311]. Modon solutions can be used as a basis for a theory of instantons in drift wave turbulence. Instantons are temporally localized solutions which correspond to trajectories of least action. Instanton solutions are those of steepest descent, and so dominate the time-asymptotic PDF. They thus serve as tractable models of intermittency phenomena.

Schematically speaking, nonlinear drift waves have an 'anti-shielding effect', which corresponds to vortex coalescence. (An explicit illustration by direct numerical simulation is seen in [261].) A longer lifetime is expected for a larger-amplitude modon, so that a stretched, non-Gaussian PDF is obtained [55, 312, 313]. The PDF of the local Reynolds stress $\mathcal{R}$ was then obtained from the fluctuation PDF. The Reynolds stress PDF $P(\mathcal{R})$ was found to be of the form:

$$P(\mathcal{R}) \sim \exp\left(-\frac{C}{\kappa}\mathcal{R}^{3/2}\right), \tag{6.2.2}$$

where κ is the mean-square noise forcing, and C stands for a normalization coefficient that includes the effect of the spatial shape of the modon. In this case, an exponential tail is obtained. In addition, as the external forcing becomes larger, the tail extends to a larger value of $\mathcal{R}$. The divergence of $\mathcal{R}$ is the torque that drives plasma flow. This result suggests that the noise source for the zonal flow, which has been discussed in previous sections, is given by a *non-Gaussian* distribution. Further research in this direction is needed.

6.2.2. Nonlinearity in noise. In the renormalization model for drift waves, the noise related to g is a function of the amplitude of the turbulence [16, 188, 189, 302, 309, 314–316]. This gives small but finite power-law tails in the study of multiple-scale turbulence and bifurcation. The presence of non-Gaussian tails suggests that large-scale but rare events could play a dominant role in determining the average. A detailed calculation of the turbulent noise has been developed in [317] and has been applied to the case of zonal flow excitation [49, 307].

The role of turbulent noise is particularly important when one studies subcritical bifurcation. A dynamical model for a relevant, reduced degree of freedom has been developed for the L–H transition [318]. A Langevin equation for the radial electric field in the plasma edge $X = e\rho_{\mathrm{p}}E_r/T$ is derived. The damping term in (6.2.1) is given as $\Lambda X = (1 + 2q^2)^{-1}(qR/\rho_s ec_s n_i)J_r$, where J_r is the normalized current. As has been discussed in a model of the L–H transition, the deterministic equation for steady state thus becomes $\Lambda X = 0$ with multiple solutions for X. The noise amplitude g is dependent on X, so we have a case of nonlinear noise. The stationary solution for the PDF of X, $P_{eq}(X)$, may be expressed as $P_{eq}(X) \propto g^{-1}\exp(-S(X))$ by use of the nonlinear potential $S(X) = \int^X 4\Lambda(X')g(X')^{-2}X'\,dX'$. The minimum of $S(X)$ (apart from a correction of order $\ln g$) predicts the most probable state of X. The phase boundary is

$$S(X_H) = S(X_L) + \tfrac{1}{2}\ln(\Lambda_L/\Lambda_H), \tag{6.2.3}$$

where $\Lambda_{L,H} = 2|X\partial\Lambda_X/\partial X|$ at $X = X_{L,H}$. This is an extension of the *Maxwell construction rule* in the thermodynamics. The statistical average of the gradient-flux relation $Q_r[p']$ is derived. The transition rate from one metastable state to a more stable state is calculated by use of the nonlinear potential [318], in a manner similar to the Kramers barrier transition calculation [319]. Statistical averages determine the boundary of the phase [320].

Related topics include self-organized criticality (SOC) models [321–330] and observations of avalanche phenomena in DNS [155, 331–334], for which [2] provides supplementary explanations.

6.3. Non-Markovian theory

The nonlinear analysis explained in section 3 was presented in simplified limits. One is the limit where the turbulent decorrelation of drift waves is absent, that is, a drift wave-packet has two integrals of motion. As a consequence, drift wave-packets are considered to move on a surface in phase-space set by the initial conditions. These BGK-type solutions are addressed. The other is the limit in which the turbulent decorrelation of drift waves is so fast that the Markovian approximation is used to model nonlinear interactions. In general, the nonlinear decorrelation time of drift waves is not zero, even though it may be short. Non-Markovian theory is necessary to treat the intermediate cases [335]. Recent advances in this direction are discussed in this section.

6.3.1. Hamiltonian structure of the dynamics. The conservation property of drift waves in the presence of zonal flow is expressed by the invariance of the action along rays, e.g. equation (3.4.7).

The action conservation equation is a Hamiltonian equation for the wave-packet density. In order to consider this statistical dynamics property, the response of wave-packets in the presence of the zonal flow described is reduced perturbatively. One writes $N(\boldsymbol{x}; \boldsymbol{k}, t) = \langle N(\boldsymbol{x}; \boldsymbol{k}, t)\rangle + \tilde{N}(\boldsymbol{x}; \boldsymbol{k}, t)$, where $\langle N(\boldsymbol{x}; \boldsymbol{k}, t)\rangle$ is an average over temporal variations with respect to zonal flows, and $\tilde{N}(\boldsymbol{x}; \boldsymbol{k}, t)$ denotes the deviation. The dynamical equation for $\langle N(\boldsymbol{x}; \boldsymbol{k}, t)\rangle$ is an example of a Zwanzig–Mori equation. For an intermediate scale zonal flow, $k \gg K_r \gg L_n^{-1}$, a non-Markovian phase-space kinetic equation of the form is obtained:

$$\begin{aligned}
&\frac{\partial}{\partial t}\langle N(\boldsymbol{x}; \boldsymbol{k}, t)\rangle - \mathcal{L}_{w,0}\langle N(\boldsymbol{x}; \boldsymbol{k}, t)\rangle \\
&\qquad = \int_0^t dt' \left\{ \frac{\partial}{\partial \boldsymbol{x}} \cdot \boldsymbol{D}^{XX}(t-t') \cdot \frac{\partial}{\partial \boldsymbol{x}} + \frac{\partial}{\partial \boldsymbol{x}} \cdot \boldsymbol{D}^{XK}(t-t') \cdot \frac{\partial}{\partial \boldsymbol{k}} \right\} \langle N(\boldsymbol{x}; \boldsymbol{k}, t')\rangle \\
&\qquad\quad + \int_0^t dt' \left\{ \frac{\partial}{\partial \boldsymbol{k}} \cdot \boldsymbol{D}^{KX}(t-t') \cdot \frac{\partial}{\partial \boldsymbol{x}} + \frac{\partial}{\partial \boldsymbol{k}} \cdot \boldsymbol{D}^{KK}(t-t') \cdot \frac{\partial}{\partial \boldsymbol{k}} \right\} \langle N(\boldsymbol{x}; \boldsymbol{k}, t')\rangle,
\end{aligned} \tag{6.3.1}$$

where $\boldsymbol{D}^{XX}$, $\boldsymbol{D}^{XK}$, $\boldsymbol{D}^{KX}$ and $\boldsymbol{D}^{KK}$ are 2×2 tensors, given by

$$\boldsymbol{D}^{XX}_{\mathrm{i},j}(t-t') = \left\langle V_{\mathrm{ZF},i}(\boldsymbol{x},t) V_{\mathrm{ZF},j}(\boldsymbol{x}(t \mid t'), t') \right\rangle, \tag{6.3.2a}$$

$$\boldsymbol{D}^{XK}_{i,j}(t-t') = \left\langle V_{\mathrm{ZF},i}(\boldsymbol{x},t) W_{\mathrm{ZF},j}(\boldsymbol{x}(t \mid t'), \boldsymbol{k}(t \mid t'), t') \right\rangle, \tag{6.3.2b}$$

where $\boldsymbol{D}^{KX}$ and $\boldsymbol{D}^{KK}$ are given by replacing V_{ZF} and W_{ZF} accordingly, $\boldsymbol{W}_{\mathrm{ZF}} = -\partial/\partial\boldsymbol{x}(\boldsymbol{k}\cdot\boldsymbol{V}_{\mathrm{ZF}})$, and i, j stand for the x and y directions. (The tensor form is necessary if one considers poloidal inhomogeneity, as is discussed in section 3.3.4.) If the Markovian approximation is now employed, one finds $\boldsymbol{D}^{\alpha\beta}_{i,j} = \int^t \mathrm{d}t' \boldsymbol{D}^{\alpha\beta}_{i,j}(t-t')$, where α, β vary over X, K. The two quantities $D^{XX}_{x,x}$ and $D^{KK}_{y,y}$ reduce to what has been previously obtained in the limit of the short lifetime of the drift waves.

Equation (6.3.1) describes the evolution of drift waves in the presence of a statistical ensemble of zonal flows. First, it is a non-Markovian equation, and includes the finite memory time. Second, this equation includes cross-interaction between the wavenumber space and the real space. Note that the cross-interaction terms are also derived in the diffusion approximation. As a noticeable consequence of the non-Markovian effect, [335] illustrated super-diffusion and sub-diffusion phenomena in the transient response. (The cross-interaction term is small for the pure zonal flow case.)

The Kubo number $\mathcal{K}$ may be defined as the ratio of the decorrelation time of drift waves to the bounce frequency of wave-packets in the trough of the zonal flow, $\mathcal{K} = \omega_{\mathrm{bounce}}/\gamma_{\mathrm{drift}}$. The analyses in sections 3.5.4, 3.5.5 and 3.5.7 are developed for $\mathcal{K} < 1$, while that in section 3.5.6 is given for the limit $\mathcal{K} \to \infty$. (For the details of the bounce frequency, see section 3.5.6.) Equation (6.3.1) allows a study that covers a wide range of the Kubo number. Evaluations of the Lagrangian correlations in the rhs of equation (6.3.2) have been studied by using of the method of decorrelation trajectories [336–338]. Analysis of these effects has begun [181]. One important fact is that the poloidal wavenumber of drift waves k_y is no longer constant when the $\boldsymbol{E} \times \boldsymbol{B}$ flow exhibits the poloidal asymmetry. This is in contrast to the case of stationary and purely $m = 0$ zonal flow. The transparency of the analysis which was brought by the introduction of the WKE could be maintained by introducing Casimir invariants for the Hamiltonian dynamics with multiple fields [339]. New insights will be given by future research.

6.4. Envelope formalism

The zonal flow problem belongs to the class of problems concerned with understanding interactions in multi-component systems, with each component having its own range of characteristic space–time scales. So far, we have discussed two approaches to the multi-scale interaction problem. The first uses parametric (modulational) theory, and is based on a modal interaction expansion. The second is wave kinetics and adiabatic theory, and is based on a description employing rays and eikonal theory. A third multi-scale expansion approach exists, and is commonly referred to as the envelope formalism. This section is devoted to describing the envelope formalism approach to the zonal flow problem.

The envelope formalism uses reductive perturbation theory to develop a description in terms of the dispersion relation of a rapidly varying carrier wave (associated with the primary perturbation) and the amplitude of a slowly varying intensity envelope, associated with the mean field. The envelope evolves slowly in space and time, as compared to the carrier. The envelope formalism complements the parametric and wave kinetic approach in that:

(a) it is not restricted by the structure inherent to a modal expansion, and thus can represent a wider and richer class of nonlinear phenomena (i.e. solitons, collapse, etc) than simple parametric theory can.

(b) it is not restricted to an eikonal description, and so can capture the physics of the competition between diffraction and nonlinearity, unlike wave kinetics.

Anticipated by Landau, the rigorous envelope formalism was pioneered by Newell and Whitehead [35] in 1969, with the aim of describing secondary pattern formation slightly above marginality in Rayleigh–Benard convection. The most notable application of the envelope formalism in plasma physics is to the classic problem of Langmuir turbulence and Langmuir collapse, as studied by Zakharov in 1972 [110]. It is worth mentioning here that the Zakharov equations are the coupled envelope equations for the amplitudes of the electric field E and density perturbation $\tilde{n}$ in Langmuir turbulence, i.e.

$$-2i\omega_{\mathrm{pe}}\frac{\partial}{\partial t}E = \tilde{n}E - \gamma v_{\mathrm{The}}^2\nabla^2 E, \tag{6.4.1a}$$

$$\frac{\partial^2}{\partial t^2}\tilde{n} - c_{\mathrm{s}}^2\nabla^2\tilde{n} = \nabla^2|E|^2. \tag{6.4.1b}$$

Depending on dimensionality, initial conditions and the number of degrees of freedom, many different nonlinear phenomena, including soliton formation, collapse, secondary radiation, etc, can be described using this simple model. The simplicity and flexibility of the Zakharov equations have greatly stimulated interest in both Langmuir turbulence and in the application of the envelope formalism to other multi-scale nonlinear problems. The first application of the envelope formalism to convective cell dynamics (and thus zonal flows) was by Taniuti and collaborators in 1979 [340], and an extension of Sagdeev *et al* [5] was given using the full systematology of reductive perturbation methods in [341].

Here, we discuss only an especially simple application of the envelope formalism [342, 343] to the problem of zonal flow generation in drift wave turbulence. We consider a plasmas in two-dimensional geometry with $T_{\mathrm{i}} = 0$, but with a mean $\boldsymbol{E} \times \boldsymbol{B}$ flow. To implement the envelope formalism, we write $e\tilde{\phi}/T_{\mathrm{e}} = N \exp \mathrm{i}(\boldsymbol{k}\cdot\boldsymbol{x} - \omega t) + \mathrm{c.c.}$ and assume the drift wave envelope $N(\boldsymbol{X}, T)$ varies *slowly* in space and time. The fast variation obeys the usual dispersion relation $\omega = k_\theta V_{\mathrm{d}}(1 + k_\perp^2\rho_{\mathrm{s}}^2)^{-1}$. Here, for the slowly varying parameters, the ordering $T = \varepsilon t$, $\boldsymbol{X} = (\varepsilon x, \varepsilon y)$ expresses the scale separation. (In this section, ε is a small parameter, not the inverse aspect ratio.) Note that nonlinearities associated with like-scale interactions are ignored. Now, expanding in ε throughout yields the equations for the envelope N and the mean fields $\langle n\rangle$ and $\langle\phi\rangle$, which are

$$\begin{aligned}\mathrm{i}\frac{\partial N}{\partial\tau} &+ \frac{1}{2}\left(\frac{\partial^2\omega_k}{\partial k_x^2}\frac{\partial^2}{\partial X^2} + \frac{\partial^2\omega_k}{\partial k_y^2}\frac{\partial^2}{\partial Y^2} + 2\left(\frac{\partial^2\omega_k}{\partial k_x\partial k_y}\right)\frac{\partial^2}{\partial X\partial Y}\right)N\\ &+ \rho_{\mathrm{s}}^2\omega_{\mathrm{ci}}\left(k\times\nabla\frac{e\langle\phi\rangle}{T_{\mathrm{e}}}\right)\cdot\hat{z}N - \frac{\rho_{\mathrm{s}}^2\omega_{\mathrm{ci}}}{1+k_\perp^2\rho_{\mathrm{s}}^2}(k\times\nabla\langle n\rangle)\cdot\hat{z}N = 0,\end{aligned} \tag{6.4.2a}$$

$$\begin{aligned}&\left(\varepsilon\frac{\partial}{\partial\tau} - \boldsymbol{v}_{\mathrm{g}}\cdot\nabla\right)\left(\frac{\partial^2}{\partial X^2} + \frac{\partial^2}{\partial Y^2}\right)\frac{e\langle\phi\rangle}{T_{\mathrm{e}}}\\ &\quad + 2\rho_{\mathrm{s}}^2\omega_{\mathrm{ci}}\left(k_x k_y\left(\frac{\partial^2}{\partial Y^2} - \frac{\partial^2}{\partial X^2}\right) + \left(k_x^2 - k_y^2\right)\frac{\partial^2}{\partial X\partial Y}\right)|N|^2 = 0,\end{aligned} \tag{6.4.2b}$$

$$\left(\varepsilon\frac{\partial}{\partial\tau} - \boldsymbol{v}_{\mathrm{g}}\cdot\nabla\right)\langle n\rangle + V_{\mathrm{d}}\frac{\partial}{\partial Y}\frac{e\langle\phi\rangle}{T_{\mathrm{e}}} = 0. \tag{6.4.2c}$$

Note that equation (6.4.2b) shows that the structure of the secondary flow is determined, in part, by the anisotropy of the underlying turbulence—i.e. via terms $\sim (k_x^2 - k_y^2)$, etc. The system of equations (6.4.2a)–(6.4.2c) constitutes the set of envelope equations for the drift wave–zonal flow system, including the more general case of drift wave–convective cell systems [344–349].

For the particular case of zonal flow, $\partial/\partial Y \to 0$, and collisional damping of the zonal flow $\gamma_{\rm damp}$ is important, the envelope equation is a cubic nonlinear Schrödinger equation

$$\mathrm{i}\frac{\partial N}{\partial \tau} + \frac{1}{2}\frac{\partial^2 \omega_k}{\partial k_x^2}\frac{\partial^2}{\partial X^2}N + \left(\frac{2\rho_{\rm s}^4\omega_{\rm ci}^2 k_y^2 k_x}{\partial \omega_k/\partial k_x}\right)|N|^2 N = 0. \tag{6.5}$$

Straightforward analysis then predicts modulational instability for drift wave numbers such that $1 + \rho_{\rm s}^2 k_y^2 - \rho_{\rm s}^2 k_x^2 > 0$. The most unstable zonal flow wavenumber is $q_{x,\max} = \omega_{\rm ci}^2(1+\rho_{\rm s}^2 k_\perp^2)^5 V_{\rm d}^{-2}(1+\rho_{\rm s}^2 k_y^2 - \rho_{\rm s}^2 k_x^2)^{-1} N_0$, where N_0 is the maximum drift wave amplitude. The domains of zonal flow and streamer instability are shown in [2]. A similar analysis for the collisional case has been performed as well. The results are given in [29].

From the expression for $q_{x,\max}$, weakly collisional zonal flow will have radial scale $\Delta r \sim (\rho_{\rm s}^2/L_n)(\tilde{n}/n_0)^{-1} F_{\rm ZF}(\rho_{\rm s}\boldsymbol{k}_\perp)$. Here $F_{\rm ZF}(\rho_{\rm s}\boldsymbol{k}_\perp)$ is determined by the $\rho_{\rm s}\boldsymbol{k}_\perp$-dependence of $q_{x,\max}$. Note that the scale is amplitude dependent. For $\tilde{n}/n_0 \sim \rho_{\rm s}/L_n$, $\Delta r \sim \rho_{\rm s} F_{\rm ZF}(\rho_{\rm s}\boldsymbol{k}_\perp)$, so a wide range of zonal flow scales may be excited. Finally, note that zonal flows will be strongly localized near caustics, where $\partial\omega_k^2/\partial k_{\rm i}^2 \to 0$. Strongly anisotropic collapse, to localized, singular shear layers, is possible at caustics.

There is considerable work on the envelope formalism beyond the simple analysis described above. Weiland and collaborators have explored the effect of finite $T_{\rm i}$ and ion temperature perturbations [350]. More recent extension includes the study of electromagnetic perturbations [351]. Spineanu and Vald have studied the structure of zonal flow and have analysed possible poloidal dependence [210, 352]. Gurcan *et al* have examined zonal flow and streamer formation in ETG turbulence, which is isomorphic to quasi-geostrophic turbulence, since both waves and flows have Boltzmann ions [353–355]. They determined the criterion for collapse to singular shear layers and addressed the problem of pattern competition between streamers and zonal flows using techniques from the Langmuir problem.

7. Laboratory experiments on zonal flows physics

In this section, we discuss laboratory experiments relevant to zonal flows. Experimental studies of zonal flows in plasmas are few and far between. Thus, this section is written with two aims in mind, namely, both to review existing work and also to outline possible future directions for studies of zonal flows, in the hope that more experimental work will be stimulated.

This section is organized as follows. Section 7.1 presents experimental results on determining zonal flow characteristics. Section 7.2 discusses zonal flow dynamics and their interaction with ambient turbulence. We present our suggestions for future experimental research, including possibilities for basic experiments designed for zonal flow measurements, in section 7.3.

7.1. Characteristics of zonal flows

The characteristics of zonal flows are described in sections 2, 3 and 4, and are summarized in table 2. Here, we reiterate some of those which are most relevant to experimental measurements and tests [145].

7.1.1. Spatial structure. In confined plasmas, the equilibrium profile is usually treated as a smooth function of radius, the characteristic scale length of which is less than or equal to the minor radius (excluding the case of transport barriers) or of the barrier thickness (for

Table 11. Experimental characteristics of zonal flows.

	Zonal flow (narrow sense)	GAMs
Fluctuation structure	$m = n = 0$ for $\tilde{\phi}$	$m = n = 0$ for $\tilde{\phi}$
	$\hat{n} \ll \hat{\phi}$	$m = 1, n = 0$ for $\tilde{n}$
		$\lvert\tilde{n}/n_0\rvert = \sqrt{2} q_r \rho_s \lvert e\tilde{\phi}/T_e\rvert$
Real frequency	$\Omega_{ZF} \simeq 0$	$\omega_{GAM} \simeq v_{Thi}/R$
Autocorrelation time	$\varepsilon \nu_{ii}^{-1}$, or other (TBD)	ν_{ii}^{-1} or other (TBD)
Radial wavelength	$a\rho_i > q_r^{-2} > \rho_i^2$	$\leftarrow$
Radial coherence length	Several tens of $\rho_i \sim \sqrt{a\rho_i}$	$\leftarrow$
Amplitude (vorticity)	Order of $\rho_i^{-1} V_d$	TBD

barriers). In the presence of turbulence, the flux surface-averaged flow velocity can vary radially for two reasons. One is the $\boldsymbol{E} \times \boldsymbol{B}$ zonal flow structure, which is discussed in this review. The other possible origin is the corrugation of flux surface-averaged pressure. This latter type of localized diamagnetic flow, which is nothing but a symptom of flux surface-averaged pressure corrugation, must be carefully distinguished from true zonal flows in experiments. Such pressure corrugations may be induced by avalanches, streamers and other transport events.

Turbulence-driven zonal flows are radially localized, with a broad spectrum of radial scales ranging from the microscale (i.e. turbulence eddy sizes of $\Delta r \sim$ several ion gyro-radii) through mesoscales (i.e. a fraction of minor radius). Gyrokinetic simulations of ITG turbulence show that the component of the zonal flow has $q_r \rho_i \sim 0.1$ [145], for typical tokamak core plasma parameters, though the sensitivity of this value to variable system parameters is unclear. The associated electrostatic potential ϕ_{ZF} is poloidally symmetric ($q_\theta = 0$).

We note that the magnitude of zonal flow velocity, as predicted from tokamak core turbulence simulations, is typically small (i.e. $V_{ZF} = 10^{-2} v_{th,i}$), but the associated $\boldsymbol{E} \times \boldsymbol{B}$ shearing rate is significant enough to regulate turbulence and transport [145, 356]. Obviously, this indicates that the zonal flow shear spectrum peaks at a higher $q_r \rho_i$, than the zonal flow velocity and potential spectra. This is apparent from the results of gyrofluid simulations, as shown in figure 3 of [356]. This suggests that the difficulties in measuring zonal flows in the experiments come mainly from the fact that it is neccesary to simultaneously ensure sensing long correlation lengths in the toroidal direction ($n = 0$) and poloidal direction ($m = 0$) along with fast radial variation (on the scale of several ion gyro-radii). Finally, achieving the goals of detecting the variability of the portion of the zonal flow spectrum responsible for transport regulation and identifying a causal link between flows and turbulence are further complicated by the fact that the 'relevant' shearing scales are determined by their autocorrelation times, as well as their shear strength. Features of the zonal flows contrasting the zero frequency zonal flows from GAM components are listed above in table 11.

7.1.2. Temporal behaviour. The frequency spectra of zonal flows and GAMs depend on plasma conditions, and for this reason edge turbulence deserves a later, separate discussion. In the core, the zonal flow frequency spectrum at a fixed q_r has a broad peak at $\omega = 0$, and a width indicating a finite lifetime, $\tau_{ac,ZF} = (\Delta\omega_{ZF})^{-1}$. Zonal flows thus have frequency components which significantly outlive the ambient turbulence ($\Delta\omega_{ZF} < \Delta\omega_{drift}$, or equivalently $\tau_{ac,ZF} > \tau_{ac,drift}$). Their lifetime $\tau_{ac,ZF}$ is determined either by collisions, turbulent transfer processes (as are explained in section 3), by external noise (explained in section 6), or by the instability of the zonal flow pattern.

In general, the question of the nature of zonal flow damping boils down to a comparison between the strength of collisional and nonlinear processes.

7.1.3. Toroidal geometry and GAMs. In toroidal geometry, the poloidal direction is no longer an ignorable coordinate, and there exists an inevitable poloidal angle dependency of many key quantities (for instance, B depends on the poloidal angle). While the flux surface-average of $\boldsymbol{E}\times\boldsymbol{B}$ flows are mainly in the poloidal direction [9, 10], the toroidal return flow has a $\sin\theta$ dependence. In general toroidal geometry, the zonal flow magnitude $V_{\mathrm{ZF}} = -E_{\mathrm{r}}/B = B^{-1}\partial\phi_{\mathrm{ZF}}/\partial r$, i.e. $(RB_\theta B^{-1})\partial\phi_{\mathrm{ZF}}/\partial\psi$ (ψ being the magnetic flux function) has a slight in–out asymmetry due to a flux-expansion factor 'RB_θ' [11]. Due to the presence of geodesic curvature in various toroidal devices, the zonal flow contains a linearly damped oscillation called a geodesic acoustic mode (GAM) [68], as discussed in detail in sections 3.1.2 and 4.5.2. Since GAM pressure fluctuation has dominant mode numbers $n = 0$, $m = 1$ (due to toroidal coupling), it has $k_\parallel = 1/qR$, so that $\omega_{\mathrm{GAM}} = Gv_{\mathrm{th,i}}/R$. Here G is a coefficient of the order of 1, and ion Landau damping for GAMs scales like $\sim \exp\{-\omega^2/2k_\parallel^2 v_{\mathrm{th,i}}^2\} \sim \exp\{-G^2q^2/2\}$. Thus, one would expect a 'GAM peak' to be clearly visible in the frequency spectrum when GAM energy is appreciable. In conclusion, some key features of the GAM are not only a well-defined linear oscillation frequency, $\omega_{\mathrm{GAM}} = Gv_{\mathrm{th},i}/R$, but also the existence of sideband pressure fluctuations with $n = 0$ and $m = 1$. Properly distinguishing between oscillatory GAMs and classical zonal flows (which are quasi-stationary) is a major challenge to experimentalists interested in zonal flow physics. This issue is particularly relevant since the finite characteristic frequency of GAMs renders them easier to detect experimentally than the zero-frequency zonal flows.

Finally, we briefly comment on stellarators (helical systems). Turbulence-driven zonal flow properties in stellarators have not been discussed widely to date, but have recently begun to be addressed in print [357, 358]. The questions of the effective damping and inertia of zonal flows in systems for which axisymmetry is absent, are particularly acute. In particular, new or enhanced damping mechanisms may be present, and the continued status of zonal flows as 'modes of minimal inertia' is not certain. For these, experiments on future stellarators with quasi-axisymmetry such as the National Compact Stellarator Experiment (NCSX) [359] and CHS-qa [360] would be illuminating.

7.1.4. Experimental studies of zonal flow structure via potential measurements

Flux surface-averaged radial electric field. The most direct evidence of zonal flows comes from measurements of the $\boldsymbol{E}\times\boldsymbol{B}$ flow V_{ZF}, the associated radial electric field E_{r}, or the associated electrostatic potential ϕ_{ZF}. As the importance of the flow shear decorrelation mechanism [9–11] in enhancing confinement has become widely recognized [206, 223, 361], there have been significant advances in the diagnostic capabilities for measuring E_{r} using the motional Stark effect (MSE) [362] or the heavy ion beam probe (HIBP) [363, 364], and in measuring the poloidal velocity V_θ of carbon impurity ions using charge exchange recombination spectroscopy (CHERS), and then calculating E_{r} from the radial force balance relation [365–367]. However, an order of magnitude improvement in the *temporal* resolution of these diagnostics is required to distinguish the temporal evolution of zonal flows from that of the mean $\boldsymbol{E}\times\boldsymbol{B}$ flow. The 'mean equilibrium' profile must also be measured with a radial resolution sufficient to distinguish profile corrugation induced by spatially intermittent turbulent transport from zonal flows. As discussed at the beginning of this section, while zonal flows are typically long lived as compared to turbulence eddies, their auto-correlation rate can reach 5 KHz for typical tokamak core parameters [145].

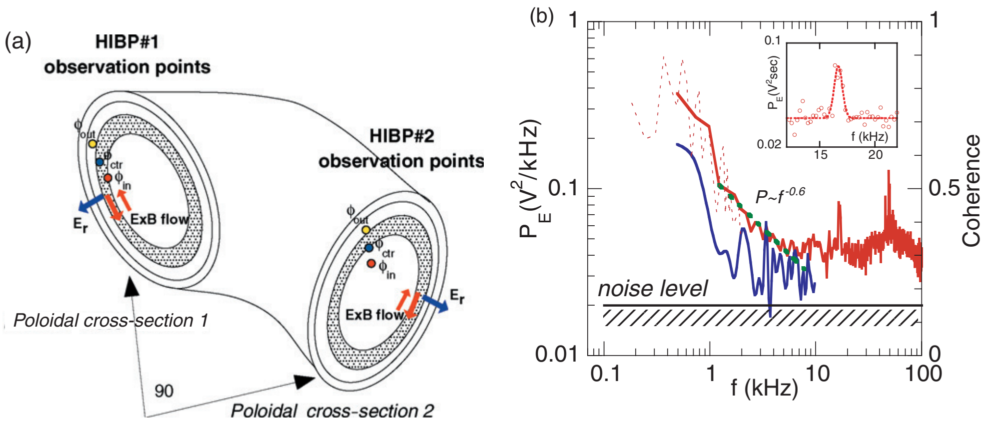

Figure 45. Identification of zonal flow on CHS. Geometry of measurements and fluctuation spectra: (*a*) observation points of dual heavy ion beam probes in CHS (blue), (*b*) power spectra of a electric field (red), and coherence between electric fields from the HIBPs. In the frequency range from 0.3 to 1 kHz, the activity to show long range correlation is found to be zonal flow. A peak at the GAM frequency is shown by an insert. Fluctuations in the range of tens of kilohertz are drift wave turbulence [372].

Identification of zonal flow by use of HIBP. The HIBP is capable of measuring the electrostatic potential $\phi_{\rm es}$, associated with the radial electric field. Its relatively fine temporal resolution has allowed detailed analyses of the edge transport barrier of the H-mode [368, 369] and the ITB dynamics in stellarators [364, 370, 371]. By use of a single HIBP, the radial resolution of which has not been better than 1 cm, the mean $E_{\rm r}$ was measured. This is believed to be mainly determined by neoclassical (collisional) particle transport, rather than by turbulence. The identification of the core zonal flow has been achieved very recently by use of a dual-HIBP system, i.e. two HIBPs are set in different toroidal angles, thus allowing the measurement of the toroidally symmetric $n = 0$ component, which is the critical element of the zonal flow measurement [372, 373]. This has made a path to the direct measurement of zonal flows in the plasma core. Figure 45 illustrates the power spectrum of the radial electric field in the core of CHS plasma, indicating the zonal flow component near $\omega \sim 0$ and the peak of the GAM oscillations. Measuring $E_{\rm r}$ at fixed radius r_1 by one HIBP, and $E_{\rm r}$ at various radii r_2 by the other HIBP, the coherence of the radial electric field at r_1 and r_2 is directly measured. The low frequency part ($\omega/2\pi < 1$ kHz) has high coherence, demonstrating a long coherence length. Cross-coherence takes a large positive value at $r_1 = r_2$, i.e. $n = 0$. As the relative distance $r_1 - r_2$ varies, the cross-coherence value between two measured electric field varies, alternately, between large positive values and large negative values. By this measurement, the radial wavelength of the zonal flow was identified. In the case of figure 45, the radial wavelength of the zonal flow is about 1–2 cm. This rapid radial variation is another essential feature of the zonal flow. The amplitude of this zonal flow is also observed to be few 100 V m^{-1}, and the $\boldsymbol{E} \times \boldsymbol{B}$ shearing rate remains smaller than the diamagnetic velocity divided by the plasma size. The sample volume still remains of the order of the radial wavelength. This limit of spatial resolution may be an obstacle for measuring the precise peak height of the zonal flow. The decorrelation rate of the zonal flow, $\Delta\omega_{\rm ZF}$, is found to be smaller than (or at most) $2\pi \times 10^3$ s^{-1} in this observation, and is close to the inverse time of the global energy confinement time. (The energy confinement time is a few milliseconds in low density ECH plasmas.) The radial scan of the measurement point has revealed that the zonal flows exist over a wide region of radii.

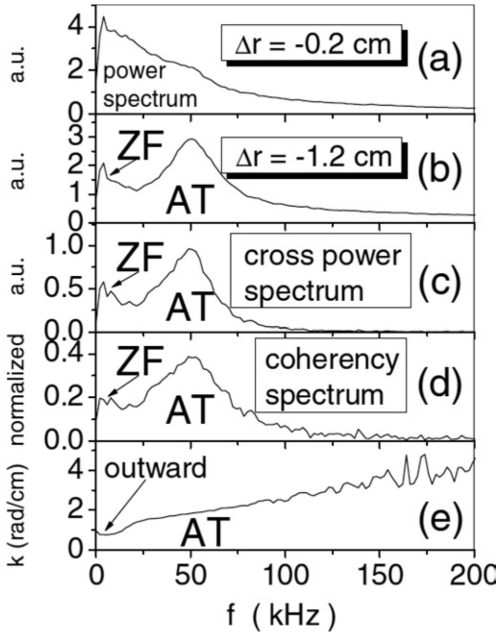

Figure 46. Spectra measured with the modified forked probe. Peaks of zonal flow and ambient turbulence (AT) are shown: (*a*) Auto power spectrum of $\tilde{V}_{\theta 1}(\Delta r = -0.2\,\mathrm{cm})$, (*b*) Auto power spectrum of $\tilde{V}_{\theta 2}(\Delta r = -0.2\,\mathrm{cm})$, (*c*) Cross power spectrum, (*d*) Coherency spectrum and (*e*) Wavenumber spectrum. (c)–(e) were calculated from the long distance correlation between $\tilde{V}_{\theta 1}$ and $\tilde{V}_{\theta 2}$ [374].

To date, this result seems the most direct and convincing experimental confirmation for the presence of the zonal flow in core plasmas.

Measurement at edge. Near the edge of tokamak plasmas, Langmuir probes are applied to the study of long range electric field fluctuations. In the study of [374], radial electric fields are measured at different poloidal angles simultaneously, and the low frequency component is identified. Although the poloidal angle between two forked probes is limited (the distance between them in toroidal direction is about $1/10$ of the minor radius), the observation gives a strong support for the presence of the poloidally symmetric, low frequency radial electric field perturbations as is shown in figure 46. The amplitude and radial wavenumber are evaluated as $\tilde{V}_{\mathrm{ZF}}/V_{\mathrm{Thi}} \simeq 0.5$–$0.9\%$ and $q_{\mathrm{r}}\rho_{\mathrm{i}} \simeq 0.06$–$0.1$. The half-width at half-maximum of the spectrum is not clearly identified.

Edge transport barrier. Another measurement of the electric field by use of the HIBP has been performed on the JFT-2M tokamak [368, 369] in conjunction with the L-to-H transition. The radially localized response of the electric field structure near the last closed flux surface is precisely measured. The jump of the radial electric field and associated change of the fluctuations have been measured at the onset of the L–H transition. The high temporal resolution of the potential measurement has allowed the determination of the rate of variation of the radial electric field at the onset of the L–H transition. Results indicate $(\partial E_{\mathrm{r}}/\partial t)E_{\mathrm{r}}^{-1} \sim \mathrm{O}(10\,\mu\,\mathrm{s}^{-1})$. This is in the range of theoretical predictions for the rate of radial electric field bifurcation. So far, an accurate decomposition of the measured radial electric field into the zonal flow and the 'mean flow' has not been possible, and remains a significant challenge for future experimental research on zonal flows.

Observation of potential fluctuations in GAM frequency range. The long range oscillation in the core plasma, which is attributed to the GAM, has been observed on CHS by use of dual HIBP systems as is illustrated in figure 45. The frequency of $\omega/2\pi \simeq 17$ kHz is close to the GAM frequency at the observed ion temperature [372]. The half-width at half-maximum of the spectral peak is a few kilohertz. The measurement of other wave parameters, e.g. the parity of the density perturbation, the radial wavelength and others, is ongoing.

The experimental evidence for the presence of GAMs in tokamaks has also increased. The measurement of potential fluctuations by use of the HIBP has been performed on the JIPP-TIIU tokamak [363]. Low frequency fluctuations in the range of 20 kHz have been identified in the vicinity of the plasma edge and core, as well [363, 375–376]. This was the most advanced measurement of potential fluctuation in the mid-1990s. This fluctuation was conjectured to be a GAM oscillation. Further analysis of the measured data is ongoing.

Motivated by the recent community-wide interest in measuring zonal flows, HIBP measurement data obtained from TEXT tokamak plasmas in the early 1990s have been re-analysed recently in detail [377]. The measured potential fluctuation has the following properties. For a range of minor radius from $r/a = 0.6$ to $r/a = 0.95$, the $m = 0$ component of the potential fluctuation with radial correlation length below 2 cm (smaller than the sample volume size) was found to be oscillating with a well-defined frequency which matches that predicted for the GAM [68]. Outside of this radial range, no significant $m = 0$ fluctuation in potential was detected.

It should be noted, however, that conclusive measurements of the long toroidal correlation length ($n = 0$ component) have *not* yet been completed (except by the dual HIBP measurement on CHS). In particular, the pertinence of the measured potential fluctuations to zonal flows (as opposed to GAMs) is still unclear. Even the dual HIBP experiments need future experiments for more conclusive results. It would also be illuminating to explore, via numerical simulation, whether or not GAMs in that particular frequency and parameter regime could play a significant role in regulating turbulence.

7.2. Zonal flow dynamics and interaction with ambient turbulence

As is illustrated in figure 45, the zonal flow amplitude and drift wave fluctuations are simultaneously measured on CHS by use of the dual HIBP system. This provides a possibility to identify the causal relation between the zonal flow and ambient turbulent fluctuations. The detailed measurements and analyses are ongoing, and a definitive conclusion has not yet been obtained. Therefore, in this section, we discuss indirect measurements on zonal flows. Such experiments attempt to detect and to elucidate the physics of zonal flows by indirect means. In some cases, such indirect approaches strike at the heart of the fundamental physical processes thought to generate zonal flows (i.e. triad interactions between two high frequency drift waves and the zonal flow). Thus, these approaches are motivated by concerns of both physics and expediency.

7.2.1. Zonal flow generation mechanisms. As discussed in section 3.2, zonal flows in electrostatic turbulence in a simple geometry are generated by the Reynolds' stress associated with the nonlinear coupling of higher-k components of the ambient fluctuations [32]. In the more general context of electromagnetic turbulence in toroidal geometry, the evolution of the zonal flow can be written in the following schematic way $(\partial/\partial t)V_{\mathrm{ZF}}$ = Reynolds' stress + Maxwell's stress + Stringer–Winsor + damping. Most theoretical discussions on zonal flows have focused on the role of Reynolds' stress, since it is believed to be relevant regardless of geometry, values of the plasma beta, and the nature of fluctuations. However, some [378] argued that, in the transition region between the core and edge of tokamak plasmas, the Stringer–Winsor (SW) term, can play a major role in generation of the GAM component of zonal flows. The SW mechanism is basically a torque on the plasma pressure column caused by the interaction of pressure inhomogeneity with the in–out asymmetry in magnetic field strength [378]. In the results of Braginskii fluid simulation described in [209], it was found that the SW term was greater than the Reynolds' stress term for a typical parameter set for the transition core/edge region. However, more recent related fluid simulations by other teams found that the SW effect has a different sign from that of the Reynolds' stress and can make zonal flow generation weaker [274, 379].

As discussed in section 3, for electromagnetic turbulence, the Maxwell's stress term associated with the $J \times B$ nonlinearity can be appreciable. In the ideal MHD limit of purely Alfvenic turbulence, the Maxwell's stress cancels the Reynolds' stress exactly, and the state is called the purely Alfvenic state. This establishes that zonal flow can be driven only through non-ideal MHD effects.

7.2.2. Experimental studies on zonal flow dynamics. It is encouraging to note that the Reynolds' stress has been measured using Langmuir probes on the TJ-2 stellarator [380] and the H-1 tokamak [381]. One should note that the dominant nonlinear mode coupling channel for zonal flow generation is the three-mode coupling involving two high-k fluctuations and the zonal flow, i.e. a non-local (distant) interaction in k. An increase of this nonlinear mode coupling is an indicator, albeit indirect, of increased zonal flow generation [382]. The strength of interaction can be quantified by bi-coherence measurements and there have been bi-coherence analyses of the probe measurements on DIII-D edge [383–385], which support the notion that the nonlinear couplings, which are necessary for zonal flow generation, increases abruptly just prior to the H-mode transition. A relevant experiment has been performed on H-1 heliac [386], confirming the dominance of non-local interaction in the generation of the poloidally extended structures. A related work, to excite convective cells externally [387], was reported. The role of geodesic curvature coupling (i.e. the relative importance of Reynolds' stress drive and the SW drive/damping) have been further investigated on the Kiel stellarator [388].

7.2.3. Experimental studies on zonal flow interaction with turbulence. Given the difficulty in measuring $\tilde{\phi}$, E_r, etc, most fluctuation diagnostics measure density fluctuations. Therefore, there exist many fusion plasma devices in which zonal-flow-related experiments can be tried via density fluctuation measurements. We summarize some experiments along these lines using different methods. An experiment and analysis based on line-integrated measurements of density fluctuations on DIII-D tokamak edge using the phase contrast imaging (PCI) [389] was able to demonstrate that the fluctuation spectrum as a function of k_r and ω, $S(k_r, \omega)$ resembles that obtained from ITG turbulence simulations. However, this line-integrated measurement could not demonstrate that the observed fluctuations were symmetric in both poloidal and toroidal directions (i.e. $m = 0, n = 0$). The estimated upper bounds on the mode number was of the order of 30.

One way of examining zonal flow properties is to estimate the zonal flow velocity (which advects the ambient turbulence) by analyzing the 'measured' ambient turbulence density fluctuation spectra. We note that for this approach, the instantaneous Doppler-shift of the density fluctuation with wave vector k should exceed the decorrelation rates of both the zonal

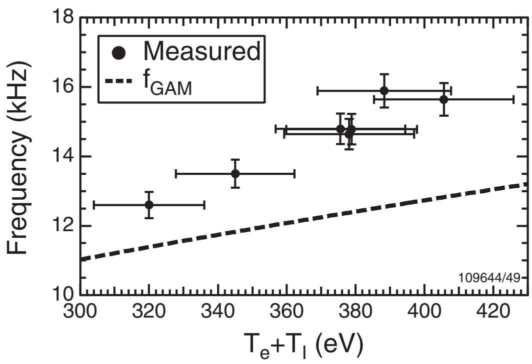

Figure 47. Frequency of observed oscillations (attributed to GAM) and dependence on temperature. Measurement of D III-D is compared to the calculated GAM frequency (left) [392, 393].

flows and turbulence, thus allowing the invocation of Taylor's hypothesis [390]. Significant progress in this approach has been made by using a two-dimensional array of beam emission spectroscopy (BES) diagnostics on the plasma edge. BES measurements and analyses have identified that density fluctuations are advected by the zonal-flow-like field [391]. The estimated flow amplitude was of the order $10^{-2} v_{\mathrm{th,i}}$ roughly in the range observed in numerical simulations [145]. The alleged zonal flow also has a well-defined frequency close to that of the GAM [392] (see figure 47). A signal was readily observed at high q and not observed at low q [393], as expected from the q-dependence of GAM Landau damping, as discussed in section 7.1.3. Unfortunately, another important aspect of the GAM oscillation is that the zonal flow ($n = 0, m = 0$) is accompanied by the $n = 0, m = 1$ component of density fluctuations. This prediction could not be confirmed. This shortcoming was partly due to the fact that the BES arrays were located near the low field midplane side of the tokamak, where GAM density fluctuations are expected to be very weak. From a simple theory, the GAM amplitude, at a given flux surface, is expected to be highest at the top and at the bottom of the tokamak. The poloidal mode number of density fluctuations corresponding to the GAM frequency from this experiment was predicted to be on the order of 10 [392].

Another way of estimating the zonal flow velocity, which of course advects the ambient turbulence, is to measure the Doppler shift of the ambient turbulence density fluctuation frequency spectra, using Doppler reflectometry [394]. An ocsillation at 20–30 kHz was observed in the core of T-10 tokamak and was attributed to the GAM [395]. From a measurement of the edge plasma of ASDEX-U, a coherent peak in the spectrum near the GAM frequency has been observed in addition to a stronger and broader peak at much lower frequency which appears to be 'zero frequency' zonal flow [396]. The dependence of the peak frequency on the edge electron temperature is in broad agreement with GAM frequency for various operation modes of plasmas including ohmic, L-mode and quiescent H(QH)-mode plasmas as reported in [396].

Very recently, the GAM fluctuations at edge are measured by HIBP on JFT-2M, and the modulation of the amplitude of high frequency fluctuations by the oscillation at GAM frequency was reported [397].

7.2.4. Measurements of zonal flow effects on confinement. Another indirect way of demonstrating the existence of zonal flow is by identifying the change in transport and confinement due to zonal flows. These include the expected changes in turbulence-driven transport onset conditions (for instance, a change akin to the Dimits shift) and transport scaling with key macroscopic variables (for instance, ion–ion collisions, which damp zonal flows, or parameters which enter the neoclassical dielectric function). Such studies should emerge from systematic dimensionless parameter scans of plasmas.

7.3. Suggestions on future experiments and information needed from simulations and theory

After a summary (not exhaustive) of the recent experimental progress in pursuing the measurements of zonal flows, we discuss some future experimental plans and possibilities for further progress and list key physics information which future experiments will need from numerical simulations and theories for the identification of zonal flows.

We mentioned that an order of magnitude improvement in the *temporal* resolution of the present day diagnostics, together with the identification of the $n = 0$ component, is required to distinguish zonal flows from the 'mean $\boldsymbol{E} \times \boldsymbol{B}$ flows'. Regarding HIBP measurements, two HIBP systems are operating on CHS, providing simultaneous measurements of the electric field perturbation pattern and structure. Initial data from the dual HIBP system has already yielded the essential direct observation of the zonal flow. Future progress on CHS experiments are promising, and will play a central role for the experimental study of zonal flow in core plasmas. Studies of higher resolution are planned on the National Spherical Torus Experiment (NSTX) using a new spectroscopic technique with a higher temporal resolution [398] and on the Alcator C-Mod tokamak and NSTX using a two-dimensional gas puff image (GPI) of edge turbulence [399, 400].

Regarding bi-coherence analysis of turbulence spectra, a conclusive result in this endeavour requires the precise measurement of the zonal flow component, together with the other two 'legs' of the three-wave coupling triad that resonate with the measured zonal flow. The coherent part of this nonlinear interaction with the zonal flow of interest must be measured, so as to quantify the acceleration of the zonal flow by the background turbulence. This process can be extended to electromagnetic fluctuations in high β plasmas and stellarators [401]. Then the incoherent part of the nonlinear interactions must be measured to quantify the stochastic noise term. Through these processes, one has solid understanding of the physical process which governs the generation of the zonal flow.

For further elucidation of the implications of the experimental results based on the measurements of density fluctuations, the following information from direct numerical simulations will be extremely useful. First, for an identification of density fluctuations which accompany the zonal flows, simulations should quantify the expected level of density fluctuations not only for the $n = 0$, $m = 0$ mode, but also for the sidebands $n = 0$, $m = 1$, etc. We note that most 'zonal flow characteristics' listed in print to date [145] are based on pure ITG turbulence, with adiabatic electron response where $\tilde{n}/n = 0$ for $n = 0$, $m = 0$ mode. With recent advances in gyrokinetic simulations including more realistic electron dynamics as described in section 4, such information should now be available and should be extremely useful for experiments measuring density fluctuations, such as phase contrast imaging (PCI) [402]. Of course, for detailed comparisons between experiment and simulations, more comprehensive spectral information than that usually presented (such as $S(k_r)$ or $S(\omega)$ at a fixed k_r, etc) would be desirable, especially $S(k_r, \omega)$ and $S(k_r, \omega, k_\theta)$ for $m = 0, \pm 1, \pm 2, \ldots$, etc. Another way to systematically demonstrate the effects of zonal flows is to scan the plasma parameters and compare the detailed spatio-temporal behaviour of the ambient turbulence measured by comprehensive two-dimensional microwave imaging [403, 404] to results from direct numerical simulations. This, however, requires that the simulation code should be validated via comparison to simpler experiments.

Second, for the purpose of identifying zonal flows by the measurement of high-k density fluctuations which are advected by the flows, the temporal scale separation of the various physical frequencies required for Taylor's hypothesis [390] should be established in order to strengthen the validity of the experiments and analyses. The relevant frequencies involved are: $\boldsymbol{k} \cdot \boldsymbol{V}_{\mathrm{E}}$, the instantaneous Doppler-shift of the frequency of ambient turbulence, due to zonal flows, $\Delta\omega_{\mathrm{drift}}$, the decorrelation rate of the ambient turbulence, and $\Delta\omega_{\mathrm{ZF}}$, the decorrelation rate of the zonal flow itself. While the estimate that $\Delta\omega_{\mathrm{ZF}} < \Delta\omega_{\mathrm{drift}} < \boldsymbol{k} \cdot \boldsymbol{V}_{\mathrm{E}}$ [145] is often quoted, this was only one case for a 'typical' set of tokamak core parameters. Preferably, such information should be available from direct numerical simulation, for each experiment.

The reason why the measurement of the zonal flow has been so rare in the experiment of plasma confinement, which has lasted already about five decades, was explained at the beginning of section 7. That is, the need of high resolution of the electric field measurement in radius and time, simultaneous with the capacity to measure long poloidal and toroidal correlation length, is really demanding. These difficulties must be overcome in the future, because the understanding of the drift wave–zonal flow turbulence is a crucial element of the understanding of anomalous transport.

8. Summary and discussion

In this final section, we present the conclusions of this review of zonal flow physics and briefly discuss directions of, and areas for, future research. There is no question that zonal flows exist, are ubiquitous constituents of drift wave turbulence in confined plasma, and also occur in many places in nature. Research has also demonstrated that zonal flows are an essential element of the mechanisms of self-regulation of drift wave turbulence and of the formation of edge and ITBs. The development of the understanding of zonal flow phenomena has made a concrete contribution to controlled fusion research, in general, and to the design of ITER and other future experiments, in particular.

The theory of zonal flows is now a well-developed subject. We have shown that it is convenient and illuminating to classify the diversity of zonal flow dynamics according to the degree of stochasticity of drift wave ray propagation in the zonal flow field, and by the ratio of the zonal flow autocorrelation time to the 'bounce time' of a drift wave-packet trapped in a zonal flow field. A variety of approximation methods have been utilized to calculate the rate of zonal shear amplification, for both the coherent and the stochastic regimes, and for a variety of different geometries. All of this wide variety of calculational approaches have the common element of their foundation in the disparity of time scales between the primary drift waves and secondary zonal flows. The back reaction of zonal flows onto the primary drift wave spectrum via shearing, both coherent and stochastic, is now well understood. Such insight has facilitated the construction of simple but self-consistent models which describe the various states of the drift wave–zonal flow system. The development of more advanced theories, such as probabilistic approaches and models, is proceeding in the research community.

Numerical simulations of zonal flows have identified their generation in a broad regime of models of low frequency microturbulence. In addition, some aspects of zonal flow structure, generation by modulational instability and saturation scaling trends have been critically tested by numerical simulation, with a high degree of success. However, the further development and application of detailed computational diagnostics to *quantitative* tests of zonal flow theory is still quite desirable. Experimental research on zonal flow phenomena is still in its youth. While several experiments have identified various elements characteristic of zonal flow phenomena, critical tests of basic zonal flow physics and of the basic theory remain incomplete.

We now discuss some of the frontiers of, and possible future developments in, the physics of drift wave–zonal flow turbulence. In the realm of theory, the critical problem is that of identifying and evaluating zonal flow saturation mechanism in the collisionless regime. Further and deeper work on tertiary shear flow instability, nonlinear wave kinetics, trapped wave-packets and turbulent trapping will be valuable and surely will be forthcoming. Such works need to confront the reality of realistic geometry, including that of the stellarator, as well. The advancement in meeting the challenge of complex geometry and dynamics will strengthen an already powerful theoretical basis, which commonly helps to solve the expected mysteries presented by future space and astronomical observations. In addition, the role of convective cells (i.e. alternatively nonlinear streamers) in the drift wave–zonal flow system must be better understood. General convective cells, which vary in the poloidal direction, can be induced by drift wave turbulence, and may have a strong impact on the dynamical evolution of transport in the system. The structure of such convective cells may be strongly influenced by magnetic shear. The partition of excitation energy between drift waves, zonal flows and convective cells has not been fully addressed, and requires intensive study in the future. *This issue lies at the heart of the 'pattern selection' problem, as to which type of secondary structure is the ultimate 'attractor state' for a given set of system parameters.* More generally, the nonlinear theory of wave kinetics, particularly the regime near primary wave marginality (i.e. $\gamma_k \to 0$), remains unexplored and thus merits further development. This is a general theme in plasma theory, and progress on this topic will sow the seeds for future benefits in a number of problems. Another area of likely activity is the study of the interaction of zonal flow with mean $\boldsymbol{E} \times \boldsymbol{B}$ sheared flows and other questions pertinent to confinement, such as turbulence propagation. Also, further study of electromagnetic effects on zonal flows is necessary, including, in particular, $A_\perp$ effects ($A_\perp$ is the vector potential in the direction perpendicular to the magnetic field), which are critical to high beta plasmas, such as those found in spherical tori. The more general questions of the interaction between zonal flow dynamics and those of magnetic dynamos, etc, remain to be clarified, as well. In particular, *magnetic stresses tend to grow with increasing ß, and so compete against Reynold's stresses, thereby reducing the rate of shear amplification*. As a consequence, the suppression of turbulence by velocity shear is *weakened*, so that heat transport and dynamo activity *increase*. This interesting set of trade-offs and competitions is made possible by the fact that zonal flows are in general more effective at quenching transport then zonal fields. Finally, since zonal flow shearing is effectively a process whereby smaller scales are strained by larger scales, it is fundamentally an intermittency phenomenon. Future theoretical research must address such intermittency, in order that predictive capacity be optimized. In particular, the astute reader will surely have noted that all discussion of zonal flow shearing, herein and elsewhere, is, as usual in plasma physics, organized in the either coherent shearing models, where $k_\mathrm{r} V'_{\boldsymbol{E}\times\boldsymbol{B}} t$, or stochastic shearing models, where $\delta k_\mathrm{r} \sim \sqrt{D_k t}$. In reality, nondiffusive Levy-flights on k_r, with $k_\mathrm{r} \sim t^\alpha$, $\frac{1}{2} < \alpha < 1$, are surely possible and will appear as intermittent, strong shearing events. To describe such phenomena, a fractional kinetic theory [405] will be necessary. Insights from SOC-type models [180] may be useful, as well.

Future simulation research must progress further from observation and identification of zonal flow phenomena to quantitative numerical experiments and tests. More advanced numerical diagnostics must be developed, and more systematic regime surveys must be implemented. Though numerical simulation has contributed much to our understanding of drift wave–zonal flow turbulence, its full potential has not yet been tapped. Finally, it must be said that the greatest opportunities for future research on zonal flows lie in the realm of experiment. Particular challenges include the simultaneous study, correlation and synthesis of generation dynamics in real space (i.e. via vorticity transport) and $\boldsymbol{k}$-space (i.e. via nonlinear mode coupling), and the development of methods to control zonal flows. More generally, future experiments must emphasize *challenging* the theory and confronting it with stressful quantitative tests.

Finally, it should be emphasized that the zonal flow dynamics problem represents one well-defined example of a broad class of bifurcation phenomena in confined plasmas. As such, it can and will join with other firm webs of interacting feedback loops which collectively govern plasma dynamics. For example, in burning plasmas, both burning and quenching can be expected to appear as dual, bistable states. Transitions between them, either periodic or intermittent, could be triggered by transport events, for which the dynamics of drift wave–zonal flow turbulence in high temperature D–T plasmas would be of central importance. Internal transport barrier formation in burning plasmas is another example of events from this category. The predictability of such transition phenomena merits intense theoretical study. However, interest in zonal flow physics is not limited to the realm of fusion plasma physics. Zonal flow generation is an example of a broad class of problems dealing with the amplification of an axial vector field with global symmetry by microscopic turbulence which is driven by the gradient of a scalar field. This category of problems also includes the magnetic dynamo (solar, terrestrial and galactic), accretion disc dynamics, jet formation, the global circulation of the ocean, etc. Thus, the study of zonal flows is a splendid opportunity for plasma and fusion science to demonstrate its capability to make a significant contribution to this now classic lore of problems.

Acknowledgments

The authors have benefited tremendously from the efforts of their collaborators in the course of research on topics related to the material of this review. For their many contributions, we thank (listed alphabetically): M Beer, K H Burrell, B A Carreras, S Champeaux, L Chen, A Das, A Fukuyama, A Fujisawa, A V Gruzinov, I Gruzinov, O Gurcan, K Hallatschek, C Hidalgo, F L Hinton, C H Holland, D W Hughes, P K Kaw, E Kim, Y-B Kim, V B Lebedev, Z Lin, M Malkov, N Mattor, R Moyer, R Nazikian, M N Rosenbluth, H Sanuki, V D Shapiro, R Singh, A Smolyakov, F Spineanu, U Stroth, E J Synakowski, S Toda, G Tynan, M Vlad, M Yagi and A Yoshizawa.

We are also grateful for useful and informative discussions with (listed alphabetically): R Balescu, S Benkadda, P Beyer, N Brummell, F Busse, G Carnevale, J W Connor, A Dimits, J F Drake, X Garbet, A Hasegawa, C W Horton, K Ida, Y Idomura, F Jenko, C Jones, Y Kishimoto, Y Kiwamoto, J A Krommes, E Mazzucato, G McKee, Y Miura, K Molvig, V Naulin, W Nevins, D E Newman, H Park, F W Perkins, T Rhodes, R Z Sagdeev, Y Sarazin, B Scott, K C Shaing, M Shats, K-H Spatscheck, H Sugama, R D Sydora, W Tang, S Tobias, L Villard, E Vishniac, F Wagner, M Wakatani, W Wang, T-H Watanabe, T Watari, J Weiland, S Yoshikawa, W R Young, M Zarnstorff, F Zonca, S Zweben. We thank the authors who permitted reproduction of their figures and Mr S Keating for careful proofreading of the manuscript.

This work was partly supported by the US DOE under Grant Nos FG03-88ER53275 and FG02-04ER54738, by the Grant-in-Aid for Specially Promoted Research (16002005) and by the Grant-in-Aid for Scientific Research (15360495) of the Ministry of Education, Culture, Sports, Science and Technology of Japan, by the Collaboration Programs of NIFS and of the Research Institute for Applied Mechanics of Kyushu University, by the Asada Eiichi Research Foundation, and by the US DOE Contract No DE-AC02-76-CHO-3073. A large

Table A1. Quasi-isomorphism between ITG and ETG.

Key issue	ITG	ETG
Linear response in the electrostatic limit		
$\tilde{n}_{\mathrm{i}}$	From gyrokinetic equation	$-e\phi/T_{\mathrm{i}}$: pure adiabatic
$\tilde{n}_{\mathrm{e}}$	$e(\phi - \langle\phi\rangle)/T_{\mathrm{e}}$: adiabatic with zonal flow	From gyrokinetic equation
Disparity in transport channels caused by particular turbulence	$\chi_{\mathrm{i}} \sim \chi_{\phi} > \chi_{\mathrm{e}}, D$	$\chi_{\mathrm{e}} \sim \chi_J > D, \chi_{\mathrm{i}}, \chi_{\phi}$
Zonal flow strength in nonlinear regime	Typically strong	Typically weaker
Radial correlation length of ambient turbulence at nonlinear saturation	Several ρ_{i}	Uncertain—current research
Isomorphism breaker	Zonal flow	Residual magnetization of ion response Electromagnetic effect Debye shielding

part of this paper was completed during the stay of three of the authors (PHD, KI and TSH) at Kyushu University, and they gratefully acknowledge the hospitality of and support by Kyushu University. P H Diamond thanks the Isaac Newton Institute for Mathematical Sciences of the University of Cambridge, for support and hospitality during the final stages of completion of this project.

Appendix A. Near-isomorphism between ITG and ETG

Here the quasi-isomorphism between ITG and ETG are tabulated in table A1.

In this table, D, χ_{ϕ} and X_J are diffusivities of particle, momentum and current. Note that ETG turbulence will transport current much like ITG turbulence transports momentum. X_J is like a hyper-resistivity.

Appendix B. Hierarchy of nonlinear governing equations

In this appendix, the hierarchy of nonlinear governing equations is explained. The steps for reduction, and physics lost in the process of reduction are also listed, as summarized in table B1.

As is explained in the main text, most simulations mentioned above have used the conventional nonlinear gyrokinetic equation [212], which ignores the velocity space nonlinearity, which is formally smaller than the $\boldsymbol{E}\times\boldsymbol{B}$ nonlinearity. The conventional nonlinear gyrokinetic equation fails to obey the fundamental conservation laws, such as energy (of particles and fluctuation fields), and phase-space volume at a non-trivial order. For longer times, well after the initial nonlinear saturation of turbulence, even very small errors in the governing equation can accumulate (in time, regardless of computational method) and muddy the physics predictions. A recent simulation [236] in cylindrical geometry used a fully nonlinear energy conserving and phase-space conserving form of the nonlinear gyrokinetic equation [214]. The importance of using governing equation with proper conservation laws is demonstrated in this series of simulations, with and without velocity space nonlinearity.

Table B1. Hierarchy of governing equations.

Nonlinear equations: from fundamental, primitive to reduced, simplified	Steps for reduction	Physics lost due to reduction
Vlasov–Klimontovich equation [406]		
⇓	Remove high frequency terms ($\geqslant\omega_{ci}$)	High frequency phenomena [411]
Gyrokinetic equation: conservative [214, 407–410]		
⇓	Neglect velocity space nonlinearity	Conservation of energy between particles and fields, of phase-space volume, nonlinear trapping of particles along $\boldsymbol{B}$. (Influence is illustrated in figure B.1.)
Gyrokinetic equation: conventional [212]		
⇓	Take moments in velocity space	Some nonlinear kinetic effects including inelastic Compton scattering [414], accuracy in damping rates of zonal flow [42, 43] and damped mode [415]
Gyrofluid equation [215, 412, 413]		
⇓	Expansion in finite Larmor radius terms; ordering for collisional plasmas	Most kinetic effects associated with long mean free paths and finite size orbits.
Fluid equations [416–421]		

The authors reported that neglecting velocity space nonlinearity in an ITG simulation resulted in undesirable consequences. The energy was no longer conserved between particles and fluctuating fields, and a precious indicator of the quality of numerical integration was lost. The zonal flow pattern and the radial heat transport pattern were affected as well. (See an extended description in [2].)

References

[1] Glanz J 1996 *Science* **274** 1600
[2] Diamond P H, Itoh S-I, Itoh K and Hahm T S 2004 Zonal flows in plasma—a review *Research Report* NIFS-805, National Institute of Fusion Science
[3] Arnold V I and Meshalkin 1960 *Usp. Mater. Nauk* **15** 247
[4] Hasegawa A, Maclennan C G and Kodama Y 1979 *Phys. Fluids* **22** 2122
[5] Sagdeev R Z, Shapiro V D and Shevchenko V I 1978 *Sov. J. Plasma Phys.* **4** 306
[6] Okuda H and Dawson J M 1973 *Phys. Fluids* **16** 408
[7] Balk A, Nazarenko S V and Zakharov V E 1990 *Sov. Phys.—JETP* **71** 249
[8] Hasegawa A and Wakatani M 1987 *Phys. Rev. Lett.* **59** 1581
[9] Biglari H, Diamond P H and Terry P W 1990 *Phys. Fluids* B **2** 1
[10] Itoh S-I and Itoh K 1990 *J. Phys. Soc. Japan* **59** 3815
[11] Hahm T S and Burrell K H 1995 *Phys. Plasmas* **2** 1648
[12] Terry P W 2000 *Rev. Mod. Phys.* **72** 109
[13] Diamond P H, Rosenbluth M N, Hinton F L, Malkov M, Fleisher J and Smolyakov A 1998 *Plasma Physics and Controlled Nuclear Fusion Research* (Vienna: IAEA) IAEA-CN-69/TH3/1
[14] Diamond P H, Rosenbluth M N, Sanchez E, Hidalgo C, Van Milligen B, Estrada T, Brañas B, Hirsch M, Hartfuss H J and Carreras B A 2000 *Phys. Rev. Lett.* **84** 48
[15] Diamond P H *et al* 2001 *Nucl. Fusion* **41** 1067
[16] Yoshizawa A, Itoh S-I and Itoh K 2002 *Plasma and Fluid Turbulence* (Bristol: Institute of Physics Publishing)
[17] Hammett G *et al* 1993 *Plasma Phys. Control. Fusion* **35** 973
[18] Lin Z, Hahm T S, Lee W W, Tang W M and White R B 1998 *Science* **281** 1835
[19] Waltz R, Kerbel G and Milovich J 1994 *Phys. Plasmas* **1** 2229

[20] Sagdeev R Z and Galeev A A 1969 *Nonlinear Plasma Theory* ed T O'Neil and D L Book (New York: Benjamin)

[21] Dyachenko A I, Nazarenko S V and Zakharov V E 1995 *Phys. Lett.* A **165** 330

[22] Dubrulle B and Nazarenko S V 1997 *Physica* D **110** 123

[23] Monin A S and Piterbarg L I 1987 *Sov. Phys. Dokl.* **32** 622

[24] Smolyakov A I and Diamond P H 1999 *Phys. Plasmas* **6** 4410

[25] Chen L, Lin Z and White R B 2000 *Phys. Plasmas* **7** 3129

[26] Tur A V, Chechkin A V and Yanovsky V V 1992 *Phys. Fluids* B **4** 3513

[27] Smolyakov A I and Diamond P H 2000 *Phys. Plasmas* **7** 1349

[28] Gruzinov A V, Diamond P H and Lebedev V B 1994 *Phys. Plasmas* **1** 3148

[29] Champeaux S and Diamond P H 2001 *Phys. Lett.* A **288** 214

[30] Drake J F, Finn J M, Guzdar P, Shapiro V, Shevchenko V, Waelbroeck I, Hassam A B, Liu C S and Sagdeev R 1992 *Phys. Fluids* B **4** 488

[31] Rosenbluth M N and Shapiro V D 1994 *Phys. Plasmas* **1** 222

[32] Diamond P H and Kim Y B 1991 *Phys. Fluids* B **3** 1626

[33] Lichtenberg A J and Liebermann M A 1984 *Regular and Stochastic Motion* (New York: Springer)

[34] Rechester A B and Rosenbluth M N 1978 *Phys. Rev. Lett.* **40** 38

[35] Newell A C and Whitehead J A 1969 *J. Fluid Mech.* **38** 279

[36] Taniuti T and Wei C C 1968 *J. Phys. Soc. Japan* **24** 941

[37] Satya Y S and Kaw P K 1977 *Phys. Rev. Lett.* **31** 1453

[38] Kaw P, Singh R and Diamond P H 2002 *Plasma Phys. Control. Fusion* **44** 51

[39] Smolyakov A I, Diamond P H and Malkov M 2000 *Phys. Rev. Lett.* **84** 491

[40] Mima K and Nishikawa K 1984 *Basic Plasma Physics II* ed A A Galeev and R N Sudan (Amsterdam: North-Holland) chapter 6.5

[41] Kraichnan R H 1967 *Phys. Fluids* **10** 1417

[42] Rosenbluth M N and Hinton F L 1998 *Phys. Rev. Lett.* **80** 724

[43] Hinton F L and Rosenbluth M N 1999 *Plasmas Phys. Control. Fusion* **41** A653

[44] Hinton F L 1991 *Phys. Fluids* B **3** 696

[45] May R 1974 *Stability and Complexity in Model Ecosystems* (Cambridge: Cambridge University Press)

[46] Diamond P H, Liang Y-M, Carreras B A and Terry P W 1994 *Phys. Rev. Lett.* **72** 2565

[47] Itoh K and Itoh S-I 1996 *Plasma Phys. Control. Fusion* **38** 1

[48] Itoh K, Itoh S-I and Fukuyama A 1999 *Transport and Structural Formation in Plasmas* (Bristol: Institute of Physics Publishing)

[49] Malkov M and Diamond P H 2001 *Phys. Plasmas* **8** 3996

[50] Diamond P H *et al* 1993 *Plasma Physics and Controlled Nuclear Fusion Research 1992* vol 2 (Vienna: IAEA) p 97

[51] Lin Z *et al* 1999 *Phys. Rev. Lett.* **83** 3645

[52] Dimits A M, Williams T J, Byers J A and Cohen B I 1996 *Phys. Rev. Lett.* **77** 71

[53] Rogers B N, Dorland W and Kotschenreuther M 2000 *Phys. Rev. Lett.* **85** 5336

[54] Idomura Y, Wakatani M and Tokuda S 2000 *Phys. Plasmas* **7** 3551

[55] Kim E and Diamond P H 2002 *Phys. Plasmas* **9** 71

[56] Itoh S-I and Kawai Y (ed) 2002 *Bifurcation Phenomena in Plasmas* (Fukuoka: Kyushu University Press)

[57] Goldman M V 1984 *Rev. Mod. Phys.* **56** 709

[58] Zel'dovich Ya B and Novikov I D 1983 *The Structure and Evolution of the Universe* vol 2 (Chicago, IL: University of Chicago Press) p 242

[59] Zeldovich Ya B, Ruzmaikin A A and Sokoloff D D 1983 *Magnetic Fields in Astrophysics* (New York: Gordon and Breach)

[60] Moffatt H K 1978 *Magnetic Field Generation in Electrically Conducting Fluids* (New York: Cambridge University Press)

[61] Parker E N 1979 *Cosmical Magnetic Fields* (Oxford: Clarendon)

[62] Diamond P H, Hughes D W and Kim E-J 2005 Self-consistent mean field electrodynamics in two and three dimensions *The Fluid Mechanics of Astrophysics and Geophysics* vol 12, ed A M Soward, C A Jones, D W Hughes and N O Weiss (London: Taylor and Francis) p 145

[63] Yoshizawa A, Itoh S-I, Itoh K and Yokoi N 2004 *Plasma Phys. Control. Fusion* **46** R25

[64] Horton C W 1999 *Rev. Mod. Phys.* **71** 735

[65] Okuda H, Chu C and Dawson J M 1975 *Phys. Fluids* **18** 243

[66] Diamond P H 2002 *US–Japan Workshop on Transport and Structure Formation of Plasmas (Kyushu University, 2002)*

[67] Galeev A A and Sagdeev R Z 1968 *Sov. Phys.—JETP* **26** 233
[68] Winsor N, Johnson J L and Dawson J M 1968 *Phys. Fluids* **11** 2448
[69] Stringer T 1969 *Phys. Rev. Lett.* **22** 770
[70] Sagdeev R Z and Galeev A A 1969 *Dokl. Akad. Nauk SSSR* **189** 1204
Sagdeev R Z and Galeev A A 1970 *Sov. Phys.—Dokl.* **14** 1198 (Engl. Transl.)
[71] Rosenbluth M N, Rutherford P H, Taylor J B, Frieman E A and Kovrizhnikh L M 1971 *Plasma Physics and Controlled Nuclear Fusion Research 1970* vol 1 (Vienna: IAEA) p 495
[72] Stix T H 1973 *Phys. Fluids* **16** 1260
[73] Hazeltine R D 1974 *Phys. Fluids* **17** 961
[74] Hassam A B and Kulsrud R M 1978 **21** 2271
[75] Hirshman S P 1978 *Nucl. Fusion* **18** 917
[76] Hirshman S P and Sigmar D J 1981 *Nucl. Fusion* **21** 1079
[77] Hinton F L and Hazeltine R D 1981 *Rev. Mod. Phys.* **48** 239
[78] Helander P and Sigmar D J 2002 *Collisional Transport in Magnetized Plasmas* (Cambridge: Cambridge University Press)
[79] Hassam A B and Drake J F 1993 *Phys. Fluids* B **5** 4022
[80] Itoh S-I and Itoh K 1988 *Phys. Rev. Lett.* **60** 2276
[81] Shaing K S and Grume E C 1989 *Phys. Rev. Lett.* **63** 2369
[82] Taguchi M 1988 *Plasma Phys. Control. Fusion* **30** 1897
[83] Taguchi M 1991 *Plasma Phys. Control. Fusion* **33** 859
[84] Hassam A B, Antonsen T M, Drake J F and Liu C S 1991 *Phys. Rev. Lett.* **66** 309
[85] Hsu C T, Shaing K C and Gormley R 1994 *Phys. Plasmas* **1** 132
[86] Hugill J 1994 *Plasma Phys. Control. Fusion* **36** B173
[87] Wobig H and Kisslinger J 1995 *Plasma Phys. Control. Fusion* **37** 893
[88] Rozhansky Y and Tendler M 1996 Plasma rotation in tokamaks *Review of Plasma Physics* vol 19, ed B B Kadomtsev (New York: Consultants Bureau) p 147
[89] Galeev A A, Sagdeev R Z, Liu C S and Novakovskii S V 1996 *J. Exp. Theor. Phys.* **82** 875
[90] Morris R C, Haines M G and Hastie R J 1996 *Phys. Plasmas* **3** 4513
[91] Lebedev V B, Yushmanov P N, Diamond P H, Novakovskii S V and Smolyakov A I 1996 *Phys. Plasmas* **3** 3023
[92] Novakovskii S V *et al* 1997 *Phys. Plasmas* **4** 4272
[93] Azumi M 1989 private communication
[94] Stringer T E 1993 *Nucl. Fusion* **33** 1249
[95] Itoh K, Itoh S-I, Yagi M and Fukuyama A 1998 *Phys. Plasmas* **5** 4121
[96] Lin Z *et al* 2000 *Phys. Plasmas* **7** 1807
[97] Chen Y *et al* 2003 *Nucl. Fusion* **43** 1121
[98] Candy J *et al* 2003 *J. Comput. Phys.* **186** 545
[99] Beer M 1995 *PhD Thesis* Princeton University
[100] Waltz R *et al* 1996 *Proc. Int. IAEA Conf. on Plasma Physics and Controlled Fusion Research (Montreal, 1996)* paper IAEA/CN-64/D1-6
[101] Beer M and Hammett G 1998 *Proc. Varenna–Lausanne Int. Workshop (Societa Italiana di Fisica, Editrice Compositori, Bologna, 1998)* p 19
[102] Kim E J, Holland C and Diamond P H 2003 *Phys. Rev. Lett.* **91** 075003
[103] Sagdeev R Z, Shapiro V D and Shevchenko V I 1978 *JETP Lett.* **27** 340
Sagdeev R Z, Shapiro V D and Shevchenko V I 1978 *Pis'ma Zh. Eksp. Teor. Fiz.* **27** 361
[104] Hallatschek K and Diamond P H 2003 *New J. Phys.* **5** 29.1
[105] Shukla P K *et al* 2001 *Eur. Phys. J.* D **20** 103
[106] Manfredi G, Roach C M and Dendy R O 2001 *Plasma Phys. Control. Fusion* **43** 825
[107] Manfredi G, Roach C M and Dendy R O 2001 *Plasma Phys. Control. Fusion* **43** 1001
[108] McCarthy D R, Lashmore-Davies C N and Thyagaraja A 2004 *Phys. Rev. Lett.* **93** 065004
[109] Connor J W, Hastie R J and Taylor J B 1979 *Proc. R. Soc.* A **365** 1
[110] Zakharov V E 1972 *Sov. Phys.—JETP* **35** 908
[111] Malkov M and Diamond P H 2001 *Phys. Plasmas* **9** 3996
[112] Itoh K, Itoh S-I and Hallatschek K 2005 *Plasma Phys. Control. Fusion* **47** 451
[113] Kadomtsev B B 1965 *Plasma Turbulence* (New York: Academic)
[114] Chen L *et al* 2001 *Nucl. Fusion* **41** 747
[115] Guzdar P N, Kleva R G, Das A and Kaw P K 2001 *Phys. Rev. Lett.* **87** 1015001
[116] Lakhin V P 2003 *Plasma Phys. Rep.* **29** 137

[117] Some of the explicit equations have been given in the reduced set of equations in chapter 11 of Ref. [16]

[118] Yagi M, Itoh S-I, Itoh K and Fukuyama A 1997 *Plasma Phys. Control. Fusion* **39** 1887

[119] Craddock G G and Diamond P H 1991 *Phys. Rev. Lett.* **67** 1535

[120] Zonca F 1999 *Phys. Plasmas* **6** 1917

[121] Rebut P H and Hugon M 1985 *Plasma Physics and Controlled Nuclear Fusion Research 1984* vol 2 (Vienna: IAEA) p 197

See also: Callen J D *et al* 1986 *Plasma Physics and Controlled Nuclear Fusion Research* vol 2 (Vienna: IAEA) p 157

[122] Gruzinov I and Diamond P H 2002 *Phys. Lett.* A **302** 119

[123] Yoshizawa A, Yokoi N, Itoh S-I and Itoh K 1998 *Phys. Plasmas* **6** 3194

[124] Kuo H L 1963 *Phys. Fluids* **6** 195

[125] Deardorff J W 1965 *Phys. Fluids* **8** 1027

[126] Gage K S and Reid W H 1968 *J. Fluid Mech.* **33** 21

[127] See, e.g. Lehnert B 1966 *Phys. Fluids* **9** 1367

[128] Inoue S, Itoh K and Yoshikawa S 1980 *J. Phys. Soc. Japan* **49** 367

[129] Shaing K C 1991 *Comments Plasma Phys. Control. Fusion* **14** 41

[130] Hassam A B 1991 *Comments Plasma Phys. Control. Fusion* **14** 275

[131] Sugama H and Wakatani M 1991 *Phys. Fluids* B **3** 1110

[132] Waelbroeck F L *et al* 1992 *Phys. Fluids* B **4** 1441

[133] Chu M S *et al* 1995 *Phys. Plasmas* **2** 2236

[134] Miller R L, Waelbroeck F W, Lao L L and Taylor T S 1994 *Int. Conf. on Plasma Physics and Controlled Nuclear Fusion Research* vol 3 (Seville: IAEA) p 231

[135] Medvedev M V and Diamond P H 1995 *Phys. Plasmas* **2** 727

[136] Bai L, Fukuyama A and Uchida M 1998 *Plasma Phys. Control. Fusion* **40** 785

[137] Waltz R E, Kerbel G D, Milovich J and Hammett G W 1995 *Phys. Plasmas* **2** 2408

[138] Sanuki H 1984 *Phys. Fluids* **27** 2500

[139] Itoh S-I, Itoh K, Ohkawa T and Ueda N 1989 *Plasma Physics and Controlled Nuclear Fusion Research 1988* vol 2 (Vienna: IAEA) p 23

[140] Goldreich P and Lynden-Bell D 1965 *Mon. Not. R. Atron. Soc.* **130** 125

[141] Zhang Y Z and Mahajan S M 1992 *Phys. Fluids* B **4** 1385

[142] Itoh S-I, Itoh K, Fukuyama A and Yagi M 1994 *Phys. Rev. Lett.* **72** 1200

[143] Shaing K C *et al* 1989 *Plasma Physics and Controlled Nuclear Fusion Research 1988* vol 2 (Vienna: IAEA) p 13

[144] Hirshman S P and Molvig K 1979 *Phys. Rev. Lett.* **42** 648

[145] Hahm T S, Burrell K H, Lin Z, Nazikian R and Synakowski E J 2000 *Plasma Phys. Control. Fusion* **42** A205

[146] Krommes J A 2000 *Phys. Plasmas* **7** 1148

[147] See, e.g. Kubo R, Toda M and Hashitsume N 1985 *Statical Physics II* (Berlin: Springer)

[148] Hinton F L and Wong S K 1985 *Phys. Fluids* **28** 3082

[149] Connor J W *et al* 1987 *Plasma Phys. Control. Fusion* **29** 919

[150] Itoh K *et al* 1998 *Plasma Phys. Control. Fusion* **40** 661

[151] Hahm T S and Burrell K H 1996 *Plasma Phys. Control. Fusion* **38** 1427

[152] Hahm T S *et al* 1998 *Plasma Phys. Control. Fusion* **40** 657

[153] Meshalkin N and Sinai Y 1965 *Appl. Math Mech.* **25** 1140

[154] Kim E J and Diamond P H 2002 *Phys. Plasmas* **9** 4530

[155] Holland C *et al* 2002 Investigations of the role of nonlinear couplings in structure formation and transport regulation: experiment, simulation, and theory, THP1/3

[156] Dorland W 1993 *PhD Thesis* Princeton University

[157] Rosenbluth M N 2002 private communication

[158] Lashmore-Davies C N, McCarthy D R and Thyagaraja A 2001 *Phys. Plasmas* **8** 5121

[159] Itoh K *et al* 2004 *J. Phys. Soc. Japan* **73** 2921

[160] Diamond P H and Gruzinov A V 1997 *Phys. Rev. Lett.* **78** 3306

[161] Malkov M, Diamond P H and Rosenbluth M N 2001 *Phys. Plasmas* **9** 5073

[162] Breizman B N 1978 *Sov. Phys.—JETP* 45 **271**

Breizman B N 1977 *Zh. Eksp. Teor. Fiz.* **72** 518

[163] Itoh K and Itoh S-I 1985 *J. Phys. Soc. Japan* **54** 1228

[164] Bazdenkov S V and Pogutse O P 1990 *JETP Lett.* **57** 410

[165] Itoh S-I, Itoh K, Fukuyama A and Miura Y 1991 *Phys. Rev. Lett.* **67** 2485
[166] Itoh S-I, Itoh K and Fukuyama A 1993 *Nucl. Fusion* **33** 1445
[167] Zohm H 1994 *Phys. Rev. Lett.* **72** 222
[168] Pogutse O P, Kerner W, Gribkov V, Dazdenkov S and Osipenko M 1994 *Plasma Phys. Control. Fusion* **36** 1963
[169] Sugama H and Horton W 1995 *Plasma Phys. Control. Fusion* **37** 345
[170] Vojtsekhovich L A, Dnestrovskij A Yu and Parail V V 1995 *Nucl. Fusion* **35** 631
[171] Lebedev V B, Diamond P H, Gruzinova I and Carreras B A 1995 *Phys. Plasmas* **2** 3345
[172] Toda S *et al* 1996 *Plasma Phys. Control. Fusion* **38** 1337
[173] Takayama A and Wakatani M 1996 *Plasma Phys. Control. Fusion* **38** 1411
[174] Aoyagi T, Yagi M and Itoh S-I 1997 *J. Phys. Soc. Japan* **66** 2689
[175] Thyagaraja A, Haas F A and Harvey D J 1999 *Phys. Plasmas* **6** 2380
[176] Wersinger J M, Finn J M and Ott E 1980 *Phys. Rev. Lett.* **44** 453
[177] Bian N, Benkadda S, Garcia O E, Paulsen J-V and Garbet X 2003 *Phys. Plasmas* **10** 1382
[178] Watanabe T-H and Sugama H 2002 **9** 3659
[179] Marchenko V S 2002 *Phys. Rev. Lett.* **89** 185002
[180] Diamond P H and Malkov M 2002 *Phys. Scr.* T **98** 63
[181] Balescu R 2003 *Phys. Rev.* E **68** 046409
[182] Itoh K, Hallatschek K, Toda S, Itoh S-I, Diamond P H, Yagi M and Sanuki H 2004 *Plasma Phys. Control. Fusion* **46** A335
[183] Itoh K, Itoh S-I and Fukuyama A 1992 *Phys. Rev. Lett.* **69** 1050
[184] Drake J F, Zeiler A and Biskamp D 1995 *Phys. Rev. Lett.* **75** 4222
[185] Walleffe F 1997 *Phys. Fluids* **9** 883
[186] Itoh K, Itoh S-I, Fkuyama A, Yagi Toda M S and Kawasaki M 2002 Modelling of bifurcations in magnetic confinement plasmas *Bifurcation Phenomena in Plasmas* ed S-I Itoh and N Kawai (Fukuoka: Kyushu University Press) p 416
[187] Itoh S-I and Itoh K 2001 *Plasma Phys. Control. Fusion* **43** 1055
[188] Itoh S-I, Kitazawa A, Yagi M and Itoh K 2002 *Plasma Phys. Control. Fusion* **44** 1311
[189] Itoh S-I, Itoh K, Yagi Kawasaki M M and Kitazawa A 2002 *Phys. Plasmas* **9** 1947
[190] Kishimoto Y 2004 *Invited talk at 9th H-mode Workshop (San Diego, 2003) Plasma Phys. Control. Fusion* **46** submitted
[191] Itoh K, Itoh S-I, Spineanu F, Vlad M O and Kawasaki M 2003 *Plasma Phys. Control. Fusion* **45** 911
[192] Holland C and Diamond P H 2004 *Phys. Plasmas* **11** 1043
[193] Jenko F 2003 *13th Toki Conf. (Toki, 2003)* paper I-1
[194] Yagi M *et al* 2003 *13th Toki Conf. (Toki, 2003)* paper I-6
[195] Malkov M, Diamond P H and Smolyakov A 2001 *Phys. Plasmas* **8** 1553
[196] Terry P W *et al* 2001 *Phys. Rev. Lett.* **87** 185001
[197] Kim E-J and Diamond P H 2003 *Phys. Rev. Lett.* **91** 075001
[198] Kim E-J and Diamond P H 2004 *Phys. Plasmas* **11** L77
[199] Hamaguchi S and Horton W 1992 *Phys. Fluids* B **4** 319
[200] Kim Y-J, Kishimoto Y, Wakatani M and Tajima T 1996 *Phys. Plasmas* **3** 3689
[201] Waltz R E, Staebler G M, Dorland W, Hammett G W, Kotschenreuther M and Konings J A 1997 *Phys. Plasmas* **4** 2482
[202] Itoh K, Itoh S-I, Fukuyama A, Sanuki H and Yagi M 1994 *Plasma Phys. Control. Fusion* **36** 123
[203] Li J and Kishimoto Y 2002 *Phys. Rev. Lett.* **89** 115002
[204] Jenko F *et al* 2002 *19th IAEA Fusion Energy Conf. (Lyon, 2002)* paper TH/1-2
[205] Weynants R R, Jachmich S and Van Oost G 1998 *Plasma Phys. Control. Fusion* **40** 635
[206] Burrell K H 1997 *Phys. Plasmas* **4** 1499
[207] Tynan G R *et al* 1992 *Phys. Rev. Lett.* **68** 3032
[208] Shats M G *et al* 2000 *Phys. Rev. Lett.* **84** 6042
[209] Hallatschek K and Biskamp D 2001 *Phys. Rev. Lett.* **86** 1223
[210] Spineanu F and Vlad M A 2002 *Phys. Rev. Lett.* **89** 185001
[211] Tang W 2004 *Phys. Plasmas* **9** 1856
[212] Frieman E A and Chen L 1982 *Phys. Fluids* **25** 502
[213] Sydora R D, Decyk V K and Dawson J M 1996 *Plasma Phys. Control. Fusion* **38** A281
[214] Hahm T S 1988 *Phys. Fluids* **31** 2670
[215] Beer M A and Hammett G W 1996 *Phys. Plasmas* **3** 4046
[216] Lee W, Tang W W M and Okuda H 1980 *Phys. Fluids* **23** 2007

[217] Dimits A M *et al* 1994 *Plasma Physics and Controlled Nuclear Fusion Research* vol III (Vienna: IAEA) p 457
[218] Sydora R D *et al* 1990 *Phys. Rev. Lett.* **64** 2015
[219] Parker S E, Lee W W and Santoro R A 1993 *Phys. Rev. Lett.* **71** 2042
[220] Cummings J C 1995 *PhD Thesis* Princeton University
[221] Kishimoto Y *et al* 1998 *Plasma Phys. Control. Fusion* **40** A663
[222] Hahm T S *et al* 1999 *Phys. Plasmas* **6** 922
[223] Synakowski E J *et al* 1997 *Phys. Plasmas* **4** 1736
[224] Mazzucato E *et al* 1996 *Phys. Rev. Lett.* **77** 3145
[225] Dimits A *et al* 2000 *Phys. Plasmas* **7** 969
[226] Hallatschek K 2004 *Phys. Rev. Lett.* **93** 065001
[227] Diamond P H *et al* 1997 *Phys. Rev. Lett.* **78** 1472
[228] Lebedev V B and Diamond P H 1997 *Phys. Plasmas* **4** 1087
[229] Falchetto G L and Ottaviani M 2004 *Phys. Rev. Lett.* **92** 25002
[230] Kim E, Diamond P H and Hahm T S 2004 *Phys. Plasmas* **11** 4454
[231] Hahm T S 2002 *Plasma Phys. Control. Fusion* **44** A87
[232] Mikkelsen D R *et al* 2002 *Plasma Physics and Controlled Nuclear Fusion Research* (Vienna: IAEA) IAEA-CN-69/EXP5/03
[233] Parker S E, Chen Y, Wan W, Cohen B I and Nevins W M 2004 *Phys. Plasmas* **11** 2594
[234] Hahm T S, Diamond P H, Lin Z, Itoh K and Itoh S-I 2004 *Plasma Phys. Control. Fusion* **46** A323
[235] Zonca F, Chen L and White R 2004 *Phys. Plasmas* **11** 2488
[236] Villard L *et al* 2004 *Nucl. Fusion* **44** 172
[237] Li J *et al* 2003 *13th Int. Toki Conf. (Toki, 2003)* paper P2-38
[238] Jenko F and Scott B D 1998 *Phys. Rev. Lett.* **80** 4883
[239] Tange T *et al* 1977 *J. Phys. Soc. Japan* **42** 2006
[240] Hahm T S 1992 *Phys. Fluids* B **4** 2801
[241] Carerras B A *et al* 1992 *Phys. Fluids* B **4** 3115
[242] Dupree T H 1972 *Phys. Fluids* **15** 334
[243] Watanabe T-H and Sugama H 2004 *Phys. Plasmas* **11** 1476
[244] Wong K-L *et al* 1997 *Phys. Lett.* A **236** 33
[245] Wong K-L *et al* 2000 *Phys. Lett.* A **276** 281
[246] Park K-L *et al* 2004 private communication
[247] Rhodes T *et al* 2004 private communication
[248] Porkolab M *et al* 2004 private communication
[249] Jenko F *et al* 2000 *Phys. Plasmas* **7** 1904
[250] Labit B and Ottaviani M 2003 *Phys. Plasmas* **10** 126
[251] Li J and Kishimoto Y 2004 *Phys. Plasmas* **11** 1493
[252] Lin Z *et al* 2004 *Plasma Physics and Controlled Nuclear Fusion* (Vienna: IAEA)
[253] Jenko F and Dorland W 2002 *Phys. Rev. Lett.* **89** 225001
[254] Hahm T S and Tang W M 1989 *Phys. Fluids* B **1** 1185
[255] Jenko F *et al* 2001 *Phys. Plasmas* **8** 4096
[256] Busse F H 1994 *Chaos* **4** 123
[257] Hasegawa A and Mima K 1978 *Phys. Fluids* **21** 87
[258] Rossby C G 1940 *Q. J. R. Meteo. Soc.* **66** (Suppl.) 68
[259] Horton W and Hasegawa A 1994 *Chaos* **4** 227
[260] Rhines P B 1975 *J. Fluid Mech.* **69** 417
[261] Naulin V 2002 *New J. Phys.* **4** 28.1
[262] Scott B D 1995 *Plasma Physics and Controlled Nuclear Fusion Research* vol III (Vienna: IAEA) p 447
[263] Carreras B A, Lynch V E and Garcia L 1993 *Phys. Fluids* B **5** 1795
[264] Guzdar P N, Drake J F, McCarthy D, Hassam A B and Liu C S 1993 *Phys. Fluids* B **5** 3712
[265] Sugama H, Wakatani M and Hasegawa A 1988 *Phys. Fluids* **31** 1601
[266] Sugama H and Horton W 1994 *Phys. Plasmas* **1** 345
[267] Naulin V 2003 *Phys. Plasmas* **10** 4016
[268] Sugama H and Horton W 1994 *Phys. Plasmas* **1** 2220
[269] Wakatani M *et al* 2002 Shear flow generation due to electromagnetic instabilities *19th IAEA Fusion Energy Conf. (Lyon, 2002)* paper TH/P1-18

[270] Rogers B N, Drake J F and Zeiler A 1998 *Phys. Rev. Lett.* **81** 4396
[271] Rogers B N *et al* 1995 *Phys. Plasmas* **2** 2397
[272] Xu X Q *et al* 2002 *New J. Phys.* **4** 53
[273] Scott B D *et al* 2001 *Plasma Physics and Controlled Nuclear Fusion Research* (Vienna: IAEA)
[274] Scott B D 2003 *Phys. Lett.* A **320** 53
[275] Scott B D 2003 private communication
[276] Scott B D 2004 Energetics of the interaction between electromagnetic $E \times B$ turbulence and zonal flows *Phys. Plasmas* submitted
[277] Dimits A M *et al* 2000 *Nucl. Fusion* **40** 661
[278] Dimits A M *et al* 2000 *Phys. Plasmas* **7** 969
[279] Parker S *et al* 1999 *Phys. Plasmas* **6** 1709
[280] Gossard E E and Hooke W H 1975 *Waves in the Atmosphere* (Amsterdam: Elsevier)
[281] Charney J G 1948 *Geophys. Publ. Oslo* **17** 1
[282] Hasegawa A 1983 *J. Phys. Soc. Japan* **52** 1930
[283] Marcus P S, Kundu T and Lee C 2000 *Phys. Plasmas* **7** 1630
[284] Or A C and Busse F H 1987 *J. Fluid. Mech.* **174** 313
[285] Busse F H 1976 *Icarus* **29** 255
[286] Busse F H 1983 *J. Fluid. Mech.* **121** 375
[287] Grote E and Busse F A 2001 *Fluid Dyn. Res.* **28** 349
[288] Jones C A *et al* 2003 *Geophys. Res. Lett.* **30** 1731
[289] Brummell N H and Hart J F 1993 *Geophys. Astrophys. Fluid Dyn.* **68** 85
[290] Christensen U R 2001 *Geophys. Astrophys. Fluid Dyn.* **28** 2553
[291] Zhang K K and Busse F H 1989 *Geophys. Astrophys. Fluid Dyn.* **49** 97
[292] Busse F H 2000 *Ann. Rev. Fluid Mech.* **32** 383
[293] Takagi M and Matsuda Y 2003 *Reports of RIAM* No. S-1 (11–14 Feburary, 2003)
[294] Schubert G 1983 *Venus* (University of Arizona Press) pp 681–765
[295] Thompson R 1970 *Atmos. J. Sci.* **27** 1107
[296] Fels S B and Lindzen R E 1973 *Geophys. Fluid. Dyn.* **6** 149
[297] Gierasch P J 1975 *Atmos. J. Sci.* **32** 1038
[298] Horton C W 1984 *Basic Plasma Physics II* ed A A Galeev and R N Sudan (Amsterdam: North-Holland) chapter 6.4
[299] Cheng C Z and Okuda H 1977 *Phys. Rev. Lett.* **38** 708
[300] Okuda H 1974 *Phys. Fluids* **17** 375
[301] Sanuki H and Weiland J 1980 *J. Plasma Phys.* **23** 29
[302] Krommes J A 1999 *Plasma Phys. Control. Fusion* **41** A641
[303] Scott B D 1992 *Phys. Fluids* B **4** 2468
[304] Das A, Sen A, Mahajan S and Kaw P 2001 *Phys. Plasmas* **8** 5104
[305] Champeaux S *et al* 2001 *APS Invited Lecture*
[306] Carreras B A *et al* 2002 Anomalous diffusion in plasma turbulence models *19th IAEA Fusion Energy Conf. (Lyon, 2002)* (Vienna: IAEA) paper TH/2-3
[307] Krommes J A and Kim C B 2000 *Phys. Rev.* E **62** 8508
[308] Balescu R 1997 *Statistical Dynamics: Matter out of Equilibrium* (London: Imperial College Press)
[309] Krommes J A 2002 *Phys. Rep.* **360** 1
[310] Makino M, Kamimura T and Taniuti T 1981 *J. Phys. Soc. Japan* **50** 980
[311] Meiss J D and Horton C W 1983 *Phys. Fluids* **26** 990
[312] Kim E J and Diamond P H 2002 *Phys. Rev. Lett.* **88** 225002
[313] Kim E J *et al* 2003 *Nucl. Fusion* **43** 961
[314] Itoh S-I and Itoh K 1999 *J. Phys. Soc. Japan* **68** 1891
Itoh S-I and Itoh K 1999 *J. Phys. Soc. Japan* **68** 2661
Itoh S-I and Itoh K 2000 *J. Phys. Soc. Japan* **69** 408
Itoh S-I and Itoh K 2000 *J. Phys. Soc. Japan* **69** 3253
[315] Itoh S-I and Itoh K 2000 *J. Phys. Soc. Japan* **69** 427
[316] Yagi M *et al* 2002 Multiple-scale turbulence and bifurcation *19th IAEA Fusion Energy Conf. (Lyon, 2002)* (Vienna: IAEA) TH1/4
[317] Bowman J C, Krommes J A and Ottaviani M 1993 *Phys. Fluids* B **5** 3558
[318] Itoh S-I, Itoh K and Toda S 2002 *Phys. Rev. Lett.* **89** 215001
[319] Chandrasekhar S 1943 *Rev. Mod. Phys.* **15** 1

[320] Itoh S-I, Itoh K and Toda S 2003 *Plasma Phys. Control. Fusion* **45** 823
See also: Itoh S-I *et al* 2002 Statistical theory of L–H transition and its implication to threshold database *19th IAEA Fusion Energy Conf. (Lyon, 2002)* (Vienna: IAEA) PDP/04
[321] Bak P, Tang C and Wiesenfeld K 1987 *Phys. Rev. Lett.* **59** 381
[322] Diamond P H and Hahm T S 1995 *Phys. Plasmas* **2** 3640
[323] Newman D E, Carreras B A, Diamond P H and Hahm T S 1996 *Phys. Plasmas* **3** 1858
[324] Carreras B A, Newman D, Lynch V E and Diamond P H 1996 *Phys. Plasmas* **3** 2903
[325] Dendy R O and Helander P 1997 *Plasma Phys. Control. Fusion* **39** 1947
[326] Carreras B A *et al* 1998 *Phys. Plasmas* **5** 3632
[327] Carreras B A *et al* 1999 *Phys. Plasmas* **6** 1885
[328] Gruzinov I, Diamond P H and Rosenbluth M N 2002 *Phys. Rev. Lett.* **89** 255001
[329] Gruzinov I, Diamond P H and Rosenbluth M N 2003 *Phys. Plasmas* **10** 569
[330] Krommes J A 2000 *Phys. Plasmas* **7** 1752
[331] Nevins W M 2000 *Bull. Am. Phys. Soc.* **45** 158
[332] Krasheninnikov S I *et al* 2002 Blobs and cross-field transport in the tokamak edge plasmas *19th IAEA Fusion Energy Conf. (Lyon, 2002)* (Vienna: IAEA) TH4/1
[333] Ghendrih Ph *et al* 2002 Theoretical analysis of long range turbulent transport in the scrape-off-layer *19th IAEA Fusion Energy Conf. (Lyon, 2002)* (Vienna: IAEA) THP2/14
[334] Nevins W M *et al* 2002 Simulations of boundary turbulence in tokamak experiments *19th IAEA Fusion Energy Conf. (Lyon, 2002)* THP3/7
[335] Balescu R 2000 *Plasma Phys. Control. Fusion* **42** B1
[336] Vlad M, Spineanu F, Misguich J H and Balescu R 1998 *Phys. Rev.* E **58** 7359
[337] Vlad M, Spineanu F, Misguich J H and Balescu R 2001 *Phys. Rev.* E **63** 066304
[338] Vlad M, Spineanu F, Misguich J H and Balescu R 2003 *Phys. Rev.* E **67** 026406
[339] Krommes J A 2003 *13th Int. Toki Conf.* paper I-20
[340] Kodama Y and Taniuti T 1979 *J. Phys. Soc. Japan* **47** 1706
[341] Shukla P K *et al* 1981 *Phys. Rev.* A **23** 321
[342] Nozaki K, Taniuti T and Watanabe K 1979 *J. Phys. Soc. Japan* **46** 983
[343] Nozaki K, Taniuti T and Watanabe K 1979 *J. Phys. Soc. Japan* **46** 991
[344] Petviashvili V I 1977 *Fiz. Plazmy* **3** 270
Petviashvili V I 1977 *Sov. J. Plasma Phys.* **3** 150 (Engl. Transl.)
[345] Flierl G R 1979 *Dyn. Atmos. Oceans* **3** 15
[346] Lakhin V P, Mikhailovskii A B and Onishcenko O G 1987 *Phys. Lett.* A **119** 348
[347] Kono M and Miyashita E 1988 *Phys. Fluids* **31** 326
[348] Spatschek K H, Laedke E W, Marquardt Chr, Musher S and Wenk H 1990 *Phys. Rev. Lett.* **64** 3027
[349] Spatschek K H 1999 *Plasma Phys. Control. Fusion* **41** A115
[350] Weiland J, Sanuki H and Liu C S 1981 *Phys. Fluids* **24** 93
[351] Mahajan S and Weiland J 2000 *Plasma Phys. Control. Fusion* **42** 987
[352] Spineanu F, Vlad M, Itoh K, Sanuki H and Itoh S-I 2004 *Phys. Rev. Lett.* **93** 25001
[353] Gurcan O D and Diamond P H 2004 *Phys. Plasmas* **11** 572
[354] Gurcan O D and Diamond P H 2004 *Phys. Plasmas* **11** 332
[355] Gurcan O D and Diamond P H 2004 *Phys. Plasmas* **11** 4973
[356] Hahm T S *et al* 1999 *Phys. Plasmas* **6** 922
[357] Jenko F and Kendl A 2002 *Phys. Plasmas* **9** 4103
[358] Kendl A, Scott B D, Ball R and Dewar R L 2003 *Phys. Plasmas* **10** 3684
[359] Zarnstorff M *et al* 2001 *Plasma Phys. Control. Fusion* **43** 237
[360] Okamura S *et al* 2001 *Nucl. Fusion* **41** 1865
[361] Ida K 1998 *Plasma Phys. Control. Fusion* **40** 609
[362] Levinton F M *et al* 1998 *Phys. Rev. Lett.* **80** 4887
[363] Hamada Y 1997 *Fusion Eng. Des.* **34–35** 25–35
[364] Fujisawa A 2003 *Plasma Phys. Control. Fusion* **45** R1
[365] Groebner R J *et al* 1990 *Phys. Rev. Lett.* **64** 3015
[366] Ida K, Hidekuma S, Miura Y, Fujita T, Mori M, Hoshino K, Suzuki N, Yamauchi T and JFT-2M group 1990 *Phys. Rev. Lett.* **65** 1364
[367] Bell R E *et al* 1998 *Phys. Rev. Lett.* **81** 1429
[368] Ido T *et al* 2002 *Phys. Rev. Lett.* **88** 055006
[369] Miura Y *et al* 2001 *Nucl. Fusion* **41** 973

[370] Fujisawa A *et al* 2000 *Phys. Plasmas* **7** 4152

[371] Stroth U *et al* 2001 *Phys. Rev. Lett.* **86** 5910

[372] Fujisawa A *et al* 2004 *Phys. Rev. Lett.* **93** 165002

[373] Fujisawa A *et al* 2004 *31st EPS Conf. on Controlled Fusion and Plasma Physics (London, 2004)* paper O2-04

[374] Xu G S, Wan B N, Song M and Li J 2003 *Phys. Rev. Lett.* **91** 125001

[375] Hamada Y *et al* 1994 *Plasma Phys. Control. Fusion* **36** 1743

[376] Hamada Y, Nishizawa A, Kawasumi Y, Fujisawa A, Iguchi H and JIPP T-IIU group 1997 *Fusion Eng. Des.* **34–35** 657

Hamada Y, Nishizawa A, Kawasumi Y, Fujisawa A, Iguchi H and JIPP T-IIU group 1997 *Fusion Eng. Des.* **34–35** 663

[377] Schoch P *et al* 2003 *Phys. Rev. Lett.* submitted

[378] Hassam A B *et al* 1994 *Phys. Plasmas* **1** 337

[379] Kishimoto Y and Li J Q 2003 *ITC-13*

[380] Hidalgo C *et al* 1999 *Phys. Rev. Lett.* **83** 2203

[381] Xu Y H *et al* 2000 *Phys. Rev. Lett.* **84** 3867

[382] Diamond P H *et al* 2000 *Phys. Rev. Lett.* **84** 4842

[383] Tynan G R *et al* 2001 *Phys. Plasmas* **8** 2691

[384] Moyer R A *et al* 2001 *Phys. Rev. Lett.* **87** 135001

[385] Holland C *et al* 2002 *Plasma Phys. Control. Fusion* **44** A453

[386] Shats M G and Solomon W M 2002 *Phys. Rev. Lett.* **88** 045001

[387] Sugai H, Pecseli H L, Rasmussen J J and Thomsen K 1983 *Phys. Fluids* **26** 1389

[388] Ramisch M, Stroth U, Niednerand M and Scott B D 2003 *New J. Phys.* **5** 12

[389] Coda S, Porkolab M and Burrell K H 2001 *Phys. Rev. Lett.* **86** 4835

[390] Taylor G I 1915 *Phil. Trans. R. Soc.* A **215** 1

[391] Jackubowski M, Fonck R J and Mckee G 2002 *Phys. Rev. Lett.* **89** 265003

[392] McKee G R *et al* 2003 *Phys. Plasmas* **10** 1712

[393] McKee G R *et al* 2003 *Plasma Phys. Control. Fusion* **45** A477

[394] Hirsch M and Holzhauer E 2004 *Plasma Phys. Control. Fusion* **46** 593

[395] T-10 Team 2002 Transport and turbulence studies in the T-10 tokamak *(Lyon, 2002)* (Vienna: IAEA) paper OV/5-2

[396] Conway G D, Scott B, Schirmer J, Reich M, Kendl A and ASDEX Upgrade Team 2004 *31st EPS Conf. on Controlled Fusion and Plasma Physics (London, 2004)* paper P4.124

[397] Ido T *et al* 2004 Electrostatic fluctuation and fluctuation-induced particle flux during formation of the edge transport barrier in the JFT-2M tokamak *20th IAEA Conf. on Fusion Energy* (Portugal: IAEA) EX/4-6Rb

[398] Paul S *et al* 2004 *Rev. Sci. Instrum.* **75** 4077

[399] Zweben S *et al* 2004 *Nucl. Fusion* **44** 134

[400] Terry J *et al* 2003 *Phys. Plasmas* **10** 1739

[401] Punzmann H and Shats M G 2004 *Phys. Rev. Lett.* **93** 125003

[402] Porkolab M and Rost C 2003 private communication

[403] Mazzucato E 2004 *Plasma Phys. Control. Fusion* **46** 1271

[404] Park H *et al* 2004 *Rev. Sci. Instrum.* **75** 3787

[405] Zaslavsky G M 2002 *Phys. Rep.* **371** 461

[406] Klimontovich Yu L 1967 *The Statistical Theory of Non-Equilibrium Processes in a Plasma* (Cambridge, MA: MIT)

[407] Dubin D H *et al* 1983 *Phys. Fluids* **26** 3524

[408] Hahm T S, Lee W W and Brizard A 1988 *Phys. Fluids* **31** 1940

[409] Brizard A 1989 *J. Plasma Phys.* **41** 541

[410] Hahm T S 1996 *Phys. Plasmas* **3** 4658

[411] Stix T H 1992 *Waves in Plasmas* (New York: AIP) p 247

[412] Dorland W and Hammett G W 1993 *Phys. Fluids* B **5** 812

[413] Snyder P B, Hammett G W and Dorland W 1997 *Phys. Plasmas* **4** 3974

[414] Mattor N 1992 *Phys. Fluids* B **4** 3952

[415] Sugama H, Watanabe T-H and Horton C W 2001 *Phys. Plasmas* **8** 2617

[416] Braginskii S I 1965 *Review of Plasma Physics* vol 1, ed M A Leontovich (New York: Consultants Bureau) p 205

[417] Yagi M and Horton W 1994 *Phys. Plasmas* **1** 2135
[418] Scott B 1997 *Plasma Phys. Control. Fusion* **39** 1635
[419] Zeiler A, Drake J F and Rogers B 1997 *Phys. Plasmas* **4** 2134
[420] Xu X Q *et al* 2000 *Phys. Plasmas* **7** 1951
[421] Simakov A N and Catto P J 2003 *Phys. Plasmas* **10** 4744